

Durham E-Theses

Magnetoresistivity tensor of arsenic (25.5 at. %) – Antimony alloy single crystals.

Akgoz, Yakup Cevdet

How to cite:

Akgoz, Yakup Cevdet (1974) *Magnetoresistivity tensor of arsenic (25.5 at. %) – Antimony alloy single crystals.*, Durham theses, Durham University. Available at Durham E-Theses Online:
<http://etheses.dur.ac.uk/8131/>

Use policy

The full-text may be used and/or reproduced, and given to third parties in any format or medium, without prior permission or charge, for personal research or study, educational, or not-for-profit purposes provided that:

- a full bibliographic reference is made to the original source
- a [link](#) is made to the metadata record in Durham E-Theses
- the full-text is not changed in any way

The full-text must not be sold in any format or medium without the formal permission of the copyright holders.

Please consult the [full Durham E-Theses policy](#) for further details.

MAGNETORESISTIVITY TENSOR OF
ARSENIC (25.5 at.%) - ANTIMONY
ALLOY SINGLE CRYSTALS

by

YAKUP CEVDET AKGÖZⁿ B.Sc.

A thesis submitted to the University of Durham
for the degree of
Doctor of Philosophy
November 1974

Department of Applied Physics and Electronics
Science Laboratories
Durham City



ABSTRACT

An experimental investigation of the galvanomagnetic effects in a particular A7 structure material and a theoretical study of the symmetry properties of the transport tensors are presented.

For the experimental study, arsenic-antimony alloy single crystals have been grown at the minimum melting point composition (25.5 at.%As) where the solidus and liquidus touch on the phase diagram. Dislocation etch pit studies have been made on the (111) cleavage faces. Measurements have been made between 1.5K and 300K of the twelve components that define the low-field magnetoresistivity tensor and of the orientation dependence of the tensor components $\rho_{11}(B_1, B_2, 0)$, $\rho_{11}(B_1, 0, B_3)$ and $\rho_{21}(B_1, 0, B_3)$. A least-mean-squares fit to the data has been used to obtain the model parameters for a two band, multivalley, ellipsoidal Fermi surface. The alloy model parameters are compared and contrasted with those of the parent elements. The alloy is semimetallic.

In the theoretical work, the forms of the magnetic field dependent transport tensors are established for all 32 crystallographic point groups. A formulation of galvanomagnetic and thermomagnetic effects based on the separation of the tensor components into "even" and "odd" functions of the applied magnetic field is given. It is shown that the Umkehr effect is a natural result of the anisotropy of crystals.

ACKNOWLEDGEMENTS

First I would like to express my sincere gratitude to my supervisor Dr. G.A. Saunders for his enthusiastic guidance, interest and sustained encouragement in the course of this research project.

I am grateful to Professor D.A. Wright for use of the many facilities in the Department and the Turkish Ministry of Education (Milli Eğitim Bakanlığı) for a postgraduate grant.

My thanks also go to the workshop staff for their technical assistance and Dr. Ö.T. Akıncı for his careful electron microprobe analysis of the samples.

Finally, I would like to thank Mrs. C.A. Kitching for her careful typing of the manuscript.

CONTENTS

	Page
Abstract	ii
Acknowledgements	iii
<u>CHAPTER 1: GENERAL INTRODUCTION</u>	1
<u>CHAPTER 2: SYMMETRY IN THE A7 STRUCTURE</u>	
2.1 Introduction.	4
2.2 The rhombohedral space lattice and the A7 structure.	5
2.2.1 Relationships between Miller indices referred to various axial sets.	18
2.3 Which crystal system does the A7 structure belong to?	21
2.4 The reciprocal space lattice.	23
2.5 Symmetry of the Brillouin zone in the A7 structure.	26
<u>CHAPTER 3: SPACE TIME SYMMETRY RESTRICTIONS ON THE FORM OF TRANSPORT TENSORS.</u>	
3.1 Introduction.	33
3.2 Tensors in crystals.	34
3.2.1 Polar and axial tensors.	36
3.2.2 Intrinsic symmetry of tensors.	38
3.3 Tensor calculus	39
3.3.1 Tensor addition.	39
3.3.2 Tensor products.	40
3.3.3 Some properties of symmetric second rank tensors.	47
3.4 Effects of crystal symmetry on the forms of the tensors representing macroscopic physical properties of crystals.	49

	Page
3.4.1 Neumann's principle.	49
3.4.2 Crystal symmetry restrictions - CLASSICAL METHODS.	50
3.4.3 Crystal symmetry restrictions - GROUP THEORETICAL METHODS.	53
3.5 Space-time symmetry restrictions on the form of transport tensors.	71
3.5.1 Constant and field dependent tensors.	71
3.5.2 The transformation law for field dependent tensors.	72
3.5.3 Crystal symmetry restrictions on the form of the transport tensors - the magnetoresistivity tensor $\rho_{ij}(\vec{B})$.	73
3.5.4 ————— the magnetothermoelectric power tensor $\alpha_{ij}(\vec{B})$.	82
3.5.5 The Umkehr effect.	83
 <u>CHAPTER 4: A FORMULATION OF TRANSPORT TENSORS IN ANISOTROPIC MEDIA: GALVANOMAGNETIC AND THERMOMAGNETIC EFFECTS.</u>	
4.1 Introduction.	85
4.2 Transport tensors. Case (1): $\vec{B}=0$.	86
4.3 Transport tensors. Case (2): $\vec{B}=(B_1, B_2, B_3)$.	93
4.3.1 Galvanomagnetic effects.	95
4.3.2 Thermomagnetic effects.	114
 <u>CHAPTER 5: THE EFFECT OF CONSTANT ENERGY SURFACE MODELS AND SOME BASIC TRANSPORT THEORY ASSUMPTIONS ON THE FORM OF TRANSPORT TENSORS.</u>	
5.1 Introduction.	123
5.2 Constant energy surface symmetry restrictions on the form of the magnetoresistivity tensor.	124
5.3 The effect of constant energy surface models on the form of $\alpha_{ij}(\vec{B})$ - the diffusion and phonon drag thermopowers.	128

	Page
5.4	The Umkehr effect in $\rho_{ij}(\vec{B})$. 138
5.4.1	The A7 structure semimetals. 139
5.4.2	n-type Germanium. 141
5.5	The Umkehr effect in $\alpha_{ij}(\vec{B})$. 143
 <u>CHAPTER 6: MAGNETORESISTIVITY TENSOR OF</u>	
<u>As(25.5 at.%)–Sb ALLOY SINGLE CRYSTALS.</u>	
6.1	Introduction. 145
6.2	Growth and dislocation etch pits of As(25.5at.%)–Sb single crystals. 146
6.2.1	Crystal growth. 146
6.2.2	Dislocation etch pit studies. 148
6.2.3	Orientation of crystals. 152
6.2.4	Conversely oriented etch pits in the A7 structure semimetals. 153
6.3	Galvanomagnetic effects of As(25.5 at.%)–Sb alloy single crystals. 155
6.3.1	Experimental procedure and results. 157
6.3.2	Computation 162
6.3.3	Discussion of the model parameters. 165
6.4	Electron and hole tilt angles in the A7 structure semimetals. 167
References	vii
APPENDIX I.	xiii
APPENDIX II.	xv
APPENDIX III.	xviii
PUBLICATIONS.	xxii

CHAPTER ONE

GENERAL INTRODUCTION

Measurement of the galvanomagnetic effects has long been a valuable method for obtaining information about the motion of charge carriers in crystals under the influence of electric and magnetic fields. The elemental group V semimetals bismuth, antimony and arsenic have always been among the first materials, particularly bismuth, in which new experimental studies of transport effects have been carried out. Low field galvanomagnetic data on these semimetals have been (following Abeles and Meiboom 1956) successfully interpreted using multivalley ellipsoidal Fermi surface models by several workers in the field. Similar studies have been carried out on certain Bi-Sb alloys (see Goldsmid 1970 and references therein). The present concern is to extend these low field galvanomagnetic studies to arsenic-antimony alloy single crystals grown at the minimum melting point composition (25.5 at.% As) where the solidus and liquidus touch on the phase diagram (figure 6.1). A condensed discussion of the experimental results and their significance is given in chapter 6.

However, while the low field galvanomagnetic measurements of As(25.5 at.%) - Sb alloy single crystals (hereafter referred to as the As-Sb alloy or the alloy) were in progress, there were two important publications in the field (Fuchser et al (1970)



and Aubrey (1971) which developed a compact expression for the magnetoconductivity tensor which is not restricted to the low field condition. Furthermore Aubrey (1971) derived explicit expressions for each component of $\sigma_{ij}(\vec{B})$ in terms of carrier densities and mobilities for the tilted multivalley ellipsoidal model of the group V semimetals which are valid over the classical range of magnetic fields. This formulation, in fact, provides a theory for the so called intermediate field region in which galvanomagnetic data have not previously been interpreted completely. Galvanomagnetic measurements in this region (Saunders and Sumengen 1972, Jacobson 1973, Akgöz and Saunders 1974, Sumengen et al 1974) are more practical and easier experimentally, capable of providing more and comprehensive data and of wider application than measurements of low field tensor components. In fact, the anisotropy of the galvanomagnetic effects is most pronounced in this region. With this development a new dimension has been added to the area of galvanomagnetic effect studies.

During our investigations of this new area, some basic questions have come to notice:

is $\rho_{ij}(\vec{B})$ a tensor?; how does the crystal symmetry restrict its form?; how do we define magnetoresistance and Hall effect now?; what is the Umkehr effect?.....

A large part of this thesis (section (3.5) of chapter 3, chapter 4 and chapter 5) has been devoted to answering these and related questions.

A few remarks about notation may be found useful. A vector is denoted by a letter with an arrow attached to it such as (\vec{B}, \vec{E}, \dots). A two-headed arrow sign is attached to tensors such as ($\vec{T}, \vec{\mu}, \vec{p}, \dots$), but transition is readily made to the suffix notation. Subscripts denote cartesian components of vectors (or tensors) and run from 1 to 3 unless otherwise stated. Throughout the text, the Einstein summation convention is used.

CHAPTER TWO

SYMMETRY IN THE A7 STRUCTURE

2.1 INTRODUCTION

The relatively low symmetry of the A7 structure has a dominating influence on the electronic properties of the group V semimetals. There have been a variety of descriptions of this structure in the literature: different workers have used different definitions of such parameters as the primitive lattice translation vectors, axial systems, indices of planes and directions, and unit cells. As a result it can be difficult to relate the results of one worker with those of another.

In this chapter the more commonly used crystallographic conventions are collected and compared and the appropriate transformations from one to another are presented. One problem has been the choice of a particular convention on which to base this study. For reasons which will be dealt with in the course of this chapter, a right-handed crystallographic orthogonal set has been shown to be the most convenient axial set (both in real and reciprocal space) for use as a frame of reference for the A7 structure. The major purpose of this chapter is to give a complete description of the A7 structure on this basis. One particular difficulty discussed is the classification of the A7 structure into a crystal system.

The point symmetries of the Brillouin zone appropriate to the A7 structure are listed. These symmetry points display the possible location of the Fermi surface pockets in the Brillouin zone.

2.2 THE RHOMBOHEDRAL SPACE LATTICE AND THE A7 STRUCTURE

Arsenic, antimony, bismuth and bismuth-antimony and arsenic-antimony solid solutions crystallize in the A7 structure (arsenic structure) which belongs to the point group $\bar{3}m$ (D_{3d}). The A7 structure, which is based on a rhombohedral space lattice, is obtained by associating a basis of two atoms with each lattice point. The most symmetrical point group in each crystal system is called holosymmetric; $\bar{3}m$ is a holosymmetric point group.

This point group consists of the following symmetry operations:

Symmetry operation	Description of the operation
E	the identity;
C_3^+ , C_3^-	rotations of $+\frac{2\pi}{3}$ and $-\frac{2\pi}{3}$ about the trigonal axis;
C'_{21} , C'_{22} , C'_{23}	three two-fold rotations about axes perpendicular to trigonal axis;
I	the inversion;

S_6^+ , S_6^-

rotations of $-\pi/3$ and $+\pi/3$ about the trigonal axis, followed by inversion.

σ_{d1} , σ_{d2} , σ_{d3}

three reflection planes containing the z-axis, which make 120° angles with respect to each other, and are each perpendicular to one of the two-fold axes ($C_{2i} \perp \sigma_{di}$; $i = 1, 2, \text{ and } 3$).

Positive rotations are defined as anticlockwise. Thus the symmetry elements of the A7 structure comprise 3 diad (binary) axes normal to three mirror planes, mutually oriented at 120° , which intersect in an inversion triad (trigonal) axis.

Each lattice site of the rhombohedral space lattice has the point group symmetry $\bar{3}m$. There are three primitive translation vectors of equal magnitude and usually denoted by $a = |\vec{a}_1| = |\vec{a}_2| = |\vec{a}_3|$. The angle between any \vec{a}_i ($i = 1, 2, 3$) is called the rhombohedral angle; the restrictions imposed by the requirement of rhombohedral symmetry are

$$\alpha < 120^\circ, \neq 60^\circ, \neq 90^\circ, \neq 109^\circ 28' . \quad (2.1)$$

The two restrictions $\alpha \neq 60^\circ$ and $\alpha \neq 109^\circ 28'$ do not appear in any of the commonly used textbooks of solid state physics. The following seven space groups possess the rhombohedral space lattice:

$R3(C_3^4)$, $R\bar{3}(S_6^2)$, $R32(D_3^7)$ $R3c(C_{3v}^6)$, $R\bar{3}m(D_{3d}^5)$, $R3m(C_{3v}^5)$,
 $R\bar{3}c(D_{3d}^6)$.

Two of these space groups $R3c$ and $R\bar{3}c$ are nonsymmorphic, that is they have nonprimitive translations such as glide planes or screw axes. However, the space group $R\bar{3}m$ of interest here is symmorphic. Figure (2.1) shows the rhombohedral space lattice in which primitive rhombohedral and hexagonal unit cells are drawn.

The origin can be placed either at a lattice point or at an atomic site (both have been used in the literature); this choice makes no difference to unit cell volume or to the directions of lattice translation vectors \vec{a}_i but it does, of course, translate their origin along the threefold axis. Figure (2.2) shows the same hexagonal and primitive rhombohedral unit cells constructed when the origin is taken at an atomic site. However, in the present work (following the International Tables for X-Ray Crystallography) a lattice point (which is an inversion centre) is chosen as the origin. It must be emphasized that in the A7 structure there is another inversion centre which is the centre of the primitive rhombohedral (prh) and face-centred rhombohedral (fcr) unit cells in real space - this corresponds to the T point of the first Brillouin zone in the reciprocal space.

Four types of axial system can be used to describe crystals having the A7 structure and their various physical properties. Each axial set is associated with a unit cell in the following way:

- (i) The crystallographic orthogonal set → Wigner-Seitz unit cell.
- (ii) Rhombohedral axes → primitive rhombohedral unit cell.
- (iii) Hexagonal axes → hexagonal unit cell.
- (iv) Face-centred cubic orthogonal axial set → face-centred rhombohedral unit cell.

We now proceed to define them in turn and study their relationships.

(1) A crystallographic orthogonal axial set is defined in the A7 structure in the following way: the z-axis coincides with the three-fold (trigonal) axis, the x-axis with one of the three two-fold (binary) axes, which are each perpendicular to one of the three mirror planes, and the y-axis (bisectrix) completes the orthogonal set. It is often convenient and necessary, from both experimental and theoretical points of view, to specify a (+x, +y, +z) right handed set. A lattice point is taken as the origin, see figures (2.1), (2.2), (2.3), (2.4) and (2.5). In figure (2.5), the positive direction of the primitive

translation vectors are chosen outwards from the origin; the \vec{a}_1 are shown projected onto the xy plane and their projections are labelled $[\vec{a}_{1prh}]_{proj}$. The +z direction is defined along $(\vec{a}_1 + \vec{a}_2 + \vec{a}_3)$. Three options obtain for choice of the y-axis, namely along each of the directions $[\vec{a}_{1prh}]_{proj}$; $[\vec{a}_{2prh}]_{proj}$ is taken and the +y direction is defined along this projection outwards from the origin. The +x completes the right handed orthogonal axial set. In the orientation of the crystals used here, +y and -y directions have been identified in two ways firstly from the symmetry shown on the Laue-back reflection pictures, secondly from the orientation of the triangular etch pits on the xy plane; these experimental techniques will be explained in detail in a later chapter.

The Wigner-Seitz unit cell is the smallest cell which can be constructed from the plane perpendicular bisectors of vectors from the origin to other lattice points. This is the smallest volume from which the entire crystal can be reproduced by translation through the primitive translation vectors. This unit cell automatically displays the point symmetry of the crystal and because of this property it is called the symmetrical unit cell. Figure (2.6) shows a drawing of the Wigner-Seitz cell of the A7 structure and includes the (+x, +y, +z) orthogonal crystallographic right handed set and also $\frac{1}{2}\vec{a}_1$. It is bounded from above and below by the plane perpendicular bisectors of the primitive translation vectors $\pm \vec{a}_1, \pm \vec{a}_2, \pm \vec{a}_3$; the other sides

which are normal to the xy plane are determined by the plane perpendicular bisectors of the vectors $\pm(\vec{a}_1 - \vec{a}_2)$, $\pm(\vec{a}_1 - \vec{a}_3)$, $\pm(\vec{a}_2 - \vec{a}_3)$. These sides intersect the xy plane in a hexagon, see the inner cross section of figure (2.5). The centre Γ is a lattice point and has the full $\bar{3}m$ point group symmetry.

The primitive translation vectors in the rhombohedral space lattice can be written in the crystallographic orthogonal axial system as follows

$$\begin{aligned}\vec{a}_1 &= \frac{\sqrt{3}}{2} s\hat{x} - \frac{1}{2}s\hat{y} + r\hat{z}, \\ \vec{a}_2 &= \quad \quad \quad s\hat{y} + r\hat{z}, \\ \vec{a}_3 &= -\frac{\sqrt{3}}{2} s\hat{x} - \frac{1}{2}s\hat{y} + r\hat{z}.\end{aligned}\tag{2.2}$$

where \hat{x} , \hat{y} , \hat{z} are unit vectors along the crystallographic x, y, z axes, and $s = a \cos\theta$ and $r = a \sin\theta$; θ is the angle between \vec{a}_1 and its projection on the xy plane. The relationships between \vec{a}_{2prh} (or in short notation \vec{a}_2), s, and r are shown in figure (2.3). The parameters s, r, and θ are listed in table (2.1) with the pertinent crystal structure parameters of the A7 structure semimetals.

(ii) The primitive rhombohedral unit cell is a parallelepiped with edges \vec{a}_1 , \vec{a}_2 , \vec{a}_3 (the primitive translation vectors). This unit cell is shown in figure (2.1) when a

lattice point is chosen as the origin and in figure (2.2) when an atomic site is the origin. There are two atoms per prh unit cell located at the positions $3ur\hat{z}$ and $(3r - 3ur)\hat{z}$ along the trigonal axis. The length of the body diagonal of the prh unit cell is $3r = |(\vec{a}_1 + \vec{a}_2 + \vec{a}_3)|$. The distance along the body diagonal from the origin to the nearest atom in the cell is $3ur$ and the shorter distance along z-axis between adjacent atoms is $6ur$. When $\alpha = 60^\circ$; the value $u = \frac{1}{4}$ corresponds to the face centred cubic structure. The position of any atom in the A7 structure relative to the origin is

$$\vec{R}(p) = \vec{t}_n + (2p - 3)ur\hat{z} \quad (2.3)$$

where $p = 1$ or 2 and

$$\vec{t}_n = n_1\vec{a}_1 + n_2\vec{a}_2 + n_3\vec{a}_3, \quad (2.4)$$

\vec{t}_n is a general vector in rhombohedral space. When $n_1, n_2,$ and n_3 take integer values \vec{t}_n becomes a rhombohedral lattice vector. If the indices of a direction are defined as the components of a vector in real space, then they can be designated as $[n_1 \ n_2 \ n_3]_{prh}$ where $n_i (i = 1, 2, 3)$ represent a direction referred to the primitive translation vectors \vec{a}_i and thus are related directly to the prh unit cell. By combining equations (2.2), (2.3), and (2.4), the position vector can be written in the crystallographic axial set as

$$\vec{R}(p) = \frac{\sqrt{3}}{2} (n_1 - n_3) \hat{x} + \frac{1}{2}(-n_1 + 2n_2 - n_3)\hat{y} + \left\{ (n_1 + n_2 + n_3) + 3(2p-3)u \right\} r\hat{z} \quad (2.5)$$

The following relationships between r, s and the prh unit cell parameters hold

$$r = a \sin \theta = \frac{a \sqrt{1 + 2 \cos \alpha}}{\sqrt{3}},$$

$$s = a \cos \theta = \frac{a \sqrt{2(1 - \cos \alpha)}}{\sqrt{3}}. \quad (2.6)$$

Thus, the ratio $\frac{r}{s}$ is related to the prh angle α by

$$\frac{r}{s} = \frac{\sqrt{1 + 2 \cos \alpha}}{\sqrt{2(1 - \cos \alpha)}}. \quad (2.7)$$

When this ratio takes certain special values, the rhombohedral space lattice transforms to one of the space lattices below:

- 1) $\frac{r}{s} = \sqrt{2}$, $\alpha = 60^\circ$ Face-centred cubic space lattice.
- 2) $\frac{r}{s} = \frac{1}{\sqrt{2}}$, $\alpha = 90^\circ$ Simple cubic lattice.
- 3) $\frac{r}{s} = \frac{1}{2\sqrt{2}}$, $\alpha = 109^\circ 28'$ Body-centred cubic space lattice.

These three cases correspond to the restrictions on the rhombohedral space lattice given in equation (2.1). The rhombohedral space lattice, which the A7 structure is based upon, lies in the range $\frac{r}{s} > \sqrt{2}$ and $\alpha < 60^\circ$ (see table (2.1) for the values of $\frac{r}{s}$ and α of the A7 structure semimetals). The volume of the prh unit cell is given by

\vec{a}_1

$$V_{\text{prh}} = \vec{a}_1 \cdot (\vec{a}_2 \wedge \vec{a}_3) = \frac{3\sqrt{3}}{2} s^2 r \quad (2.8)$$

Referred to the prh axes, the indices of a direction will be designated by $[n_1 \ n_2 \ n_3]_{\text{prh}}$ and the Miller indices of a plane or parallel planes by $(hkl)_{\text{prh}}$. A set of equivalent directions and a form of planes will be designated by $\langle n_1 \ n_2 \ n_3 \rangle_{\text{prh}}$ and $\{hkl\}_{\text{prh}}$ respectively. The directions $[111]_{\text{prh}}$, $[\bar{1}2\bar{1}]_{\text{prh}}$, and $[10\bar{1}]_{\text{prh}}$ correspond to the +z (+ trigonal), +y (+ bisectrix) and +x (+ binary) directions respectively; $(111)_{\text{prh}}$ is the cleavage plane.

(iii) The International Tables for X-Ray Crystallography give hexagonal axes as an alternative to prh axes for $R\bar{3}m$ crystals. These axes have often been referred to by workers measuring the lattice parameters of A7 structure crystals. They can be oriented in two different ways relative to the primitive translation vectors \vec{a}_1 . These so-called "obverse" and "reverse" settings are shown in figure (2.1) as $(\vec{a}_1 \text{ hex}, \vec{a}_2 \text{ hex}, \vec{c}_{\text{hex}})$ and $(\vec{a}'_1 \text{ hex}, \vec{a}'_2 \text{ hex}, \vec{c}_{\text{hex}})$ respectively. In this work the "obverse" orientation is adopted. The \vec{c}_{hex} - axis coincides with the z-axis; $\vec{a}_1 \text{ hex}$ and $\vec{a}_2 \text{ hex}$ axes are at an angle of 120° to each other in the xy plane (see figure 2.1). The hexagonal unit cell, which is constructed from $\vec{a}_1 \text{ hex}$, $\vec{a}_2 \text{ hex}$, and \vec{c}_{hex} bases vectors, is triply primitive and contains six atoms. The hexagonal unit cell edge vectors are expressed in the crystallographic orthogonal set as

$$\begin{aligned}
 \vec{a}_1 \text{ hex} &= \frac{\sqrt{3}}{2} s \hat{x} - \frac{3}{2} s \hat{y} \quad , \\
 \vec{a}_2 \text{ hex} &= \frac{\sqrt{3}}{2} s \hat{x} + \frac{3}{2} s \hat{y} \quad , \\
 \vec{c} \text{ hex} &= 3 r z. \qquad \qquad \qquad (2.9)
 \end{aligned}$$

The volume of the unit cell is given by

$$V_{\text{hex}} = \vec{a}_1 \text{ hex} \cdot (\vec{a}_2 \text{ hex} \wedge \vec{c}_{\text{hex}}) = 3V_{\text{prh}} = \frac{9\sqrt{3}}{2} s^2 r . \quad (2.10)$$

The relations between the hexagonal and the prh unit cell parameters are

$$\begin{aligned}
 |\vec{a}_1 \text{ hex}| &= |\vec{a}_2 \text{ hex}| = \sqrt{3}s = a \sqrt{2(1 - \cos\alpha)} \quad , \\
 |\vec{c} \text{ hex}| &= 3r = a \sqrt{3(1 + 2\cos\alpha)} \quad . \quad (2.11)
 \end{aligned}$$

To index the crystallographic planes and directions of the A7 structure crystals referred to the hexagonal unit cell, either a three or four axes may be used. The fourth-axis shown in figure (2.5) in the xy plane and coincides with the (-x) direction. Thus, it is given by

$$\vec{a}_3 \text{ hex} = -(\vec{a}_1 \text{ hex} + \vec{a}_2 \text{ hex}) = -\sqrt{3} s \hat{x}. \quad (2.12)$$

Referred to the three hexagonal axes, a direction, a set of equivalent directions, a plane and a form of equivalent planes will be represented by $[n_1 \ n_2 \ n_3]_{\text{hex}}$,

$\langle n_1 \ n_2 \ n_3 \rangle_{\text{hex}}$, $(hkl)_{\text{hex}}$, and $\{hkl\}_{\text{hex}}$ respectively.

The Miller-Bravais (four-axis) indices for planes ($hkl\ell$) are obtained from the three-axis indices when the condition $h + k + i = 0$ is imposed. The indices of a direction referred to the four-axis (four-index) hexagonal system can not be easily obtained from the three-axis $[n_1 n_2 n_3]_{\text{hex}}$ indices (for discussion, see Bloss 1971). This has not been pointed out in the literature for $R\bar{3}m$ crystals and incorrect four-axis (four-index) directional indices have been used (for example, by Doershel 1972 and Windmiller 1966). However, if the four-axis (four-index) directional indices are represented by $[uvw]$ such that $t = -(u+v)$, then the three-axis directional indices $[n_1 n_2 n_3]_{\text{hex}}$ are obtained from the following equations:

$$n_1 = 2u + v, n_2 = u + 2v, n_3 = w$$

or

$$u^\dagger = \frac{1}{3}(2n_1 - n_2), v = \frac{1}{3}(2n_2 - n_1), t = -(u + v), \\ w = n_3. \quad (2.13)$$

For example, the direction $[101]_{\text{hex}}$ referred to the three-axis hexagonal axes corresponds to $\frac{1}{3}[2\bar{1}\bar{1}3]$ direction referred to the four-axis (four-index) hexagonal axes. The four-axis (four-index) directional indices have the advantage over the three-axis (three-index) indices that similar directions have similar indices.

[†] Not to be confused with the atomic position parameter u in equation (2.5)

(iv) The yz and xz cross-sections of the face-centred rhombohedral (fcr) unit cell are shown in figures (2.3) and (2.4) respectively. In figure (2.5) the fcr unit cell translations $\vec{a}_1 \text{ fcr}$ are shown projected onto the xy plane and their projections are labelled $[\vec{a}_1 \text{ fcr}]_{\text{proj}}$. To be consistent with the other unit cell settings the projection $[\vec{a}_2 \text{ fcr}]_{\text{proj}}$ is taken in the -y direction, see figure (2.3). The $\vec{a}_i \text{ fcr}$ are expressed in the crystallographic orthogonal set as

$$\begin{aligned}\vec{a}_1 \text{ fcr} &= -\sqrt{3} s\hat{x} + s\hat{y} + r\hat{z}, \\ \vec{a}_2 \text{ fcr} &= -2s\hat{y} + r\hat{z}, \\ \vec{a}_3 \text{ fcr} &= \sqrt{3} s\hat{x} + s\hat{y} + r\hat{z}.\end{aligned}\tag{2.14}$$

The fcr unit cell contains eight atoms and the volume of the cell is given by

$$\begin{aligned}V_{\text{fcr}} &= 4V_{\text{prh}} = \vec{a}_1 \text{ fcr} \cdot (\vec{a}_2 \text{ fcr} \wedge \vec{a}_3 \text{ fcr}) = \\ &= 6\sqrt{3} s^2 r.\end{aligned}\tag{2.15}$$

The body diagonals of the fcr and prh unit cells are the same. The relation between the prh unit cell parameters and the fcr unit cell parameters is given by

$$|\vec{a}_i \text{ fcr}| = \sqrt{4s^2 + r^2} = a\sqrt{3 - 2\cos\alpha}.\tag{2.16}$$

The axial angle α_{fcr} between any two $\vec{a}_i \text{ fcr}$ ($i = 1, 2, 3$) is related to the prh angle α by

$$\cos \alpha_{fcr} = \frac{(2\cos \alpha - 1)}{(3 - 2\cos \alpha)} \quad (2.17)$$

Referred to the fcr unit cell, the interplanar angles and angles between directions in the A7 structure materials have been calculated by Salkovitz (1956), Vickers (1957) and Bacon et al (1964). For the indices referred to this cell, the convention that will be adopted here is the same as that for the prh and hexagonal unit cells with a subscript fcr. The directions $[111]_{fcr}$, $\frac{1}{2}[1\bar{2}1]_{fcr}$, and $\frac{1}{2}[\bar{1}01]_{fcr}$ correspond to the +z, +y, and +x directions respectively.

The reason that many workers in the field have chosen to use the face-centred cubic (fcc) cartesian axes is that there is a close relationship between the space lattice of the A7 structure and the fcc space lattice (see Falicov and Golin 1965). The primitive translation vectors \vec{a}_1 are expressed in this cartesian axial set as

$$\begin{aligned} \vec{a}_1 &= a_0 \{ e, 1, 1 \} , \\ \vec{a}_2 &= a_0 \{ 1, e, 1 \} , \\ \vec{a}_3 &= a_0 \{ 1, 1, e \} \end{aligned} \quad (2.18)$$

where $\{ \}$ indicates rectangular coordinates. The parameter e is related to the prh angle α by

$$\cos \alpha = \frac{1 + 2e}{(2 + e^2)} \quad (2.19)$$

and $\epsilon = 0$ corresponds to $\alpha = 60^\circ$ (which is the fcc lattice) so that ϵ is a measure of the distortion of the lattice from fcc. The parameter a_0 is related to ϵ and a by

$$a_0 = \frac{a}{\sqrt{2 + \epsilon^2}} \quad (2.20)$$

All these parameters have been calculated and are collected in table (2.1)

2.2.1 Relationships between Miller indices referred to various axial sets

Each unit cell considered above may be convenient for studying different properties of the A7 structure crystals, so it is often necessary to know how the Miller indices of planes and the indices of directions alter when the choice of the unit cell is altered. To this end, we will give the matrices representing the transformations of the Miller indices of planes and the indices of directions from one unit cell to the other and vice versa. The Miller indices of planes will be denoted by a column matrix in a round bracket with a subscript specifying the unit cell under consideration (i.e. prh, hex, fcr). The following matrix equations represent the transformations of the Miller indices of planes:

- 1) The transformation from the prh unit cell to the hexagonal unit cell is

$$\begin{pmatrix} 1 & \bar{1} & 0 \\ 0 & 1 & \bar{1} \\ 1 & 1 & 1 \end{pmatrix} \begin{pmatrix} h \\ k \\ l \end{pmatrix}_{\text{prh}} = \begin{pmatrix} h \\ k \\ l \end{pmatrix}_{\text{hex}} \quad (2.21)$$

and the reverse transformation equation is

$$\frac{1}{3} \begin{pmatrix} 2 & 1 & 1 \\ \bar{1} & 1 & 1 \\ \bar{1} & \bar{2} & 1 \end{pmatrix} \begin{pmatrix} h \\ k \\ l \end{pmatrix}_{\text{hex}} = \begin{pmatrix} h \\ k \\ l \end{pmatrix}_{\text{prh}} \quad (2.22)$$

2) The transformation from the prh unit cell to the fcr unit cell is

$$\begin{pmatrix} \bar{1} & 1 & 1 \\ 1 & \bar{1} & 1 \\ 1 & 1 & \bar{1} \end{pmatrix} \begin{pmatrix} h \\ k \\ l \end{pmatrix}_{\text{prh}} = \begin{pmatrix} h \\ k \\ l \end{pmatrix}_{\text{fcr}} \quad (2.23)$$

and the reverse transformation equation is

$$\frac{1}{2} \begin{pmatrix} 0 & 1 & 1 \\ 1 & 0 & 1 \\ 1 & 1 & 0 \end{pmatrix} \begin{pmatrix} h \\ k \\ l \end{pmatrix}_{\text{fcr}} = \begin{pmatrix} h \\ k \\ l \end{pmatrix}_{\text{prh}} \quad (2.24)$$

3) The transformation from the fcr unit cell to the hexagonal one is

$$\frac{1}{2} \begin{pmatrix} \bar{1} & 1 & 0 \\ 1 & \bar{1} & 1 \\ 2 & 2 & 2 \end{pmatrix} \begin{pmatrix} h \\ k \\ l \end{pmatrix}_{\text{fcr}} = \begin{pmatrix} h \\ k \\ l \end{pmatrix}_{\text{hex}} \quad (2.25)$$

and the reverse transformation is

$$\frac{1}{3} \begin{pmatrix} \bar{4} & \bar{2} & 1 \\ 2 & \bar{2} & 1 \\ 2 & 4 & 1 \end{pmatrix} \begin{pmatrix} h \\ k \\ l \end{pmatrix}_{\text{hex}} = \begin{pmatrix} h \\ k \\ l \end{pmatrix}_{\text{fcr}} \quad (2.26)$$

The indices of a direction will be designated by a column matrix in a square bracket with a subscript specifying the unit cell. The matrix equation that transforms the indices of a direction

1) from the prh unit cell to the hexagonal unit cell is

$$\frac{1}{3} \begin{pmatrix} 2 & \bar{1} & \bar{1} \\ 1 & 1 & \bar{2} \\ 1 & 1 & 1 \end{pmatrix} \begin{bmatrix} n_1 \\ n_2 \\ n_3 \end{bmatrix}_{\text{prh}} = \begin{bmatrix} n_1 \\ n_2 \\ n_3 \end{bmatrix}_{\text{hex}} \quad (2.27)$$

and the reverse transformation is

$$\begin{pmatrix} 1 & 0 & 1 \\ \bar{1} & 1 & 1 \\ 0 & \bar{1} & 1 \end{pmatrix} \begin{bmatrix} n_1 \\ n_2 \\ n_3 \end{bmatrix}_{\text{hex}} = \begin{bmatrix} n_1 \\ n_2 \\ n_3 \end{bmatrix}_{\text{prh}} \quad (2.28)$$

2) from the prh unit cell to the fcr one is

$$\frac{1}{2} \begin{pmatrix} 0 & 1 & 1 \\ 1 & 0 & 1 \\ 1 & 1 & 0 \end{pmatrix} \begin{bmatrix} n_1 \\ n_2 \\ n_3 \end{bmatrix}_{\text{prh}} = \begin{bmatrix} n_1 \\ n_2 \\ n_3 \end{bmatrix}_{\text{fcr}} \quad (2.29)$$

and the reverse transformation is

$$\begin{pmatrix} \bar{1} & 1 & 1 \\ 1 & \bar{1} & 1 \\ 1 & 1 & \bar{1} \end{pmatrix} \begin{bmatrix} n_1 \\ n_2 \\ n_3 \end{bmatrix}_{\text{fcr}} = \begin{bmatrix} n_1 \\ n_2 \\ n_3 \end{bmatrix}_{\text{prh}} \quad (2.30)$$

3) from the fcr unit cell to the hexagonal unit cell is

$$\frac{1}{3} \begin{pmatrix} \bar{4} & 2 & 2 \\ \bar{2} & \bar{2} & 4 \\ 1 & 1 & 1 \end{pmatrix} \begin{bmatrix} n_1 \\ n_2 \\ n_3 \end{bmatrix}_{\text{fcr}} = \begin{bmatrix} n_1 \\ n_2 \\ n_3 \end{bmatrix}_{\text{hex}} \quad (2.31)$$

and the reverse transformation is

$$\frac{1}{2} \begin{pmatrix} \bar{1} & 0 & 2 \\ 1 & \bar{1} & 2 \\ 0 & 1 & 2 \end{pmatrix} \begin{bmatrix} n_1 \\ n_2 \\ n_3 \end{bmatrix}_{\text{hex}} = \begin{bmatrix} n_1 \\ n_2 \\ n_3 \end{bmatrix}_{\text{fcr}} \quad (2.32)$$

where the three-axis hexagonal basis is referred to for the hexagonal indices and the usual matrix multiplication is used throughout.

2.3 WHICH CRYSTAL SYSTEM DOES THE A7 STRUCTURE BELONG TO?

There are problems associated with the classification of materials belonging to $\bar{3}m$ point group into a crystal system. The 32 point groups have been collected into sets called crystal systems according to the highest-ranking rotation axis which they contain. In this classification

crystals with one triad (3 or $\bar{3}$) axis are said to belong to the trigonal system and those with one hexad (6 or $\bar{6}$) axis to the hexagonal system. Many crystallographers group these two systems into an all-inclusive hexagonal system because a crystal with a single principal axis either 3 or $\bar{3}$ may have either a hexagonal or rhombohedral lattice. Other authors subdivide into hexagonal and rhombohedral sub-systems; the basis of this classification rests on lattice type rather than on the minimal symmetry. The point is that some crystals belonging to the $\bar{3}m$ point group are built on a primitive rhombohedral space lattice for which a primitive rhombohedral unit cell can always be chosen, while other crystals belonging to the same point group are built on a hexagonal space lattice for which a hexagonal cell must be chosen as the primitive cell. As can be seen from figure (2.7), crystals belonging to space groups $R\bar{3}m$ (D_{3d}^5) and $R\bar{3}c$ (D_{3d}^6) have a rhombohedral space lattice while those in $P\bar{3}1m$ (D_{3d}^1), $P\bar{3}1c$ (D_{3d}^2), $P\bar{3}m1$ (D_{3d}^3), $P\bar{3}c1$ (D_{3d}^4) have a hexagonal one. The symmetry of the lattice points of these two space lattices is different, namely $\bar{3}m$ for rhombohedral, and $6/mmm$ for hexagonal. The space group for the A7 structure (arsenic structure) isogonal with point group $\bar{3}m$ is $R\bar{3}m$.

To study the symmetry of electronic wave functions in the A7 structure the symmetry of the Brillouin zone (which is directly related to the rhombohedral space lattice)

is usually considered. The suggestion that any crystal with a 3-fold or a 6-fold axis is referred to a hexagonal system and a multiple unit cell be taken for rhombohedral crystals, which seems to be supported by many crystallographers including among others Buerger (1971), Azároff (1968), is not practical in the theory of the Brillouin zones and in the study of electronic properties of A7 structure crystals. We leave this controversial problem (i.e. into which crystal system should the A7 structure be classified?) to crystallographers and go on further to study the symmetry of the reciprocal lattice of the A7 structure.

2.4 THE RECIPROCAL SPACE LATTICE

The primitive reciprocal lattice translations \vec{b}_i are defined in terms of the primitive rhombohedral translations by the following equations:

$$\vec{b}_i = 2\pi \frac{\vec{a}_j \wedge \vec{a}_k}{\vec{a}_i \cdot (\vec{a}_j \wedge \vec{a}_k)}$$

or
$$\vec{b}_i \cdot \vec{a}_j = 2\pi \delta_{ij} \quad (2.33)$$

where $i, j, k = 1, 2, 3$ and δ_{ij} is the Kronecker delta. The periodic repetition of \vec{b}_i generates the reciprocal space lattice. A right handed orthogonal set (which coincides with the crystallographic orthogonal set defined in section 2.2) will be represented in reciprocal space by k_x -, k_y -, and k_z - axes with unit vectors \hat{x} , \hat{y} , and \hat{z} along these axes. By using the equations (2.2) and (2.33) the primitive reciprocal translations \vec{b}_i are expressed in this orthogonal

set as

$$\begin{aligned}
 \vec{b}_1 &= \frac{2\pi}{\sqrt{3}s} \hat{x} - \frac{2\pi}{3s} \hat{y} + \frac{2\pi}{3r} \hat{z}, \\
 \vec{b}_2 &= \frac{4\pi}{3s} \hat{y} + \frac{2\pi}{3r} \hat{z}, \\
 \vec{b}_3 &= \frac{2\pi}{\sqrt{3}s} \hat{x} - \frac{2\pi}{3s} \hat{y} + \frac{2\pi}{3r} \hat{z}
 \end{aligned} \tag{2.34}$$

where s and r have been defined in section (2.2).

The angle β (the primitive reciprocal rhombohedral angle) between any two \vec{b}_i is given by

$$\cos \beta = \frac{(s^2 - 2r^2)}{(s^2 + 4r^2)} \tag{2.35}$$

and this angle is related to the prh angle α by

$$\cos \beta = -\frac{\cos \alpha}{(1 + \cos \alpha)}. \tag{2.36}$$

The restrictions imposed on the prh angle α by the rhombohedral space lattice are also imposed on the primitive reciprocal rhombohedral angle β by the reciprocal lattice. The lengths of the primitive reciprocal lattice translations are equal to each other and they are related to the prh unit cell parameters by

$$\begin{aligned}
 |\vec{b}_1| &= |\vec{b}_2| = |\vec{b}_3| = b = \\
 &= \frac{2\pi}{a} \sqrt{\frac{(1 + \cos \alpha)}{(1 - \cos \alpha)(1 + 2 \cos \alpha)}}.
 \end{aligned} \tag{2.37}$$

A general vector in reciprocal space is given by

$$\vec{G} = h\vec{b}_1 + k\vec{b}_2 + l\vec{b}_3 \quad (2.38)$$

when h , k and l are integers, the vector \vec{G} becomes a reciprocal lattice vector such that its head and tail coincide with reciprocal space lattice points. In reciprocal space a direction and a plane will be denoted by $[hkl]^*$ and $(hkl)^*$ respectively; both refer to primitive reciprocal translations. The direction $[hkl]^*$ is perpendicular to the plane $(hkl)_{prh}$ with the same indices. Thus Miller indices of a crystallographic plane can be defined as the components of a vector in reciprocal space. By using the equations (2.34) and (2.38), \vec{G} becomes

$$\begin{aligned} \vec{G} &= \frac{2\pi}{3s} (h-l)\hat{x} + \frac{2\pi}{3s} (-h+2k-l)\hat{y} + \frac{2\pi}{3r} (h+k+l)\hat{z} \\ &= k_x\hat{x} + k_y\hat{y} + k_z\hat{z}. \end{aligned} \quad (2.39)$$

Falicov and Golin (1965) have started from the fcc cartesian axial set in real space (equation 2.18) and have expressed the primitive reciprocal lattice translations as

$$\begin{aligned} \vec{b}_1 &= b_0 \quad \left\{ -(1 + \epsilon), 1, 1 \right\} , \\ \vec{b}_2 &= b_0 \quad \left\{ 1, -(1 + \epsilon), 1 \right\} , \\ \vec{b}_3 &= b_0 \quad \left\{ 1, 1, -(1 + \epsilon) \right\} \end{aligned} \quad (2.40)$$

where b_0 is related to e and a by

$$b_0 = \frac{2\pi \sqrt{e^2 + 2}}{a (e^2 - e + 2)} \quad (2.41)$$

The parameters b, β, b_0 and the volume of the first Brillouin zone ($V_{BZ} = (2\pi)^3/V_{prh}$) for the group V semimetals have been calculated and are collected in table (2.2). A comparison between the equation (2.2) and (2.34) shows that the reciprocal lattice to the rhombohedral space lattice is itself rhombohedral. Thus, the unit cells that we have studied in section (2.3) can also be associated with the reciprocal lattice. However, in reciprocal space we will only study the symmetrical properties of the first Brillouin zone (i.e. the symmetrical unit cell in reciprocal space).

2.5 SYMMETRY OF THE BRILLOUIN ZONE IN THE A7 STRUCTURE

In reciprocal space, a symmetrical unit cell can be constructed by constructing the plane perpendicular bisectors of the vectors connecting the origin (which is a reciprocal lattice point) to all reciprocal lattice points and then by taking the smallest volume about the origin enclosed by these intersecting planes. The zone constructed in this way is known as the first Brillouin zone. To label the irreducible representations of symmetry points uniquely, it is convenient to restrict the wave vector \vec{k} to the first Brillouin zone. In this convention \vec{k} is called the reduced wave vector and the Brillouin zone the reduced zone (from now on we will use the expression the Brillouin zone instead of the first Brillouin zone).

Figure (2.8) shows the Brillouin zone appropriate to the A7 structure crystals. Although the geometrical shape of this Brillouin zone has been presented by many authors (see for example: Mase 1953 , Jones 1960, Cohen 1961), there has been a tendency for small errors to creep in which have been proliferated throughout the literature. The boundary planes above and below are the planes normal to and bisectors of the vectors $\pm(\vec{b}_1 + \vec{b}_2 + \vec{b}_3)$. These two faces are regular hexagons and are parallel to the trigonal plane. The six foursided faces (rectangles) are determined by the plane perpendicular bisectors of the vectors $\pm(\vec{b}_1 + \vec{b}_2)$, $\pm(\vec{b}_1 + \vec{b}_3)$, $\pm(\vec{b}_2 + \vec{b}_3)$. The remaining inclined six-sided faces (irregular hexagons) are the plane perpendicular bisectors of the vectors $\pm \vec{b}_1$, $\pm \vec{b}_2$, $\pm \vec{b}_3$. A simple description of the shape of this zone can be given in the following way: it is constructed from two types of sides, long and short (eighteen of each). The length of the long and short sides are equal to the sides of the rectangles. The sides of the regular hexagons are long.

At absolute zero the energy states of a crystal will be filled with electrons - in accord with the Pauli exclusion principle - up to an energy level (called the Fermi level) such that all electrons in the system are accounted for. That surface in reciprocal space separating the full from the empty states is called the Fermi surface. Electrons well inside the Fermi surface cannot be excited thermally or by electric or magnetic fields because the states within the

appropriate energy range are already occupied. Only the electrons near the Fermi surface can be excited and hence electron transport is mainly due to these electrons.

It is well known that in the band structure of a solid, the energy E , as a function of the wave vector \vec{k} , has the point group symmetry of the crystal (Jones 1960), a result which may be expressed as

$$E(R_i \vec{k}) = E(\vec{k}) \quad (2.42)$$

where R_i is the i^{th} point group operation.

In addition time reversal symmetry imposes a centre of inversion

$$E(\vec{k}) = E(-\vec{k}). \quad (2.43)$$

Equations (2.42) and (2.43) imply that, whether the full symmetry of the crystal has an inversion element or not, the energy E , as a function of the wave vector \vec{k} possesses inversion symmetry. Thus, constant energy surfaces in general, and the Fermi surface in particular have the symmetry of one of the following Laue groups:

$$\bar{1}, \frac{2}{m}, \frac{2}{m} \frac{2}{m} \frac{2}{m}, \frac{4}{m}, \frac{4}{m} \frac{2}{m} \frac{2}{m}, \bar{3}, \frac{3}{m} \frac{2}{m}$$

$$\frac{6}{m}, \frac{6}{m} \frac{2}{m} \frac{2}{m}, \frac{2}{m} \bar{3}, \frac{4}{m} \frac{3}{m} \frac{2}{m}.$$

A Laue group is a point group which contains the inversion "I" as an element. The associated Laue group of the 21

remaining point groups may be obtained by taking the direct product of the point group under consideration and the inversion group C_1 ; for example, the point group $D_{3d}(\bar{3} \frac{2}{m})$ is the direct product of D_3 and C_1 i.e.

$$D_{3d} = D_3 \otimes C_1 \quad (2.44)$$

where Schoenflies symbols are used for the point groups. Due to this, in group theory, Laue groups are called inversion groups.

Following the recent works by Jan (1972) and Cracknell (1973) we give a procedure to identify the space group of $E(\vec{k})$ in crystals. If the space group of a crystal is known, the space group for its constant-energy surface $E(\vec{k})$ in general and its Fermi surface in particular can be found by three steps: firstly, find the associated symmorphic space group of the space group of the crystal (this can be found by using the International Tables for X-ray Crystallography 1952); secondly, if the inversion "I" is not an element of this symmorphic space group, add "I" to it as shown in equation (2.44) for the point groups; thirdly, find the space group of the associated reciprocal lattice of this final space group. Twenty four possible Fermi surface symmetries have been found and listed by Jan (1972). In fact, these correspond to 24 space groups which are the symmorphic space groups associated with the 11 Laue groups. The point group $\bar{3}m$ of the A7 structure is a Laue group itself. When

$\bar{3}m$ is associated with a hexagonal space lattice, the symmetry of the Fermi surface is either $P\bar{3}1m$ or $P\bar{3}m1$ depending on the relationship between the basis \vec{a}_1 and the mirror planes (see figure 2.7a and b). On the other hand, if $\bar{3}m$ is associated with the rhombohedral space lattice (which is the case for the A7 structure crystals), the symmetry of the Fermi surface is $R\bar{3}m$ (or D_{3d}^5).

For multivalley constant-energy surfaces, the formalism given in the preceding paragraph may not be the most convenient way of studying the symmetry properties of such surfaces. It may be more convenient to consider the point group symmetry of the individual pockets on their own. For the particular case of the A7 structure of interest here, points of high symmetry on the surface and inside the Brillouin zone (figure 2.8) are given in tables (2.3) and (2.4) respectively; in tables (2.5) and (2.6), respectively are given the symmetry of the lines on the surface and inside of the Brillouin zone. We follow the notation used by Cohen (1961) for the symmetry points and lines of the Brillouin zone. In addition, we introduce some more points and lines of special symmetry and label only one twelfth (in volume) of the Brillouin zone which is named the "basic section" of the zone. The whole Brillouin zone is obtained from this basic section by the symmetry operations of the point group $\bar{3}m$. The point symmetries and their elements are listed in the third columns of tables (2.3) and (2.4). Referred to the right-handed crystallographic orthogonal set which is

uniquely represented in reciprocal space by $(+k_x, +k_y, +k_z)$, we give for the first time the coordinates of the symmetry points in the second columns of tables (2.3) and (2.4). In the second columns of tables (2.5) and (2.6), we list the special lines; for example, in table (2.5), (T,W) represents a line on the surface of the Brillouin zone with T and W its end points. The point Q in the first column of table (2.5) represents a point anywhere on the line (T,W). Referred to the same $(+k_x, +k_y, +k_z)$ set, the coordinates of the points (which are located arbitrarily on the corresponding line) are given in the third columns of tables (2.5) and (2.6).

To explain the contents of tables (2.3) to 2.6), the following notes can be considered:

(i) For the point symmetries we use the International symbols, and for their associated elements Schoenflies symbols are used.

(ii) The range of the values of the variables k_x , k_y , and k_z are calculated to be

$$|k_x| \leq \overline{\Gamma K} \equiv \frac{\pi}{6\sqrt{3}s} \left(4 + \frac{s^2}{r^2}\right)$$

$$|k_y| \leq \overline{\Gamma N} \equiv \frac{\pi}{6s} \left(4 + \frac{s^2}{r^2}\right)$$

$$|k_z| \leq \overline{\Gamma T} \equiv \frac{\pi}{r}$$

where numerical values of s and r , for the A7 structure semimetals, are given in table (2.1).

(iii) The relative setting of the associated symmetry elements of the symmetry points are referred to figure (2.9).

(iv) The multiplicity factors, which are listed in the last columns of the tables, represent the number of equivalent symmetry points (which are obtained by applying $\bar{3}m$ symmetry elements about Γ) in the first Brillouin zone.

(v) The symmetry points, which are equivalent as far as the constant-energy ellipsoids are concerned, are grouped together and the associated multiplicity factor is calculated by considering the total number of these points in the first Brillouin zone.

(vi) The Fermi surface pockets can be centred on any of the symmetry points of the Brillouin zone. The number of the pockets can be determined by the multiplicity factors (as an example, for antimony, see Valicov and Lin 1966).

To summarize, it may be said that tables (2.3) to (2.6) represent the symmetry of the Fermi surface of the A7 structure and display, the conditions imposed on the Fermi surface by the crystal symmetry.

TABLE (2.1): Room temperature crystal structure parameters of the group V semimetals. $|\vec{a}_i|$, α_{prh} , and u for As, Sb, and Bi are taken from Schiferl and Barrett(1969).

Parameter	Bi	Sb	As	As(25.5 at .%) -Sb
$ \vec{a}_i \equiv a$	4.7458	4.5067	4.132	4.418
$\alpha_{prh} \equiv \alpha$	57.23	57.11	54.126	56.2
u	0.23389	0.23349	0.22707	0.232 †
$ \vec{a}_{i \text{ hex}} $	4.5460	4.3084	3.7598	4.1618
$ \vec{c}_{\text{hex}} $	11.862	11.2740	10.5475	11.1222
r	3.9541	3.7580	3.5158	3.7074
s	2.6245	2.4875	2.1707	2.4028
r/s	1.5066	1.5107	1.6197	1.5429
θ	56.43	56.50	58.31	57.05
V_{prh}	70.7608	60.4136	43.0403	55.6105
$ \vec{a}_{i \text{ fcr}} $	6.5716	6.2348	5.5866	6.0695
α_{fcr}	87.53	87.42	84.60	86.58
ϵ	.41739	.43543	.88288	.57205
a_o	3.2185	3.0456	2.4784	2.8960

Units: $\vec{a}_i (i = 1,2,3)$, $\vec{a}_{i \text{ hex}} (i = 1,2)$, \vec{c}_{hex} , r, s , $\vec{a}_{i \text{ fcr}} (i = 1,2,3)$, a_o , in Ångströms; α_{prh} , θ , α_{fcr} , in decimal degrees; V_{prh} , in (Å)³; u and ϵ are constants.

† estimated by assuming a linear change of u throughout As-Sb solid solutions.

TABLE (2.2): Room temperature reciprocal lattice parameters of the group V semimetals.

Parameter	B ₁	Sb	As	As(25.5 at.% -Sb)
$ \vec{b}_1 \equiv b$	1.6816	1.7738	2.0195	1.8325
β	110.56	110.60	111.68	110.94
b_0	1.1112	1.1761	1.3367	1.2361
V_{BZ}	3.5054	4.1059	5.7632	4.4605

Units: \vec{b}_1 (1 = 1,2,3), b_0 , in Ångströms;

V_{BZ} , in (Å)⁻³; β , in decimal degrees.

TABLE (2.3): Points of high symmetry on the surface of the Brillouin zone. The coordinates of the points are referred to the right handed orthogonal set $(+k_x, +k_y, +k_z)$ and the origin is at Γ .

Point	coordinates	Point symmetry and the associated elements	Multiplicity factor
T	$(0, 0, \frac{\pi}{r})$	$\bar{3}m:E C_3^+ C'_{21} C'_{22} C'_{23}$ $I S_6^+ \sigma_{d1} \sigma_{d2} \sigma_{d3}$	1
L	$(0, \frac{2\pi}{3s}, \frac{\pi}{3r})$	$\frac{2}{m}:E C'_{21} I \sigma_{d1}$	3
X	$(\frac{\pi}{\sqrt{3}s}, \frac{\pi}{3s}, \frac{2\pi}{3r})$	$\frac{2}{m}:E C'_{22} I \sigma_{d2}$	3
K	$(\frac{\pi}{6\sqrt{3}s} f_1, \frac{\pi}{6s} f_1, 0)$	$2:E C'_{23}$	6
K'	$(\frac{\pi}{6\sqrt{3}s} f_1, \frac{\pi}{6s} f_1, \frac{2\pi}{3r})$	$2:E C'_{22}$	
W	$(\frac{\pi}{3\sqrt{3}s} f_2, \frac{\pi}{3s} f_2, \frac{\pi}{r})$	$2:E C'_{23}$	6
W'	$(f_3, \frac{2\pi}{3s} f_2, \frac{\pi}{3r})$	$2:E C'_{21}$	
U	$(\frac{\pi}{2\sqrt{3}s} f_2, \frac{\pi}{6s} f_2, \frac{\pi}{r})$	$m:E \sigma_{d2}$	6
U'	$(\frac{\pi}{2\sqrt{3}s} f_2, \frac{\pi}{6s} f_2, \frac{\pi}{3r})$	$m:E \sigma_{d2}$	
Z	$(0, \frac{\pi}{3s} f_2, \frac{\pi}{r})$	$m:E \sigma_{d2}$	
N	$(0, \frac{\pi}{6s} f_1, 0)$	$m:E \sigma_{d1}$	
N'	$(0, \frac{\pi}{6s} f_1, \frac{2\pi}{3r})$	$m:E \sigma_{d1}$	6
N''	$(\frac{\pi}{4\sqrt{3}s} f_1, \frac{\pi}{12s} f_1, 0)$	$m:E \sigma_{d2}$	

$$f_1 = 4 + \left(\frac{s}{r}\right)^2, f'_1 = 4 - \left(\frac{s}{r}\right)^2, f_2 = 2 - \left(\frac{s}{r}\right)^2, f'_2 = 2 + \left(\frac{s}{r}\right)^2,$$

$$f_3 = \frac{\pi}{3r} \sqrt{4s^2 - f_1} + \frac{\pi}{3\sqrt{3}s} f_2.$$

TABLE (2.4): Symmetry points inside the Brillouin zone.
 The coordinates of the points are referred
 to the right handed orthogonal $(+k_x, +k_y, +k_z)$ set.

Point	Coordinates	Point symmetry and the associated elements	Multiplicity factor
Γ	$(0,0,0)$	$\bar{3}_m: E \quad C_3^+ \quad C'_{21} \quad C'_{22} \quad C'_{23}$ $I \quad S_6^+ \quad \sigma_{d1} \quad \sigma_{d2} \quad \sigma_{d3}$	1
H	$(0, k_y, k_z)$	$m: E \quad \sigma_{d1}$	6
G	(k_x, k_y, k_z)	$1: E$	12

TABLE (2.5): Lines of symmetry on the surface of the Brillouin zone (see figure 2.8). The coordinates of the points, which are located between the end points of the indicated lines, are referred to the right handed orthogonal $(+k_x, +k_y, +k_z)$ set.

Point	Location Line	Coordinates	Point symmetry and the associated elements	Multiplicity factor
Q	(T,W)	$(k_x, \sqrt{3}k_x, \frac{\pi}{r})$	2: E C' ₂₃	6
M	(T,U)	$(\sqrt{3}k_y, k_y, \frac{\pi}{r})$	m: E σ_{d2}	} 6
M'	(T,Z)	$(0, k_y, \frac{\pi}{r})$	m: E σ_{d1}	
Y	(W', L)	$(k_x, \frac{2\pi}{3s}, \frac{\pi}{3r})$	2: E C' ₂₁	6
R	(U', N'')	$(\sqrt{3}k_y, k_y, k_z)$	m: E σ_{d2}	} 6
R'	(Z, N')	$(0, k_y, k_z)$	m: E σ_{d1}	
V	(X,K')	$(k_x, k_y, \frac{2\pi}{3r})$	2: E C' ₂₂	6
S	(U,X)	$(\sqrt{3}k_y, k_y, k_z)$	m: E σ_{d2}	} 6
S'	(X, U')	$(\sqrt{3}k_y, k_y, k_z)$	m: E σ_{d2}	

TABLE (2.6): Lines of symmetry inside the Brillouin zone (see figure 2.8). The coordinates of the points, which are located between the end points of the indicated lines, are referred to the right handed orthogonal $(+k_x, +k_y, +k_z)$ set.

Point	location line	Coordinates	Point symmetry and the associated elements	Multiplicity factor
Λ	(Γ, T)	$(0, 0, k_z)$	$3m: E C_3^{\pm} \sigma_{di}$ $(i = 1, 2, 3)$	} 2
Σ	(Γ, K)	$(k_x, \sqrt{3}k_x, 0)$	$2: E, C'_{23}$	
Δ	(Γ, X)	$(\sqrt{3}k_y, k_y, \frac{2s}{r} k_y)$	$m: E \sigma_{d2}$	6
Λ'	(Γ, L)	$(0, k_y, \frac{s}{2r} k_y)$	$m: E \sigma_{d1}$	6
Σ'	(Γ, Z)	$(0, k_y, \frac{3s}{f_2 r} k_y)$	$m: E \sigma_{d1}$	6
F	(Γ, N)	$(0, k_y, 0)$	$m: E \sigma_{d1}$	} 6
F'	(Γ, N'')	$(\sqrt{3}k_y, k_y, 0)$	$m: E \sigma_{d2}$	

$$f_2 = 2 - \left(\frac{s}{r}\right)^2$$

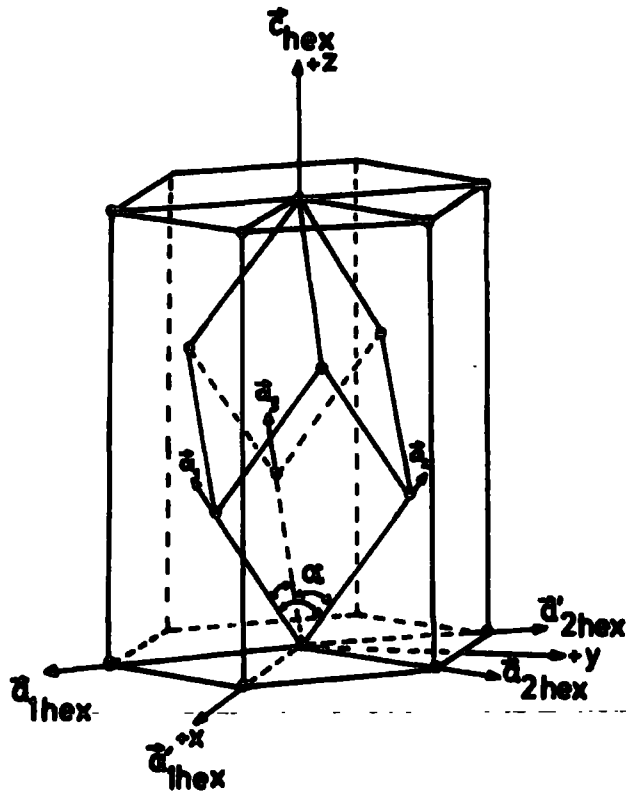


FIGURE (2.1): The "obverse" ($a_{1hex}, a_{2hex}, c_{hex}$) and "reverse" ($a_{1hex}, a_{2hex}, c_{hex}$) settings of the hexagonal unit cell and the primitive rhombohedral unit cell (a_1, a_2, a_3) drawn in the rhombohedral space lattice. The common origin of the unit cells is a lattice point. The $(+x, +y, +z)$ right handed crystallographic orthogonal set relative to the unit cell axes is shown. The rh angle α is also shown.

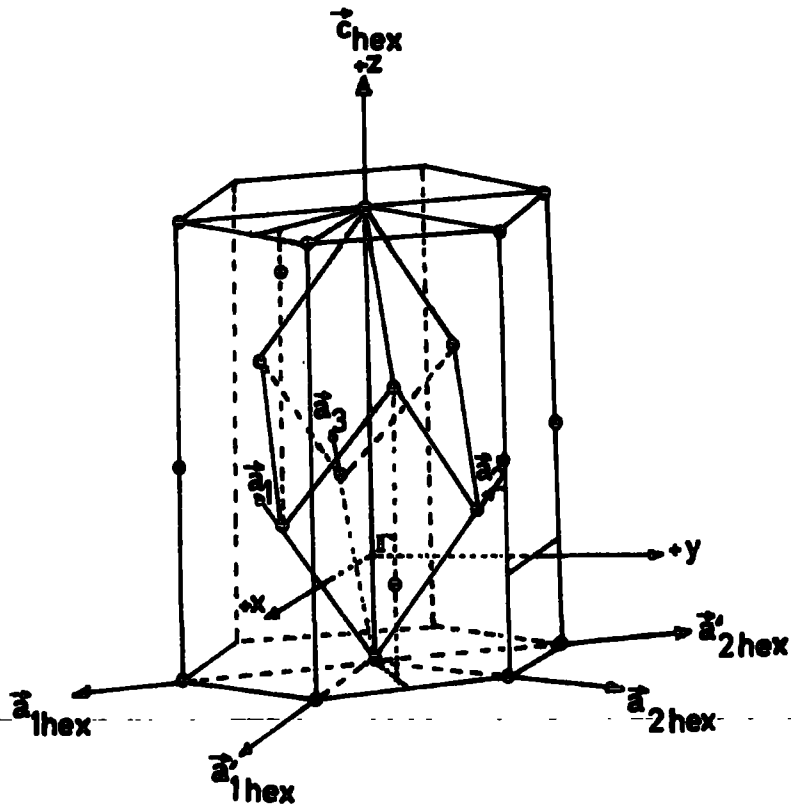


FIGURE (2.2): The prh unit cell and the two equivalent hexagonal unit cells of the A7 structure; heavy dots represent atomic sites. The common origin of the unit cells is an atomic site. Notice that Γ is the origin of the unit cells shown in figure (2.1). The $(+x,+y,+z)$ set is also indicated.

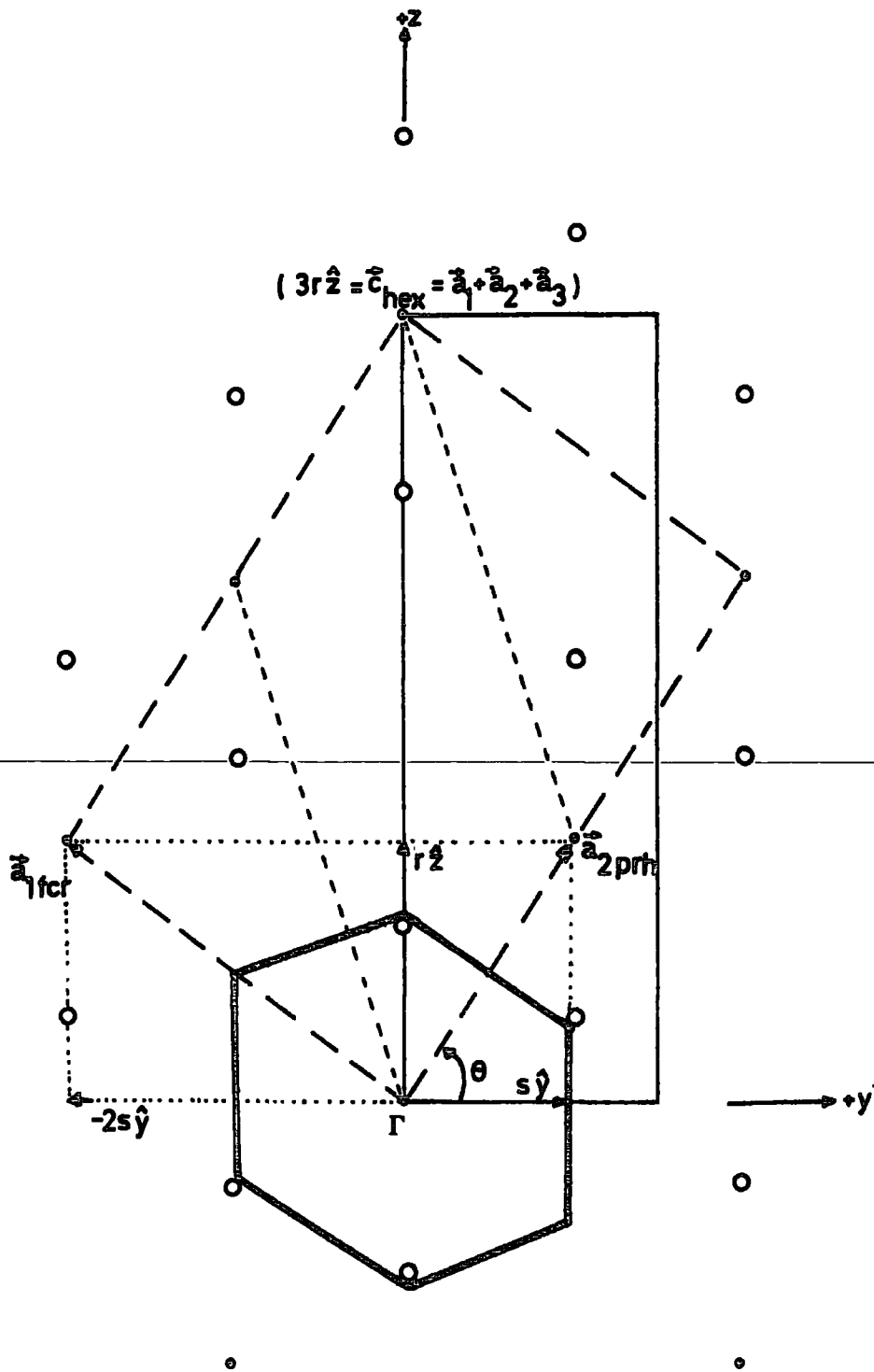


FIGURE (2.3): $(+y, +z)$ Cross-section of the A7 structure. Four unit cell cross sections are shown. (i.e. prh, hex, fcr, and Vigner-Seitz unit cells). Circles represent the positions of the atoms and dots are the rhombohedral lattice points.

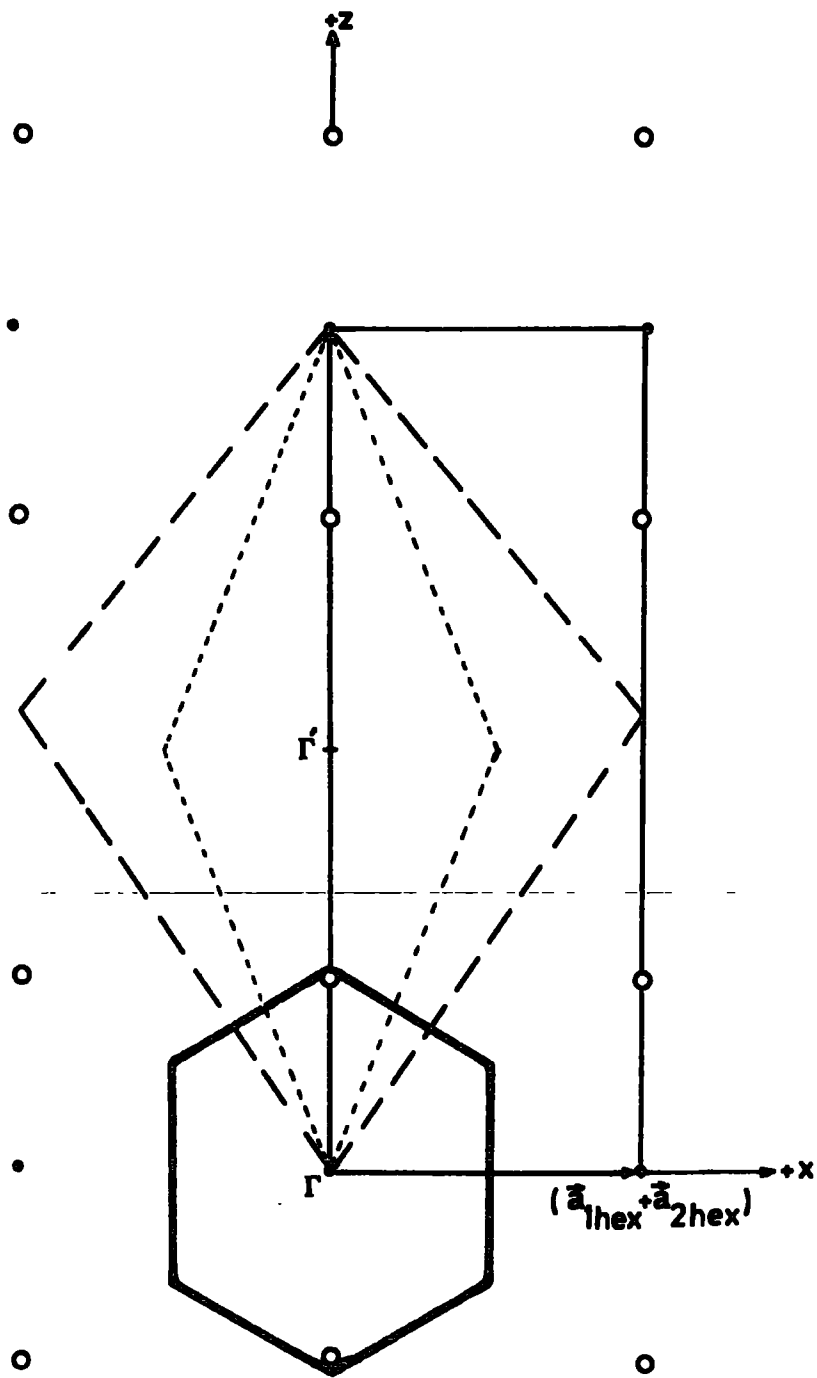


FIGURE (2.4): (+x, +z) Cross-section of the A7 structure. Γ' is an alternative inversion centre point to the point Γ .

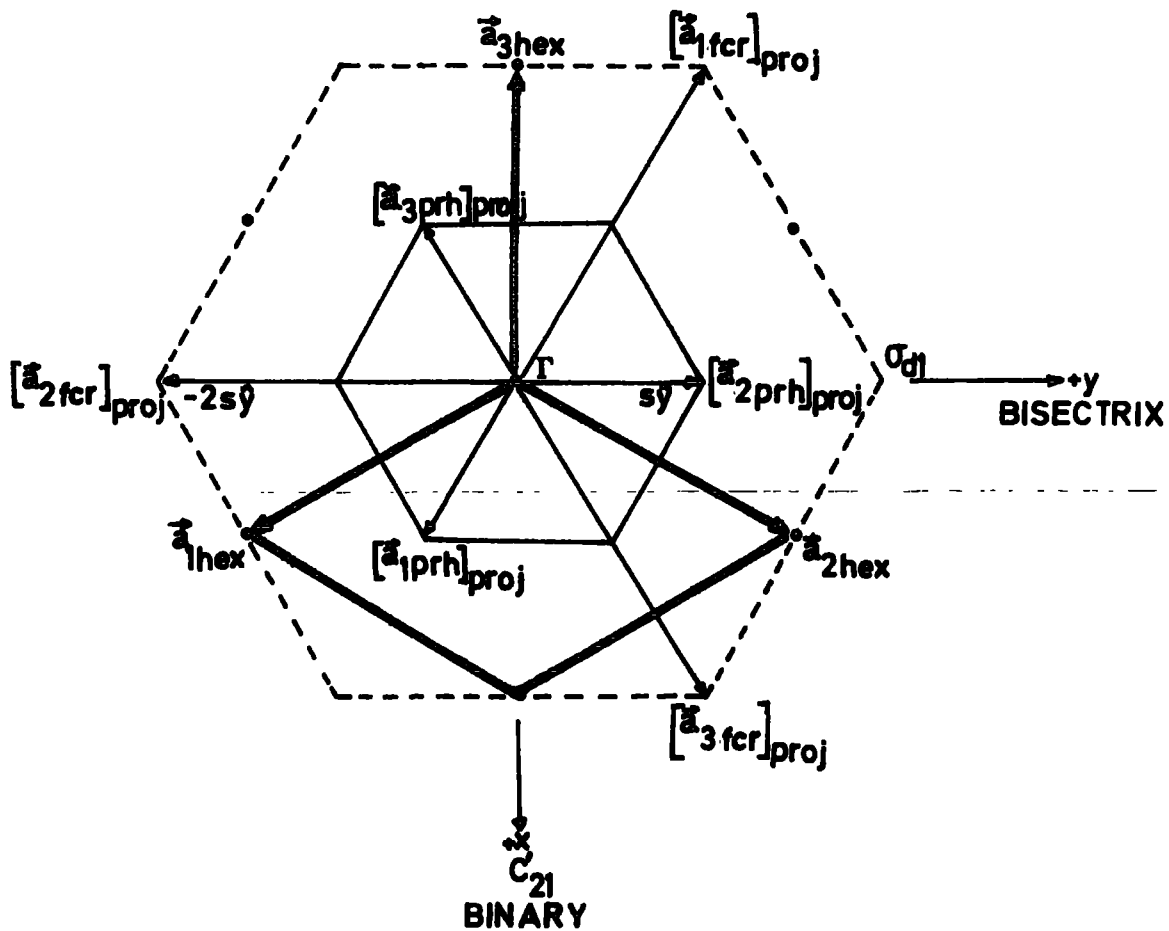


FIGURE (2.5): xy cross-section of the A7 structure. The cross-section of the hexagonal unit cell and the projection of the other cells on the xy plane are shown.

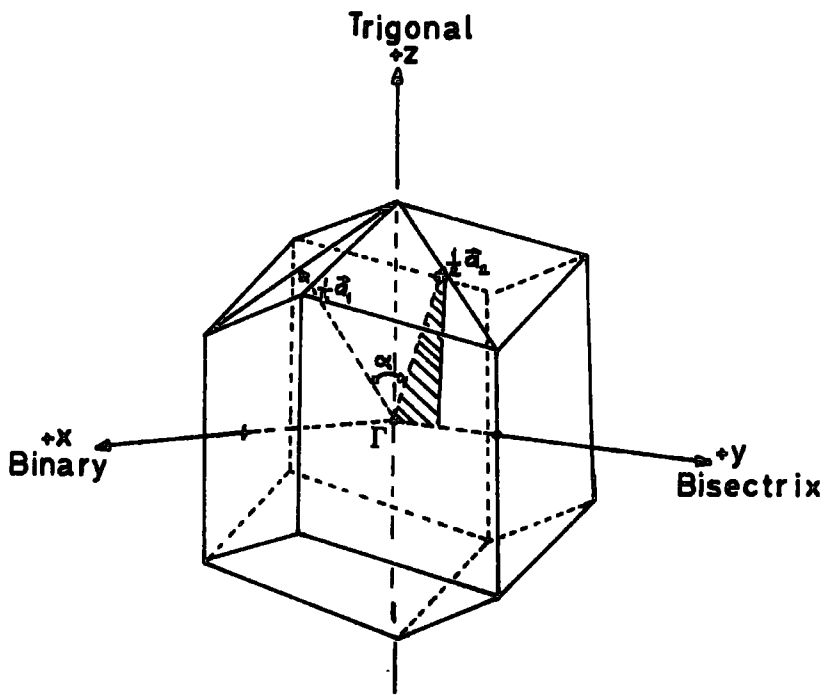


FIGURE (2.6): Wigner-Seitz unit cell for the A7 structure. The right handed crystallographic orthogonal (+x, +y, +z) set is shown. The primitive rhombohedral angle α is also indicated.

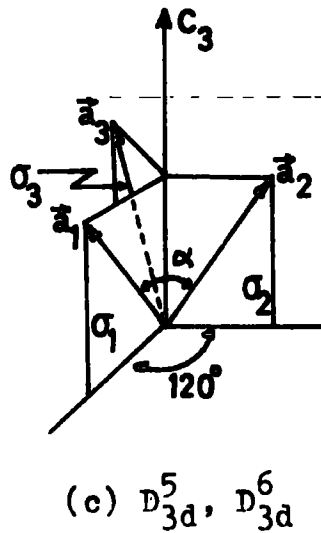
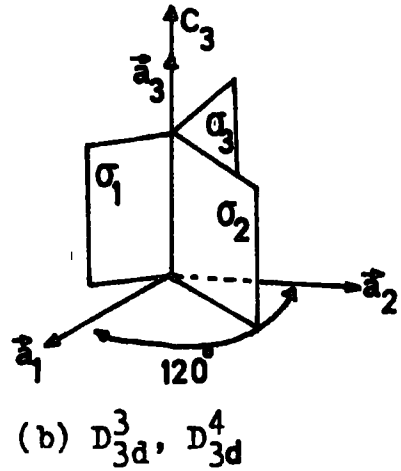
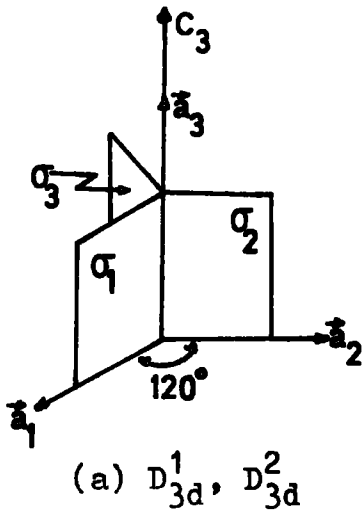


FIGURE 2.7 (a,b,c): Space groups isogonal with point group $\bar{3}m(D_{3d})$. The appropriate primitive translations and mirror planes are shown. C_3 is the common 3-fold rotational axis. Notice while it is possible to construct a primitive hexagonal unit cell in cases (a) and (b), this is not possible in case (c).

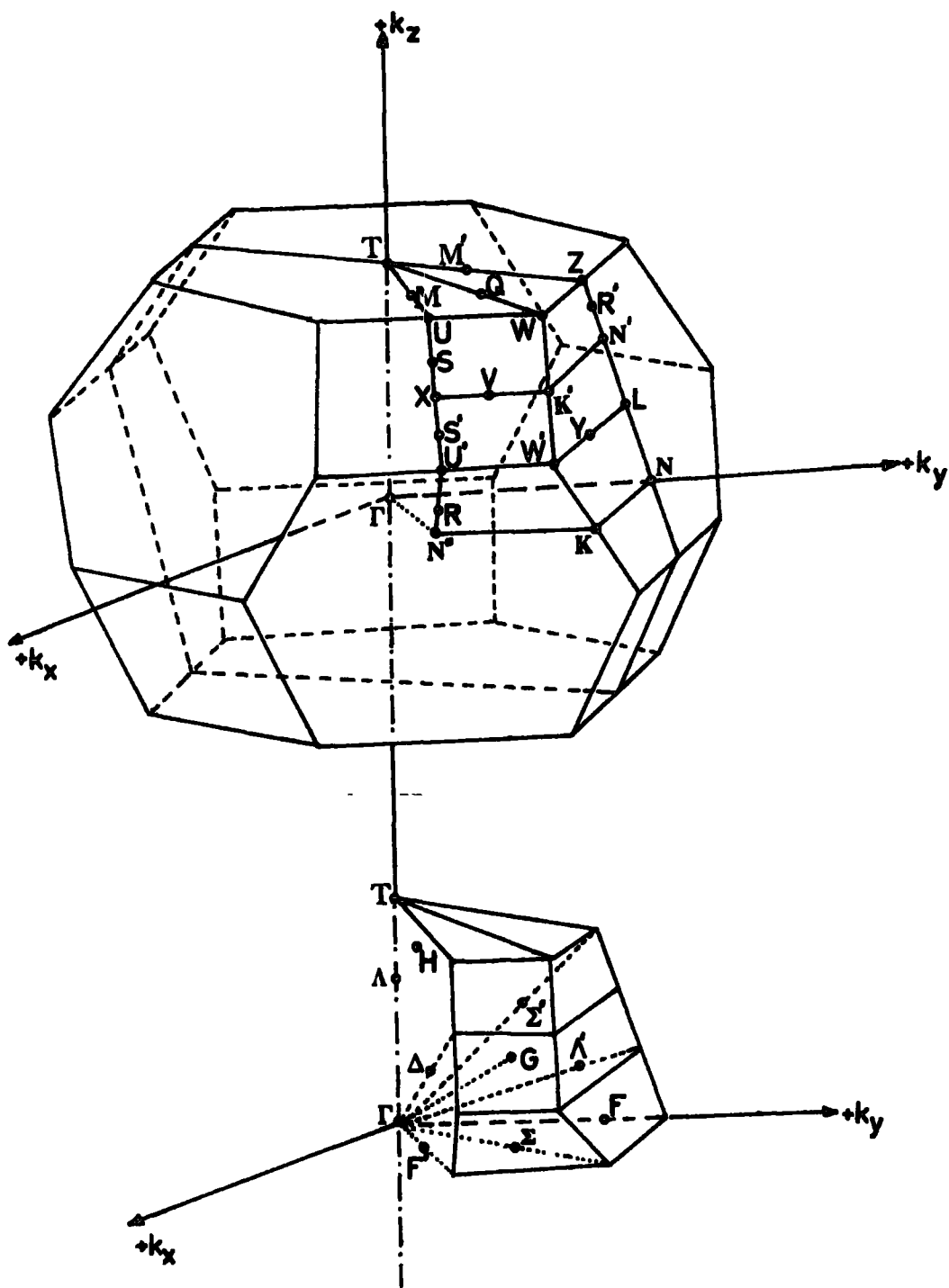


FIGURE (2.8): The Brillouin zone for the A7 structure showing special points and lines of symmetry. The "basic section" of the zone is shown underneath; special points and lines of symmetry inside this section are indicated. Point G, inside the basic section, is a general point with no symmetry.

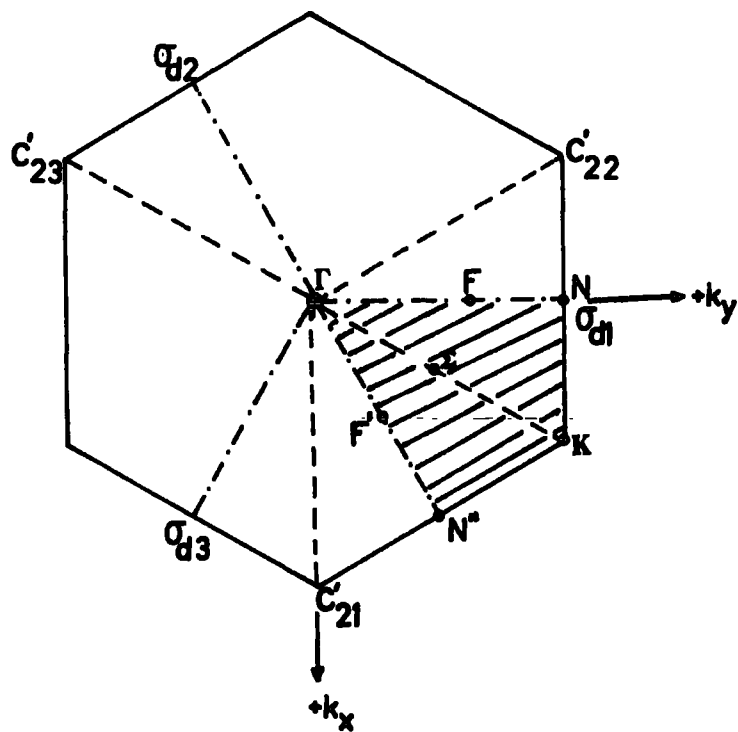


FIGURE (2.9): k_x k_y cross section of the Brillouin zone.

The two-fold rotational axes and mirror planes with their notation are indicated. The shaded area is the cross section of the basic section of the Brillouin zone.

CHAPTER THREE

SPACE-TIME SYMMETRY RESTRICTIONS ON THE FORM OF TRANSPORT TENSORS

3.1 INTRODUCTION

In section two of this chapter the basic transformation properties of tensors are reviewed and in section three an outline of tensor calculus is given. It is hoped that these two sections will serve as a guide and source of reference to the rest of the work presented in this thesis in which tensors are employed throughout.

In section four classical and group theoretical methods are used to study the limitations of crystal symmetry on the forms of tensors. An alternative formula to that of Bhagavantam's is given. Furthermore to find the precise forms of tensors a new approach is suggested - the Projection operator method.

In the last section (section five) the field dependent tensor transformation law in conjunction with Onsager reciprocity relations is used to establish the forms of transport tensors. For this purpose a set of generating symmetry elements for each 11 enantiomorphous point groups are derived and listed.

The forms taken by the magnetic field dependent magnetoresistivity and magnetothermoelectric power tensors are tabulated in the so-called "dot notation". Each tensor component is divided into "even" and "odd" parts with respect to the magnetic induction \vec{B} . Furthermore it is shown that the Umkehr effect (which is usually thought to be an anomalous effect) can occur in any component of the field dependent transport tensors which contains both "even" and "odd" parts in \vec{B} and to be a direct result of the anisotropy of the crystal.

3.2 TENSORS IN CRYSTALS

A tensor of rank n has 3^n components which transforms under coordinate transformations as

$$T'_{ijk\dots n} = R_{ip} R_{jq} R_{kr} \dots R_{nu} T_{pqr\dots u} \quad (3.1)$$

where R_{ip}, R_{jq}, \dots are the components of the transformation matrix which is a direction cosine matrix itself; $T_{pqr\dots u}$ and $T'_{ijk\dots n}$ are the original and transformed tensor components respectively. According to this definition a tensor of zero rank is a scalar and a tensor of first rank is a vector. To make the tensor concept clear, let us consider a vector \vec{A} which is a first rank tensor itself. In a given

reference frame the vector \vec{A} is determined uniquely by a set three components A_i ($i = 1, 2, 3$). If a new coordinate system is introduced the same vector \vec{A} is determined by a set of components B_i ; these new components are related in a definite way to the old. It is the law of transformation of components of a vector that is the essence of the vector idea, and the same is true of tensors. Since tensors are physical quantities or physical properties that are independent of the choice of the reference frames they form an ideal tool for the study of natural laws.

In solid state physics, most of the physical properties of single crystals depend on the direction in which they are measured. Therefore, physical properties of single crystals must be regarded as anisotropic, or at least potentially anisotropic. A great simplification occurs when the equations representing physical properties are written in tensor form. Tensors also facilitate the transformation of equations from one set of coordinates to another. Here orthogonal transformations in Cartesian space and therefore Cartesian tensors are only considered. A physical property of a crystal is defined by a relationship between two or more measurable quantities associated with the crystal. These measurable quantities are fields induced in matter by external causes and are called physical tensors. Typical examples are current density \vec{J} and electric field intensity \vec{E} which are first

rank tensors. The linear relationship between these physical tensors (ohm's law) defines the property tensor ρ_{ij} . Let us show that ρ_{ij} transforms like a second rank tensor: In a given cartesian coordinate system, in suffix notation, the vectors E_i and J_j are related by

$$E_i = \rho_{ij} J_j. \quad (3.2)$$

If these vectors transform to a primed coordinate system as

$$E'_m = R_{mi} E_i \quad (3.3)$$

and

$$J'_n = R_{nj} J_j \quad (3.4)$$

then $E'_m = R_{mi} \rho_{ij} J_j = R_{mi} R_{nj} \rho_{ij} J'_n =$

$$= R_{mi} R_{nj} \rho_{ij} J'_n = \rho'_{mn} J'_n. \quad (3.5)$$

Here R_{mi} and R_{nj} are the components of a 3×3 transformation matrix and $(i, j, m, n = 1, 2, 3)$. From equations (3.2) and (3.5) we can conclude that ρ_{ij} transforms as a tensor of second rank.

3.2.1 Polar and Axial tensors.

There are some tensors which obey the transformation law.

$$T'_{ijk\dots n} = \pm R_{ip} R_{jq} R_{kr} \dots R_{nu} T_{pqr\dots u} \quad (3.6)$$

where the negative sign is taken for transformations which change right-handed coordinate axes into left-

handed and vice versa, and the positive sign for transformations which do not change the hand of axes. A transformation which does change the hand of axes can always be considered to be a combination of a rotation of the axes and a reversal of their sense, i.e. rotation followed by a reflection or inversion. Tensors which transform according to equation (3.6) are called axial tensors (or pseudotensors) while a true tensor, which transform according to equation (3.1), is referred to as a polar tensor. To prevent the description of polar and axial tensors from becoming too abstract, let us take the magnetic induction vector \vec{B} which can be considered as a prototype axial vector (a first rank tensor). Vector \vec{B} cannot only be represented by a line of a certain length drawn in a certain direction, but also a sense of rotation is associated with the direction of it. When an electric current circulates in a coil, a magnetic induction \vec{B} is produced along the axis of the coil, the direction of \vec{B} is solely determined by the sense of the circulating current in the coil. On the other hand a polar vector (e.g. electric current density vector \vec{J} or electric field strength \vec{E}) can be represented unambiguously by a directed arrow.

3.2.2 Intrinsic symmetry of tensors.

A tensor $T_{ijk\dots n}$ is said to be symmetric in the indices i and j , if $T_{ijk\dots n} = T_{jik\dots n}$. Similarly, a tensor is antisymmetric with respect to a pair of its indices, say i and j , if an interchange of these indices merely changes the sign of the tensor components, i.e. $T_{ijk\dots n} = -T_{jik\dots n}$. Symmetry and antisymmetry are preserved under coordinate transformations. The property of a tensor being symmetric or antisymmetric is referred to as the intrinsic symmetry of the tensor. This intrinsic symmetry is something inherent to the physical property tensor and persists irrespective of the symmetry of the crystal under consideration.

As an example, let us consider transport tensors which are the main concern of this work. It is well known that the intrinsic symmetry of transport tensors are the Onsager reciprocity relations (see Onsager 1931a and b) which are due to the principle of microscopic reversibility. This principle may most concisely expressed by quoting Casimir (1945):

"...that the fundamental equations governing the motion of individual particles are symmetric with respect to past and future, or, mathematically speaking, that they are invariant under a transformation $(t) \rightarrow (-t)$."

Although, in principle, the intrinsic symmetry of transport tensors (i.e. Onsager reciprocity relations) and thus the principle of microscopic reversibility is a result of time reversal symmetry (see Fumi 1952b), it is derived from the principles of irreversible thermodynamics which is beyond the scope of this work.

3.3 TENSOR CALCULUS

The simplicity and elegance which tensors bring to the study of the physical properties of single crystals leads us to outline the language of tensors which is called tensor calculus.

3.3.1. Tensor addition

Tensor addition is defined only for tensors of equal rank. Two tensors are added by simply adding their corresponding components. It could be extended to include three or more tensors. This addition operation is commutative and associative. A useful application of tensor addition (or subtraction) operation is that any tensor of rank two say T_{ij} may be expressed as the sum of a symmetric $T_{ij}^{(s)}$ and an antisymmetric $T_{ij}^{(a)}$ tensor, i.e.

$$T_{ij} = T_{ij}^{(s)} + T_{ij}^{(a)} . \quad (3.7)$$

The symmetric $T_{ij}^{(s)}$ and antisymmetric $T_{ij}^{(a)}$ parts respectively are given by

$$T_{ij}^{(s)} = \frac{1}{2} (T_{ij} + T_{ji}) \quad (3.8)$$

and $T_{ij}^{(a)} = \frac{1}{2} (T_{ij} - T_{ji})$. (3.9)

3.3.2 Tensor products

(i) Outer product

The simplest example of outer product of tensors is the product of two tensors A_p and B_q of rank one (i.e. two vectors \vec{A} and \vec{B}), defined as:

$$T_{pq} = A_p B_q \quad (p, q = 1, 2, 3). \quad (3.10)$$

The nine products in equation (3.10) which are conveniently written in a square array as

$$\begin{pmatrix} A_1 B_1 & A_1 B_2 & A_1 B_3 \\ A_2 B_1 & A_2 B_2 & A_2 B_3 \\ A_3 B_1 & A_3 B_2 & A_3 B_3 \end{pmatrix} \quad \text{or} \quad \begin{pmatrix} T_{11} & T_{12} & T_{13} \\ T_{21} & T_{22} & T_{23} \\ T_{31} & T_{32} & T_{33} \end{pmatrix} \quad (3.11)$$

Note that $\vec{A}\vec{B} \neq \vec{B}\vec{A}$. To see that in equation (3.10) T_{pq} is a tensor of second rank, consider its transformation rule

$$\begin{aligned} T'_{ij} &= A'_i B'_j = (R_{ip} A_p) (R_{jq} B_q) = \\ &= R_{ip} R_{jq} A_p B_q = R_{ip} R_{jq} T_{pq} \end{aligned} \quad (3.12)$$

which is equivalent to equation (3.1) for rank two. Similarly the nine products in equation (3.12) can conveniently be written in a square array as

$$\begin{pmatrix} A_1 B_1 & A_1 B_2 & A_1 B_3 \\ A_2 B_1 & A_2 B_2 & A_2 B_3 \\ A_3 B_1 & A_3 B_2 & A_3 B_3 \end{pmatrix} \text{ or } \begin{pmatrix} T'_{11} & T'_{12} & T'_{13} \\ T'_{21} & T'_{22} & T'_{23} \\ T'_{31} & T'_{32} & T'_{33} \end{pmatrix} \quad (3.13)$$

Another example is the outer product of two second rank tensors S_{pq} and T_{vw} . Each tensor has nine components so that it is possible to form 81 products as

$$Q_{pqvw} = S_{pq} T_{vw} \quad (3.14)$$

On transformation of the orthogonal axes equation (3.14) transforms as

$$\begin{aligned} Q'_{ijmn} &= S'_{ij} T'_{mn} = \\ &= (R_{ip} R_{jq} S_{pq}) (R_{mv} R_{nw} T_{vw}) = \\ &= R_{ip} R_{jq} R_{mv} R_{nw} S_{pq} T_{vw} = \\ &= R_{ip} R_{jq} R_{mv} R_{nw} Q_{pqvw} \end{aligned} \quad (3.15)$$

From their transformation rule it is clearly seen that the 81 component quantity (i.e. Q_{pqvw}) is a fourth rank tensor. The extension of the above argument to tensors of rank other than two is obvious. Generally the outer product of two tensors of rank m and n gives a tensor of rank $(m+n)$. In the literature, for the

outer product of tensors, the names: dyadic product, exterior product, ordered product can frequently be encountered.

(ii) Inner product (single contraction).

The inner product of two tensors is obtained from the exterior product by putting equal two neighbouring indices belonging to each of the tensors respectively, and by summing over the resulting "dummy" index.

Inner product is indicated by inserting a dot between the symbols of the tensors. An obvious example to this type of product is the well known dot product of two vectors \vec{A} and \vec{B} (which are first rank tensors) i.e.

$$\vec{A} \cdot \vec{B} = A_i B_i \quad (3.16)$$

which is a scalar.

To give more examples, let \vec{T} be a second rank tensor and \vec{A} be a vector, then

$$\vec{T} \cdot \vec{A} = T_{ij} A_j \quad (3.17)$$

The quantities $T_{ij} A_j$ are components of a vector. In the same fashion

$$\vec{A} \cdot \vec{T} = A_j T_{j1} \quad (3.18)$$

It can easily be shown that the dot products

$\vec{T} \cdot \vec{A}$ and $\vec{A} \cdot \vec{T}$ are the same only if \vec{T} is symmetric. If both \vec{S} and \vec{T} are second rank tensors, then their inner product $\vec{S} \cdot \vec{T}$ is also a second rank tensor whose components are

$$Q_{ik} = \tilde{S} \cdot \tilde{T} = S_{ij} T_{jk}. \quad (3.19)$$

If \tilde{C} is a third rank tensor and \tilde{T} is second rank, the components of the resultant third rank tensor produced by single contraction are

$$P_{ijk} = \tilde{C} \cdot \tilde{T} = C_{ijn} T_{nk}. \quad (3.20)$$

Thus, in general, the single contraction of an n^{th} rank tensor with an m^{th} rank tensor is an $(n+m-2)^{\text{th}}$ rank tensor. The "." implies that the repeated indices are those which are at the right of the sequence for the left-hand tensor and at the left of the sequence for the right-hand tensor, i.e. if \tilde{T} is an n^{th} rank tensor and \tilde{S} is an m^{th} rank tensor, the $(n+m-2)^{\text{th}}$ rank tensor \tilde{Q} , in suffix notation is given by

$$Q_{ij \dots ru \dots w} = \tilde{T} \cdot \tilde{S} = T_{ij \dots rs \dots} S_{su \dots w}. \quad (3.21)$$

As in the case of the outer product, different names have also been used for the inner product. These are interior product, dot product and contracted product. If \vec{A} and \vec{B} are two vectors and \vec{T} is a second rank tensor, an operation which is usually called double product is given by

$$\vec{A} \cdot \vec{T} \cdot \vec{B} = (\vec{A} \cdot \vec{T}) \cdot \vec{B} = \vec{A} \cdot (\vec{T} \cdot \vec{B}). \quad (3.22)$$

Equation (3.22) which is a scalar quantity is written in suffix notation as

$$\vec{A} \cdot \vec{T} \cdot \vec{B} = A_i T_{ij} B_j. \quad (3.23)$$

$\vec{A} \cdot \vec{T} \cdot \vec{B}$ is equal to $\vec{B} \cdot \vec{T} \cdot \vec{A}$ when \vec{T} is a symmetric second rank tensor for which $T_{ij} = T_{ji}$. Similar types of expressions to equation (3.22) are frequently used in solid state physics, particularly to represent ellipsoidal constant energy surfaces.

It is very important to note that the dot product operation (the inner product or single contraction) can be represented by matrix multiplication; this is certainly true for first and second rank tensors. Let us show this by examples. Equation (3.17) can be written in matrix notation as

$$\vec{T} \cdot \vec{A} = \begin{pmatrix} T_{11} & T_{12} & T_{13} \\ T_{21} & T_{22} & T_{23} \\ T_{31} & T_{32} & T_{33} \end{pmatrix} \cdot \begin{pmatrix} A_1 \\ A_2 \\ A_3 \end{pmatrix} \quad (3.24)$$

where the components of the second rank tensor \vec{T} are regarded as the components of a 3 by 3 square matrix and the components of the vector \vec{A} are written as a column matrix. Equation (3.18) may be worked out in a similar manner, except that now the vector \vec{A} must be written as row matrix in order to perform the multiplication;

$$\vec{A} \cdot \vec{T} = (A_1 \ A_2 \ A_3) \cdot \begin{pmatrix} T_{11} & T_{12} & T_{13} \\ T_{21} & T_{22} & T_{23} \\ T_{31} & T_{32} & T_{33} \end{pmatrix} \cdot \quad (3.25)$$

By writing the second rank tensors \vec{S} and \vec{T} as 3 by 3 square matrices equation (3.19) becomes

$$\vec{Q} = \vec{S} \cdot \vec{T} = \begin{pmatrix} S_{11} & S_{12} & S_{13} \\ S_{21} & S_{22} & S_{23} \\ S_{31} & S_{32} & S_{33} \end{pmatrix} \cdot \begin{pmatrix} T_{11} & T_{12} & T_{13} \\ T_{21} & T_{22} & T_{23} \\ T_{31} & T_{32} & T_{33} \end{pmatrix} \quad (3.26)$$

Similarly, equation (3.23) can be written in matrix notation as

$$\vec{A} \cdot \vec{T} \cdot \vec{B} = (A_1 \ A_2 \ A_3) \cdot \begin{pmatrix} T_{11} & T_{12} & T_{13} \\ T_{21} & T_{22} & T_{23} \\ T_{31} & T_{32} & T_{33} \end{pmatrix} \cdot \begin{pmatrix} B_1 \\ B_2 \\ B_3 \end{pmatrix} \quad (3.27)$$

Matrix representation of tensor products (i.e. inner product) involving higher than second rank tensors has found to be complicated and therefore left beyond the scope of this work. Thus these types of tensor products will have to be written in suffix notation only. On the other hand, tensors up to second rank can clearly be represented by matrices. Referred to an orthogonal set of axes, a scalar (zero rank tensor) has one component and thus can be thought of as a 1×1 matrix, a vector (first rank tensor) has three components which can be represented by a 3×1 column matrix or 1×3 row matrix, and a second rank tensor has nine components which can be displayed as a 3×3 square matrix. Furthermore, the transformation rule for the first and second rank tensors can also be represented by matrices.

	Suffix notation	Matrix notation
Vectors	$\hat{A}'_i = R_{ij} A_j$	$\hat{A}' = RA$
Second rank tensors	$T'_{ij} = R_{ip} R_{jq} T_{pq}$	$T' = RTR^t$

Here primes represent the transformed tensors and R^t is the transpose of the transformation 3x3 matrix.

In fact, the above mentioned matrix representation of tensors are the only resemblance between tensors and matrices. For example, a third rank tensor has 27 components and these would require a 3x3x3 cubical array for proper systematic display. Although customarily higher order tensors have usually been displayed in array form, this is merely for display purposes and for tensor products and transformations, matrix algebra cannot be applied properly.

(iii) Double inner product (double contraction).

The double contraction operation of n^{th} rank tensor \tilde{T} with an m^{th} rank tensor \tilde{S} is a $(m+n-4)^{\text{th}}$ rank tensor \tilde{Q} written as

$$\tilde{Q} = \tilde{T} : \tilde{S} \quad (3.28)$$

In suffix notation equation (3.28) becomes

$$Q_{ij\dots otu\dots w} = T_{ij\dots opq} S_{pqt\dots w} \quad (3.29)$$

where the duplication of the indices p and q implies double summation. If both \tilde{T} and \tilde{S} are second rank tensors, then $\tilde{T}:\tilde{S}$ is a scalar given by $T_{ij} S_{ij}$. If \tilde{T} is a third rank tensor and \tilde{S} is second rank, then the double contraction gives a vector whose components are

$$\tilde{T}:\tilde{S} = T_{ijk} S_{jk} \quad (3.30)$$

If the tensors to be combined are of high rank, triple contractions can also be defined.

3.3.3 Some properties of symmetric second rank tensors.

If \tilde{T} is a tensor of rank two and its components are such that $T_{ij} = T_{ji}$ then \tilde{T} is a symmetric second rank tensor. The importance attached to a symmetric second rank tensor is that a lot of physical properties are represented by this tensor. Referred to an orthogonal triad a symmetric second rank tensor can at most have six number of independent components. There is always some orientation of these orthogonal axes such that the components of the symmetric second rank tensor T_{ij} will all be zero for $i \neq j$. The orthogonal set of axes in which this is true are usually called the principal axes of the tensor. One of the consequences of this is that any symmetric second rank tensor may be characterized by a maximum of three quantities, i.e. the components along the principal axes of the tensor. In other words a symmetric second rank tensor can always be transformed to a

diagonal form for a certain orthogonal set of axes.

It is also possible to describe a symmetric second rank tensor geometrically. This is called the representation quadric. It is a property of a quadric that it possesses three mutually perpendicular axes which are called principal axes. These axes turn out to be the same as the principal axes of a symmetric second rank tensor. In general, the representation quadric is defined as

$$T_{ij} x_i x_j = 1. \quad (3.31)$$

Referred to the principal axes, equation (3.31) becomes

$$T_{11} x_1^2 + T_{22} x_2^2 + T_{33} x_3^2 = 1. \quad (3.32)$$

A tensor inverse to a second rank tensor in general and to a symmetric second rank tensor in particular can always be defined. The procedure of finding this inverse tensor is the same as that of finding the inverse of a 3x3 matrix. The directions of the principal axes of both a symmetric second rank tensor and its inverse coincide.

3.4 EFFECT OF CRYSTAL SYMMETRY ON THE FORMS OF THE TENSORS REPRESENTING MACROSCOPIC PHYSICAL PROPERTIES OF CRYSTALS.

The relationships between the symmetry of crystals and their macroscopic physical properties have been a subject of study for a long time. In all such studies, many of the physical properties of crystals have been expressed by relations between tensors. Such tensor relations are called "constitutive equations". Here, in this section, the use of symmetry to simplify the forms of tensors describing various physical properties of crystals will be outlined. In addition, the use of group theoretical methods to find the number of independent components of tensors and their precise identification will be generalized.

3.4.1 Neumann's principle

Neumann's principle which states that a bulk physical property of a crystal must possess at least the point group symmetry of the crystal. The first implication of this principle is that any given physical property may possess a higher symmetry than that possessed by the crystal. The second implication is that under any symmetry transformation of coordinates appropriate to the point group of the crystal, all components of the tensor representing a physical property are unchanged.

Mathematically speaking, this second implication of Neumann's principle is that the transformed tensor shall be indistinguishable from the original and consequently the primes may be removed from the tensor transformation equations (3.1) and (3.6). For example, when R represents a symmetry element of the crystal point group, equation (3.1) for a polar tensor \tilde{T} of any rank must be replaced by

$$T_{ijk\dots n} = R_{ip}R_{jq}R_{kr}\dots R_{nu} T_{pqr\dots u} \quad (3.33)$$

An axial tensor \tilde{T} of any rank, however, transforms according to

$$T_{ijk\dots n} = \pm R_{ip}R_{jq}R_{kr}\dots R_{nr} T_{pqr\dots u} \quad (3.34)$$

which is the unprimed form of equation (3.6).

3.4.2 Crystal symmetry restrictions - CLASSICAL METHODS

Equations (3.33) and (3.34) can be considered as the mathematical expressions for Neumann's principle. The classical way of studying the effect of crystal symmetry to simplify the forms of tensors describing various properties of crystals is the direct use of the tensor transformation equation (3.33) for polar tensors and (3.34) for axial tensors. The procedure can be stated as follows: the symmetry elements of the point group of the crystal are successively applied to the tensor equation and each time it is demanded that the equations should remain invariant. As a result, some of the tensor components may vanish and relations between the others may be

established. Various examples of the use of this method can be found in the classical books of Nye (1960) and Bhagavantam (1966).

However, in order to secure the maximum simplification in the form of a tensor all the symmetry elements of the point group need not be used. A set of generating elements for each of the 32 crystallographic point groups may be used instead. To this end, a set of generating elements for each point group have been listed by Birss (1966), (see column 8 of table 3 in his book, pp. 36-38).

The number of the generating elements for a point group is considerably less than that of the symmetry elements of the point group. For example, for the point group $\bar{3}m$ this number is 3 out of 12 symmetry elements. These are: I , C_3^+ and C_2' . The members of a set of generating elements of a point group are not unique, but they must satisfy the following two conditions:

- (a) any sort of multiplication between the generating elements should not yield a symmetry element which is already a member of the set, and
- (b) all the symmetry elements of the point group should be obtained (or generated) from the generating set by multiplication.

There is, however, another classical method to simplify the forms of tensors. This is the so called "direct inspection method" devised by Fumi (1952a). The basis

for this method is that orthogonal coordinate products transform like the components of a tensor.

Mathematically this means that the tensor transformation equation

$$T_{ij} = R_{ip} R_{jq} T_{pq} \quad (3.35)$$

can be replaced by

$$x_i x_j = R_{ip} R_{jq} x_p x_q \quad (3.36)$$

which is the transformation equation for the coordinate products. In equation (3.36) x_1 , x_2 and x_3 stand for the orthogonal set. Thus, the transformation law for a second rank polar tensor (equation 3.35) turns out to be the same as the transformation law for the products of coordinates (equation 3.36). This method seems to be practical only when orthogonal coordinates do not transform into linear combinations of themselves under crystal symmetry operations. Therefore, application of this method to trigonal and hexagonal point groups need special consideration.

To conclude, it may be said that the safest and most systematic classical way of studying the effect of crystal symmetry on the forms of tensors is the use of Neumann's principle (equations 3.33 and 3.35) in conjunction with the generating elements for each of the 32 crystallographic point groups.

3.4.3. Crystal symmetry restrictions - GROUP THEORETICAL METHODS.

1) Number of independent non-zero components

Bhagavantam and Suryanarayana (1949) have described a group theoretical method (hereafter will be called Bhagavantam's method) of determining the number of independent non-zero components of tensors representing various physical properties of crystals in each of the 32 crystallographic point groups. This number (n_i) can be obtained by (for more details, see, Bhagavantam 1966 p.83).

$$n_i = \frac{1}{g} \sum_j h_j X_j(R) X_i(R). \quad (3.37)$$

Here g is the total number of symmetry elements of the point group under consideration, h_j is the number of elements in the j^{th} class, $X_i(R)$ is the character relative to the symmetry operation R in the particular irreducible representation and $X_j(R)$ is the character of the symmetry element R in the tensor representation. In Bhagavantam's method, it is assumed that all tensors transform like the total symmetric irreducible representation; therefore, the value of $X_i(R)$ is taken to be equal to 1 for all R .

The value of $\chi_j(R)$ is calculated in two steps: firstly, a character equation appropriate to the tensor under consideration is obtained (see, Bhagavantam 1966, tables VII (a, b, c) pp. 88-90); secondly, this character equation is evaluated for each R of the point group under consideration. The character equation covers properties such as the nature of the tensor (polar or axial) and its intrinsic symmetry. Thus Bhagavantam's method is also called the character method. It has been extensively used to calculate the number of independent non-zero components of various physical tensors in a recent book by Wooster (1973). It has also been successfully used by Sumengen (1971) and Sumengen and Saunders (1972b) who have calculated the number of independent non-zero components of the low field galvanomagnetic and thermomagnetic tensors for the A7 structure materials.

To calculate the number of independent non-zero components of tensors, a group theoretical method alternative to that of Bhagavantam's has been described by Jahn (1937, 1949). This method avoids the character calculations.

It consists of finding first the explicit form of the tensor representation under consideration for the full group of all symmetry operations and then obtaining the form for the individual point groups by reducing this representation. At present, we will not give a full description of this method because it is, in general, based on the representation theory which we have not included in this work.

Before giving a generalization of Bhagavantam's method, let us describe the contents of tables (3.1) and (3.2) which will be frequently referred to in the examples.

Notes to table (3.1)

- (i) In general, the use of matrices to represent symmetry operations is a common practice in group theory. The set of symmetry elements of the crystallographic point groups can be represented by matrices. Here as an example the matrix form of the 12 symmetry operations of the point group $\bar{3}m$ are listed.
- (ii) The character of a symmetry element is defined as the trace of its matrix, that is, the sum of the diagonal elements of the matrix.
- (iii) The matrices are referred to a right handed orthogonal set: $x//C'_{21}$, $y//\sigma_{d1}$, $z//C_3^{\pm}$. Anticlockwise rotations are taken as positive. The passive convention is adopted, that is, matrix operators move the coordinate axes and leave the points (or bodies) fixed.

TABLE (3.1) : Matrix representation of the symmetry elements (see section 2.2 for their description) of point group D_{3d} ($\bar{3}m$):

$$E = \begin{pmatrix} 1 & 0 & 0 \\ 0 & 1 & 0 \\ 0 & 0 & 1 \end{pmatrix},$$

$$C_3^+ = \begin{pmatrix} \frac{1}{2} & \frac{\sqrt{3}}{2} & 0 \\ -\frac{\sqrt{3}}{2} & \frac{1}{2} & 0 \\ 0 & 0 & 1 \end{pmatrix}, \quad C_3^- = \begin{pmatrix} \frac{1}{2} & \frac{\sqrt{3}}{2} & 0 \\ \frac{\sqrt{3}}{2} & \frac{1}{2} & 0 \\ 0 & 0 & 1 \end{pmatrix},$$

$$C'_{21} = \begin{pmatrix} 1 & 0 & 0 \\ 0 & -1 & 0 \\ 0 & 0 & -1 \end{pmatrix}, \quad C'_{22} = \begin{pmatrix} \frac{1}{2} & \frac{\sqrt{3}}{2} & 0 \\ \frac{\sqrt{3}}{2} & \frac{1}{2} & 0 \\ 0 & 0 & -1 \end{pmatrix}, \quad C'_{23} = \begin{pmatrix} \frac{1}{2} & \frac{\sqrt{3}}{2} & 0 \\ -\frac{\sqrt{3}}{2} & \frac{1}{2} & 0 \\ 0 & 0 & -1 \end{pmatrix};$$

$$I = \begin{pmatrix} -1 & 0 & 0 \\ 0 & -1 & 0 \\ 0 & 0 & -1 \end{pmatrix},$$

$$S_6^+ = \begin{pmatrix} \frac{1}{2} & \frac{\sqrt{3}}{2} & 0 \\ \frac{\sqrt{3}}{2} & \frac{1}{2} & 0 \\ 0 & 0 & -1 \end{pmatrix}, \quad S_6^- = \begin{pmatrix} \frac{1}{2} & \frac{\sqrt{3}}{2} & 0 \\ -\frac{\sqrt{3}}{2} & \frac{1}{2} & 0 \\ 0 & 0 & -1 \end{pmatrix},$$

$$\sigma_{d1} = \begin{pmatrix} -1 & 0 & 0 \\ 0 & 1 & 0 \\ 0 & 0 & 1 \end{pmatrix}, \quad \sigma_{d2} = \begin{pmatrix} \frac{1}{2} & \frac{\sqrt{3}}{2} & 0 \\ \frac{\sqrt{3}}{2} & \frac{1}{2} & 0 \\ 0 & 0 & 1 \end{pmatrix}, \quad \sigma_{d3} = \begin{pmatrix} \frac{1}{2} & \frac{\sqrt{3}}{2} & 0 \\ -\frac{\sqrt{3}}{2} & \frac{1}{2} & 0 \\ 0 & 0 & 1 \end{pmatrix}.$$

TABLE (3.2): Character table for point group $\bar{3}m$ (D_{3d}).

D_{3d}	E	$2C_3 \begin{cases} C_3^+ \\ C_3^- \end{cases}$	$3C_2 \begin{cases} C_{21}' \\ C_{22}' \\ C_{23}' \end{cases}$	I	$2S_6 \begin{cases} S_6^+ \\ S_6^- \end{cases}$	$3\sigma_d \begin{cases} \sigma_{d1} \\ \sigma_{d2} \\ \sigma_{d3} \end{cases}$
A_{1g}	1	1	1	1	1	1
A_{2g}	1	1	-1	1	1	-1
E_g	2	-1	0	2	-1	0
A_{1u}	1	1	1	-1	-1	-1
A_{2u}	1	1	-1	-1	-1	1
E_u	2	-1	0	-2	-1	0

Notes to table (3.2)

(i) The symbol in the upper left-hand corner of the table identifies the particular point group (here point group D_{3d}). The special symbols used are those first suggested by Mulliken (1933). A or B denote always one dimensional representations, E two dimensional, F three dimensional. The two dimensional symbol E should not be confused with the identity operation E.

(ii) The symbol A denotes the irreducible representation which is symmetric under the main symmetry operations about the principal axis; here C_3^+ or C_3^- . Subscripts on the basic symbols are identified as follows:

1 = Symmetric under σ_{d_i} ($i = 1, 2, 3$) operations

2 = antisymmetric under σ_{d_i} operations

g (gerade) = symmetric under an I (inversion) operation

u (ungerade) = antisymmetric under an I (inversion) operation.

Polar tensors transform like A_{1g} and axial tensors like A_{1u} .

(iii) The symmetry elements of $\bar{3}m$ are grouped in 6 classes. This grouping is based on the fact that all the symmetry operations in the class have the same character (or trace) and are related by similarity transformations. By a class we mean all the symmetry operations of a point group which obey the relation

$$R^{-1} C_1 R = C_1 \quad (3.38)$$

where C_1 is a chosen symmetry operation and R runs over all the symmetry operations of the particular point group.

(iv) Here we shall not attempt to explain how to construct the character tables for the crystallographic point groups. This rather specialized technique, which is beyond the scope of this work, involves a number of theorems on the representation theory. Fortunately, all the character tables we are likely to require already exist in the literature. They can be found in most of the books on applied group theory (see, for example, Tinkham 1964 pp. 323-30; Hall 1969 pp. 343-54; Bradley and Cracknell 1972 pp. 57-60).

We now give a generalized form of equation (3.37) as

$$n_i = \frac{1}{g} \sum_j h_j X_i(R_j) \{ X(R_j) \}^r \quad (3.39)$$

Here g and h_j have the same meanings as in equation (3.37), $X_i(R_j)$ is the character of the i^{th} irreducible representation corresponding to the j^{th} class, $X(R_j)$ is the trace of the R_j^{th} symmetry element in the j^{th} class, and r is the rank of the tensor under consideration. If we know the nature of the tensor (i.e. polar or axial), the value of $X_i(R_j)$ can be directly obtained from the character table: a polar tensor transforms like a totally symmetric one dimensional irreducible representation (A_{1g} in table 3.2) and an axial tensor transforms like a one dimensional, antisymmetric under an improper rotation, irreducible representation (A_{1u} in table 3.2). $X(R_j)$ is obtained from the matrix representation table (table 3.1) and is the trace of the j^{th} matrix. Let us explain this method by examples. In all these examples, the number of independent non-zero components of certain tensors are going to be calculated for the point group $\bar{3}m$ of major interest here.

Example one. Consider the thermoelectric power tensor $\alpha_{ij}^{(o)}$, a second rank polar tensor. Let us calculate the number of independent non-zero components of this tensor. Because of its polar nature it transforms like A_{1g} . Thus $X_i(R_j) \rightarrow X_{A_{1g}}(R_j) = 1$ for all j (j runs from 1 to 6, i.e., the number of classes in point group $\bar{3}m$).

From table (3.2)

$$\begin{aligned}
 g &= 12; \\
 h_1 &= 1, h_2 = 2, h_3 = 3, \\
 h_4 &= 1, h_5 = 2, h_6 = 3.
 \end{aligned}
 \tag{3.40}$$

From table (3.1), the traces of the matrix operations are

$$\begin{aligned}
 X(R_1) &= 3, \quad X(R_2) = 0, \quad X(R_3) = -1, \\
 X(R_4) &= -3, \quad X(R_5) = 0, \quad X(R_6) = 1
 \end{aligned}
 \tag{3.41}$$

where $R_1 = E$, $R_2 = C_3^+$ or C_3^- , $R_3 = C'_{21}$ or C'_{22} or C'_{23} ,
 $R_4 = I$, $R_5 = S_6^+$ or S_6^- , $R_6 = \sigma_{d1}$ or σ_{d2} or σ_{d3} .

Substitution of all the above values into equation (3.39) yields

$$\begin{aligned}
 n_i &= \frac{1}{12} \left\{ h_1 X_1(R_1) [X(R_1)]^2 + h_2 X_1(R_2) [X(R_2)]^2 + \right. \\
 &\quad + h_3 X_1(R_3) [X(R_3)]^2 + h_4 X_1(R_4) [X(R_4)]^2 + \\
 &\quad \left. + h_5 X_1(R_5) [X(R_5)]^2 + h_6 X_1(R_6) [X(R_6)]^2 \right\} = \\
 &= \frac{1}{12} \left\{ (1)(1)(3)^2 + (2)(1)(0)^2 + (3)(1)(-1)^2 + \right. \\
 &\quad \left. + (1)(1)(-3)^2 + (2)(1)(0)^2 + (3)(1)(1)^2 \right\} = 2
 \end{aligned}
 \tag{3.42}.$$

where the symbol i should be replaced by A_{1g} . Thus the number of independent non-zero components of the thermoelectric power tensor for $\bar{3}m$ symmetry is two - a very well known result.

Example two. Consider the low field Nernst tensor $\alpha_{ijk_1}^{(1)}$, an axial third rank tensor. It transforms like A_{1u} . Thus the values of $X_i(R_j)$ are obtained from table (3.2) as

$$\begin{aligned} X_1(R_1) &= X_1(R_2) = X_1(R_3) = 1, \\ X_1(R_4) &= X_1(R_5) = X_1(R_6) = -1 \end{aligned} \quad (3.43)$$

where i should be replaced by A_{1u} .

The rest of the parameters take the same values as in example one with the exception of r , the rank of the tensor, which is 3.

Substitution of the values into equation (3.39) yields

$$\begin{aligned} n_1 &= \frac{1}{12} \left\{ h_1 X_1(R_1) [X(R_1)]^3 + h_2 X_1(R_2) [X(R_2)]^3 + \right. \\ &+ h_3 X_1(R_3) [X(R_3)]^3 + h_4 X_1(R_4) [X(R_4)]^3 + \\ &+ h_5 X_1(R_5) [X(R_5)]^3 + h_6 X_1(R_6) [X(R_6)]^3 \left. \right\} (i \rightarrow A_{1u}) \\ &= \frac{1}{12} \left\{ (1)(1)(3)^3 + (2)(1)(0)^3 + (3)(1)(-1)^3 + (1)(-1)(-3)^3 + \right. \\ &+ (2)(-1)(0)^3 + (3)(-1)(1)^3 \left. \right\} = 4. \end{aligned} \quad (3.44)$$

Thus the number of independent components of $\alpha_{ijk_1}^{(1)}$ for $\bar{3}m$ symmetry is 4. Sümengen and Saunders (1972b) have obtained the same number by using Bhagavantam's method.

For physical reasons some tensors possess intrinsic symmetry (see, section 3.2.2). However this property, is not included in equation (3.39). Partly following Lyubarskii (1960) p. 168 and Bhagavantam (1966) p. 97, a formula to

include the intrinsic symmetry of tensors is given by

$$n_i = \frac{1}{g} \sum_j h_j \chi_i(R_j) \left\{ \frac{1}{N_p} \sum_{N_p} (\pm) \chi(R_j^m) \chi(R_j^n) \dots \chi(R_j^p) \right\}. \quad (3.45)$$

Here N_p is the order of the permutation P , $m, (n, \dots, p)$ are the cycle lengths of the permutations, $\chi(R_j^m)$ is the trace of a new matrix which is obtained by taking the m^{th} power of the j^{th} matrix. The minus sign is taken when the relevant permutation changes the sign of the tensor under consideration. Now let us explain how to use equation (3.45) with an example.

Example three. Consider the low field Hall effect tensor $\rho_{ijk_1}^{(1)}$, a third rank axial tensor. It is antisymmetric with respect to its indices i and j , that is, $ijk_1 = -jik_1$. Thus the permutation group consists of the two permutations ($N_p=2$)

$$\begin{array}{lll} 1^{\text{st}} & (1) (2) (3) & m=1, n=1, p=1 \\ 2^{\text{nd}} & (12) (3) & m=2, n=1 \end{array} \quad (3.46)$$

In the first permutation there are 3 cycles (1), (2), (3) and each cycle length is 1 ($m=1, n=1, p=1$).

In the second permutation there are two cycles (12) and (3), the length of the first cycle is two ($m=2$) and the second is one ($n=1$); in the first cycle, interchange of the indices 1,2 changes the sign of the tensor; thus for this case the minus sign in equation (3.45) should be used.

If these values of N_p , m , n and p are used, equation (3.45) becomes

$$\begin{aligned} n_1 &= \frac{1}{g} \sum_j h_j x_1(R_j) \left\{ \frac{1}{2} x(R_j) x(R_j) x(R_j) \right. \\ &\quad \left. - \frac{1}{2} x(R_j^2) x(R_j) \right\} = \\ &= \frac{1}{g} \sum_j h_j x_1(R_j) \frac{1}{2} \left\{ x^3(R_j) - x(R_j^2) x(R_j) \right\} . \end{aligned} \quad (3.47)$$

Now in this equation, with the exception of $x(R_j^2)$, all the values of the parameters can be found exactly the same way as those of examples one and two.

Let us calculate the value of $x(R_j^2)$ by giving an example.

Consider the matrix operation C'_{21} , the value of $x(R_j)$ is -1 (see, table 3.1 and equation 3.41) and that of $x(R_j^2)$ is 3. Here we have obtained the number 3 by taking the square of the matrix C'_{21} .

The result, namely the number of independent non-zero components of $\rho_{ijk_1}^{(1)}$, is

$$\begin{aligned} n_1 &= \frac{1}{12} \left\{ (1)(1) \frac{1}{2} [(3)^3 - (3)(3)] + (2)(1) \frac{1}{2} [(0)^3 - (2)(0)] \right. \\ &\quad + (3)(1) \frac{1}{2} [(-1)^3 - (3)(-1)] + (1)(-1) \frac{1}{2} [(-3)^3 - (3)(-3)] \\ &\quad \left. + (2)(-1) \frac{1}{2} [(0)^3 - (2)(0)] + (3)(-1) \frac{1}{2} [(1)^3 - (3)(1)] \right\} = \\ &= 2. \end{aligned} \quad (3.48)$$

Thus there are two independent low field Hall coefficients for the A7 structure materials, a well-known result.

We conclude this section by pointing out that the method which we have described here is simple, systematic and more general than that of Bhagavantam.

2) Forms of tensors - the projection operator

Up to this stage we have calculated the number of independent non-zero components of tensors only. In other words we do not know which are the zero (or non-zero) components and what are the relationships between the non-zero tensor components. To find the forms of these tensors, in addition to the above calculations, one of the classical methods need to be used. Apparently group theory has been used only by Fumi (1952b) to tackle this second stage. Although there is complete agreement between his results and ours, his method seems complicated. Especially in his paper a crucial step, the construction of bases, does not seem clear (at least it seems so to the present author). However, his paper has always been a helpful source during the progress of this particular subject.

Here we suggest a novel approach to find the precise forms of tensors. An operator (which will be called the projection operator, because it has a similar structure to that of the projection operator which is used in quantum mechanics to project out basis functions (see, for example, Tinkham 1964 pp. 40-42, Falicov 1966 pp. 57-58)), appropriate to each crystallographic point group is constructed. This is done by using the character table and the matrix form of the symmetry operations of the point

group under consideration.

This projection operator can be written

$$P_{op}^i = \frac{1}{g} \sum_j X_i(R_j) R_j. \quad (3.49)$$

Here g and $X_i(R_j)$ are the same symbols as in equation (3.39), the index j runs over all the symmetry operations of the point group. Classes are not involved. Let us construct the projection operator for the point group $\bar{3}m$. To achieve this end, the following ingredients are needed.

- (a) the character table (table 3.2),
- (b) the nature of the tensor (polar or axial),
- (c) the twelve symmetry operations of the point group $\bar{3}m$ (see, table 3.1).

For (b), let us reconsider example one, the thermoelectric power tensor $\alpha_{ij}^{(o)}$, a second rank polar tensor which transforms like A_{1g} . Thus, from table (3.2), $X_i(R_j) = 1$ for all R_j ($j=1,2,3, \dots, 12$) and $g = 12$.

We now write the projection operator (equation 3.49) for $\bar{3}m$ symmetry as

$$P_{op}^i = \frac{1}{12} \left\{ E + C_3^+ + C_3^- + C_{21} + C_{22} + C_{23} + I + S_6^+ + S_6^- + \sigma_{d1} + \sigma_{d2} + \sigma_{d3} \right\} \quad (3.50)$$

where $i \rightarrow A_{1g}$.

Already in section (3.4.2) we have mentioned that Cartesian coordinate products transform like the components of a tensor (equation 3.36).

If the tensor components are denoted by the coordinate products that are their indices, the unsimplified form of

the thermoelectric power tensor can be written as

$$\alpha_{ij}^{(0)} = \begin{pmatrix} xx & xy & xz \\ yx & yy & yz \\ zx & zy & zz \end{pmatrix}. \quad (3.51)$$

Now we apply the projection operator, that is, equation 3.50, to all the components of this tensor (equation 3.51). The operator is applied to each tensor component separately. Let us see the effect of P_{op}^i on the xx component. To find this, we need to know how the Cartesian coordinates x, y, z transform under the symmetry operations of the point group. For this purpose, transformed form of the x, y, z coordinates under the point group $\bar{3}m$ symmetry operations are listed in table (3.3).

TABLE (3.3): Transformation of x, y, z in point group $D_{3d}(\bar{3}m)$.
 ($+x // C_{21}^+$, $+y // C_{d1}$ or projection of \bar{a}_2 on the xy plane,
 $+z // C_3^+ // (\bar{a}_1 + \bar{a}_2 + \bar{a}_3) // [111]$).

Point group symmetry operation	Transformed form of		
	x	y	z
E	x	y	z
C_3^+	$-\frac{1}{2}x + \frac{\sqrt{3}}{2}y$	$-\frac{\sqrt{3}}{2}x - \frac{1}{2}y$	z
C_3^-	$-\frac{1}{2}x - \frac{\sqrt{3}}{2}y$	$\frac{\sqrt{3}}{2}x - \frac{1}{2}y$	z
C_{21}^+	x	$-y$	$-z$
C_{22}^+	$-\frac{1}{2}x - \frac{\sqrt{3}}{2}y$	$-\frac{\sqrt{3}}{2}x + \frac{1}{2}y$	$-z$
C_{23}^+	$-\frac{1}{2}x + \frac{\sqrt{3}}{2}y$	$\frac{\sqrt{3}}{2}x + \frac{1}{2}y$	$-z$
I	$-x$	$-y$	$-z$
S_6^+	$\frac{1}{2}x + \frac{\sqrt{3}}{2}y$	$-\frac{\sqrt{3}}{2}x + \frac{1}{2}y$	$-z$
S_6^-	$\frac{1}{2}x - \frac{\sqrt{3}}{2}y$	$\frac{\sqrt{3}}{2}x + \frac{1}{2}y$	$-z$
d_1	$-x$	y	z
d_2	$\frac{1}{2}x + \frac{\sqrt{3}}{2}y$	$\frac{\sqrt{3}}{2}x - \frac{1}{2}y$	z
d_3	$\frac{1}{2}x - \frac{\sqrt{3}}{2}y$	$-\frac{\sqrt{3}}{2}x - \frac{1}{2}y$	z

By using table (3.3), the effect of P_{op}^1 on the xx component becomes

$$\begin{aligned} P_{op}^1(xx) &= \frac{1}{12} \left\{ x^2 + \left(-\frac{1}{2}x + \frac{\sqrt{3}}{2}y\right)^2 + \left(-\frac{1}{2}x - \frac{\sqrt{3}}{2}y\right)^2 + x^2 + \right. \\ &\quad \left. + \left(-\frac{1}{2}x - \frac{\sqrt{3}}{2}y\right)^2 + \left(\frac{1}{2}x + \frac{\sqrt{3}}{2}y\right)^2 + (-x)(-x) + \left(\frac{1}{2}x + \frac{\sqrt{3}}{2}y\right)^2 + \right. \\ &\quad \left. + \left(\frac{1}{2}x - \frac{\sqrt{3}}{2}y\right)^2 + (-x)(-x) + \left(\frac{1}{2}x + \frac{\sqrt{3}}{2}y\right)^2 + \left(\frac{1}{2}x - \frac{\sqrt{3}}{2}y\right)^2 \right\} = \\ &= \frac{1}{2}(x^2 + y^2), \end{aligned}$$

similarly

$$P_{op}^1(yy) = \frac{1}{2}(x^2 + y^2)$$

$$P_{op}^1(zz) = z^2$$

$$P_{op}^1(xy) = P_{op}^1(xz) = P_{op}^1(yx) = P_{op}^1(yz) = P_{op}^1(zx) = P_{op}^1(zy) = 0.$$

(3.52)

Here attention should be paid to the order of the multiplication of the x, y, z coordinates. For example,

$$\left(-\frac{1}{2}x + \frac{\sqrt{3}}{2}y\right)^2 = \frac{1}{4}x^2 - \frac{\sqrt{3}}{4}xy - \frac{\sqrt{3}}{4}yx + \frac{3}{4}y^2$$

$$\text{but } \neq \frac{1}{4}x^2 - \frac{\sqrt{3}}{2}xy \text{ (or } -\frac{\sqrt{3}}{2}yx) + \frac{3}{4}y^2. \quad (3.53)$$

A tensor component which is operated on will be called the original tensor component and the projected out component or a linear combination of components will be called the resultant component.

We interpret the operations in equation (3.52) as follows:

(i) If the projection operator operating on an original component projects out zero, we say that this original component vanishes. Thus the application of the projection operator on a tensor component has the property of yielding zero unless the tensor component being operated on is a non-zero component itself.

(ii) If the result is not zero, we say that the original component does not vanish. The linear relationships between the projected out components are taken to be the same relationships between the corresponding original components. For example in equation (3.52), the projection operator has been projected out $\frac{1}{2}(x^2+y^2)$ from both the (xx) and (yy) original components. Therefore we take $xx=yy$. Thus we then identify the two independent non-zero components of the thermoelectric power tensor as $xx(=yy)$ and zz . Hence the final form of the tensor (equation 3.51) becomes trivial.

This projection operator approach may be mathematically formulated and generalized as follows:

Let $U_1(x,y,z), U_2(x,y,z), \dots, U_n(x,y,z)$ represent the original tensor components where n is the rank of the tensor and let $f_1(x,y,z), f_2(x,y,z), \dots$ represent the resultant components.

If $P_{op}^i U_k(x,y,z)=0$, we say that the original k^{th} component ($k = 1,2,3, \dots, n$) is zero.

$$\text{If } \left. \begin{array}{l} P_{op}^i U_k(x,y,z) = f_1(x,y,z) \\ P_{op}^i U_{k'}(x,y,z) = f_1(x,y,z) \end{array} \right\} \begin{array}{l} \text{We take } U_k(x,y,z) = U_{k'}(x,y,z) \\ \text{where } k, k' = 1, 2, 3 \dots n \text{ and} \\ k \neq k' \end{array}$$

$$\text{or if } \left. \begin{array}{l} P_{op}^i U_k(x,y,z) = f_2(x,y,z) \\ P_{op}^i U_{k'}(x,y,z) = -5f_2(x,y,z) \end{array} \right\} \begin{array}{l} \text{We take} \\ U_k(x,y,z) = -5U_{k'}(x,y,z). \end{array}$$

(3.54)

In the related field we could not find a theorem to account for this case - probably there is not one.

The intrinsic symmetry (if any) of tensors, however, is not contained in equation (3.50). We have found it convenient to impose this extra condition on the non-zero components of the tensor obtained by the projection operator approach. To explain this and take the opportunity to give another example of using the projection operator, let us reconsider example three - the low field Hall effect tensor. It transforms like A_{1u} ($i \rightarrow A_{1u}$). The projection operator for this tensor is

$$P_{op}^i = \frac{1}{12} \{ E + C_3^+ + C_3^- + C_{21}' + C_{22}' + C_{23}' - I - S_6^+ - S_6^- - \sigma_{d1} - \sigma_{d2} - \sigma_{d3} \}.$$

(3.55)

Again the components of $\rho_{1jk_1}^{(1)}$ are denoted by the coordinate products that are their indices. For example the two components $\rho_{111}^{(1)}$ and $\rho_{123}^{(1)}$ are denoted by X^3 and xyz respectively. The projection operator (equation 3.55) operating on the original tensor components yields

$$P_{op}^i (x^3) = \frac{1}{4} (x^3 - xy^2 - yxy - y^2x) \quad (a)$$

$$P_{op}^i (xy^2) = \frac{1}{4} (-x^3 + xy^2 + yxy + y^2x) \quad (b)$$

$$P_{op}^i (xyz) = \frac{1}{2} (xyz - yxz) \quad (c)$$

$$P_{op}^i (xyz) = \frac{1}{2} (xzy - yzx) \quad (d)$$

$$P_{op}^i (yxy) = \frac{1}{4} (-x^3 + xy^2 + yxy + y^2x) \quad (e)$$

$$P_{op}^i (yxz) = \frac{1}{2} (yxz - xyz) \quad (f)$$

$$P_{op}^i (y^2x) = \frac{1}{4} (-x^3 + xy^2 + yxy + y^2x) \quad (g)$$

$$P_{op}^i (yzx) = \frac{1}{2} (yzx - xzy) \quad (h)$$

~~$$P_{op}^i (zxy) = \frac{1}{2} (zxy - zyx) \quad (i)$$~~

$$P_{op}^i (zyx) = \frac{1}{2} (zxy - zyx) \quad (j)$$

P_{op}^i projects out zero from the rest of tensor components, i.e. $xyx \ xzx \ x^2y \ x^2z \ xz^2 \ yx^2 \ y^3 \ yzy \ y^2z \ yz^2 \ zx^2 \ z^2x \ zy^2 \ z^2y \ zxz \ zyz \ z^3$. (3.56)

From (c) and (f)	$xyz = -yxz$	}	(3.57)
" (d) " (h)	$xzy = -zyx$		
" (i) " (j)	$zxy = -zyx$		
from (a), (b), (e) and (g)	$x^3 = -xy^2 = -yxy = -y^2x$		

Thus we have identified four independent components. In fact these can be considered the independent components of $\alpha_{ijk_1}^{(1)}$ (low field Nernst tensor) which has no intrinsic symmetry. As we have already mentioned in example three,

(1)
 ρ_{ijk_1} is antisymmetric with respect to its indices i and j , i.e. $ijk_1 = -jik_1$. Application of this condition to the equalities in equation (3.57) yields

$$\begin{aligned} xyz &= -yxz \\ xzy &= -zxy = zyx = -yzx \\ zxy &= -xzy = -zyx = yzx \end{aligned} \left. \vphantom{\begin{aligned} xyz \\ xzy \\ zxy \end{aligned}} \right\} yzx$$

$$x^3 = -xy^2 = -yxy = -y^2x = 0. \quad (3.58)$$

Hence the precise form of $\rho_{ijk_1}^{(1)}$ follows - there are two independent components: $xyz \rightarrow \rho_{123}^{(1)}$ and $yzx \rightarrow \rho_{231}^{(1)}$.

To make sure that this projection operator method holds generally, we have found the precise forms of some other tensors of different rank and kind; in every case a complete agreement between these forms and those obtained by classical methods have been reached.

3.5 SPACE-TIME SYMMETRY RESTRICTIONS ON THE FORM OF TRANSPORT TENSORS.

The purpose of this section is to establish the form of transport tensors for each of the 32 crystallographic point groups. Here we assume that the time (or time-reversal) symmetry restrictions are given; as we have already mentioned in section (3.2.2), the time-reversal symmetry restrictions are embodied in the Onsager reciprocity relations:

$$\begin{aligned} \rho_{ij}(\vec{B}) &= \rho_{ji}(-\vec{B}) \\ \kappa_{ij}(\vec{B}) &= \kappa_{ji}(-\vec{B}) \end{aligned} \tag{3.59}$$

$$\pi_{ij}(\vec{B}) = T \alpha_{ji}(-\vec{B}). \tag{3.60}$$

Therefore, we shall be concerned with the space (or spatial) symmetry restrictions only.

3.5.1 Constant and field dependent tensors.

If the components are functions of the applied fields, the tensor is called a field dependent tensor. According to this definition all the tensors which have been described in the previous sections of this chapter should accurately be classified as constant tensors. However, the magnetoresistivity tensor $\rho_{ij}(\vec{B})$ which is a function of the magnetic field is a field dependent tensor, although the low field expansion coefficients of $\rho_{ij}(\vec{B})$ are constant tensors.

3.5.2 The transformation law for field dependent tensors.

Here we follow closely the formalism given by Grabner and Swanson (1962) and write the transformation law for field dependent tensors as: all the components of a field dependent tensor must be invariant under the symmetry operations of a point group of a crystal applied to both the components of the tensor and their arguments. This may be regarded as an extension of Neumann's principle to the field dependent tensors. The phenomenological coefficients (or transport tensors): $\rho_{ij}(\vec{B})$, $\alpha_{ij}(\vec{B})$, $\pi_{ij}(\vec{B})$, $\gamma_{ij}(\vec{B})$ and their inverses are magnetic field dependent second rank polar tensors. The field dependent transformation law for $\rho_{ij}(\vec{B})$ is

$$\rho_{ij}(|R|R_{1q}B_q, |R|R_{2q}B_q, |R|R_{3q}B_q) = R_{im}R_{jn}\rho_{mn}(B_1, B_2, B_3) \quad (3.61)$$

where $|R|$ is the determinant of the 3x3 matrix representing a symmetry operation of the crystal point group. The same transformation equation applies to the other transport tensors and their inverses. Since the magnetic induction is an axial vector, its components transform as

$$B_i = |R| R_{ij}B_j. \quad (3.62)$$

3.5.3 Crystal symmetry restrictions on the form of the transport tensors - the magnetoresistivity tensor $\rho_{ij}(\vec{B})$.

Since a centre of inversion leaves (3.62) invariant, it may be added to the existing space symmetry. Therefore, we need consider only those 11 point groups involving proper rotations alone: the symmetry restrictions reduce to those imposed by the enantiomorphous groups, which are obtained from the space group by replacement of every translation by the identity and every improper rotation by its proper counterpart. The symmetry elements of the enantiomorphous point groups are listed in Table (3.4).

As a reference frame a right handed orthogonal axial set is chosen, adjusted to each of the 32 point groups by taking the z-axis along the rotation axis or rotation-inversion axis of highest order (an exception is the pair of cubic point groups 23 and $\frac{2}{m}\bar{3}$ for which the z-axis is taken along a twofold axis). In this choice of an (x,y,z) orthogonal axial set we follow Nye (1960) page 282 (he writes x_1, x_2, x_3) except that we take the first setting of the monoclinic point groups $2, m, 2/m$ given in the International Tables for X-ray Crystallography (1952). The symmetry elements, which are represented as 3×3 unitary matrices referred to these axial sets are subscripted x,y,z (with the usual exception of the trigonal and hexagonal point groups in which z// C_3 or C_6 , x// C'_2 , y completes the orthogonal right handed set - for Laue group $6/mmm$ the y axis is parallel to C''_2) in

the convention adopted by Bradley and Cracknell (1972); $m = x, y, z$; $j = 1, 2, 3, 4$; $p = a, b, c, d, e, f$. For rotations we use the passive convention, that is bodies (here crystals) are fixed, the axes are rotated - anticlockwise and clockwise rotations are represented by + and - superscripts respectively. It is not always necessary to use all the symmetry elements of the enantiomorphous group to secure maximum simplification of the transport tensors: a set of generating elements suffices. Previously, Birss (1966) has listed the generating elements for constant tensors. Here in table (3.4) we list the generating elements required to find the effect of spatial symmetry on the magnetic field dependent transport tensors; to find these generating elements, the following rules have been used in sequence:

(i) The identity element E is neglected because it brings no simplification.

(ii) Those symmetry elements that leave the magnetic induction or one of its components invariant are chosen; the only exception to this rule is that we add the element C_{31}^+ (which, when applied, yields interrelations between tensor components) to the generating elements of the cubic point groups.

(iii) Any two perpendicular two-fold axes require a third perpendicular to both of them. Therefore, when there are three mutually perpendicular two-fold symmetry elements successive application of any two of them will give the result of the third: we are able to neglect any one.

(iv) For n -fold rotations where $n > r$ (r is the rank of the tensor under consideration — 2 for transport tensors), application of one symmetry element for which $n > r$ is enough (Hermann 1934). For example, the point group C_6 contains four rotations (namely C_3^+ , C_6^+) about the z -axis for which $n > 2$ which are consistent with (ii). Therefore, we need choose one only; our choice is C_3^+ (see Table 3.4).

As these rules suggest, it is possible to make several different choices for a complete set of the generating elements provided that the number of them stays the same. Multiplication of two or more generating elements in a set does not yield a member of that particular set.

By successive multiplication of the generating elements in a particular set, by themselves or with each other, it is possible to obtain all the elements of the associated enantiomorphous point group.

The spatial symmetry restricted forms of $\rho_{1j}(\vec{B})$ have been constructed by systematic substitution into equation (3.61) and (3.62) of the generating elements (in their matrix representation) taken in turn followed by application of the Onsager relation (3.59). The components of $\rho_{1j}(\vec{B})$, obtained when the magnetic field is directed along the x, y and z axes (we write 1,2,3 for x, y, z respectively) in turn, are listed for all 32 crystallographic point groups in Table (3.5). Each tensor component is separated into "even" and "odd" parts in the magnetic induction \vec{B} . The theoretical and practical consequences of this separation will

be discussed in the next chapter. Now let us find the form taken by $\rho_{1j}(\vec{B})$ in the point group $\bar{3}m$.

From table (3.4):

the enantiomorphous point group is 32 (or D_3),

the generating elements are C_3^+ and C_{21}' .

Note that the rest of the symmetry elements of the enantiomorphous point group 32(D_3) may be obtained by multiplication as

$$\begin{aligned} C_3^+ C_3^+ C_3^+ &= E & C_3^+ C_{21}' &= C_{22}' \\ C_3^+ C_3^+ &= C_3^- & C_3^+ C_3^+ C_{21}' &= C_{23}' \end{aligned} \quad (3.63)$$

The matrix forms of C_3^+ and C_{21}' are given in table (3.1).

Substitution of C_3^+ into equation (3.62) yields

$$\begin{pmatrix} -\frac{1}{2} & \frac{\sqrt{3}}{2} & 0 \\ \frac{\sqrt{3}}{2} & -\frac{1}{2} & 0 \\ 0 & 0 & 1 \end{pmatrix} \begin{pmatrix} B_1 \\ B_2 \\ B_3 \end{pmatrix} = \begin{pmatrix} -\frac{1}{2}B_1 + \frac{\sqrt{3}}{2}B_2 \\ -\frac{\sqrt{3}}{2}B_1 - \frac{1}{2}B_2 \\ B_3 \end{pmatrix} \quad (3.64)$$

Similarly C_{21}' yields

$$\begin{pmatrix} 1 & 0 & 0 \\ 0 & -1 & 0 \\ 0 & 0 & -1 \end{pmatrix} \begin{pmatrix} B_1 \\ B_2 \\ B_3 \end{pmatrix} = \begin{pmatrix} B_1 \\ -B_2 \\ -B_3 \end{pmatrix} \quad (3.65)$$

First, let us find the effect of C_3^+ on the form of

$\rho_{1j}(0,0,B_3)$ [or in short $\rho_{1j}(B_3)$].

From equation (3.64) $B_3 \rightarrow B_3$ under C_3^+ operation.

Using this and the matrix form of C_3^+ in equation (3.61),

the following nine equalities for $\rho_{ij}(B_3)$ are obtained.

$$\begin{aligned} \rho_{11}(B_3) &= R_{11}R_{11} \rho_{11}(B_3) + R_{11}R_{12} \rho_{12}(B_3) + R_{12}R_{11} \rho_{21}(B_3) + \\ &+ R_{12}R_{12} \rho_{22}(B_3) = \\ &= \frac{1}{4} \rho_{11}(B_3) - \frac{\sqrt{3}}{4} \rho_{12}(B_3) - \frac{\sqrt{3}}{4} \rho_{21}(B_3) + \frac{3}{4} \rho_{22}(B_3). \end{aligned} \quad (a)$$

Similarly

$$\rho_{22}(B_3) = \frac{3}{4} \rho_{11}(B_3) + \frac{\sqrt{3}}{4} \rho_{12}(B_3) + \frac{\sqrt{3}}{4} \rho_{21}(B_3) + \frac{1}{4} \rho_{22}(B_3) \quad (b)$$

$$\rho_{33}(B_3) = \rho_{33}(B_3) \quad (c)$$

$$\rho_{12}(B_3) = \frac{\sqrt{3}}{4} \rho_{11}(B_3) - \frac{3}{4} \rho_{21}(B_3) + \frac{1}{4} \rho_{12}(B_3) - \frac{\sqrt{3}}{4} \rho_{22}(B_3) \quad (d)$$

$$\rho_{21}(B_3) = \frac{\sqrt{3}}{4} \rho_{11}(B_3) - \frac{3}{4} \rho_{12}(B_3) + \frac{1}{4} \rho_{21}(B_3) - \frac{\sqrt{3}}{4} \rho_{22}(B_3) \quad (e)$$

$$\rho_{13}(B_3) = -\frac{1}{2} \rho_{13}(B_3) + \frac{\sqrt{3}}{2} \rho_{23}(B_3) \quad (f)$$

$$\rho_{31}(B_3) = -\frac{1}{2} \rho_{31}(B_3) + \frac{\sqrt{3}}{2} \rho_{32}(B_3) \quad (g)$$

$$\rho_{23}(B_3) = -\frac{\sqrt{3}}{2} \rho_{13}(B_3) - \frac{1}{2} \rho_{23}(B_3) \quad (h)$$

$$\rho_{32}(B_3) = -\frac{\sqrt{3}}{2} \rho_{31}(B_3) - \frac{1}{2} \rho_{32}(B_3). \quad (i)$$

From equation (f) and (h) $\rho_{13}(B_3) = \rho_{23}(B_3) = 0$

From equation (g) and (i) $\rho_{31}(B_3) = \rho_{32}(B_3) = 0$

From equations (a), (b), (d), and (e)

$$\rho_{12}(B_3) = -\rho_{21}(B_3) \quad (3.66)$$

$$\rho_{11}(B_3) = \rho_{22}(B_3). \quad (3.67)$$

The effect of C_3^+ on $\rho_{1j}(B_1)$ and $\rho_{1j}(B_2)$ brings no simplification.

Now let us find the effect of C_{21}^i on the form of $\rho_{1j}(B_1)$. From equation (3.65) $B_1 \rightarrow B_1$ under the operation C_{21}^i . Again using $(B_1 \rightarrow B_1)$ and the matrix form of C_{21}^i in equation (3.61), the following nine equalities are obtained.

$$\left. \begin{aligned} \rho_{11}(B_1) &= \rho_{11}(B_1) \\ \rho_{22}(B_1) &= \rho_{22}(B_1) \\ \rho_{33}(B_1) &= \rho_{33}(B_1) \end{aligned} \right\} \text{No simplification.} \quad (3.68)$$

$$\rho_{12}(B_1) = -\rho_{12}(B_1) \quad \therefore \quad \rho_{12}(B_1) = 0$$

$$\rho_{21}(B_1) = -\rho_{21}(B_1) \quad \therefore \quad \rho_{21}(B_1) = 0$$

$$\rho_{13}(B_1) = -\rho_{13}(B_1) \quad \therefore \quad \rho_{13}(B_1) = 0$$

$$\rho_{31}(B_1) = -\rho_{31}(B_1) \quad \therefore \quad \rho_{31}(B_1) = 0$$

$$\left. \begin{aligned} \rho_{23}(B_1) &= \rho_{23}(B_1) \\ \rho_{32}(B_1) &= \rho_{32}(B_1) \end{aligned} \right\} \text{both contain "even" and "odd" terms.} \quad (3.69)$$

Now we consider the effect of C_{21}^i on $\rho_{1j}(B_2)$.

From equation (3.65) $(B_2 \rightarrow -B_2)$; using this and the matrix form of C_{21}^i in equation (3.61), another nine equalities can be obtained as

$$\left. \begin{aligned} \rho_{11}(-B_2) &= \rho_{11}(B_2) \\ \rho_{22}(-B_2) &= \rho_{22}(B_2) \\ \rho_{33}(-B_2) &= \rho_{33}(B_2) \end{aligned} \right\} \text{all "even" in } B_2. \quad (3.70)$$

$$\left. \begin{aligned} \rho_{12}(-B_2) &= -\rho_{12}(B_2) \\ \rho_{21}(-B_2) &= -\rho_{21}(B_2) \\ \rho_{13}(-B_2) &= -\rho_{13}(B_2) \\ \rho_{31}(-B_2) &= -\rho_{31}(B_2) \end{aligned} \right\} \text{all "odd" in } B_2. \quad (3.71)$$

$$\left. \begin{aligned} \rho_{23}(-B_2) &= \rho_{23}(B_2) \\ \rho_{32}(-B_2) &= \rho_{32}(B_2) \end{aligned} \right\} \text{both are "even" in } B_2. \quad (3.72)$$

Finally, let us find the effect of C_{21}^i on $\rho_{ij}(B_3)$.

From equation (3.65) $B_3 \rightarrow -B_3$; using this and the matrix form of C_{21}^i in equation (3.61) yields

$$\left. \begin{aligned} \rho_{11}(-B_3) &= \rho_{11}(B_3) \\ \rho_{22}(-B_3) &= \rho_{22}(B_3) \\ \rho_{33}(-B_3) &= \rho_{33}(B_3) \end{aligned} \right\} \text{all "even" in } B_3. \quad (3.73)$$

$$\left. \begin{aligned} \rho_{12}(-B_3) &= -\rho_{12}(B_3) \\ \rho_{21}(-B_3) &= -\rho_{21}(B_3) \end{aligned} \right\} \text{both "odd" in } B_3. \quad (3.74)$$

From equations (3.66) and (3.74)

$$\rho_{12}(B_3) = -\rho_{21}(B_3). \quad (3.75)$$

Now the form of $\rho_{1j}(B_1)$ can be written from equations (3.68) and (3.69); the form of $\rho_{1j}(B_2)$ from equations (3.70), (3.71) and (3.72); and that of $\rho_{1j}(B_3)$ from equations (3.67), (3.73) and (3.75).

The final forms of $\rho_{1j}(B_1)$, $\rho_{1j}(B_2)$ and $\rho_{1j}(B_3)$ can be obtained by application of the Onsager relation (equation 3.59) to equations (3.67) to (3.75) and are given in table (3.5). The dot notation used is that of Nye (1960) who has given a large number of those physical properties which can be represented by constant tensors. We list — in addition to the form of $\rho_{1j}(\vec{B})$ — interrelations between the tensor components which occur in the tetragonal and cubic point groups. These relations come out in the application of the generating elements; in the cubic point groups application of the symmetry element C_{31}^+ alone yields the relations.

For the point groups (422, 4mm, $\bar{4}2m$, 4/mmm) there is an alternative setting of the x and y axes, i.e. x// C_{2a} //[110] and y// C_{2b} // $[\bar{1}10]$; $\rho_{1j}(\vec{B})$ takes the same form for both the original and this new orthogonal set.

In general, it is always possible for any crystal to define orthogonal axial sets other than the conventional crystallographic axes. To obtain the reconstructed form of $\rho_{1j}(\vec{B})$, it is necessary only to find the symmetry elements of the new axes themselves and then look for the enantiomorphous point group with the same symmetry in

table (3.5). The new form that $\rho_{1j}(\bar{B})$ takes is then that of this lower symmetry point group. A practical use of this general result is that, when the components of $\rho_{1j}(\bar{B})$ are to be measured in a sample obtainable in a specific direction other than one of the conventional crystallographic axes, the appropriate form of $\rho_{1j}(\bar{B})$ and its non-zero components can readily be found—a useful guide to the experimentalist. The procedure is best clarified by examples.

(i) For the cubic point groups 23 and $\frac{2}{m}\bar{3}$, another right handed orthogonal axial set—with the $z(3)$ -axis taken in the $C_{31}^+ // [111]$ direction and an arbitrary choice of x and y axes—can also be chosen, the form of $\rho_{1j}(\bar{B})$ is then the same as that for the enantiomorphous group 3 ; in table (3.5) we have given the form of $\rho_{1j}(\bar{B})$ referred to this second axial set.

(ii) For the other cubic groups 432 , $\bar{4}3m$ and $\frac{4}{m}\bar{3}\frac{2}{m}$, a second axial set that can be chosen as $x // C_{2b} // [1\bar{1}0]$, $y // [11\bar{2}]$, $z // C_{31}^+ // [111]$; the appropriate form of $\rho_{1j}(\bar{B})$ (now identical to that for the point group 32 ; inspection of the symmetry elements given in table (3.4) for the point group 432 shows that the elements of 32 are contained in them) is also given in table (3.5). This form of $\rho_{1j}(\bar{B})$ is of interest to us because the Umkehr effect can in principle be observed in a suitable sample having this configuration; this point will be discussed in chapter 5.

In general to measure a component $\rho_{ij}(B_1, B_2, B_3)$ in the nomenclature of Table (3.5) one would cut a rectangular parallelepiped sample, pass a current along the long direction j and measure the voltage developed in the i direction; the magnetic field can be applied along any direction 1, 2 or 3 or if the orientation dependence is required the magnetic field can be taken stepwise around a plane (see Akgoz and Saunders 1974 for a specific example). The magnetothermal conductivity tensor $K_{ij}(\vec{B})$ takes the same form as $\rho_{ij}(\vec{B})$ and to obtain the components a similar experimental configuration can be used.

3.5.4. Crystal symmetry restrictions on the forms of the transport tensors - the magnetothermoelectric power tensor $\alpha_{ij}(\vec{B})$.

Although $\alpha_{ij}(\vec{B})$ and $\rho_{ij}(\vec{B})$ are second rank magnetic field dependent tensors, they differ in that the Onsager relations relate a component of $\rho_{ij}(\vec{B})$ to another component of the same tensor (equation 3.59); for $\alpha_{ij}(\vec{B})$, the Onsager relations relate a component of $\alpha_{ij}(\vec{B})$ to a component of $\pi_{ij}(\vec{B})$ (see equation 3.60) and do not impose any restrictions on the form of $\alpha_{ij}(\vec{B})$. Thus, with the exception of the restrictions imposed by the Onsager relation (equation 3.59), the forms taken by $\alpha_{ij}(\vec{B})$ can be obtained by using the same procedure as the one described for $\rho_{ij}(\vec{B})$ in the previous section. The relation (equation 3.60) can only be used to find the form of $\pi_{ij}(\vec{B})$ when the

form of $\alpha_{ij}(\vec{B})$ is known and vice versa.

In table (3.6), we give the forms taken by $\alpha_{ij}(\vec{B})$ for each 32 crystallographic point groups. Here the full forms of "even" and "odd" parts of $\alpha_{ij}(\vec{B})$ are given, whereas in table (3.5) half of the "even" and "odd" parts are given only. This is because the "even" and "odd" parts of $\rho_{ij}(\vec{B})$ are symmetric and antisymmetric in the indices i and j respectively; but this is not so for $\alpha_{ij}(\vec{B})$.

3.5.5 The Umkehr Effect.

One clear and direct result can be obtained from tables (3.5) and (3.6) - a phenomenological explanation of the so-called Umkehr effect which is usually thought to be an anomalous effect. Experimentally the existence of this effect in $\alpha_{ij}(\vec{B})$ has been well established: for certain crystallographic directions in bismuth a different magnetothermoelectric voltage has been measured by reversing the sense of the applied magnetic field (see, for example, Gruneisen and Gielessen 1936; Smith et al 1964; Gitsu et al 1970; Michenaud et al 1970; Sumengen and Saunders 1972a). Inspection of tables (3.5) and (3.6) shows that the Umkehr effect is to be expected in any component of $\rho_{ij}(\vec{B})$ or $\alpha_{ij}(\vec{B})$ which contains both "even" and "odd" terms. Due to the Onsager relations (equation 3.59), the diagonal components of $\rho_{ij}(\vec{B})$ and $K_{ij}(\vec{B})$ must be "even" functions of \vec{B} ; thus only the off-diagonal

components can contain both "even" and "odd" terms. But for $\alpha_{ij}(\vec{B})$ and $\pi_{ij}(\vec{B})$ there is no such restriction: "even" and "odd" terms can exist in the diagonal components as well. In fact the observation of an Umkehr effect in a diagonal component $\alpha_{ii}(B_1)$ seems to be the origin of the concept of the Umkehr effect as an anomalous phenomenon. We conclude that the Umkehr effect can appear in any component of the magnetic field dependent transport tensors which contains both "even" and "odd" terms and it is a natural result of the anisotropy of crystals.

TABLE(3.4): GENERATING SYMMETRY ELEMENTS FOR THE MAGNETIC FIELD DEPENDENT TRANSPORT TENSORS

Point groups (International symbol)	Enantiomorphous point group	Symmetry elements of the enantio- morphous point group	Generating elements
$1, \bar{1}$	$1(C_1)$	E	no element
$2, m, 2/m$	$2(C_2)$	E C_{2z}	C_{2z}
$222, mm2, mmm$	$222(D_2)$	E $C_{2z} C_{2x} C_{2y}$	$C_{2z} C_{2x}$
$4, \bar{4}, 4/m$	$4(C_4)$	E $C_{4z}^+ C_{2z}$	$C_{4z}^+ C_{2z}$
$422, 4mm, \bar{4}2m,$ $4/mmm$	$422(D_4)$	E $C_{4z}^+ C_{2z} C_{2x}$ $C_{2y} C_{2a} C_{2b}$	$C_{4z}^+ C_{2z} C_{2x}$
$3, \bar{3}$	$3(C_3)$	E C_3^+	C_3^+
$32, 3m, \bar{3}m$	$32(D_3)$	E $C_3^+ C_{2i}^+$	$C_3^+ C_{2i}^+$
$6, \bar{6}, 6/m$	$6(C_6)$	E $C_6^+ C_3^+ C_2$	$C_3^+ C_2$
$622, 6mm, \bar{6}m2,$ $6/mmm$	$622(D_6)$	E $C_6^+ C_3^+ C_2$ $C_{2i}^+ C_{2i}''$	$C_3^+ C_2 C_{2i}^+$
$23, \frac{2}{m} \bar{3}$	$23(T)$	E $C_{2m} C_{3j}^+$	$C_{2z} C_{2x} C_{31}^+$
$432, \bar{4}3m, \frac{4}{m} \bar{3} \frac{2}{m}$	$432(O)$	E $C_{2m} C_{3j}^+$ $C_{4m}^+ C_{2p}$	$C_{2z} C_{2x}$ $C_{4m}^+ C_{31}^+$

TABLE(3.5): SPACE-TIME SYMMETRY RESTRICTED FORMS OF THE MAGNETORESISTIVITY TENSOR $\rho_{ij}(\vec{B})$ IN THE 32 CRYSTALLOGRAPHIC POINT GROUPS.

KEY TO NOTATION

- . zero component
 - non-zero component
 - equal components.
- All even parts and odd parts are symmetric and antisymmetric about their leading diagonals respectively.

(1, $\bar{1}$)

	EVEN	+	ODD
$\rho_{ij}(B_1) =$	$\begin{pmatrix} \bullet & \bullet & \bullet \\ & \bullet & \bullet \\ & & \bullet \end{pmatrix}$		$\begin{pmatrix} \cdot & \bullet & \bullet \\ & \cdot & \bullet \\ & & \cdot \end{pmatrix}$
$\rho_{ij}(B_2) =$	$\begin{pmatrix} \bullet & \bullet & \bullet \\ & \bullet & \bullet \\ & & \bullet \end{pmatrix}$		$\begin{pmatrix} \cdot & \bullet & \bullet \\ & \cdot & \bullet \\ & & \cdot \end{pmatrix}$
$\rho_{ij}(B_3) =$	$\begin{pmatrix} \bullet & \bullet & \bullet \\ & \bullet & \bullet \\ & & \bullet \end{pmatrix}$		$\begin{pmatrix} \cdot & \bullet & \bullet \\ & \cdot & \bullet \\ & & \cdot \end{pmatrix}$

(2, m, 2/m)

	EVEN	+	ODD
$\rho_{ij}(B_1) =$	$\begin{pmatrix} \bullet & \bullet & \cdot \\ & \bullet & \cdot \\ & & \bullet \end{pmatrix}$		$\begin{pmatrix} \cdot & \cdot & \bullet \\ & \cdot & \bullet \\ & & \cdot \end{pmatrix}$
$\rho_{ij}(B_2) =$	$\begin{pmatrix} \bullet & \bullet & \cdot \\ & \bullet & \cdot \\ & & \bullet \end{pmatrix}$		$\begin{pmatrix} \cdot & \cdot & \bullet \\ & \cdot & \bullet \\ & & \cdot \end{pmatrix}$
$\rho_{ij}(B_3) =$	$\begin{pmatrix} \bullet & \bullet & \cdot \\ & \bullet & \cdot \\ & & \bullet \end{pmatrix}$		$\begin{pmatrix} \cdot & \bullet & \cdot \\ & \cdot & \cdot \\ & & \cdot \end{pmatrix}$

(222, mm2, mmm)

	EVEN	+	ODD
$\rho_{ij}(B_1) =$	$\begin{pmatrix} \bullet & \cdot & \cdot \\ & \bullet & \cdot \\ & & \bullet \end{pmatrix}$		$\begin{pmatrix} \cdot & \cdot & \cdot \\ & \cdot & \bullet \\ & & \cdot \end{pmatrix}$
$\rho_{ij}(B_2) =$	$\begin{pmatrix} \bullet & \cdot & \cdot \\ & \bullet & \cdot \\ & & \bullet \end{pmatrix}$		$\begin{pmatrix} \cdot & \cdot & \bullet \\ & \cdot & \cdot \\ & & \cdot \end{pmatrix}$
$\rho_{ij}(B_3) =$	$\begin{pmatrix} \bullet & \cdot & \cdot \\ & \bullet & \cdot \\ & & \bullet \end{pmatrix}$		$\begin{pmatrix} \cdot & \bullet & \cdot \\ & \cdot & \cdot \\ & & \cdot \end{pmatrix}$

$(4, \bar{4}, 4/m)$

$(422, 4mm, \bar{4}2m, 4/mmm)$

$$\rho_{ij}(B_1) = \begin{matrix} \text{EVEN} & & \text{ODD} \\ \left(\begin{array}{ccc} \bullet & \bullet & \cdot \\ & \bullet & \cdot \\ & & \bullet \end{array} \right) & + & \left(\begin{array}{ccc} \cdot & \cdot & \bullet \\ & \cdot & \bullet \\ & & \cdot \end{array} \right) \end{matrix}$$

$$\rho_{ij}(B_2) = \begin{matrix} \text{EVEN} & & \text{ODD} \\ \left(\begin{array}{ccc} \bullet & \bullet & \cdot \\ & \bullet & \cdot \\ & & \bullet \end{array} \right) & + & \left(\begin{array}{ccc} \cdot & \cdot & \bullet \\ & \cdot & \bullet \\ & & \cdot \end{array} \right) \end{matrix}$$

$$\rho_{ij}(B_3) = \begin{matrix} \text{EVEN} & & \text{ODD} \\ \left(\begin{array}{ccc} \bullet & \cdot & \cdot \\ & \bullet & \cdot \\ & & \bullet \end{array} \right) & + & \left(\begin{array}{ccc} \cdot & \bullet & \cdot \\ & \cdot & \cdot \\ & & \cdot \end{array} \right) \end{matrix}$$

$$\rho_{ij}(B_1) = \begin{matrix} \text{EVEN} & & \text{ODD} \\ \left(\begin{array}{ccc} \bullet & \cdot & \cdot \\ & \bullet & \cdot \\ & & \bullet \end{array} \right) & + & \left(\begin{array}{ccc} \cdot & \cdot & \cdot \\ & \cdot & \bullet \\ & & \cdot \end{array} \right) \end{matrix}$$

$$\rho_{ij}(B_2) = \begin{matrix} \text{EVEN} & & \text{ODD} \\ \left(\begin{array}{ccc} \bullet & \cdot & \cdot \\ & \bullet & \cdot \\ & & \bullet \end{array} \right) & + & \left(\begin{array}{ccc} \cdot & \cdot & \bullet \\ & \cdot & \cdot \\ & & \cdot \end{array} \right) \end{matrix}$$

$$\rho_{ij}(B_3) = \begin{matrix} \text{EVEN} & & \text{ODD} \\ \left(\begin{array}{ccc} \bullet & \cdot & \cdot \\ & \bullet & \cdot \\ & & \bullet \end{array} \right) & + & \left(\begin{array}{ccc} \cdot & \bullet & \cdot \\ & \cdot & \cdot \\ & & \cdot \end{array} \right) \end{matrix}$$

When $B_1 = B_2 = B_3$, the following interrelations between tensor components hold:

EVEN

$$\rho_{11}(B_1) = \rho_{22}(B_2)$$

$$\rho_{22}(B_1) = \rho_{11}(B_2)$$

$$\rho_{33}(B_1) = \rho_{33}(B_2)$$

$$\rho_{12}(B_1) = -\rho_{12}(B_2)$$

ODD

$$\rho_{13}(B_1) = \rho_{23}(B_2)$$

$$\rho_{23}(B_1) = -\rho_{13}(B_2)$$

When $B_1 = B_2 = B_3$, the following interrelations between tensor components hold:

EVEN

$$\rho_{11}(B_1) = \rho_{22}(B_2)$$

$$\rho_{22}(B_1) = \rho_{11}(B_2)$$

$$\rho_{33}(B_1) = \rho_{33}(B_2)$$

ODD

$$\rho_{23}(B_1) = -\rho_{13}(B_2)$$

$(23, \frac{2}{m} \bar{3})$

	EVEN	+	ODD
$\rho_{ij}(B_1) =$	$\begin{pmatrix} \bullet & \cdot & \cdot \\ & \bullet & \cdot \\ & & \bullet \end{pmatrix}$		$\begin{pmatrix} \cdot & \cdot & \cdot \\ & \cdot & \bullet \\ & & \cdot \end{pmatrix}$
$\rho_{ij}(B_2) =$	$\begin{pmatrix} \bullet & \cdot & \cdot \\ & \bullet & \cdot \\ & & \bullet \end{pmatrix}$		$\begin{pmatrix} \cdot & \cdot & \bullet \\ & \cdot & \cdot \\ & & \cdot \end{pmatrix}$
$\rho_{ij}(B_3) =$	$\begin{pmatrix} \bullet & \cdot & \cdot \\ & \bullet & \cdot \\ & & \bullet \end{pmatrix}$		$\begin{pmatrix} \cdot & \bullet & \cdot \\ & \cdot & \cdot \\ & & \cdot \end{pmatrix}$

When $B_1=B_2=B_3$, the following interrelations between tensor components hold:

EVEN

$\rho_{11}(B_1) = \rho_{22}(B_2) = \rho_{33}(B_3)$
 $\rho_{22}(B_1) = \rho_{33}(B_2) = \rho_{11}(B_3)$
 $\rho_{33}(B_1) = \rho_{11}(B_2) = \rho_{22}(B_3)$

ODD

$\rho_{23}(B_1) = -\rho_{13}(B_2) = \rho_{12}(B_3)$

 Referred to the orthogonal axial set:
 $z//C_{31}^+//[111], x$ and y arbitrary,
 the form of $\rho_{ij}(\vec{B})$ is

	EVEN	+	ODD
$\rho_{ij}(B_1) =$	$\begin{pmatrix} \bullet & \bullet & \bullet \\ & \bullet & \bullet \\ & & \bullet \end{pmatrix}$		$\begin{pmatrix} \cdot & \bullet & \bullet \\ & \cdot & \bullet \\ & & \cdot \end{pmatrix}$
$\rho_{ij}(B_2) =$	$\begin{pmatrix} \bullet & \bullet & \bullet \\ & \bullet & \bullet \\ & & \bullet \end{pmatrix}$		$\begin{pmatrix} \cdot & \bullet & \bullet \\ & \cdot & \bullet \\ & & \cdot \end{pmatrix}$
$\rho_{ij}(B_3) =$	$\begin{pmatrix} \bullet & \cdot & \cdot \\ & \bullet & \cdot \\ & & \bullet \end{pmatrix}$		$\begin{pmatrix} \cdot & \bullet & \cdot \\ & \cdot & \cdot \\ & & \cdot \end{pmatrix}$

$(432, \bar{4}3m, \frac{4}{m} \bar{3} \frac{2}{m})$

	EVEN	+	ODD
$\rho_{ij}(B_1) =$	$\begin{pmatrix} \bullet & \cdot & \cdot \\ & \bullet & \cdot \\ & & \bullet \end{pmatrix}$		$\begin{pmatrix} \cdot & \cdot & \cdot \\ & \cdot & \bullet \\ & & \cdot \end{pmatrix}$
$\rho_{ij}(B_2) =$	$\begin{pmatrix} \bullet & \cdot & \cdot \\ & \bullet & \cdot \\ & & \bullet \end{pmatrix}$		$\begin{pmatrix} \cdot & \cdot & \bullet \\ & \cdot & \cdot \\ & & \cdot \end{pmatrix}$
$\rho_{ij}(B_3) =$	$\begin{pmatrix} \bullet & \cdot & \cdot \\ & \bullet & \cdot \\ & & \bullet \end{pmatrix}$		$\begin{pmatrix} \cdot & \bullet & \cdot \\ & \cdot & \cdot \\ & & \cdot \end{pmatrix}$

When $B_1=B_2=B_3$, the following interrelations between tensor components hold:

EVEN

$\rho_{11}(B_1) = \rho_{22}(B_2) = \rho_{33}(B_3)$
 $\rho_{22}(B_1) = \rho_{11}(B_2) = \rho_{11}(B_3)$

ODD

$\rho_{23}(B_1) = -\rho_{13}(B_2) = \rho_{12}(B_3)$

 Referred to the orthogonal axial set:
 $x//C_{2b}//[1\bar{1}0], y//[11\bar{2}], z//C_{31}^+//[111],$
 the form of $\rho_{ij}(\vec{B})$ is

	EVEN	+	ODD
$\rho_{ij}(B_1) =$	$\begin{pmatrix} \bullet & \cdot & \cdot \\ & \bullet & \bullet \\ & & \bullet \end{pmatrix}$		$\begin{pmatrix} \cdot & \cdot & \cdot \\ & \cdot & \bullet \\ & & \cdot \end{pmatrix}$
$\rho_{ij}(B_2) =$	$\begin{pmatrix} \bullet & \cdot & \cdot \\ & \bullet & \bullet \\ & & \bullet \end{pmatrix}$		$\begin{pmatrix} \cdot & \bullet & \bullet \\ & \cdot & \cdot \\ & & \cdot \end{pmatrix}$
$\rho_{ij}(B_3) =$	$\begin{pmatrix} \bullet & \cdot & \cdot \\ & \bullet & \cdot \\ & & \bullet \end{pmatrix}$		$\begin{pmatrix} \cdot & \bullet & \cdot \\ & \cdot & \cdot \\ & & \cdot \end{pmatrix}$

TABLE (3.6) : SPATIAL SYMMETRY RESTRICTED FORMS OF THE
MAGNETOTHERMOELECTRIC POWER TENSOR $\alpha_{ij}(\vec{B})$ IN THE
32 CRYSTALLOGRAPHIC POINT GROUPS.

KEY TO NOTATION

- . zero component
- non-zero component
- equal components
- components numerically equal, but opposite in sign.

(1, $\bar{1}$)

	EVEN	+	ODD
$\alpha_{ij}(B_1) =$	$\begin{pmatrix} \bullet & \bullet & \bullet \\ \bullet & \bullet & \bullet \\ \bullet & \bullet & \bullet \end{pmatrix}$		$\begin{pmatrix} \bullet & \bullet & \bullet \\ \bullet & \bullet & \bullet \\ \bullet & \bullet & \bullet \end{pmatrix}$
$\alpha_{ij}(B_2) =$	$\begin{pmatrix} \bullet & \bullet & \bullet \\ \bullet & \bullet & \bullet \\ \bullet & \bullet & \bullet \end{pmatrix}$		$\begin{pmatrix} \bullet & \bullet & \bullet \\ \bullet & \bullet & \bullet \\ \bullet & \bullet & \bullet \end{pmatrix}$
$\alpha_{ij}(B_3) =$	$\begin{pmatrix} \bullet & \bullet & \bullet \\ \bullet & \bullet & \bullet \\ \bullet & \bullet & \bullet \end{pmatrix}$		$\begin{pmatrix} \bullet & \bullet & \bullet \\ \bullet & \bullet & \bullet \\ \bullet & \bullet & \bullet \end{pmatrix}$

(2, m, 2/m)

	EVEN	+	ODD
$\alpha_{ij}(B_1) =$	$\begin{pmatrix} \bullet & \bullet & \cdot \\ \bullet & \bullet & \cdot \\ \cdot & \cdot & \bullet \end{pmatrix}$		$\begin{pmatrix} \cdot & \cdot & \bullet \\ \cdot & \cdot & \bullet \\ \bullet & \bullet & \cdot \end{pmatrix}$
$\alpha_{ij}(B_2) =$	$\begin{pmatrix} \bullet & \bullet & \cdot \\ \bullet & \bullet & \cdot \\ \cdot & \cdot & \bullet \end{pmatrix}$		$\begin{pmatrix} \cdot & \cdot & \bullet \\ \cdot & \cdot & \bullet \\ \bullet & \bullet & \cdot \end{pmatrix}$
$\alpha_{ij}(B_3) =$	$\begin{pmatrix} \bullet & \bullet & \cdot \\ \bullet & \bullet & \cdot \\ \cdot & \cdot & \bullet \end{pmatrix}$		$\begin{pmatrix} \bullet & \bullet & \cdot \\ \bullet & \bullet & \cdot \\ \cdot & \cdot & \bullet \end{pmatrix}$

(222, mm2, mmm)

	EVEN	+	ODD
$\alpha_{ij}(B_1) =$	$\begin{pmatrix} \bullet & \cdot & \cdot \\ \cdot & \bullet & \cdot \\ \cdot & \cdot & \bullet \end{pmatrix}$		$\begin{pmatrix} \cdot & \cdot & \cdot \\ \cdot & \cdot & \bullet \\ \cdot & \bullet & \cdot \end{pmatrix}$
$\alpha_{ij}(B_2) =$	$\begin{pmatrix} \bullet & \cdot & \cdot \\ \cdot & \bullet & \cdot \\ \cdot & \cdot & \bullet \end{pmatrix}$		$\begin{pmatrix} \cdot & \cdot & \bullet \\ \cdot & \cdot & \cdot \\ \bullet & \cdot & \cdot \end{pmatrix}$
$\alpha_{ij}(B_3) =$	$\begin{pmatrix} \bullet & \cdot & \cdot \\ \cdot & \bullet & \cdot \\ \cdot & \cdot & \bullet \end{pmatrix}$		$\begin{pmatrix} \cdot & \bullet & \cdot \\ \bullet & \cdot & \cdot \\ \cdot & \cdot & \cdot \end{pmatrix}$

$(4, \bar{4}, 4/m)$

$(422, 4mm, \bar{4}2m, 4/mmm)$

	EVEN		ODD
$\alpha_{ij}(B_1) =$	$\begin{pmatrix} \bullet & \bullet & \cdot \\ \bullet & \bullet & \cdot \\ \cdot & \cdot & \bullet \end{pmatrix}$	+	$\begin{pmatrix} \cdot & \cdot & \bullet \\ \cdot & \cdot & \bullet \\ \bullet & \bullet & \cdot \end{pmatrix}$
$\alpha_{ij}(B_2) =$	$\begin{pmatrix} \bullet & \bullet & \cdot \\ \bullet & \bullet & \cdot \\ \cdot & \cdot & \bullet \end{pmatrix}$	+	$\begin{pmatrix} \cdot & \cdot & \bullet \\ \cdot & \cdot & \bullet \\ \bullet & \bullet & \cdot \end{pmatrix}$
$\alpha_{ij}(B_3) =$	$\begin{pmatrix} \bullet & \bullet & \cdot \\ \bullet & \bullet & \cdot \\ \cdot & \cdot & \bullet \end{pmatrix}$	+	$\begin{pmatrix} \bullet & \bullet & \cdot \\ \bullet & \bullet & \cdot \\ \cdot & \cdot & \bullet \end{pmatrix}$

	EVEN		ODD
$\alpha_{ij}(B_1) =$	$\begin{pmatrix} \bullet & \cdot & \cdot \\ \cdot & \bullet & \cdot \\ \cdot & \cdot & \bullet \end{pmatrix}$	+	$\begin{pmatrix} \cdot & \cdot & \cdot \\ \cdot & \cdot & \bullet \\ \cdot & \bullet & \cdot \end{pmatrix}$
$\alpha_{ij}(B_2) =$	$\begin{pmatrix} \bullet & \cdot & \cdot \\ \cdot & \bullet & \cdot \\ \cdot & \cdot & \bullet \end{pmatrix}$	+	$\begin{pmatrix} \cdot & \cdot & \bullet \\ \cdot & \cdot & \cdot \\ \bullet & \cdot & \cdot \end{pmatrix}$
$\alpha_{ij}(B_3) =$	$\begin{pmatrix} \bullet & \cdot & \cdot \\ \cdot & \bullet & \cdot \\ \cdot & \cdot & \bullet \end{pmatrix}$	+	$\begin{pmatrix} \cdot & \cdot & \cdot \\ \cdot & \cdot & \cdot \\ \bullet & \cdot & \cdot \end{pmatrix}$

When $B_1=B_2=B_3$, the following interrelations between tensor components hold:

When $B_1=B_2=B_3$, the following interrelations between tensor components hold:

EVEN

$$\begin{aligned} \alpha_{11}(B_1) &= \alpha_{22}(B_2) \\ \alpha_{22}(B_1) &= \alpha_{11}(B_2) \\ \alpha_{33}(B_1) &= \alpha_{33}(B_2) \\ \alpha_{12}(B_1) &= -\alpha_{21}(B_2) \\ \alpha_{21}(B_1) &= -\alpha_{12}(B_2) \end{aligned}$$

EVEN

$$\begin{aligned} \alpha_{11}(B_1) &= \alpha_{22}(B_2) \\ \alpha_{22}(B_1) &= \alpha_{11}(B_2) \\ \alpha_{33}(B_1) &= \alpha_{33}(B_2) \end{aligned}$$

ODD

$$\begin{aligned} \alpha_{23}(B_1) &= -\alpha_{13}(B_2) \\ \alpha_{32}(B_1) &= -\alpha_{31}(B_2) \\ \alpha_{13}(B_1) &= \alpha_{23}(B_2) \\ \alpha_{31}(B_1) &= \alpha_{32}(B_2) \end{aligned}$$

ODD

$$\begin{aligned} \alpha_{23}(B_1) &= -\alpha_{13}(B_2) \\ \alpha_{32}(B_1) &= -\alpha_{31}(B_2) \end{aligned}$$

$(23, \frac{2}{m} \bar{3})$

	EVEN	+	ODD
$\alpha_{ij}(B_1) =$	$\begin{pmatrix} \bullet & \cdot & \cdot \\ \cdot & \bullet & \cdot \\ \cdot & \cdot & \bullet \end{pmatrix}$		$\begin{pmatrix} \cdot & \cdot & \cdot \\ \cdot & \cdot & \bullet \\ \cdot & \bullet & \cdot \end{pmatrix}$
$\alpha_{ij}(B_2) =$	$\begin{pmatrix} \bullet & \cdot & \cdot \\ \cdot & \bullet & \cdot \\ \cdot & \cdot & \bullet \end{pmatrix}$		$\begin{pmatrix} \cdot & \cdot & \bullet \\ \bullet & \cdot & \cdot \\ \cdot & \cdot & \cdot \end{pmatrix}$
$\alpha_{ij}(B_3) =$	$\begin{pmatrix} \bullet & \cdot & \cdot \\ \cdot & \bullet & \cdot \\ \cdot & \cdot & \bullet \end{pmatrix}$		$\begin{pmatrix} \cdot & \bullet & \cdot \\ \bullet & \cdot & \cdot \\ \cdot & \cdot & \cdot \end{pmatrix}$

When $B_1=B_2=B_3$, the following interrelations between tensor components hold:

EVEN

$$\alpha_{11}(B_1) = \alpha_{22}(B_2) = \alpha_{33}(B_3)$$

$$\alpha_{22}(B_1) = \alpha_{33}(B_2) = \alpha_{11}(B_3)$$

$$\alpha_{33}(B_1) = \alpha_{11}(B_2) = \alpha_{22}(B_3)$$

ODD

$$\alpha_{23}(B_1) = \alpha_{31}(B_2) = \alpha_{12}(B_3)$$

$$\alpha_{32}(B_1) = \alpha_{13}(B_2) = \alpha_{21}(B_3)$$

Referred to the orthogonal axial set: $z//C_{31}^+//[111]$, x and y arbitrary, the form of $\alpha_{ij}(\vec{B})$ is

	EVEN	+	ODD
$\alpha_{ij}(B_1) =$	$\begin{pmatrix} \bullet & \bullet & \bullet \\ \bullet & \bullet & \bullet \\ \bullet & \bullet & \bullet \end{pmatrix}$		$\begin{pmatrix} \bullet & \bullet & \bullet \\ \bullet & \bullet & \bullet \\ \bullet & \bullet & \bullet \end{pmatrix}$
$\alpha_{ij}(B_2) =$	$\begin{pmatrix} \bullet & \bullet & \bullet \\ \bullet & \bullet & \bullet \\ \bullet & \bullet & \bullet \end{pmatrix}$		$\begin{pmatrix} \bullet & \bullet & \bullet \\ \bullet & \bullet & \bullet \\ \bullet & \bullet & \bullet \end{pmatrix}$
$\alpha_{ij}(B_3) =$	$\begin{pmatrix} \bullet & \bullet & \cdot \\ \bullet & \bullet & \cdot \\ \cdot & \cdot & \bullet \end{pmatrix}$		$\begin{pmatrix} \bullet & \bullet & \cdot \\ \bullet & \bullet & \cdot \\ \cdot & \cdot & \bullet \end{pmatrix}$

$(432, \bar{4}3m, \frac{4}{m} \bar{3} \frac{2}{m})$

	EVEN	+	ODD
$\alpha_{ij}(B_1) =$	$\begin{pmatrix} \bullet & \cdot & \cdot \\ \cdot & \bullet & \cdot \\ \cdot & \cdot & \bullet \end{pmatrix}$		$\begin{pmatrix} \cdot & \cdot & \cdot \\ \cdot & \cdot & \bullet \\ \cdot & \bullet & \cdot \end{pmatrix}$
$\alpha_{ij}(B_2) =$	$\begin{pmatrix} \bullet & \cdot & \cdot \\ \cdot & \bullet & \cdot \\ \cdot & \cdot & \bullet \end{pmatrix}$		$\begin{pmatrix} \cdot & \cdot & \bullet \\ \bullet & \cdot & \cdot \\ \cdot & \cdot & \cdot \end{pmatrix}$
$\alpha_{ij}(B_3) =$	$\begin{pmatrix} \bullet & \cdot & \cdot \\ \cdot & \bullet & \cdot \\ \cdot & \cdot & \bullet \end{pmatrix}$		$\begin{pmatrix} \cdot & \bullet & \cdot \\ \bullet & \cdot & \cdot \\ \cdot & \cdot & \cdot \end{pmatrix}$

When $B_1=B_2=B_3$, the following relations between inter-tensor components hold:

EVEN

$$\alpha_{11}(B_1) = \alpha_{22}(B_2) = \alpha_{33}(B_3)$$

$$\alpha_{22}(B_1) = \alpha_{11}(B_2) = \alpha_{11}(B_3)$$

ODD

$$\alpha_{23}(B_1) = -\alpha_{13}(B_2) = \alpha_{12}(B_3)$$

Referred to the orthogonal axial set: $x//C_{2b}//[1\bar{1}0]$, $y//[11\bar{2}]$, $z//C_{31}^+//[111]$, the form of $\alpha_{ij}(\vec{B})$ is

	EVEN	+	ODD
$\alpha_{ij}(B_1) =$	$\begin{pmatrix} \bullet & \cdot & \cdot \\ \cdot & \bullet & \bullet \\ \cdot & \bullet & \bullet \end{pmatrix}$		$\begin{pmatrix} \bullet & \cdot & \cdot \\ \cdot & \bullet & \bullet \\ \cdot & \bullet & \bullet \end{pmatrix}$
$\alpha_{ij}(B_2) =$	$\begin{pmatrix} \bullet & \cdot & \cdot \\ \cdot & \bullet & \bullet \\ \cdot & \bullet & \bullet \end{pmatrix}$		$\begin{pmatrix} \bullet & \cdot & \cdot \\ \cdot & \bullet & \cdot \\ \bullet & \cdot & \cdot \end{pmatrix}$
$\alpha_{ij}(B_3) =$	$\begin{pmatrix} \bullet & \cdot & \cdot \\ \cdot & \bullet & \cdot \\ \cdot & \cdot & \bullet \end{pmatrix}$		$\begin{pmatrix} \bullet & \cdot & \cdot \\ \cdot & \bullet & \cdot \\ \cdot & \cdot & \bullet \end{pmatrix}$

CHAPTER FOUR

A FORMULATION OF TRANSPORT TENSORS IN ANISOTROPIC MEDIA:
GALVANOMAGNETIC AND THERMOMAGNETIC EFFECTS.

4.1 INTRODUCTION

The space-time symmetry restricted forms of the magnetic field dependent transport tensors tabulated in chapter three have revealed that a unique nomenclature for transport tensors in anisotropic media is needed. In this chapter a formulation of transport tensors based on the separation of the tensor components into "even" and "odd" functions of the applied magnetic field is given. Nomenclature for the galvanomagnetic and thermomagnetic effects in general and Hall effect in particular are critically reviewed. It is shown that the Hall effect be represented by the "odd" part of $\rho_{ij}(\vec{B})$ and the magnetoresistance by the "even" part. It is urged that this definition is general, simple and practical. Furthermore it is also shown that in the low field case the description of the magnetoresistance and Hall effect is in accord with the "odd" and "even" terminology.

The definition of the electrical conductivity or its inverse electrical resistivity based on expressing Joule heating in terms of σ_{ij} or ρ_{ij} is discussed. Moreover, this discussion is extended to the case when a magnetic field is applied to the medium.

4.2 TRANSPORT TENSORS.

CASE (1) : NO MAGNETIC INDUCTION, i.e. $\vec{B} = 0$.

In this case, the phenomenological linear equations in the presence of electric and thermal currents are

$$E_i = \rho_{ij} J_j + \alpha_{ij} \nabla_j T \quad (4.1)$$

$$q_i = \pi_{ij} J_j - K_{ij} \nabla_j T \quad (4.2)$$

Here $\rho_{ij}^{(0)}$ is the electrical resistivity tensor, K_{ij} is the thermal conductivity tensor, α_{ij} is the thermoelectric power tensor which represents the Seebeck effect, π_{ij} is the Peltier tensor which represents the Peltier effect, \vec{J} is the electric current density, $\vec{\nabla}T$ is the temperature gradient, \vec{q} is the heat current density and \vec{E} is the electric field intensity*. Experimental measurements are usually made with the electric current density and temperature gradient as controlled variables. When there are no temperature gradients, equation (4.1) reduces to Ohm's law

$$E_i = \rho_{ij} J_j, \quad (4.3)$$

and equation (4.2) in the absence of electric current gives Fourier's law

$$q_i = -K_{ij} \nabla_j T. \quad (4.4)$$

* Strictly \vec{E} is an electromotive force. For electrons it is given by $E_i = -\frac{1}{|e|} \frac{\partial}{\partial x_i} (\xi - |e|\varphi)$ where ξ is the chemical potential, φ is the electrostatic potential and $|e|$ is the magnitude of the electron charge.

In the absence of a magnetic induction, the Onsager reciprocity relations for transport tensors are

$$\left. \begin{aligned} \rho_{ij} &= \rho_{ji} \\ K_{ij} &= K_{ji} \end{aligned} \right\} \quad (4.5)$$

and $\pi_{ij} = T \alpha_{ji}$ (4.6)

where T is absolute temperature.

The same reciprocal relations hold for the tensors which are inverse to those given in equations (4.5) and (4.6). From relations (4.3), (4.4) and (4.5) the electrical resistivity tensor ρ_{ij} and its inverse the electrical conductivity tensor σ_{ij} the thermal conductivity tensor K_{ij} and its inverse the thermal resistivity tensor τ_{ij} are symmetric second rank constant tensors; thus their geometrical representation (i.e., quadric representation) is possible. The Onsager relation (4.6) between π_{ij} and α_{ij} is sometimes called the first Kelvin relation. Note that π_{ij} and α_{ij} possess no intrinsic symmetry; they are second rank constant tensors. The vector and tensor quantities which appear in equations (4.1) and (4.2) are polar. The spatial symmetry restricted forms of these second rank constant polar tensors are well known, see for example, Nye (1960) and Bhagavantam (1966).

At this stage we would like to open a discussion on the definition of the electrical resistivity or its inverse electrical conductivity in anisotropic media. Although equation (4.3), Ohm's law, provides the usual definition of the electrical resistivity or its inverse electrical conductivity tensor, recently Wannier (1972) has defined conductivity as the number with which E^2 is to be multiplied to get the power dissipation per unit volume, i.e.,

$$Q = \vec{J} \cdot \vec{E} = \sigma E^2. \quad (4.7)$$

In addition, we find in some books that the quantity of heat evolved per unit time and volume (i.e., power dissipation per unit volume) in a homogeneous conductor has been expressed in terms of the electrical resistivity tensor or its inverse the electrical conductivity tensor, see for example, Landau and Lifshitz (1960) p.93, Nye (1960) p.205, Mason (1966) p.217. Here we shall comment on these definitions and try to find the conditions for which Joule heating can correctly be expressed in terms of ρ_{ij} or σ_{ij} in anisotropic media.

The rate of Joule heating of a conductor is expressed by the scalar product of the current density vector \vec{J} and the electric field intensity vector \vec{E}

$$Q = \vec{J} \cdot \vec{E}. \quad (4.8)$$

When \vec{J} and \vec{E} are parallel to each other, which is true in isotropic and homogeneous cubic crystals, equation (4.8) becomes

$$Q = \vec{J} \cdot \vec{E} = \sigma E^2 = \rho J^2. \quad (4.9)$$

The difficulty in expressing Q in terms of $\vec{\rho}$ and \vec{J} or $\vec{\sigma}$ and \vec{E} arises when the vectors \vec{J} and \vec{E} do not coincide. In general, this is the case in anisotropic media. Without loss of generality, let us consider a monoclinic crystal with point group $2(C_2)$.

If the 2-fold axis coincides with z-direction (C_{2z}) the form taken by the electrical resistivity tensor ρ_{ij} is

$$\rho_{ij} = \begin{pmatrix} \rho_{11} & \rho_{12} & 0 \\ \rho_{12} & \rho_{22} & 0 \\ 0 & 0 & \rho_{33} \end{pmatrix} \quad (4.10)$$

σ_{ij} takes the same form.

Now if we cut a sample from this crystal in a rectangular parallelepiped geometry, application of an electric field to this sample may be described by the following three states:

State 1, transient state. Immediately after application of a potential difference across the sample ends, the state of the sample is:

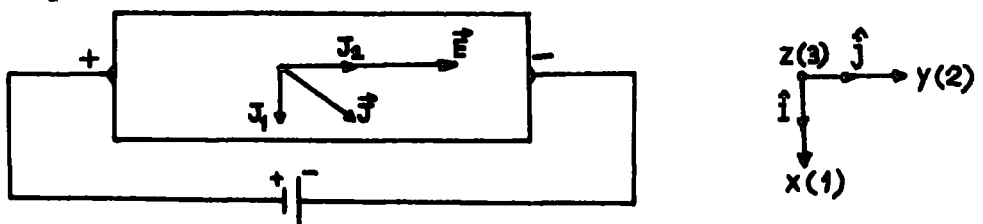


(illustration 4.1)

This state lasts a very short time, the y-directed applied electric field and the boundaries of the sample force the current to flow straight down (y-direction) the sample.

This situation gives rise to a transverse voltage difference along x-direction and hence the steady state 2 is reached.

State 2, steady state.

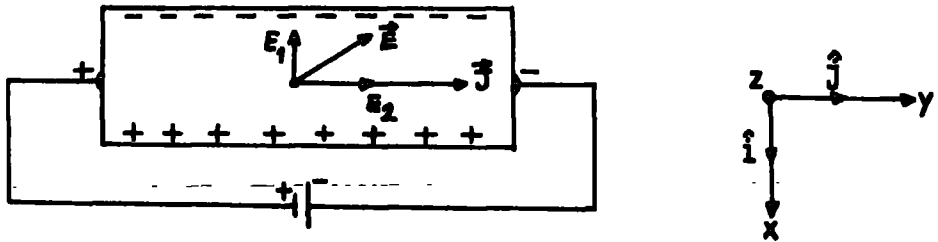


(illustration 4.2)

In this case E_1 , E_2 and $J(=J_2)$ are the measurable quantities, they are related by $E_1 = \rho_{12} J$ and $E_2 = \rho_{22} J$. The quantity of heat evolved per unit time and volume can be expressed as

$$Q_E = \vec{J} \cdot \vec{E} = (J\hat{j}) \cdot (-E_1\hat{i} + E_2\hat{j}) = JE_2 =$$

$$= \rho_{22} J^2 = \sigma_{12} E_1 E_2 + \sigma_{22} E_2^2. \quad (4.11)$$

Here \hat{i} and \hat{j} are the unit vectors along x and y directions respectively, the subscript E has been inserted on Q to denote that the electric field intensity vector is not along the sample (y-direction) and may be resolved into components along x and y directions. It is interesting to note that σ_{12} , an off diagonal component

of σ_{ij} , contributes to Joule heating.

In addition, if this sample is electrically shorted out across the x-direction, a current will then flow in this direction. We describe this state as follows:

State 3, transverse shorting (steady state).

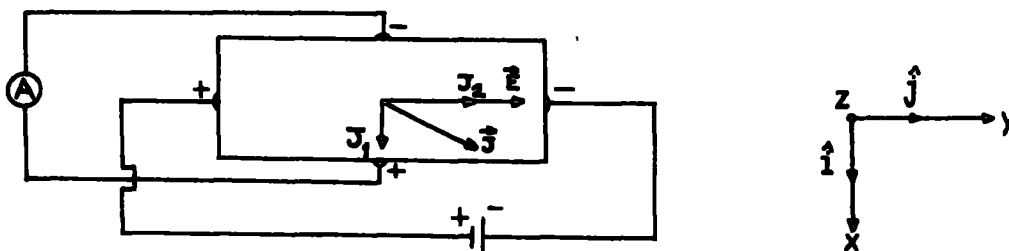


(illustration 4.3)

For this state J_1 , J_2 and $E(-E_2)$ are the measurable quantities (although when an ammeter inserted in the loop a current say I_1 will be registered, to find the current density J_1 may prove practically very difficult; to our knowledge these type of measurements have not been reported). They are related by $E_2 = \rho_{21} J_1 + \rho_{22} J_2$. Joule heating can be expressed as

$$\begin{aligned} Q_J &= \vec{J} \cdot \vec{E} = (J_1 \hat{i} + J_2 \hat{j}) \cdot (E \hat{j}) = J_2 E = \\ &= \sigma_{22} E^2 = \rho_{12} J_1 J_2 + \rho_{22} J_2^2 \end{aligned} \quad (4.12)$$

where the subscript J on Q shows that the current density is not along the sample (y-direction) and may be resolved into components along x and y directions. Notice that in equation (4.12) ρ_{12} an off-diagonal component of ρ_{ij} , contributes to Joule heating; this is contrary to state 2 in which there is no contribution from the off diagonal components of σ_{ij} .

From the preceding discussion we deduce the following results:

- (i) It seems that the Joule heating (Q_E) obtained from state 2 is not equal to the Joule heating (Q_J) obtained from state 3; but this needs to be shown experimentally.
- (ii) In state 2, using the results of equation (4.11), Joule heating in a crystal with no symmetry (i.e. triclinic) can be written as

$$Q_E = \vec{J} \cdot \vec{E} = E_i \sigma_{ij} E_j = \rho J^2 \quad (4.13)$$

where ρ is the electrical resistivity along the long direction of the sample. Note that Q_E is not equal to σE^2 .

- (iii) In state 3, using the result of equation (4.12), Joule heating, in general, can be written as

$$Q_J = \vec{J} \cdot \vec{E} = J_i \rho_{ij} J_j = \sigma E^2. \quad (4.14)$$

where σ is the electrical conductivity along the sample's long direction. Here again note that Q_J is not equal to ρJ^2 .

- (iv) From the results (i), (ii) and (iii), it appears that an expression for Joule heating in terms of ρ_{ij} or σ_{ij} depends on the shape of the sample and experimental set up.

Our conclusion is that in anisotropic media the quantity of heat evolved per unit time and volume cannot be expressed uniquely in terms of electrical resistivity tensor ρ_{ij} or its inverse electrical conductivity tensor σ_{ij} ; therefore we suggest that Joule heating should not be taken as a basis for the definition of the electrical resistivity

tensor ρ_{ij} or its inverse electrical conductivity tensor σ_{ij} . Later we shall extend this discussion to case (2), i.e., when an external magnetic induction \vec{B} is applied to the crystal.

4.3. TRANSPORT TENSORS

CASE (2) : A UNIFORM \vec{B} IS PRESENT, i.e. $\vec{B} = (B_1, B_2, B_3)$.

In this case, the phenomenological linear transport equations (equations 4.1 and 4.2) become

$$E_i = \rho_{ij}(\vec{B}) J_j + \alpha_{ij}(\vec{B}) \nabla_j T \quad (4.15)$$

$$q_i = \pi_{ij}(\vec{B}) J_j - K_{ij}(\vec{B}) \nabla_j T \quad (4.16)$$

Here $\rho_{ij}(\vec{B})$, $\alpha_{ij}(\vec{B})$, $\pi_{ij}(\vec{B})$ and $K_{ij}(\vec{B})$ are the magnetoresistivity, the magnetothermoelectric power, the magnetopeltier and the magnetothermal conductivity tensors respectively. These magnetic field dependent transport tensors actually are functions of the components of \vec{B} referred to the same cartesian axial set as that which the subscripts i and j refer to and should therefore more correctly be written in the form $\rho_{ij}(B_1, B_2, B_3)$ etc. In the presence of a magnetic induction \vec{B} the Onsager reciprocity relations, equations (4.5) and (4.6), will have to be replaced by

$$\left. \begin{aligned} \rho_{ij}(\vec{B}) &= \rho_{ji}(-\vec{B}) \\ K_{ij}(\vec{B}) &= K_{ji}(-\vec{B}) \end{aligned} \right\} \quad (4.17)$$

$$\text{and} \quad \pi_{ij}(\vec{B}) = T \alpha_{ji}(-\vec{B}). \quad (4.18)$$

Equation (4.18) is now the form taken by the Kelvin relation (cf. equation 4.6).

Over the years various names have been assigned to the magnetic field dependent transport tensors. Harman et al (1965) have used the term "galvano-thermomagnetic" to describe these tensors. A similar term "thermogalvano-magnetic" has been used by Kleiner (1966). Classifications of transport effects based on the isothermal and adiabatic experimental conditions have been given by Callen (1948), Fieschi et al. (1954), Blatt (1968) and others and usually apply for cubic crystals or better the so-called isotropic case only. Furthermore the effects have frequently been described by considering the low-field expansion coefficients alone, i.e., a Taylor series expansion up to second order terms in magnetic field components. Here we follow the usual way and divide the magnetic field dependent transport tensors into two main groups: galvanomagnetic effects and thermomagnetic effects. The components of the magnetoresistivity tensor $\rho_{ij}(\vec{B})$ represent the galvanomagnetic effects. The rest of the transport tensors $\alpha_{ij}(\vec{B})$, $\pi_{ij}(\vec{B})$ and $K_{ij}(\vec{B})$ represent the thermomagnetic effects. The low field expansion coefficients can be treated as a special case of these effects. In the following we shall give a description of these effects in anisotropic media.

4.3.1 Galvanomagnetic effects:

We consider the d.c. galvanomagnetic effects in isothermal conditions. In general, measurement of all the components of the magnetoresistivity tensor $\rho_{ij}(\vec{B})$ as a function of magnetic field strength and temperature provide sufficient experimental data to describe the galvanomagnetic effects of a particular crystal under consideration.

We write $\rho_{ij}(\vec{B})$ as a sum of "even" and "odd" functions of the applied magnetic induction \vec{B} :

$$\rho_{ij}(\vec{B}) = \rho_{ij}^{\text{even}}(\vec{B}) + \rho_{ij}^{\text{odd}}(\vec{B}) \quad (4.19)$$

where

$$\rho_{ij}^{\text{even}}(\vec{B}) = \rho_{ij}^{\text{even}}(\vec{B}); \quad \rho_{ij}^{\text{odd}}(\vec{B}) = -\rho_{ij}^{\text{odd}}(-\vec{B}). \quad (4.20)$$

The same tensor $\rho_{ij}(\vec{B})$ can also be written as the sum of symmetric (s) and antisymmetric (a) parts with respect to the indices i and j as

$$\rho_{ij}(\vec{B}) = \rho_{ij}^{(s)}(\vec{B}) + \rho_{ij}^{(a)}(\vec{B}) \quad (4.21)$$

where

$$\rho_{ij}^{(s)}(\vec{B}) = \rho_{ji}^{(s)}(\vec{B}), \quad \rho_{ij}^{(a)}(\vec{B}) = -\rho_{ji}^{(a)}(\vec{B}). \quad (4.22)$$

Now, by using the above relations together with the Onsager reciprocity relation (4.17), we shall simply show that the symmetric part of $\rho_{ij}(\vec{B})$ is an "even" function of \vec{B}

and the antisymmetric part is an "odd" function of \vec{B} .

Let us first express $\rho_{ij}^{\text{even}}(\vec{B})$ and $\rho_{ij}^{\text{odd}}(\vec{B})$ in terms of $\rho_{ij}(\pm\vec{B})$.

$$\rho_{ij}(\vec{B}) = \rho_{ij}^{\text{even}}(\vec{B}) + \rho_{ij}^{\text{odd}}(\vec{B}) \quad (4.19)$$

$$\rho_{ij}(-\vec{B}) = \rho_{ij}^{\text{even}}(-\vec{B}) + \rho_{ij}^{\text{odd}}(-\vec{B}) \quad (4.23)$$

By using equations (4.17) and (4.20), equation (4.23) becomes

$$\rho_{ij}(-\vec{B}) = \rho_{ij}^{\text{even}}(\vec{B}) - \rho_{ij}^{\text{odd}}(\vec{B}). \quad (4.24)$$

Addition and subtraction, respectively, of equation (4.24)

from equation (4.19) leads to

$$\rho_{ij}^{\text{even}}(\vec{B}) = \frac{1}{2} [\rho_{ij}(\vec{B}) + \rho_{ij}(-\vec{B})] \quad (4.25)$$

$$\rho_{ij}^{\text{odd}}(\vec{B}) = \frac{1}{2} [\rho_{ij}(\vec{B}) - \rho_{ij}(-\vec{B})]. \quad (4.26)$$

Similarly

$$\rho_{ij}(-\vec{B}) = \rho_{ij}^{(s)}(-\vec{B}) + \rho_{ij}^{(a)}(-\vec{B}). \quad (4.27)$$

Application of the Onsager's relation (equation 4.17) and equations (4.22) to the right hand side of equation (4.27) yields

$$\rho_{ij}(-\vec{B}) = \rho_{ij}^{(s)}(\vec{B}) - \rho_{ij}^{(a)}(\vec{B}). \quad (4.28)$$

Again addition and subtraction respectively of equation (4.28) from equation (4.21) yields

$$\rho_{ij}^{(s)}(\vec{B}) = \frac{1}{2} \left[\rho_{ij}(\vec{B}) + \rho_{ij}(-\vec{B}) \right] \quad (4.29)$$

$$\rho_{ij}^{(a)}(\vec{B}) = \frac{1}{2} \left[\rho_{ij}(\vec{B}) - \rho_{ij}(-\vec{B}) \right] . \quad (4.30)$$

From equations (4.25) and (4.29)

$$\rho_{ij}^{\text{even}}(\vec{B}) = \rho_{ij}^{(s)}(\vec{B}) \quad (4.31)$$

and from equations (4.26) and (4.30)

$$\rho_{ij}^{\text{odd}}(\vec{B}) = \rho_{ij}^{(a)}(\vec{B}) . \quad (4.32)$$

Thus the symmetrical part of $\rho_{ij}(\vec{B})$ is an even function of \vec{B} and the antisymmetrical part is an odd function of \vec{B} .

However, in general, the symmetric and antisymmetric parts of a field dependent second rank tensor need not be even and odd functions of \vec{B} respectively. Indeed this is the case for the magnetothermoelectric power tensor $\alpha_{ij}(\vec{B})$.

Later, in the description of $\alpha_{ij}(\vec{B})$ we shall explicitly show, in anisotropic media, that equalities (4.31) and (4.32) for $\alpha_{ij}(\vec{B})$ do not necessarily hold.

Following the above introductory remarks, we will define the magnetoresistance as the part of $\rho_{ij}(\vec{B})$ which is "even" function of \vec{B} and Hall effect as the part of $\rho_{ij}(\vec{B})$ which is "odd" function of \vec{B} (first definition). This definition was probably first suggested by Casimir (1945). Unfortunately, throughout this vast subject there have been few followers of this definition. Logan and Marcus (1952) and Grabner (1960), in their Hall effect measurements of germanium crystals,

have adopted it and so has Jan (1957), in his review article. Later, Harman and Honig (1967) in their multiband formulation of the galvanothermomagnetic effects have found it convenient to split each transport tensor entry into "even" and "odd" contributions.

On the other hand, several workers in the study of the galvanomagnetic effects (see, for example, Herring 1955, Landau and Lifshitz 1960 p. 97, Shtrikman and Thomas, 1965, Bhagavantam 1966 p. 198, Lifshitz et al. 1973 p. 168) have defined the magnetoresistance as the symmetric part of $\rho_{ij}(\vec{B})$ and Hall effect as the antisymmetric part of $\rho_{ij}(\vec{B})$; this we shall refer to as the second definition. Beer (1963) p. 71, Hurd (1974) and some of the followers of the second definition have described the magnetoresistance and Hall effect by using both the first and second definitions. In fact, because of the equalities (4.31) and (4.32) the two definitions turn out to be the same. However, for the following two reasons we prefer to use the first one:

1) Application of the symmetric and antisymmetric terminology to the other transport tensors for which equalities (4.31) and (4.32) do not hold can make the description of these tensors complicated.

2) Experimentally a component of $\rho_{ij}(\vec{B})$ which is the sum of even and odd functions of \vec{B} can be measured by using the same sample and merely reversing the sign of \vec{B} . On the other hand measurement of the symmetric and antisymmetric parts of the same component of $\rho_{ij}(\vec{B})$ (without

making use of the property of $\rho_{ij}(\vec{B})$ being even and odd functions of \vec{B} may require two samples. As an example, consider the tensor component $\rho_{23}(B_1)$ in point group $\bar{3}m$. To obtain the symmetric and antisymmetric parts of $\rho_{23}(B_1)$ the following equations may be used:

$$\rho_{23}^{(s)}(B_1) = \frac{1}{2} [\rho_{23}(B_1) + \rho_{32}(B_1)] \quad (4.33)$$

$$\rho_{23}^{(a)}(B_1) = \frac{1}{2} [\rho_{23}(B_1) - \rho_{32}(B_1)] \quad (4.34)$$

Thus, to measure $\rho_{23}(B_1)$ and $\rho_{32}(B_1)$ two differently oriented (z-cut and y-cut) samples are required. On the other hand, inspection of equations (4.25) and (4.26) shows that "even" and "odd" parts of $\rho_{23}(B_1)$ can be obtained from one sample (z-cut).

Kao and Katz (1958) have adopted another definition for the Hall and magnetoresistance effects (third definition). If the measured field (\vec{E}_{meas}) is normal to \vec{J} , they call the dependence $\vec{E}_{\text{meas}}(\vec{J}, \vec{B})$ a Hall effect; if \vec{E}_{meas} is parallel to \vec{J} , then $\vec{E}_{\text{meas}}(\vec{J}, \vec{B})$ is called the magnetoresistance. In this definition the off-diagonal even components $\rho_{ij}^{\text{even}}(\vec{B})$ ($i \neq j$) are automatically included in the Hall effect. These authors list a number of special configurations for which the crystal symmetry may impose "even" or "odd" parity on the Hall effect. Since this definition considers $\rho_{ij}^{\text{even}}(\vec{B})$ ($i \neq j$) to be part of the Hall effect, it can be a source of various Hall effects (which we shall describe later in this section). We thus believe that this definition is not practical and

and can make the issue complicated and hence should be avoided.

For completion, it is useful to define the magnetoresistance and Hall effects by considering the low field expansion coefficients. These coefficients are obtained from the Jones-Zener expansion of the magnetoresistivity tensor (which is usually carried out up to second order in magnetic field components):

$$\rho_{ij}(\vec{B}) = \rho_{ij}^{(0)} + \rho_{ijk_1}^{(1)} B_{k_1} + \rho_{ijk_1 k_2}^{(2)} B_{k_1} B_{k_2} + \dots \quad (4.35)$$

This series expansion is equivalent to a Taylor series with the coefficients given by (see Fuchser et al. 1970)

$$\rho_{ijk_1 k_2 \dots k_N}^{(N)} = \left(\frac{1}{N!} \right) \left(\frac{\partial^N \rho_{ij}(\vec{B})}{\partial B_{k_1} \dots \partial B_{k_N}} \right) \Big|_{\vec{B}=0} \quad (4.36)$$

where $i, j, k_1, k_2, \dots, k_N = 1, 2, 3$.

Hartman (1969) has given

$$\vec{\mu} \cdot \vec{B} < 1 \quad (4.37)$$

as a low-field expansion condition such that the magnitude of each term in equation (3.36) be less than one. Here $\vec{\mu}$ is the mobility tensor and \vec{B} is the antisymmetric second rank tensor form of the magnetic induction vector \vec{B} .

In equation (4.35) the coefficients are constant tensors:

$$\begin{aligned} \rho_{ij}^{(0)} &= \rho_{ji}^{(0)} && \text{(second rank symmetric polar tensor)} \\ \rho_{ijk_1}^{(1)} &= -\rho_{jik_1}^{(1)} && \text{(third rank axial tensor, antisymmetric} \\ &&& \text{with respect to } i \text{ and } j \text{ indices)} \end{aligned}$$

$$\rho_{ijk_1k_2}^{(2)} = \rho_{ji(\text{all permutations of } k_1 \text{ and } k_2)}^{(2)} \quad (\text{Fourth rank symmetric polar tensor}).$$

(4.38)

In the low field case the Hall effect and the magnetoresistance can be and often are represented by the components of the tensors $\rho_{ijk_1}^{(1)}$ and $\rho_{ijk_1k_2}^{(2)}$ respectively. This definition is in accord with the "first definition". To show this, let us consider the "even" and "odd" parity of the electric field components E_i with respect to the magnetic field

$$\begin{aligned} E_i &= E_i^{\text{even}} + E_i^{\text{odd}} = \\ &= \left[\rho_{ij}^{(0)} + \rho_{ijk_1}^{(1)} B_{k_1} + \rho_{ijk_1k_2}^{(2)} B_{k_1k_2} + \dots \right] J_j \end{aligned} \quad (4.39)$$

Here

$$E_i^{\text{even}} = \left[\rho_{ij}^{(0)} + \rho_{ijk_1k_2}^{(2)} B_{k_1} B_{k_2} + \dots \right] J_j \quad (4.40)$$

$$\text{and } E_i^{\text{odd}} = \left[\rho_{ijk_1}^{(1)} B_{k_1} + \dots \right] J_j \quad (4.41)$$

Equations (4.40) and (4.41) can be taken as the defining equations of the low-field magnetoresistance and Hall effects respectively. Throughout the text, for brevity ρ_{ij} or ρ_{ij}^0 is used in place of $\rho_{ij}^{(0)}$.



In the section (4.2) on transport tensors in the absence of a magnetic induction (i.e. case 1), we have opened a discussion on the definition of the electrical resistivity or its reciprocal electrical conductivity based on the expression of Joule heating in terms of ρ_{ij} or σ_{ij} . There we arrived at a conclusion that in anisotropic media Joule heating ($\vec{J} \cdot \vec{E}$) cannot be expressed uniquely in terms of ρ_{ij} or its reciprocal σ_{ij} and hence it should not be taken as a basis for the definition of ρ_{ij} or σ_{ij} . Now we are going to extend this discussion to case (2), i.e., when an external magnetic induction \vec{B} is applied to the crystal. In addition to the above definitions of the magnetoresistance and Hall effect (first, second and third definitions), some workers have given a description of these effects in terms of Joule heating; see for example Landau and Lifshitz (1960) p. 97, Bhagavantam (1966) p. 198, Shtrikman and Thomas (1965), Pantulu and Sudarshan (1970) and Lifshitz et al. (1973) p.168. According to this description, the Joule heat evolved in a conductor is determined only by the symmetric part of the magnetoresistivity tensor, i.e.

$$Q = \vec{J} \cdot \vec{E} = J_i E_i = J_i \rho_{ij}^{(s)}(\vec{B}) J_j \quad (4.42)$$

The lossless, antisymmetric part $\rho_{ij}^{(a)}(\vec{B})$ describes the Hall effect. Again this description needs to be critically examined. To this end, let us consider the same crystal which was studied as an example in case (1), i.e. a monoclinic crystal with point group $2(C_2)$. For this symmetry the form taken

by ρ_{ij} is given in equation (4.10) and the form of $\rho_{ij}(\vec{B})$ is given in table (3.5). For the sake of simplicity we will consult the illustrative figures (illustration 4.2) and illustration 4.3) given for state 2 and state 3 of case (1). Now consider state 2 (see illustration 4.2 in case (1)). If we apply a magnetic induction along $(\vec{B}=B_1\hat{i})$, in general, the longitudinal E_2 and transverse E_1 fields will be effected. In addition an electric field E_3 across the z-direction may be developed. In this case E_1, E_2, E_3 and $J(=J_2)$ are the measurable quantities and they are related by

$$E_1 = \overset{\text{even}}{\rho_{12}(B_1)} J_2; E_2 = \overset{\text{even}}{\rho_{22}(B_1)} J_2; E_3 = \overset{\text{odd}}{\rho_{32}(B_1)} J_2. \quad (4.43)$$

The quantity of heat evolved per unit time and volume can then be expressed as

$$\begin{aligned} Q_E &= \vec{J} \cdot \vec{E} = J\hat{j} \cdot (-E_1\hat{i} + E_2\hat{j} - E_3\hat{k}) = \\ &= JE_2 = \overset{\text{even}}{\rho_{22}(B_1)} J^2 \\ &= \left[\overset{\text{even}}{\sigma_{12}(B_1)} E_1 + \overset{\text{even}}{\sigma_{22}(B_1)} E_2 + \overset{\text{odd}}{\sigma_{23}(B_1)} E_3 \right] E_2. \end{aligned} \quad (4.44)$$

Here \hat{k} is the unit vector along the z-direction and Q_E, \hat{i}, \hat{j} and $J(=J_2)$ have the same meanings as in the equation (4.11) $\overset{\text{even}}{\rho_{22}(B_1)}$ is a field dependent tensor component and $\sigma_{12}(B_1), \sigma_{22}(B_1), \sigma_{23}(B_1)$ are the magnetoconductivity tensor components. Notice that in this set up longitudinal "even" components of $\rho_{ij}(\vec{B})$ contribute to Q_E only. On the other hand different components of $\sigma_{ij}(\vec{B})$ i.e. "even" diagonal $\overset{\text{even}}{\sigma_{ii}(\vec{B})}$,

"even" off-diagonal $\overset{\text{even}}{\sigma}_{ij}(\vec{B})$ ($i \neq j$) and "odd" $\overset{\text{odd}}{\sigma}_{ij}(\vec{B})$ components contribute to Q_E . It is obvious that when \vec{B} is in another direction a different form of equation (4.44) will result. For the set-up described by equation (4.44), inspection of this equation shows that Joule heating in general for a crystal with no symmetry (i.e. point group $1(C_1)$) can be written as

$$Q_E = \vec{J} \cdot \vec{E} = \rho_{kk}^{\text{even}}(\vec{B}) J_k^2 = E_i \sigma_{ij}(\vec{B}) E_j \quad (4.45)$$

Next consider state 3 (see illustration 4.3 in case (1)).

Since application of a magnetic induction \vec{B} along the x-direction (i.e. $\vec{B} = B_1 \hat{i}$) may develop a potential difference across the z-direction, we short-out the sample across both the x- and z-directions. For this set-up, J_1 , J_2 , J_3 and $E (=E_2)$ are the measurable quantities and they are related by

$$E (=E_2) = \rho_{21}^{\text{even}}(B_1) J_1 + \rho_{22}^{\text{even}}(B_1) J_2 + \rho_{23}^{\text{odd}}(B_1) J_3 \quad (4.46)$$

As we have mentioned in case (1), although a current in the loop in the x- or z-directions can easily be measured, to find the current density J_1 or J_3 may be difficult. Joule heating for this case can be expressed as

$$\begin{aligned} Q_J &= \vec{J} \cdot \vec{E} = (J_1 \hat{i} + J_2 \hat{j} + J_3 \hat{k}) \cdot (E \hat{j}) = \\ &= J_2 E = \overset{\text{even}}{\sigma}_{22}(B_1) E^2 = \\ &= \rho_{21}^{\text{even}}(B_1) J_1 J_2 + \rho_{22}^{\text{even}}(B_1) J_2^2 + \rho_{23}^{\text{odd}}(B_1) J_2 J_3 \end{aligned}$$

(4.47)

Note that $\sigma_{22}^{\text{even}}(B_1)$ of $\sigma_{ij}(\vec{B})$ contributes to Q_J only. But different components of $\rho_{ij}(\vec{B})$ are contributing to Q_J ; the appearance of a Hall effect term $\rho_{23}^{\text{odd}}(B_1)$ in equation (4.47) deserves attention. Here it is worth mentioning a point which could well be related to state 3; it is the well known Corbino disc geometry in which the Hall field is totally shorted and an enhancement in the magnetoresistance has been experimentally observed (see Weiss 1969 and references therein). By inspection, equation (4.47) can be generalized to a no symmetry crystal (i.e. point group $1(C_1)$) as

$$Q_J = \vec{J} \cdot \vec{E} = \sigma_{kk}^{\text{even}}(\vec{B}) E_k^2 = J_i \rho_{ij}(\vec{B}) J_j. \quad (4.48)$$

In case (2), from the preceding discussion we can deduce the following results which are similar to those in case (1):

- 1) Q_E seems not equal to Q_J but this needs to be proved experimentally.
- 2) Again, an expression for Joule heating depends strongly on the shape of the sample and the experimental set-up.

Thus, we again arrive at a similar conclusion that in anisotropic media the quantity of heat evolved per unit time and volume cannot be expressed uniquely in terms of $\rho_{ij}(\vec{B})$ or its inverse $\sigma_{ij}(\vec{B})$; therefore it should not be taken as a basis for the description of the magnetoresistance and Hall effect.

(i) MAGNETORESISTANCE

The magnetoresistance effect is the change in the electrical resistivity in the presence of a magnetic induction \vec{B} . Following a remark made by Pippard (1965) that the magnetoresistance could be proved positive, Wannier (1972) has proved a theorem under rather general assumptions that the magneto conductivity of a metal is a monotonically non-increasing function of the magnitude of \vec{B} .

We have already defined the magnetoresistance as the part of the magnetoresistivity tensor $\rho_{ij}(\vec{B})$ which is an "even" function of \vec{B} , i.e. $\overset{\text{even}}{\rho_{ij}}(\vec{B})$. This can be divided into two parts: diagonal components and off-diagonal components. The diagonal part can further be divided into two parts $\overset{\text{even}}{\rho_{ii}}(B_i)$ and $\overset{\text{even}}{\rho_{ii}}(B_k)$ ($i \neq k$). In the literature $\overset{\text{even}}{\rho_{ii}}(B_i)$ is often called the longitudinal magnetoresistance and $\overset{\text{even}}{\rho_{ii}}(B_k)$ ($i \neq k$) the transverse magnetoresistance. The off-diagonal components of $\overset{\text{even}}{\rho_{ij}}(\vec{B})$, i.e. $\overset{\text{even}}{\rho_{ij}}(B_k)$ ($i \neq j$), will be just called even off-diagonal components. Later, in a separate section we shall show that the co-existence of "even" off-diagonal components with "odd" (Hall effect) components is the main cause of the Umkehr effect in $\rho_{ij}(\vec{B})$. It is obvious that the zero field resistivity tensor components are contained in $\overset{\text{even}}{\rho_{ij}}(\vec{B})$ and they can always be obtained by putting $\vec{B}=0$. In addition to the measurements of the components of $\overset{\text{even}}{\rho_{ij}}(\vec{B})$ as a function of \vec{B} , measurements of the tensor components as a function of magnetic field direction (angular dependence) are and have always been very valuable as a source of information

about the shape of the constant energy surfaces of conductors. Recently, polar data in Bi and certain Bi-Sb alloys by Jacobson (1973), an As(25.5 at. %) - Sb alloy by Akgöz and Saunders (1974) and Bi by Sümengen et al (1974) have been used to compute the band model parameters of these materials.

(ii) HALL EFFECT

We have already defined the Hall effect as the part of $\rho_{ij}(\vec{B})$ which is an "odd" function of \vec{B} , i.e. $\rho_{ij}^{\text{odd}}(\vec{B})$. In any configuration of the sample the Hall field vanishes when \vec{B} equals zero. Hall effect measurements are usually made by employing samples in a rectangular parallelepiped geometry. A uniform constant current is maintained through the long direction of the sample. When an external magnetic field is applied to the sample, in general, a potential difference perpendicular to the current direction develops. Part of this voltage which changes sign on reversal of the sign of \vec{B} is called the Hall field. Notice that in this configuration current direction is always normal to the Hall field, but we have no condition for \vec{B} ; it can be applied to any direction although in table (3.5) we have assumed that \vec{B} is along each of the orthogonal crystallographic directions taken in turn. The components of the "odd" part of $\rho_{ij}(\vec{B})$ (see table 3.5) are then calculated by using this measured field.

If we recall equation (4.41), the linear relationship between $B_{k_1} J_j$ and E_i^{odd} allows us to find the low field Hall coefficients (which are the components of a third rank axial antisymmetric tensor). Thus the low field Hall effect of a particular material is represented by the components of $\rho_{ijk_1}^{(1)}$ which are constants themselves.

In general for the classical range of magnetic fields equation (4.41) does not hold. Again by using the "even" and "odd" parity of the measured electric field components E_i with respect to the magnetic field, we can write

$$E_i = E_i^{\text{even}} + E_i^{\text{odd}} = \left[\rho_{ij}^{\text{even}}(\vec{B}) + \rho_{ij}^{\text{odd}}(\vec{B}) \right] J_j. \quad (4.49)$$

As we have already stated, the "odd" part of (4.49) represents the Hall effect. In anisotropic media, at a constant magnetic field $\vec{B} = \vec{B}_0$, $\rho_{ij}^{\text{odd}}(\vec{B}_0)$ can be considered as the local gradient of the E_i^{odd} versus \vec{B} curve. The defining equation can be written as

$$\rho_{ij}^{\text{odd}}(\vec{B}_0) = \left(\frac{1}{J_j} \right) \left(\frac{\partial \rho^{\text{odd}}(\vec{B})}{\partial \vec{B}} \right) \Big|_{\vec{B} = \vec{B}_0} \quad (4.50)$$

Basically this definition is the tensor form of that given by Hurd (1972).

In the literature, over the years some of the components of $\rho_{ij}^{\text{odd}}(\vec{B})$ have been named as if a new Hall effect had been found. Next, and more important, several workers in the

studies of the galvanomagnetic effects have considered the "off-diagonal even" components of the magnetoresistance as part of the Hall effect; as an example we can think of the third definition. This mixing of the "even" and "odd" components of $\rho_{ij}(\vec{B})$ has been and still is a main source of names for the Hall effect. A full review of various Hall phenomena observed in crystals up to 1963 has been given in the monograph by Beer (1963). Here we shall list the names of the various Hall effects which have appeared up to now in the literature and comment on them.

1) Conventional Hall effect.

In this case, for a sample in a parallelepiped geometry, a transverse field \vec{E} is developed under the conditions such that \vec{E} , \vec{B} and \vec{J} are mutually perpendicular, where \vec{J} is along the long direction of the sample. This is true for isotropic crystals; it is also true in cubic crystals provided that \vec{E} , \vec{J} and \vec{B} are along the orthogonal crystallographic axes and also in some other point groups when \vec{E} , \vec{J} and \vec{B} are in certain special directions. The generalization of this definition to low symmetry crystals may open a way to complication.

2) Quadratic Hall effect or Even Hall effect or Transverse even effect.

The "off-diagonal even" components (which we have already mentioned in the description of the magnetoresistance) have frequently been considered as the part of the Hall effect, contrary to the first and second definitions. Measurements

involving any component of $\rho_{ij}^{\text{even}}(\vec{B})$ ($i \neq j$) can in principal cause the appearance of this effect. Different names have been assigned to these components by different workers in the field such as : quadratic Hall effect by Kohler (1934) and Shoenberg (1935); even Hall effect by Baranskii et al. (1971), Douglas and Datars (1973); a rather reasonable name "transverse even field" or "transverse even effect" has been adopted by Kachinskii (1961), Klauder and Kunzler (1961), Hurd (1972, 1974), Chiang and Shevchenko (1974). For the same effect, the name "transverse ohmic field" has also been used (see for example, Connell and Marcus 1957). As it has been pointed out by Mason et al. (1953), this even voltage is the largest source of distortion in Hall effect devices. It can only be removed by choosing the correct crystal configuration.

3) Transverse Hall effect (TH-field) and Longitudinal Hall effect (LH-field).

Grabner (1960), in his Hall effect measurements in n-type germanium has adopted such conventions as transverse Hall field (TH-field) and longitudinal Hall field (LH-field). The measured Hall field (which is an "odd" function of \vec{B}) perpendicular to \vec{B} and \vec{J} (i.e. in the direction of $\vec{B} \wedge \vec{J}$) has been called the Transverse Hall effect. Note that in this case \vec{B} is not necessarily normal to \vec{J} . The measured Hall field perpendicular to \vec{J} and $\vec{B} \wedge \vec{J}$ (i.e. in the direction of $\vec{J} \wedge (\vec{B} \wedge \vec{J})$ or in another word the measured field in the plane of \vec{B} and \vec{J}) has been called Longitudinal Hall effect. Actually, with the above conventions, Grabner's measurements

can be represented by one of the components of $\rho_{ij}^{\text{odd}}(\vec{B})$ depending on the particular orientation of his samples. It is important to notice that Grabner's Hall effect definition (as we have mentioned early) is in accord with the first definition. In fact, he has measured some of the "odd" part of the magnetoresistivity tensor.

4) Longitudinal magnetic field Hall phenomena.

In a parallelepiped sample geometry, this name has been used for a transverse potential difference developed normal to \vec{J} when the magnetic induction \vec{B} is set parallel to \vec{J} . Garcia-Moliner (1959) has predicted that such a potential difference can develop even in a cubic crystal when the current density \vec{J} is set up along a direction with no symmetry. Hattori (1968) has observed "a transverse voltage in a longitudinal magnetic field" in bismuth. In fact, he has measured $\rho_{12}^{\text{odd}}(B_2)$; a component of the Hall effect in this A7 structure material.

5) Planar Hall effect.

Apparently, Goldberg and Davis (1954) in germanium crystals first observed an electric field perpendicular to current direction in the current-magnetic field plane and for this field they have used the name "planar Hall field"; since then in the literature this effect has been known as the planar Hall effect. For the same field the name "pseudo Hall effect" has also been used by Koch (1955). Very recently Hurd (1974) has dropped the word "Hall" and defined the planar effect in the following way: in anisotropic media, with \vec{J} and

\vec{B} established in isothermal conditions, the planar effect is the appearance along a direction perpendicular to \vec{J} , and coplanar with \vec{J} and \vec{B} , of an electric field which is an "even" function of \vec{B} . From the above definitions it is clear that this effect is the measurement of the "off-diagonal even" components of $\rho_{ij}(\vec{B})$ ($i \neq j$) as a function of magnetic field direction when a constant \vec{B} is rotated in the plane determined by the i^{th} and j^{th} directions. For example, if $\vec{J} // 1$ (x-direction) and $\vec{E} // 2$ (y-direction), $\rho_{21}(B_1, B_2, 0) \Big|_{\vec{B} = \text{const.}}$ represents the planar effect.

According to the first definition, this effect is a part of the magnetoresistance, since it is an "even" function of \vec{B} .

From the above descriptions of the various Hall effects the following results can be deduced:

(I) It appears that most of the Hall effect names have arisen by consideration of the "off-diagonal even" components as though they were part of the Hall effect.

(II) The Quadratic Hall effect can be represented by the "off-diagonal even" components $\rho_{ij}(\vec{B})$ ($i \neq j$) when \vec{B} is taken along the crystallographic directions.

(III) Polar measurements of the "off-diagonal even" components $\rho_{ij}(\vec{B})$ ($i \neq j$) as a function of magnetic field direction when a constant \vec{B} is rotated in the plane determined by the i^{th} and j^{th} directions can cover the planar Hall effect.

(IV) The other Hall effects described above can either be represented by the individual components of $\rho_{ij}(\vec{B})$ or their dependence on the magnetic field direction when a constant \vec{B} is rotated in a specified crystallographic plane.

(V) From the results (I), (II), (III), (IV) and in the light of the first definition we can conclude that the effects 2 and 5 belong to the magnetoresistance; 1, 3, 4 belong to the Hall effect. Therefore, it is best not to consider them as individual effects.

(VI) Once again, in the study of the galvanomagnetic effects we suggest that workers follow the first definition —
 $\rho_{ij}^{\text{even}}(\vec{B}) \rightarrow$ magnetoresistance, $\rho_{ij}^{\text{odd}}(\vec{B}) \rightarrow$ Hall effect —
it is simple, most general and practical.

4.3.2. THERMOMAGNETIC EFFECTS

Thermoelectric effects and thermal conductivity in the presence of magnetic field are frequently called the thermomagnetic effects. As we have already stated in an earlier section the thermomagnetic effects are represented by the magnetic field dependent tensors $\alpha_{ij}(\vec{B})$, $\pi_{ij}(\vec{B})$ and $K_{ij}(\vec{B})$. $\pi_{ij}(\vec{B})$ and $\alpha_{ij}(\vec{B})$ are related by the Kelvin relation (see equation 4.18). Here, a somewhat detailed description of the magnetothermoelectric power tensor $\alpha_{ij}(\vec{B})$ together with a brief description of the other two tensors will be given.

The second rank magnetothermoelectric power tensor $\alpha_{ij}(\vec{B})$ can be expressed as a sum of "even" and "odd" functions of the applied magnetic induction \vec{B} :

$$\alpha_{ij}(\vec{B}) = \alpha_{ij}^{\text{even}}(\vec{B}) + \alpha_{ij}^{\text{odd}}(\vec{B}) \quad (4.51)$$

where
$$\alpha_{ij}^{\text{even}}(\vec{B}) = \alpha_{ij}^{\text{even}}(-\vec{B}) ; \alpha_{ij}^{\text{odd}}(\vec{B}) = -\alpha_{ij}^{\text{odd}}(-\vec{B}). \quad (4.52)$$

The same tensor can also be written as the sum of symmetric (s) and antisymmetric (a) parts with respect to the indices i and j:

$$\alpha_{ij}(\vec{B}) = \alpha_{ij}^{(s)}(\vec{B}) + \alpha_{ij}^{(a)}(\vec{B}) \quad (4.53)$$

where
$$\alpha_{ij}^{(s)}(\vec{B}) = \alpha_{ji}^{(s)}(\vec{B}) ; \alpha_{ij}^{(a)}(\vec{B}) = -\alpha_{ji}^{(a)}(\vec{B}). \quad (4.54)$$

By using the above equations (4.51) to (4.54) we will

explicitly show that $\alpha_{1j}^{(s)}(\vec{B})$ is not equal to $\alpha_{1j}^{\text{even}}(\vec{B})$ and $\alpha_{1j}^{(a)}(\vec{B})$ is not equal to $\alpha_{1j}^{\text{odd}}(\vec{B})$. Let us first express $\alpha_{1j}^{\text{even}}(\vec{B})$ and $\alpha_{1j}^{\text{odd}}(\vec{B})$ in terms of $\alpha_{1j}(\pm\vec{B})$.

$$\alpha_{1j}(\vec{B}) = \alpha_{1j}^{\text{even}}(\vec{B}) + \alpha_{1j}^{\text{odd}}(\vec{B}) \quad (4.51)$$

$$\alpha_{1j}(-\vec{B}) = \alpha_{1j}^{\text{even}}(-\vec{B}) + \alpha_{1j}^{\text{odd}}(-\vec{B}). \quad (4.55)$$

By making use of equalities (4.52), equation (4.55) becomes

$$\alpha_{1j}(-\vec{B}) = \alpha_{1j}^{\text{even}}(\vec{B}) - \alpha_{1j}^{\text{odd}}(\vec{B}). \quad (4.56)$$

Addition and subtraction respectively, of equation (4.56) from equation (4.51) leads to

$$\alpha_{1j}^{\text{even}}(\vec{B}) = \frac{1}{2} [\alpha_{1j}(\vec{B}) + \alpha_{1j}(-\vec{B})] \quad (4.57)$$

$$\alpha_{1j}^{\text{odd}}(\vec{B}) = \frac{1}{2} [\alpha_{1j}(\vec{B}) - \alpha_{1j}(-\vec{B})] \quad (4.58)$$

Equation (4.53) can be also written as

$$\alpha_{ji}(\vec{B}) = \alpha_{ji}^{(s)}(\vec{B}) + \alpha_{ji}^{(a)}(\vec{B}). \quad (4.59)$$

Use of the relations (see equations 4.54) in the right hand side of equation (4.59) yields

$$\alpha_{ji}(\vec{B}) = \alpha_{ij}^{(s)}(\vec{B}) - \alpha_{ij}^{(a)}(\vec{B}). \quad (4.60)$$

Addition and subtraction respectively, of equation (4.60) from equation (4.53) yields

$$\alpha_{ij}^{(s)}(\vec{B}) = \frac{1}{2} \left[\alpha_{ij}(\vec{B}) + \alpha_{ji}(\vec{B}) \right] \quad (4.61)$$

$$\alpha_{ij}^{(a)}(\vec{B}) = \frac{1}{2} \left[\alpha_{ij}(\vec{B}) - \alpha_{ji}(\vec{B}) \right] \quad (4.62)$$

By comparing respectively equations (4.57) and (4.58) with equations (4.61) and (4.62) it can, in general, be shown that the following inequalities hold:

$$\alpha_{ij}^{\text{even}}(\vec{B}) \neq \alpha_{ij}^{(s)}(\vec{B}), \quad (4.63)$$

$$\alpha_{ij}^{\text{odd}}(\vec{B}) \neq \alpha_{ij}^{(a)}(\vec{B}). \quad (4.64)$$

These inequalities are crucial equations in that they put an end to use of the symmetric and antisymmetric terminology in description of transport tensors. For $\rho_{ij}(\vec{B})$ the restrictions imposed by the Onsager relation (see equations 4.17) demand an equality sign instead of an inequality sign (see equations 4.31 and 4.32). This is the reason why we needed to list only the half parts of $\rho_{ij}^{\text{even}}(\vec{B})$ and $\rho_{ij}^{\text{odd}}(\vec{B})$ in table (3.5). But for $\alpha_{ij}^{\text{even}}(\vec{B})$ and $\alpha_{ij}^{\text{odd}}(\vec{B})$ the full forms were given in table (3.6).

Experimentally, "even" and "odd" parts can be measured by merely reversing the sense of the magnetic induction \vec{B} (see equations 4.57 and 4.58). On the contrary, this need not hold for the symmetric (s) and antisymmetric (a) parts. As an example consider the tensor component $\alpha_{23}(B_1)$ for the point group $\bar{3}m$. To obtain the symmetric and antisymmetric parts of $\alpha_{23}(B_1)$ the following equations may be used:

$$\alpha_{23}^{(s)}(B_1) = \frac{1}{2} \left[\alpha_{23}(B_1) + \alpha_{32}(B_1) \right] \quad (4.65)$$

$$\alpha_{23}^{(a)}(B_1) = \frac{1}{2} \left[\alpha_{23}(B_1) - \alpha_{32}(B_1) \right] . \quad (4.66)$$

That is, $\alpha_{23}(B_1)$ and $\alpha_{32}(B_1)$ need to be measured. For this two differently oriented (z - cut and y - cut) samples are required. On the other hand, inspection of equations (4.57) and (4.58) shows that "even" and "odd" parts of $\alpha_{23}(B_1)$ can be obtained from one sample (z-cut). This is a very important practical reason for using the "even" and "odd" terminology in describing field dependent transport tensors in general and $\alpha_{ij}(\vec{B})$ in particular. This further emphasises that the "even" and "odd" nomenclature for the description of transport tensors is superior to the symmetric and antisymmetric terminology.

We now define the magneto-Seebeck effect as the part of $\alpha_{ij}(\vec{B})$ which is an "even" function of \vec{B} and Nernst effect which is an "odd" function of \vec{B} . Apparently Steele and Babiskin (1955) in the measurement of the thermomagnetic effects in bismuth were the first to separate certain components of $\alpha_{ij}(\vec{B})$ into "even" and "odd" parts. Later, Harman and Honig (1967) in their multiband formulation of the galvanothermomagnetic effects have found it convenient to split each transport tensor into "even" and "odd" parts. In fact they use "Seebeck coefficient" for "even" components and "Nernst coefficient" for "odd" components of $\alpha_{ij}(\vec{B})$. Apart from these two suggestions the above description ($\alpha_{ij}^{\text{even}}(\vec{B}) \longrightarrow$ Magneto-Seebeck effect;

$\alpha_{ij}^{\text{odd}}(\vec{B})$ (Nernst effect) has not, to our knowledge, been given before. Now the magneto-Seebeck effect and Nernst effect will separately be described.

(i) MAGNETO-SEEBECK EFFECT

Following closely the description of $\rho_{ij}^{\text{even}}(\vec{B})$, the "even" part of $\alpha_{ij}(\vec{B})$, i.e. the magneto-Seebeck effect, can be divided into two parts: diagonal components and off-diagonal components. The diagonal part can further be divided into two parts $\alpha_{ii}^{\text{even}}(B_i)$ longitudinal magneto-Seebeck effect and $\alpha_{ii}^{\text{even}}(B_k)$ ($i \neq k$) transverse magneto-Seebeck effect. The off-diagonal even components $\alpha_{ij}^{\text{even}}(B_k)$ ($i \neq j$) for which we have no special name will be just called "off-diagonal even" components of $\alpha_{ij}(\vec{B})$.

(ii) NERNST EFFECT

The "odd" part of the magnetothermoelectric power tensor, i.e. $\alpha_{ij}^{\text{odd}}(\vec{B})$ represents the Nernst effect. Due to the absence of a relation like Onsager's reciprocity (see equation 4.17) in the magnetothermoelectric power $\alpha_{ij}(\vec{B})$, the diagonal components of $\alpha_{ij}^{\text{odd}}(\vec{B})$ in general can exist. This, as it will be shown later, has been the origin of the so-called "Umkehreffect" which is usually considered to be an anomalous effect.

For completion, it is useful to interpret the definition of the magneto-Seebeck and Nernst effects by considering the low-field expansion coefficients. These coefficients are usually

obtained from a power series expansion of $\alpha_{ij}(\vec{B})$ with respect to the magnetic field components:

$$\alpha_{ij}(\vec{B}) = \alpha_{ij}^{(0)} + \alpha_{ijk_1}^{(1)} B_{k_1} + \alpha_{ijk_1 k_2}^{(2)} B_{k_1} B_{k_2} + \dots \quad (4.67)$$

The coefficients (which are constant tensors) of this series are given by

$$\alpha_{ijk_1 k_2 \dots k_N}^{(N)} = \left(\frac{1}{N!} \right) \left(\frac{\partial^N \alpha_{ij}(\vec{B})}{\partial B_{k_1} \dots \partial B_{k_N}} \right) \Big|_{\vec{B} = 0} \quad (4.68)$$

where $i, j, k_1, k_2, \dots, k_N = 1, 2, 3$;

$\alpha_{ij}^{(0)}$ (second rank polar tensor)

$\alpha_{ijk_1}^{(1)}$ (third rank axial tensor)

$\alpha_{ijk_1 k_2}^{(2)}$ (fourth rank polar tensor, it is symmetric only with respect to the indices k_1 and k_2).

The effect of spatial symmetry on these constant tensors and thus the number of independent components and their identification have been studied and listed by Bhavagantam (1966), Pinchuk (1967) and Smith et al (1967). A detailed study of these low field tensors in bismuth (A7 structure, point group $\bar{3}m$) has been given by Sumengen and Saunders (1972a). In this low-field case Nernst effect and the Magneto-Seebeck effect can be represented by the components of $\alpha_{ijk_1}^{(1)}$ and $\alpha_{ijk_1 k_2}^{(2)}$ respectively provided that the power series expansion (see equation 4.67) is carried out to second order terms only. In fact, Bhagavantam (1966) has used the name Nernst effect for $\alpha_{ijk_1}^{(1)}$ and the term magnetothermoelectric power for $\alpha_{ijk_1 k_2}^{(2)}$.

To show that this description is in accord with the general definition, let us consider the "even" and "odd" parity of the thermoelectric field components E_i with respect to the magnetic field.

$$E_i = E_i^{\text{even}} + E_i^{\text{odd}} = \left[\alpha_{ij}^{(0)} + \alpha_{ijk_1}^{(1)} B_{k_1} + \alpha_{ijk_1 k_2}^{(2)} B_{k_1} B_{k_2} + \dots \right] \nabla_j T \quad (4.69)$$

Here $E_i^{\text{even}} = \left[\alpha_{ij}^{(0)} + \alpha_{ijk_1 k_2}^{(2)} B_{k_1} B_{k_2} + \dots \right] \nabla_j T \quad (4.70)$

and $E_i^{\text{odd}} = \left[\alpha_{ijk_1}^{(1)} B_{k_1} + \dots \right] \nabla_j T \quad (4.71)$

Equations (4.70) and (4.71) can be taken as the defining equations for the low-field magneto-Seebeck and Nernst effects respectively. Note that the linear relationship between $B_{k_1} \nabla_j T$ and E_i^{odd} allows us to find the low-field Nernst coefficients (which are the components of a third rank axial antisymmetric tensor). Thus the low-field Nernst effect of a particular material is represented by the components of $\alpha_{ijk_1}^{(1)}$ which are constant themselves. In general, for an arbitrary value of magnetic field, equation (4.71) does not hold. Again by using the "even" and "odd" parity of the measured thermoelectric field components E_i with respect to the applied magnetic field, E_i can be written as

$$E_i = E_i^{\text{even}} + E_i^{\text{odd}} = \left[\alpha_{ij}^{\text{even}}(\vec{B}) + \alpha_{ij}^{\text{odd}}(\vec{B}) \right] \nabla_j T. \quad (4.72)$$

As we have noted before, the "odd" part of (4.72) represents the Nernst effect. We now follow closely the definition of a Hall coefficient for an arbitrary magnetic field strength (see equation 4.50); in anisotropic media for a constant magnetic field $\vec{B}=\vec{B}_0$, $\alpha_{1j}^{\text{odd}}(\vec{B}_0)$ can be considered as a local gradient of $\underline{E}_i^{\text{odd}}$ versus \vec{B} curve. The defining equation of this Nernst coefficient is

$$\alpha_{1j}(\vec{B}_0) = \left(\frac{1}{v_j T} \right) \left(\frac{\partial \alpha_{1j}^{\text{odd}}(\vec{B})}{\partial B} \right) \Big|_{\vec{B}=\vec{B}_0} \quad (4.73)$$

In the literature, considerable theoretical work has been employed in the expression of the components of $\alpha_{1j}(\vec{B})$ in terms of mobilities and carrier densities. Once again, the well known band structure of bismuth with its large magneto-Seebeck and Nernst effect lead to this material being the first to be studied. In strong and low field limits, expressions for the components of $\alpha_{1j}(\vec{B})$ for the diffusion thermopower have been given by Harman et al (1965). Korenblit (1969), for the same limits, has given expressions for the phonon drag case. Sumengen and Saunders (1972a), for the classical range of magnetic fields, have given general and explicit expressions for some of the components of $\alpha_{1j}(\vec{B})$ for diffusion case; in fact for the first time, they have obtained a complete set of model parameters (mobilities and carrier densities) by analysing experimental results of $\alpha_{22}(\vec{B})$ for bismuth at liquid nitrogen temperatures.

In the next chapter, the form of $\alpha_{1j}(\vec{B})$ for intrinsic and p-type (Sn-doped) bismuth will be obtained for the diffusion and phonon drag cases. Measurements of the components of $\alpha_{1j}(\vec{B})$ are, in

general, more difficult than those of $\rho_{ij}(\vec{B})$. This is because of the experimental difficulties involved in attaining isothermal conditions in the presence of a temperature gradient along the sample. Smith et al (1967) have discussed the difficulties of measuring the thermomagnetic coefficients in isothermal and adiabatic conditions.

The rest of the magnetic field dependent transport tensors $\kappa_{ij}(\vec{B})$ and $\pi_{ij}(\vec{B})$ can similarly be described. They can be expressed as the sum of "even" and "odd" parts in \vec{B} :

$$\kappa_{ij}(\vec{B}) = \overset{\text{even}}{\kappa_{ij}(\vec{B})} + \overset{\text{odd}}{\kappa_{ij}(\vec{B})} \quad (4.74)$$

and
$$\pi_{ij}(\vec{B}) = \overset{\text{even}}{\pi_{ij}(\vec{B})} + \overset{\text{odd}}{\pi_{ij}(\vec{B})}. \quad (4.75)$$

Here $\overset{\text{even}}{\kappa_{ij}(\vec{B})}$ and $\overset{\text{even}}{\pi_{ij}(\vec{B})}$ are called magnetothermal conductance and magnetopeltier effect respectively; $\overset{\text{odd}}{\kappa_{ij}(\vec{B})}$ represents the Righi-Leduc effect and $\overset{\text{odd}}{\pi_{ij}(\vec{B})}$ the Ettinghausen effect.

CHAPTER FIVE

THE EFFECT OF CONSTANT ENERGY SURFACE MODELS AND SOME BASIC TRANSPORT THEORY ASSUMPTIONS ON THE FORM OF TRANSPORT TENSORS.

5.1 Introduction

Simplifications inherent in band structure models and assumptions employed in solution of the Boltzmann transport equation can restrict the forms of $\rho_{ij}(\vec{B})$ or $\alpha_{ij}(\vec{B})$. In this chapter the forms of $\rho_{ij}(\vec{B})$ and $\alpha_{ij}(\vec{B})$ obtained from transport theory are compared to the phenomenological forms established in chapter three (see section 3.5). As an example, the well-established band structure of bismuth is considered throughout. It is shown that the forms taken by $\alpha_{ij}(\vec{B})$ for the phonon-drag and carrier diffusion cases differ; the appropriate components that need to be measured to separate the two contributions are given.

From band structure considerations, an explanation of the appearance of the Umkehr effect in certain components of $\rho_{ij}(\vec{B})$ and $\alpha_{ij}(\vec{B})$ is given; here, in addition to the symmetry restrictions implicit to the band structure (i.e. the Fermi surface) model of bismuth, those arising from the well-known constant energy surface near the band extrema of n-germanium are also considered.

5.2 CONSTANT ENERGY SURFACE SYMMETRY RESTRICTIONS ON THE FORM OF THE MAGNETORESISTIVITY TENSOR.

A second way of reaching the form of $\rho_{ij}(\vec{B})$ is through the microscopic theory of electron transport. This is usually achieved by solution of the linearized Boltzmann transport equation in the relaxation time approximation. In principle when all the restrictions imposed by the band structure symmetry are included in such a calculation, the form obtained for $\rho_{ij}(\vec{B})$ should be identical to that found from the phenomenological approach in section (3.5). However, to facilitate an analytical solution to the Boltzmann equation recourse is often made for semiconductors or semimetals to representation of the constant energy surfaces in the vicinity of the symmetry related band extrema by simple models such as spheres or ellipsoids. But transport theory based on the multivalley ellipsoidal energy dependence of crystal momentum can yield results of higher symmetry than the phenomenological theory — the symmetry of the constant energy surface model determines the form of $\rho_{ij}(\vec{B})$. The simplest example is the spherical Fermi surface model of a metal with the relaxation time independent of velocity; here the "even" parts of $\rho_{ij}(\vec{B})$ are independent of the magnetic field and are simply the zero field resistivity: the magnetoresistance vanishes (see however Allgauer 1973 for a discussion of the special assumptions inherent in this simplest transport model).

The phenomenological form of $\rho_{1j}(\vec{B})$ appropriate to the A7 structure (point group $\bar{3}m$), in suffix notation, is:

$$\rho_{1j}(B_1, 0, 0) = \begin{matrix} \text{EVEN} \\ \left(\begin{array}{ccc} \rho_{11}(B_1) & 0 & 0 \\ 0 & \rho_{22}(B_1) & \rho_{23}(B_1) \\ 0 & \rho_{23}(B_1) & \rho_{33}(B_1) \end{array} \right) + \end{matrix}$$

$$+ \begin{matrix} \text{ODD} \\ \left(\begin{array}{ccc} 0 & 0 & 0 \\ 0 & 0 & \rho_{23}(B_1) \\ 0 & -\rho_{23}(B_1) & 0 \end{array} \right) \end{matrix}$$

$$\rho_{1j}(0, B_2, 0) = \begin{matrix} \text{EVEN} \\ \left(\begin{array}{ccc} \rho_{11}(B_2) & 0 & 0 \\ 0 & \rho_{22}(B_2) & \rho_{23}(B_2) \\ 0 & \rho_{23}(B_2) & \rho_{33}(B_2) \end{array} \right) + \end{matrix}$$

$$+ \begin{matrix} \text{ODD} \\ \left(\begin{array}{ccc} 0 & \rho_{12}(B_2) & \rho_{13}(B_2) \\ -\rho_{12}(B_2) & 0 & 0 \\ -\rho_{13}(B_2) & 0 & 0 \end{array} \right) \end{matrix}$$

$$\rho_{ij}(0,0,B_3) = \begin{pmatrix} \overbrace{\rho_{11}(B_3)}^{\text{EVEN}} & 0 & 0 \\ 0 & \rho_{11}(B_3) & 0 \\ 0 & 0 & \rho_{33}(B_3) \end{pmatrix} + \begin{pmatrix} \overbrace{0}^{\text{ODD}} & \rho_{12}(B_3) & 0 \\ -\rho_{12}(B_3) & 0 & 0 \\ 0 & 0 & 0 \end{pmatrix} \quad (5.1)$$

where the "even" and "odd" parts represent the magnetoresistance and Hall effect respectively. Aubrey (1971) has derived explicitly each of the components of $\sigma_{ij}(\vec{B})$ in terms of carrier densities and mobilities for the tilted ellipsoidal model of the group V semimetals. Inspection of his equations clearly shows that the form taken by $\sigma_{ij}(\vec{B})$ and therefore $\rho_{ij}(\vec{B})$ is the same as that obtained by the phenomenological approach (equation 5.1).

The way in which the constant energy surface symmetry assumptions can restrict the form of $\rho_{ij}(\vec{B})$ can be seen by consideration of Fermi surface models used for bismuth. In the first quantitative work relating the galvanomagnetic effects of bismuth to the band structure, Abeles and Meiboom (1956) used a non-tilted ellipsoidal model for the electron Fermi surface - a model which reduces the form of $\rho_{ij}(\vec{B})$ to that of the higher symmetry enantiomorphous point group 622 (see table 3.4). The components

$\rho_{23}^{\text{even}}(B_1)$, $\rho_{23}^{\text{even}}(B_2)$ and $\rho_{12}^{\text{odd}}(B_2)$ which depend upon the tilt angle of the ellipsoids must then vanish. Another example, which finds direct experimental verification, occurs when bismuth is doped with sufficient acceptors to depress the Fermi level below the conduction band edge into the L-point gap (a review of the effects of doping on semimetals is given by Saunders and Akgöz 1973). At sufficiently low temperatures the only carriers present in concentrations high enough to affect $\rho_{ij}(\vec{B})$ are holes in the ellipsoid of revolution centred at the T point. As a result of this symmetry restriction on the band structure, $\rho_{ij}(\vec{B})$ acquires the form corresponding to that for the point group 422. Gitsu et al (1969) have shown that in tin-doped bismuth $\rho_{33}(B_1) = \rho_{33}(B_2)$ which is one of the interrelations between the tensor components predicted beneath the form of $\rho_{ij}(\vec{B})$ for the point group 422 in table (3.5).

In general the form of $\rho_{ij}(\vec{B})$ can be arrived at by consideration of the symmetry of the points in the Brillouin zone where the band extrema lie.

5.3 THE EFFECT OF CONSTANT ENERGY SURFACE MODELS ON THE FORM OF $\alpha_{ij}(\vec{B})$ - THE DIFFUSION AND PHONON DRAG THERMOPOWERS.

While the phenomenological forms of $\alpha_{ij}(\vec{B})$ given in table (3.6) are strictly true, assumptions made in application of transport theory in the multivalley constant energy surface model can result in a higher apparent symmetry than that of the point group and the form of $\alpha_{ij}(\vec{B})$ is altered accordingly. The forms of $\alpha_{ij}(\vec{B})$ predicted from the theories of phonon drag and diffusion thermopower can differ and their study should allow separation of the two contributions. From solution of the Boltzmann transport equation in the relaxation time approximation, Sumengen and Saunders (1972a) have obtained a general equation for the diffusion contribution to $\alpha_{ij}(\vec{B})$. For a two-band model with electrons (e) and holes (h).

$$\alpha_{ij}(\vec{B}) = \rho_{ik}(\vec{B}) \left\{ \sigma_{kj,e}(\vec{B}) P_e + \sigma_{kj,h}(\vec{B}) P_h \right\} \quad (5.2)$$

where P_e and P_h , the partial Seebeck coefficients of electrons and holes respectively are scalar quantities (see Saunders and Öktü 1968). $\sigma_{kj,e}(\vec{B})$ and $\sigma_{kj,h}(\vec{B})$ represent the partial electron and hole conductivities. Aubrey (1971) has given the prerequisite expressions for $\sigma_{ij}(\vec{B})$ and therefore $\rho_{ik}(\vec{B})$ for the group V semimetals. Now equation (5.2) can be used to obtain the forms of $\alpha_{ij}(\vec{B})$ when carrier diffusion is the dominant transport mechanism.

However, at low temperatures phonon drag can make a large contribution to the thermopower of semimetals this is probably true for bismuth. Korenblit (1969), using anisotropic partial Seebeck tensor arising from phonon drag effects, has obtained a general expression for $\alpha_{ij}(\vec{B})$. We write, in a slightly different notation, his expression as

$$\alpha_{nk}(\vec{B}) = \rho_{nm}(\vec{B}) \left\{ \sum_I \sigma_{mj,e}^i(\vec{B}) \alpha_{jk,e}^i + \sum_r \sigma_{mj,h}^r(\vec{B}) \alpha_{jk,h}^r \right\} \quad (5.3)$$

where i and r run over the number of electron and hole ellipsoids respectively, $\sigma_{mj,e}^i(\vec{B})$ and $\sigma_{mj,h}^r(\vec{B})$ are the i^{th} electron and r^{th} hole valley magnetoconductivities respectively and $\alpha_{jk,e}^i$ and $\alpha_{jk,h}^r$ are the i^{th} electron and r^{th} hole valley phonon drag thermoelectric power tensors respectively. For bismuth equation (5.3) becomes

$$\alpha_{nk}(\vec{B}) = \rho_{nm}(\vec{B}) \left\{ \sum_{i=1}^{III} \sigma_{mj,e}^i(\vec{B}) \alpha_{jk,e}^i + \sigma_{mj,h}(\vec{B}) \alpha_{jk,h} \right\} \quad (5.4)$$

where in Korenblit's notation the hole phonon drag thermoelectric power tensor $\alpha_{jk,h}$ in the crystallographic axis reference frame is

$$\alpha_{jk,h} = \begin{pmatrix} \alpha_{11}^+ & 0 & 0 \\ 0 & \alpha_{11}^+ & 0 \\ 0 & 0 & \alpha_{33}^+ \end{pmatrix} \quad (5.5)$$

and that for electrons is

$$\alpha_{jk,e}^I = \begin{pmatrix} \alpha_{11}^- & 0 & 0 \\ 0 & \alpha_{11}^- & \alpha_{23}^- \\ 0 & \alpha_{32}^- & \alpha_{33}^- \end{pmatrix} \quad (5.6a)$$

$$\begin{matrix} \text{II, III} \\ \alpha_{jk,e}^{\text{II, III}} \end{matrix} = \begin{pmatrix} \frac{1}{4}(\alpha_{11}^- + 3\alpha_{22}^-) & \pm \frac{\sqrt{3}}{4}(\alpha_{22}^- - \alpha_{11}^-) & \mp \frac{\sqrt{3}}{2} \alpha_{23}^- \\ \pm \frac{\sqrt{3}}{4}(\alpha_{22}^- - \alpha_{11}^-) & \frac{1}{4}(3\alpha_{11}^- + \alpha_{22}^-) & -\frac{1}{2}\alpha_{23}^- \\ \mp \frac{\sqrt{3}}{2} \alpha_{32}^- & -\frac{1}{2}\alpha_{32}^- & \alpha_{33}^- \end{pmatrix} \quad (5.6b)$$

Here the upper sign refers to the second (II) and the lower sign to the third (III) ellipsoid. The ellipsoids are numbered in an anticlockwise rotational order about the [111] direction. Now by using equation (5.4) we obtain the form of the phonon drag magnetothermoelectric power tensor for bismuth when an arbitrary magnetic field B_1 , B_2 or B_3 is applied parallel to crystallographic axes x, y , or z taken in turn.

To achieve this end, we

- (i) express the components of $\rho_{nm}(\vec{B})$ in terms of $\sigma_{nm}(\vec{B})$,
- (ii) use Aubrey's (1971) expressions to find the components of $\sigma_{nm}(\vec{B})$ $\alpha_{mj,e}^{\text{I, II, III}}(\vec{B})$ and $\sigma_{mj,h}(\vec{B})$ in terms of the carrier mobilities and densities and
- (iii) obtain the electron $\alpha_{jk,e}^{\text{I, II, III}}$ and hole $\alpha_{jk,h}$ phonon drag thermoelectric power components from equations (5.6) and (5.5).

when the summation implicit in equation (5.4) has been carried out, the result obtained written out in full suffix notation is

$$\begin{aligned}
 \alpha_{ij}(B_1) &= \begin{pmatrix} \alpha_{11}(B_1) & 0 & 0 \\ 0 & \alpha_{22}(B_1) & \alpha_{23}(B_1) \\ 0 & \alpha_{32}(B_1) & \alpha_{33}(B_1) \end{pmatrix} + \begin{pmatrix} \alpha_{11}(B_1) & 0 & 0 \\ 0 & \alpha_{22}(B_1) & \alpha_{23}(B_1) \\ 0 & \alpha_{32}(B_1) & \alpha_{33}(B_1) \end{pmatrix} \\
 \alpha_{ij}(B_2) &= \begin{pmatrix} \alpha_{11}(B_2) & 0 & 0 \\ 0 & \alpha_{22}(B_2) & \alpha_{23}(B_2) \\ 0 & \alpha_{32}(B_2) & \alpha_{33}(B_2) \end{pmatrix} + \begin{pmatrix} 0 & \alpha_{12}(B_2) & \alpha_{13}(B_2) \\ \alpha_{21}(B_2) & 0 & 0 \\ \alpha_{31}(B_2) & 0 & 0 \end{pmatrix} \\
 \alpha_{ij}(B_3) &= \begin{pmatrix} \alpha_{11}(B_3) & 0 & 0 \\ 0 & \alpha_{11}(B_3) & 0 \\ 0 & 0 & \alpha_{33}(B_3) \end{pmatrix} + \begin{pmatrix} 0 & \alpha_{12}(B_3) & 0 \\ -\alpha_{12}(B_3) & 0 & 0 \\ 0 & 0 & 0 \end{pmatrix}.
 \end{aligned}
 \tag{5.7}$$

Thus the form of $\alpha_{ij}(\vec{B})$ obtained for the phonon drag thermoelectric power is identical to the phenomenological form given (for the point group $\bar{3}m$) in table (3.6).

Now we consider $\alpha_{11}(B_1)$ in particular; from equations (5.4) and (5.7)

$$\alpha_{11}(B_1) = \overset{\text{even}}{\alpha_{11}(B_1)} + \overset{\text{odd}}{\alpha_{11}(B_1)}.
 \tag{5.8}$$

$$\text{Here } \alpha_{11}^{\text{even}}(B_1) = \frac{c_1 + c_3 B_1^2}{(c_4 + c_5 B_1^2)},$$

$$\alpha_{11}^{\text{odd}}(B_1) = \frac{c_2}{(c_4 + c_5 B_1^2)} B_1 \quad (5.9)$$

where

$$c_1 = \mu_{11} \alpha_{11}^- + 3v_{11} \alpha_{11}^+ + \frac{1}{8}(\mu_{11} + 3\mu_{22})(\alpha_{11}^- + 3\alpha_{22}^-)$$

$$+ \frac{3}{8}(\mu_{22} - \mu_{11})(\alpha_{22}^- - \alpha_{11}^-) + \frac{3}{4}\mu_{23}(\alpha_{32}^- - \alpha_{23}^-),$$

$$c_2 = \frac{3}{4}(\alpha_{22}^- - \alpha_{11}^-) \mu_{11} \mu_{23} + \frac{3}{8}(\mu_{11} \mu_{33} - \frac{d_e}{\mu_{11}})(\alpha_{32}^- - \alpha_{23}^-),$$

$$c_3 = \frac{1}{4}(\mu_{11} \alpha_{11}^- + 3v_{11} \alpha_{11}^+)(3\mu_{11} \mu_{33} + \frac{d_e}{\mu_{11}}) + \frac{1}{2}d_e(\alpha_{11}^- + 3\alpha_{22}^-),$$

$$c_4 = \mu_{11} + 3v_{11} + \frac{1}{2}(\mu_{11} + 3\mu_{22}),$$

$$c_5 = \frac{1}{4}(\mu_{11} + 3v_{11})(3\mu_{11} \mu_{33} + \frac{d_e}{\mu_{11}}).$$

Here μ_{ij} and v_{ij} are the electron and hole mobility tensors respectively and $d_e = \mu_{11}(\mu_{22}\mu_{33} - \mu_{23}^2)$. Note that for bismuth $v_{11} = v_{22}$ and $v_{23} = 0$.

Now let us consider $\alpha_{11}(B_1)$ for the diffusion thermoelectric power. By putting

$$\left. \begin{aligned} \alpha_{22}^- &= \alpha_{11}^- = P_e \\ \alpha_{32}^- &= \alpha_{23}^- = 0 \end{aligned} \right\} \quad (5.10)$$

$$\alpha_{11}^+ = \alpha_{33}^+ = P_h \quad (5.11)$$

equation (5.4) reduces to equation (5.3). By using either equation (5.3) or substituting (5.10) and (5.11) into (5.9), it can easily be seen that c_2 becomes zero and therefore $\alpha_{11}^{\text{odd}}(B_1)$ is zero (in agreement with the findings of Sumengen and Saunders (1972a)). There is a marked difference between the two contributions: in the phonon drag case

$$\alpha_{11}(B_1) = \alpha_{11}^{\text{even}}(B_1) + \alpha_{11}^{\text{odd}}(B_1), \quad (5.8)$$

while in the diffusion case

$$\alpha_{11}(B_1) = \alpha_{11}^{\text{even}}(B_1), \text{ i.e. } \alpha_{11}^{\text{odd}}(B_1) = 0. \quad (5.12)$$

Thus the two effects (phonon drag and diffusion) can be separated in principle by measurements of $\alpha_{11}(+B_1)$ and $\alpha_{11}(-B_1)$.

Hansen and Nielsen (1974) have pointed out that the low field coefficient $\alpha_{11}^{(1)}$ should be a direct measure of the phonon drag thermopower due to electrons in bismuth. In the low field expansion of $\alpha_{1j}(\vec{B})$ (see equation 4.67) the phenomenological theory predicts that $\alpha_{11}^{(1)}$ is an independent non-zero component (Sumengen and Saunders 1972b). This low field component is given by

$$\alpha_{11}^{(1)} = \frac{\partial \alpha_{11}(B_1)}{\partial B_1} \Big|_{B=0} = \frac{c_2}{c_4} = \frac{\frac{3}{4} (\alpha_{22}^- - \alpha_{11}^-) \mu_{11} \mu_{23} + \frac{3}{8} (\mu_{11} \mu_{33} - \frac{d_e}{\mu_{11}}) (\alpha_{32}^- - \alpha_{23}^-)}{\mu_{11} + 3\nu_{11} + \frac{1}{2} (\mu_{11} + 3\mu_{22})}. \quad (5.13)$$

Use of the equalities (5.10) and (5.11) verifies that

$\alpha_{111}^{(1)} = 0$ for the diffusion contribution.

We shall now show that a further relationship, namely

$$\alpha_{33}^{\text{odd}}(B_1) = -\alpha_{22}^{\text{odd}}(B_1) \quad (5.14)$$

exists for the diffusion but not for the phonon drag contribution. From equation (5.2)

$$\begin{aligned} \alpha_{22}(B_1) = & \frac{\sigma_{33}(B_1)}{D_1} \left\{ \sigma_{22,e}(B_1) P_e + \sigma_{22,h}(B_1) P_h \right\} \\ & + \frac{-\sigma_{23}(B_1)}{D_1} \left\{ \sigma_{32,e}(B_1) P_e + \sigma_{32,h}(B_1) P_h \right\} \end{aligned} \quad (5.15)$$

where $D_1 = \sigma_{22}(B_1) \sigma_{33}(B_1) - \sigma_{32}(B_1) \sigma_{23}(B_1)$.

Now using Aubrey's (1971) equations (91) it can be seen that $\sigma_{33}(B_1)$, $\sigma_{22}(B_1)$ and D_1 are even functions of B_1 . Therefore the first term on the LHS of equation (5.15) is even with respect to B_1 .

Thus

$$\begin{aligned} \alpha_{22}^{\text{odd}}(B_1) = & \frac{-\sigma_{23}^{\text{even}}(B_1)}{D_1} \left\{ \sigma_{32,e}^{\text{odd}}(B_1) P_e + \sigma_{32,h}^{\text{odd}}(B_1) P_h \right\} \\ & + \frac{-\sigma_{23}^{\text{odd}}(B_1)}{D_1} \left\{ \sigma_{32,e}^{\text{even}}(B_1) P_e + \sigma_{32,h}^{\text{even}}(B_1) P_h \right\} \end{aligned} \quad (5.16)$$

where we have separated the magnetoconductivity tensor components into "even" and "odd" parts.

Again from equation (5.2)

$$\alpha_{33}(B_1) = \frac{-\sigma_{32}(B_1)}{D_1} \left\{ \sigma_{23,e}(B_1) P_e + \sigma_{23,h}(B_1) P_h \right\} + \frac{\sigma_{22}(B_1)}{D_1} \left\{ \sigma_{33,e}(B_1) P_e + \sigma_{33,h}(B_1) P_h \right\}. \quad (5.17)$$

The second term on the LHS of equation (5.17) is even with respect to B_1 .

Thus

$$\alpha_{33}^{\text{odd}}(B_1) = \frac{-\sigma_{32}^{\text{even}}(B_1)}{D_1} \left\{ \sigma_{23,e}^{\text{odd}}(B_1) P_e + \sigma_{23,h}^{\text{odd}}(B_1) P_h \right\} + \frac{-\sigma_{32}^{\text{odd}}(B_1)}{D_1} \left\{ \sigma_{23,e}^{\text{even}}(B_1) P_e + \sigma_{23,h}^{\text{even}}(B_1) P_h \right\}. \quad (5.18)$$

Again using Aubrey's (1971) equations (91) in conjunction with the "even" and "odd" terminology, it can be seen that the following equalities hold:

$$\left. \begin{aligned} \sigma_{23}^{\text{odd}}(B_1) &= -\sigma_{32}^{\text{odd}}(B_1) \\ \sigma_{23}^{\text{even}}(B_1) &= \sigma_{32}^{\text{even}}(B_1) \\ \sigma_{23,e}^{\text{odd}}(B_1) &= -\sigma_{32,e}^{\text{odd}}(B_1) \\ \sigma_{23,h}^{\text{odd}}(B_1) &= -\sigma_{32,h}^{\text{odd}}(B_1) \\ \sigma_{23,e}^{\text{even}}(B_1) &= \sigma_{32,e}^{\text{even}}(B_1) \\ \sigma_{23,h}^{\text{even}}(B_1) &= \sigma_{32,h}^{\text{even}}(B_1) = 0 \end{aligned} \right\} \quad (5.19)$$

Substitution of equalities (5.19) into equations (5.17) and (5.18) shows that

$$\boxed{\alpha_{33}^{\text{odd}}(B_1) = -\alpha_{22}^{\text{odd}}(B_1)}. \quad (5.20)$$

Thus the final form of $\alpha_{ij}(\vec{B})$ for the diffusion thermo-electric power is obtained when the equalities (5.12) and (5.20) are used in equation (5.7). We can conclude that the phonon drag and diffusion contributions can be separated by measuring the diagonal components of $\alpha_{ij}^{\text{odd}}(B_1)$. Recent measurements of $\alpha_{11}(B_3)$ and $\alpha_{33}(B_1)$ (Uher and Goldsmid (1974)) have indicated that the phonon drag contribution at very high fields persists up to well above 77K.

Another example of this separation of the contributions to the thermopower can be seen in bismuth acceptor doped so that the Fermi level lies in the L-point gap (Saunders and Akgöz 1973) - the only carriers present at moderately low temperatures would be holes in an ellipsoid of revolution centred at T point of the Brillouin zone. The drag thermopower is then given by

$$\alpha_{ij}(\vec{B}) = \rho_{ik}(\vec{B}) \left\{ \alpha_{mk,h}(\vec{B}) \alpha_{mj,h} \right\} \quad (5.21)$$

where the drag thermopower tensor $\alpha_{m,j,h}$ turns out to be that given by equation (5.5).

Thus

$$\alpha_{11}(B_1) = \rho_{11}(B_1) \left\{ \alpha_{11,h}(B_1) \alpha_{11}^+ \right\} = \alpha_{11}^+.$$

In a similar way all the components of $\alpha_{ij}(\vec{B})$ can be obtained

with the result:

$$\alpha_{ij}(B_1) = \begin{matrix} \text{EVEN} \\ \text{(Magneto-Seebeck effect)} \end{matrix} \begin{pmatrix} \alpha_{11}^+ & 0 & 0 \\ 0 & \alpha_{11}^+ & 0 \\ 0 & 0 & \alpha_{33}^+ \end{pmatrix} + \begin{matrix} \text{ODD} \\ \text{(Nernst effect)} \end{matrix} \begin{pmatrix} 0 & 0 & 0 \\ 0 & 0 & 0 \\ 0 & 0 & 0 \end{pmatrix} \quad (5.22)$$

The forms of $\alpha_{ij}(B_2)$ and $\alpha_{ij}(B_3)$ are identical to $\alpha_{ij}(B_1)$. Hence, as Korenblit (1969) has noted for a substance with a single valley, the drag thermopowers is independent of magnetic field and the Nernst effect is zero. The diffusion contribution obtained from equation (5.2) written for the case of carriers in a single valley as

$$\alpha_{ij}(\vec{B}) = \rho_{ik}(\vec{B}) \sigma_{kj}(\vec{B}) P_h \quad (5.23)$$

and its form is

$$\alpha_{ij}(B_1) = \begin{matrix} \text{EVEN} \\ \text{(Magneto-Seebeck effect)} \end{matrix} \begin{pmatrix} P_h & 0 & 0 \\ 0 & P_h & 0 \\ 0 & 0 & P_h \end{pmatrix} + \begin{matrix} \text{ODD} \\ \text{(Nernst effect)} \end{matrix} \begin{pmatrix} 0 & 0 & 0 \\ 0 & 0 & 0 \\ 0 & 0 & 0 \end{pmatrix} \quad (5.24)$$

The form of $\alpha_{ij}(B_2)$ and $\alpha_{ij}(B_3)$ are identical to $\alpha_{ij}(B_1)$. Thus the diffusion thermopower is independent of both applied magnetic field and crystallographic directions. We can conclude from this particular example that if equations (5.2) and (5.4) do describe respectively the drag and diffusion thermopowers correctly, that is if the use

of $\alpha_{mj,h}$ and P_h in equations (5.21) and (5.23) respectively is strictly correct — a proposal not yet put thoroughly to the test — then a comparison between measurements in p-type (single carrier) bismuth of $\alpha_{11}(B_k)$ and $\alpha_{33}(B_k)$ ($k=1,2,3$) should allow separation of the two thermopower contributions.

Explicit expressions for all components of $\alpha_{ij}(\vec{B})$, when \vec{B} is directed along each of the crystallographic axes (x,y, and z), have been found by following the procedure used to obtain the equations (5.9), (5.15) and (5.17). The final expressions are extensive and need not be given here. To analyse polar data, expressions for $\alpha_{ij}(B_1, B_2, 0)$, $\alpha_{ij}(B_1, 0, B_3)$ and $\alpha_{ij}(0, B_2, B_3)$ need to be derived; these are also very lengthy and are best employed in computer calculations.

5.4 The UMKEHR EFFECT IN $\rho_{ij}(\vec{B})$.

From space-time symmetry, we have already shown in chapter three (section 3.5.5) that the Umkehr effect can occur in certain off-diagonal components of the magnetoresistivity tensor. In this section we shall show that the same result can be obtained from band structure considerations. Over the years the occurrence of the Umkehr effect in $\rho_{ij}(\vec{B})$ has been a subject of some debate (see, Casimir and Gerritsen 1941; Jan 1957 for a review and references).

5.4.1. The A7 structure semimetals

To show that the Umkehr effect can occur in $\rho_{1j}(\vec{B})$, let us consider the case of $\rho_{23}(B_1)$ for the A7 structure ($\bar{3}m$ point group) semimetals. In measurements of this component, the odd and even parts can readily be separated by reversing the direction of the magnetic field from along the +x direction (+ B_1) to the -x direction (- B_1). Then with the current along the +z direction the potential difference V developed in the y-direction is

$$\begin{aligned} V_2(B_1) &= v^{\text{even}}(B_1) + v^{\text{odd}}(B_1) \\ V_2(-B_1) &= v^{\text{even}}(B_1) - v^{\text{odd}}(B_1) \end{aligned} \quad (5.25)$$

the phenomenological approach (Table 35) tells us that $V_2(B_1)$ and $V_2(-B_1)$ should not be equal because $\rho_{23}(B_1)$ is not identical to $\rho_{23}(-B_1)$. The question now is whether or not the difference is measurable. We can answer this by inserting known band model parameters into expressions for $\rho_{23}(\pm B_1)$ and thus calculating the expected magnitude of the Umkehr effect in bismuth. Following the methods of Aubrey (1971) and Saunders and Sumengen (1972), we write

$$\rho_{23}(\pm B_1) = \frac{-\sigma_{23}(\pm B_1)}{\sigma_{22}(B_1)\sigma_{33}(B_1) - \sigma_{23}(B_1)\sigma_{23}(-B_1)} \quad (5.26)$$

where

$$\sigma_{22}(B_1) = \mu_{22}a_1 + \frac{1}{2}(3\mu_{11} + \mu_{22})a_2 + 3v_{11}a_3,$$

$$\sigma_{33}(B_1) = \mu_{33}(a_1 + 2a_2) + 3v_{33}a_3,$$

$$\begin{aligned} \sigma_{23}(\pm B_1) = & (\mu_{23} \mp \frac{d_e}{\mu_{11}} B_1) a_1 - \left[\mu_{23} \pm (3\mu_{11}\mu_{33} + \frac{d_e}{\mu_{11}}) B_1 \right] a_2 \\ & \pm 3v_{11}v_{33}B_1 a_3 \end{aligned}$$

and

$$a_1 = ne \left(1 + \frac{d_e}{\mu_{11}} B_1^2 \right)^{-1}$$

$$a_2 = ne \left[1 + \frac{1}{4}(3\mu_{11}\mu_{33} + \frac{d_e}{\mu_{11}}) B_1 \right]^{-1}$$

$$a_3 = ne \left(1 + v_{11}v_{33}B_1^2 \right)^{-1}$$

$$d_e = \mu_{11}(\mu_{22}\mu_{33} - \mu_{23}^2)$$

Using the band and mobility parameters (carrier density $N = P = 3n = 4.4 \times 10^{23} \text{ m}^{-3}$, electron mobilities in $\text{m}^2 \text{V}^{-1} \text{s}^{-1}$:

$\mu_{11} = 68$, $\mu_{22} = 1.6$, $\mu_{33} = 38$, $\mu_{23} = -4.3$, hole mobilities:

$v_{11} = 12$, $v_{33} = 2.1$) obtained for bismuth at 77K by

Saunders and Sumengen 1972, we calculate that, at B_1 equal

to 0.5T, $\rho_{23}(+B_1) = 18.8 \times 10^{-7} \Omega \text{m}$ and $\rho_{23}(-B_1) = -4.9 \times$

$10^{-7} \Omega \text{m}$. Thus $\rho_{23}^{\text{even}}(B_1) = 6.9 \times 10^{-7} \Omega \text{m}$ and $\rho_{23}^{\text{odd}}(B_1) =$

$11.9 \times 10^{-7} \Omega \text{m}$: the Umkehr effect in $\rho_{23}(B_1)$ is

substantial for bismuth at 77K. Inspection of equation

(5.26) shows that the existence of even terms in $\rho_{23}(B_1)$

depends on the presence of the tilt of the electron Fermi

surface ellipsoids: if there were no tilt, there would be no

Umkehr effect in $\rho_{23}(B_1)$.

5.4.2 n-type Germanium

The co-existence of even and odd terms in $\rho_{1j}(\vec{B})$, which gives rise to the Umkehr effect, is by no means restricted to the A7 structure semimetals. It can, for example, occur in cubic crystals. This can be illustrated by considering n-type germanium (point group $\frac{4}{m} \bar{3} \frac{2}{m}$).

Consider the axial set comprising

$x//C_{2b}//[1\bar{1}0]$, $y//[11\bar{2}]$, $z//C_{31}^+//[111]$ (see Table 3.5),

which can be taken as the ellipsoidal axis system: The constant energy surfaces near each minima can be well-approximated by a set of four ellipsoids of revolution centred at the L points.

The next task is to find the form of $\rho_{1j}(\vec{B})$ in this axial set by solution of the linearized Boltzmann transport equation for this band structure model. Fuchser et al (1970) have solved the problem in the relaxation time approximation for an arbitrarily oriented electron ellipsoidal constant energy surface and have obtained

$$\alpha_{1j}(\vec{B}) = \frac{-16\sqrt{2}}{3h^3} \pi (\alpha_1 \alpha_2 \alpha_3)^{-\frac{1}{2}} \int E^{\frac{3}{2}} \frac{\partial f_0}{\partial E} (\mu_{1j}^{-1} - E)^{-1} dE. \quad (5.27)$$

Here α_i ($i = 1, 2, 3$) are inverse effective mass tensor components, E is the energy ($= \frac{\hbar^2}{2m_0} \vec{k} \cdot \vec{\alpha} \cdot \vec{k}$) and f_0 is the equilibrium distribution function. A minus sign has been included in front of this equation, the necessity of which has been confirmed by private communication with J.M. Sybert. In the axial set under consideration we have for n-type germanium

axis 1 (x - axis // [100] // c_{2b} // μ_{11} // α_1 // m_1^*

axis 2 (y - axis // [112] // $\mu_{22}(=\mu_{11})$ // $\alpha_2(=\alpha_1)$ // $m_2^*(=m_1^*)$

axis 3 (z - axis // [111] // c_{31} // μ_{33} // α_3 // m_3^* .

Thus in the absence of intervalley scattering

$$\sigma_{ij}(\vec{E}) = \sum_{k=1}^{IV} \sigma_{ij}^k(\vec{E}) = -\frac{16\sqrt{2}\pi(\alpha_1\alpha_3)^{-\frac{1}{2}}}{3h^3} \int \frac{d^3E}{E^2} \frac{\partial f_0}{\partial E} \sum_{k=1}^{IV} [(\mu_{ij}^k)^{-1} - \vec{E}]^{-1} dE \quad (5.28)$$

Where the ellipsoids of revolution are numbered in an anticlockwise order around the [001] axes. To find the total $\sigma_{ij}(\vec{E})$, the contributions from carriers in each ellipsoid are obtained by application of the following transformations to the mobility tensors and then summing over all valleys

$$\begin{aligned} \mu_{ij}^I &= R_{ip}^I R_{jq}^I \mu_{pq}^I, & \mu_{ij}^{II} &= R_{ip}^{II} R_{jq}^{II} \mu_{pq}^I, \\ \mu_{ij}^{III} &= R_{ip}^{III} R_{jq}^{III} \mu_{pq}^I, & \mu_{ij}^{IV} &= R_{ip}^{IV} R_{jq}^{IV} \mu_{pq}^I \end{aligned} \quad (5.29)$$

where R^I is a unit matrix,

$$R^{III} = \begin{pmatrix} -1 & 0 & 0 \\ 0 & \frac{1}{3} & \frac{2\sqrt{2}}{3} \\ 0 & \frac{2\sqrt{2}}{3} & \frac{1}{3} \end{pmatrix} \text{ and } R^{II,IV} = \begin{pmatrix} 0 & \mp \frac{\sqrt{2}}{3} & \pm \frac{1}{\sqrt{3}} \\ \pm \frac{\sqrt{2}}{3} & \frac{1}{3} & \frac{\sqrt{2}}{3} \\ \mp \frac{1}{\sqrt{3}} & \frac{\sqrt{2}}{3} & \frac{2}{3} \end{pmatrix}$$

Here the upper sign is for the second (II) ellipsoid and the lower sign for the fourth (IV) ellipsoid. The form obtained of $\sigma_{ij}(\vec{E})$, and thus of its inverse $\rho_{ij}(\vec{E})$, is identical to that in equation (5.1). Therefore, the off-

diagonal component $\rho_{23}(B_1)$ contains both "even" and "odd" terms: in principle, an Umkehr effect is to be expected in an n-type germanium sample with current along $[111]$ and magnetic field B_1 directed along $[1\bar{1}0]$ — when the sense of B_1 is reversed, a different voltage should be obtained in the $[11\bar{2}]$ direction. This prediction agrees with that of the phenomenological form given in table (3.5).

To conclude, the Umkehr effect is to be expected in any off-diagonal component of the magnetoresistivity tensor which contains both "even" and "odd" terms: it is directly related to the anisotropy of the constant energy surface of the crystal under consideration.

5.5 THE UMKEHR EFFECT IN $\alpha_{ij}(\vec{B})$.

From spatial symmetry arguments, we have already shown in section (3.5.5) that the Umkehr effect can occur in any component of $\alpha_{ij}(\vec{B})$ which contains both "even" and "odd" terms. We have also pointed out that this effect is well-established experimentally in bismuth. Here we shall explain briefly the appearance of the Umkehr effect in $\alpha_{ij}(\vec{B})$ by considering the Fermi surface of bismuth.

By inspection of the expanded form of equation (5.2) Sumengen and Saunders (1972a) determined for the group V semimetals which components of $\alpha_{ij}(\vec{B})$ contain both "even" and "odd" parts and therefore should exhibit the Umkehr effect. This present work does not agree with those

predictions. We have shown that when the band structure of bismuth is included analytically certain "even" and "odd" parts vanish. Inspection of the form (equation 5.7) shows which components of $\alpha_{ij}(\vec{B})$ should show the effect. Note that for those experimental configurations with \vec{B} directed along one of the crystallographic axes, x,y or z, the Umkehr effect can occur only when \vec{B} is along the x-axis, that is in all the non-zero components of $\alpha_{ij}(B_1)$. Uher and Goldsmid have recently observed the Umkehr effect in $\alpha_{33}(B_1)$ which confirms the previous observation of the effect by Steele and Babiskin (1955). Since $\alpha_{11}^{\text{odd}}(B_1)$ is zero for the diffusion contribution, an exception to this is that an Umkehr effect is to be expected in the phonon drag contribution but not in the diffusion contribution to $\alpha_{ij}(B_1)$.

Again we conclude that the appearance of the Umkehr effect in certain components of $\alpha_{ij}(\vec{B})$ is directly related to the anisotropy of the constant energy surface of the crystal under consideration.

CHAPTER SIX

MAGNETORESISTIVITY TENSOR OF ARSENIC (25.5 at.%) - ANTIMONY ALLOY SINGLE CRYSTALS

6.1 INTRODUCTION

In this chapter we discuss the experimental work carried out on the magnetoresistivity tensor of As(25.5 at.%) - Sb alloy single crystals which set the work in progress. The experimental results are interpreted to give the band model parameters of this material for the first time.

The contents of this chapter (except section 6.4) have already been published (see Akgözⁿ and Saunders 1971, Akgözⁿ et al 1972, Akgözⁿ and Saunders 1974).

6.2 GROWTH AND DISLOCATION ETCH PITS OF ARSENIC (25.5 at %) - ANTIMONY SINGLE CRYSTALS.

6.2.1 Crystal growth

A continuous series of solid solutions with the A7 structure is formed between arsenic and antimony; the lattice constant a , the rhombohedral angle α and the unit cell volume increase almost linearly with composition (Quensel et al. 1937, Trzebiatowski and Bryjak 1938). For solid solution systems in general the solidus and liquidus are separated on the phase diagram: the liquid and solid phases in equilibrium at a given temperature do not have the same composition and severe problems arise on single crystal growth—a variety of crystalline imperfections can result, including, on a gross scale, concentration gradients along the boule or dendritic or cell-like structure containing excess concentration of one component due to constitutional supercooling. Goldsmid (1970) in his review of the bismuth-antimony alloys has emphasised how difficult it is to grow homogeneous crystals of those alloys. In the arsenic-antimony system there is a feature of the phase diagram (figure 6.1) which can be used to avoid these problems: a minimum melting point at which the solidus and liquidus touch and so the liquid and solid phases in equilibrium have the same composition (25.5 at.%As). Several studies have been made of the temperature-composition dependence of the liquidus and solidus on the arsenic-antimony phase diagram by thermal, microscopic, X-ray and

chemical analysis techniques (Parravano and de Cesaris 1912, Mansuri 1928, Shih and Peretti 1956, Skinner 1965). The position of the minimum melting point on the liquidus was found to be 25.5 at.% and 612°C by Mansuri (1928) and between 22 and 29 at.%As and 612°C by Shih and Peretti (1956). The more recent and extensive work of Skinner (1965) confirms that the minimum melting temperature is 612°C; we follow Skinner and take the corresponding composition as 25.5 at.% As.

Single crystals of arsenic (25.5 at.%, 17.4 wt.%) - antimony alloys were grown from 99.9999% purity elements by a modified Bridgman technique. Evacuated (10^{-4} torr), 16mm internal diameter, quartz growth tubes with thick walls (1.6 mm), on account of the substantial vapour pressure of arsenic, were employed. Use of a single pointed end on the growth tube proved as satisfactory as employment of a constricted tube for single seed selection. A 20 mm length of 3 mm quartz rod was fused to the end of the growth tube as a spacer, because direct contact with the steel support ~~road~~ used in the furnace destroyed the temperature gradient at the tip, in which case several longitudinal crystals grew. To reduce oxidation, the arsenic was bought in sublimed form in evacuated tubes containing a suitable quantity for one run. The arsenic was weighed and transferred immediately to the growth tube (containing the antimony) and put under vacuum at once. Heating to 350°C under vacuum for 3 h distilled off any volatile oxide present; the growth tube was then sealed off. Figure (6.2) shows the growth furnace (for more

details, see Jeavons and Saunders 1968 and Jeavons 1969). A series of experiments showed that the best crystals were obtained by maintaining the temperature gradient at $10^{\circ}\text{C}/\text{cm}$ near the freezing interface and using a crystal growth rate of 2 mm h^{-1} .

Arsenic and antimony single crystals tend to grow with the z-axis nearly normal to the growth direction; but the z-axis of the alloy crystals is directed randomly between 50° and 75° with respect to the growth axis. As a rule, A7 structure crystals cleave readily to expose (111) faces; the arsenic-antimony alloys are no exception. The crystals show a perfect cleavage on the (111) face. Unlike arsenic, the alloy does not oxidise markedly on prolonged exposure to the air, and cleaved surfaces retain their shiny appearance. Debye-Scherrer powder photographs of this 25.5 at.% alloy show that the primitive rhombohedral lattice parameter a is equal to $4.418 \pm 0.001 \text{ \AA}$ and α is equal to $56^{\circ} 12' \pm 3'$.

6.2.2 Dislocation etch pit studies

Cleaved (111) faces of the crystals have been etched and examined microscopically. Several potential etching reagents were examined; an etch composed of three parts hydrofluoric acid (40%), five parts concentrated nitric acid, three parts glacial acetic acid and a few drops of bromine, aged for one month in an enclosed container, was the most successful. After immersion of the crystal for one to two seconds, followed

by washing in distilled water, this etch produced pits on the (111) cleavage plane which were much better defined than usual in metal alloys. The pits are triangular with slightly rounded corners and have pyramidal bottoms, (figures 6.3 and 6.4). The pit sides are parallel to the $\langle 10\bar{1} \rangle$ directions and, in consequence, to one of the slip line systems (figure 6.3). Akgözⁿ and Saunders (1971), by using several techniques, have established that the above etch does reveal the sites of emergence of dislocations on the (111) cleavage face of the alloy. Most of the crystals have etch pit counts of between 10^4 and 10^5 per square cm; the best crystals have counts as low as 10^3 per square cm.

Specimens were indented using a Vickers microhardness tester and then etched. No new etch pits were evident. It can be concluded that at room temperature arsenic-antimony alloys are brittle and that the dislocation mobility is essentially zero.

To relate the etch pit structure with possible dislocations, it is necessary to consider the permissible Burgers vectors and dislocation reactions for the A7 crystal structure. A standard (111) projection, including those directions particularly relevant to dislocation studies, is shown in figure (6.5). Parameters associated with dislocations most likely to occur are collected in table (6.1). The self-energy of a dislocation line is proportional to the square of Burgers vector (\vec{b}) which is presented in table (6.1) both for the

A7 structure in general and for the arsenic-antimony alloy having a rhombohedral angle α equal to $56^\circ 12'$ in particular. The sense of the angle that the Burgers vector makes with the $[111]$ direction can be found from the stereographic projection in figure (6.5) and the magnitude of this angle from table (6.1). The Frank stability rule can now be used to determine which dislocations are most likely to be stable; dislocations of large \vec{b} can lower their energies by spontaneous dissociation: a dislocation \vec{b}_1 will dissociate into two dislocations \vec{b}_2 and \vec{b}_3 , if $b_1^2 > (b_2^2 + b_3^2)$, that is if $\vec{b}_2 \cdot \vec{b}_3 > 0$. Therefore, the lowest energy dislocation should have a Burgers vector equal to the smallest Bravais lattice vector; other small values of \vec{b} can also lead to stable dislocations. These criteria evidence that dislocations with Burgers vectors $\langle 101 \rangle$, $\langle 100 \rangle$ or $\langle \bar{1}11 \rangle$ are stable in the A7 structure.

Several distinct types of pyramidal etch pits have been observed in the arsenic-antimony alloy (figure 6.4). Symmetrical pits occur together with asymmetrical pits in which the projected apex is deflected, either towards a base or a corner of the etch pit triangle. These pit types can now be related to the permissible stable dislocations. The symmetrical (S) pits are probably formed by dissolution along dislocation lines parallel to the trigonal axis: these may well be edge dislocations with one of the $\langle 10\bar{1} \rangle$ as Burgers vector. A dislocation parallel to a $\langle 110 \rangle$ direction makes an angle of 18° with the $[111]$ direction (figure 6.5). Dissolution

along this dislocation line would produce pits with the projected apex deflected towards one of the corners of the etch pit triangle (an example can be seen inside the circle labelled C in figure 6.4). Detailed measurements of the etch pit dimensions have been made to assess the angle to which the apex deflection corresponds. Etch pit depths (about 2 to 4 μm) have been measured by focusing the microscope at the surface and then at the apex, and finding the lens traverse distance. This cannot be done with great accuracy. The angle is estimated as $20^\circ \pm 5^\circ$, in reasonable agreement with the postulate that this particular pit type arises from dislocations lying parallel to $\langle 110 \rangle$ directions. For such a direction an edge dislocation with Burgers vector $\langle 10\bar{1} \rangle$ would be stable.

The commonest type of asymmetrical etch pit has a projected apex deflected towards a base of the triangle (labelled (Ba) in figure 6.4). Pit dimension measurements show that the associated dislocation makes an angle of $30^\circ \pm 5^\circ$ with the $[111]$ direction. This angle and the sense of the apex deflection, suggest that this type of pit arises from dissolution along dislocations parallel to $\langle 100 \rangle$ directions which would make an angle of 33° with the $[111]$ direction (table 6.1).

The general results obtained also hold for other A7 structure materials.

6.2.3 Orientation of the crystals.

To orient the A7 structure crystals in general and the As-Sb alloy in particular, the +y and -y directions need to be determined subsequent to and consistent with an arbitrary choice of a +z direction along the trigonal axis. To achieve this end, we have used the following two techniques:

(i) Laue back-reflection photographs.

The process involved in aligning a crystal of an A7 structure material rests upon the fact that this structure is closely related to a simple cubic structure from which it can be obtained by applying two independent, small distortion (Falicov and Golin 1965, Windmiller 1966); the normals to the $\{100\}_{\text{fcr}}$ planes exhibit pseudo-fourfold symmetry and the normals to the $\{\bar{1}11\}_{\text{fcr}}$ planes pseudo-threefold symmetry. Referred to the primitive rhombohedral unit cell, these pseudo-axes are the normals to the $\{011\}_{\text{prh}}$ and $\{100\}_{\text{prh}}$ planes respectively. Hence the quadrant in the mirror plane formed by the +y and -z axes (and the -y and +z axes) contains a pseudo-fourfold axis and that formed by the +y and +z axes (and the -y and -z axes) contains a pseudo-threefold. When a back reflection photograph is taken with the X-ray beam incident along a bisectrix axis onto a crystal with its cleavage plane horizontal, a pattern with mirror symmetry is obtained; the photograph also shows a spot corresponding to the pseudo-threefold reflection. An example for bismuth is to be found in the publication of Brown et al (1968) (figure 3) and another is given here for the As-Sb alloy (figure 6.6). If the

+z direction is chosen to be the outward normal to a cleavage surface, then the +y direction is determined since the pseudo-threefold reflection must be in the +y+z (or the -y-z) quadrant. Laue photographs taken of the arsenic-antimony alloy with the x-ray beam along the pseudo-threefold (figure 6.7) and along the pseudo-fourfold (figure 6.8) are given here to show the pseudo-symmetry. The angles between the pseudo-axes and the +y axis are listed in table (6.2).

(11) Orientation of the triangular etch pits on (111) plane.

Using technique (1), we have determined the orientation of the triangular etch pits with respect to the +x and +y axis on the (111) plane: a vector drawn from the pit centre normal to a pit side points along the +y axis, when the outward normal from the cleaved surface is taken as the +z direction (an example is shown in figure 6.3). Once this is known the crystals can be orientated by a simple visual inspection after cleaving and etching; first the +z axis is defined, the +y axis is then found from the etch pits, and finally a +x axis completes a right handed orthogonal set.

6.2.4 Conversely oriented etch pits in the A7 structure semimetals.

Apparent discrepancies in the orientation of the triangular etch pits have been mentioned by Brown et al (1968) and Akgözⁿ and Saunders (1971). Using the etching reagents quoted in the literature, we have examined the orientation of etch pits on single crystals of Bi, As, Sb, As(25.5 at.%)ⁿ-Sb and an

Sb-(2 at.%)Ge alloy. Crystals were first aligned by using Laue back-reflection photographs (technique (i)) and etched using the reagents listed in table (6.3), and the pits — on that cleavage face with the previously defined +z axis emerging from it — were examined. For a particular etchant on a given material, the pits consistently had a definite orientation. In all cases the sides of the etch pits were parallel to the binary directions and pits on the -z cleavage face (-z axis emerging from the face) were inverted with respect to those on the +z face, as required by the inversion axis of the $\bar{3}m$ point group. However, table (6.3) shows that with different etchants on a given material, two distinct and opposite orientations of triangular pits can be found; in some cases the pits were such that the +y axis pointed outwards from the pit centre normal to a base of the triangle (type A), and in others the +y axis pointed outwards through an apex of the triangle (type B). It should be noticed that even when a particular etch is used on different materials, the pits produced on each do not necessarily have the same orientation; for instance the bromine etch of Shetty and Taylor (1968) produces pits on arsenic with the opposite orientation to those it produces on antimony and the arsenic-antimony alloy.

These findings account for the apparent discrepancies in the orientation of etch pits found by different workers and previously suggested (Brown et al 1968, Akgoz and Saunders 1971) to be due to incorrect definitions or identification of axes. In particular it explains the difference in the

orientation of the pits obtained by Shetty and Taylor (1968) and Calvert and Taylor (1972), from those found by Pace et al (1970) on arsenic and antimony and by Akgoz and Saunders (1971) on the As-Sb alloy. Also accounted for are the differences in orientation between the pit orientations on Bi (Lovell and Wernick 1959, Brown et al 1968). Since the etch pit orientation depends on the reagents used, extreme care must be taken if etch pits are to be employed for assignment of the sense of the y-direction in the A7 structure crystals. ~~Hexagonal~~ type pits have been reported on arsenic (Jeavons and Saunders 1968) and on bismuth (Frawley and Childs 1970); these might represent an intermediate form between the two triangular extremes. The further question of whether all the reagents used give etch pits that mark the points of emergence of all dislocation types on the cleaved surfaces has not yet been resolved.

6.3 GALVANOMAGNETIC EFFECTS OF ARSENIC (25.5 at.%) - ANTIMONY ALLOY SINGLE CRYSTALS.

The nature of the band structure of the arsenic-antimony alloys has been the subject of some controversy. On the basis of measurements of electrical resistivity as a function of temperature, Saunders et al. (1965) first reported that these alloys show metallic (rather than semiconducting) behaviour throughout the whole composition range. But Ohyama (1965, 1966) presented electrical resistivity results which show the negative temperature coefficient typical of semiconductors; he stated that alloys in the composition range 9 to 40 at.% As are

narrow gap semiconductors above about 240K. This composition range closely parallels that (5 to 40 at.%Sb: Jain 1959) over which the bismuth antimony alloys are semiconducting, yet the band overlap of bismuth is only 0.0385eV (Smith et al. 1964) while those of antimony and arsenic are 0.20eV (Windmiller 1966) and 0.37eV (Priestley et al. 1967) respectively. Thus the band overlap change required to produce a semiconductor by alloying antimony with arsenic is much greater than that for bismuth with antimony.

To resolve the problem, Saito and Maezawa (1970) have measured the electrical resistivity and the magnetic susceptibility of alloys containing up to 21 at.% As. All samples show a positive temperature coefficient of electrical resistivity. The magnetic susceptibility parallel (χ_{\parallel}) and perpendicular (χ_{\perp}) to the trigonal axis of the alloys as a function of temperature is very similar to that of antimony itself. This evidence for retention of semimetallic behaviour as antimony is alloyed with arsenic finds further confirmation in that the extremal cross-sectional areas of the Fermi surface, measured by the de Haas-van Alphen effect, do not change with increasing arsenic concentration up to 3 at.%: the band overlap does not alter appreciably over this composition range.

Although we consider that Saito and Maezawa (1970) have now provided substantial confirmation of the original finding (Saunders et al 1965) that the arsenic-antimony alloys are

semimetallic, one aim at the onset of this work was to test that finding further, using this particular As-Sb alloy single crystals.

Reported here are systematic measurements, made at selected temperatures between 1.5 and 300K, of the low field isothermal magnetoresistivity tensor components and the angular dependence of certain components of the field dependent tensor on As(25.5 at.%) - Sb alloy single crystals. Results are interpreted using a two-carrier, multivalley band model to obtain the carrier densities and mobilities and their temperature dependences and the tilt angle of the Fermi surface pockets. These alloy model parameters are then compared and contrasted with those of the parent elements.

6.3.1 Experimental procedure and results.

Two distinct approaches have been made to measurement of the magnetoresistivity tensor $\rho_{ij}(\vec{B})$. These are first to obtain the low field tensor components and second to measure the angular dependence of certain of the magnetic field dependent tensor components for a constant magnetic field.

The low field technique has been used previously in several studies of the group V semimetals; particularly relevant here is the work on antimony (Öktü and Saunders 1967) and arsenic (Jeavons and Saunders 1969).

We have already written the low field expansion of $\rho_{ij}(\vec{B})$ up to second order in \vec{B} (see chapter 4, equations (4.35) and (4.36)). For $\bar{3}m$ point group symmetry, there are 2 independent components of ρ_{ij}^0 , 2 of $\rho_{ijk_1}^{(1)}$ (usually denoted as R_{ijk}) and 8 of $\rho_{ijk_1k_2}^{(2)}$ (usually denoted in shortened notation as A_{ij}).

Using equations (4.35) and (4.21), $\rho_{ij}(\vec{B})$ in the low field expansion can be written as

$$\rho_{ij}(\vec{B}) = \begin{matrix} \text{ODD} \\ \text{(or antisymmetric)} \end{matrix} \begin{pmatrix} 0 & R_{123}B_3 & -R_{231}B_2 \\ -R_{123}B_3 & 0 & R_{231}B_1 \\ R_{231}B_2 & -R_{231}B_1 & 0 \end{pmatrix} + \begin{matrix} \text{EVEN} \\ \text{(or symmetric(s))} \end{matrix} \begin{pmatrix} \rho_{11}^s(\vec{B}) & \rho_{12}^s(\vec{B}) & \rho_{13}^s(\vec{B}) \\ \rho_{12}^s(\vec{B}) & \rho_{22}^s(\vec{B}) & \rho_{23}^s(\vec{B}) \\ \rho_{13}^s(\vec{B}) & \rho_{23}^s(\vec{B}) & \rho_{33}^s(\vec{B}) \end{pmatrix} \quad (6.1a)$$

where

$$\rho_{11}^s(\vec{B}) = \rho_{11}^0 + A_{11}B_1^2 + A_{12}B_2^2 + A_{13}B_3^2 + 2A_{14}B_2B_3$$

$$\rho_{22}^s(\vec{B}) = \rho_{11}^0 + A_{12}B_1^2 + A_{11}B_2^2 + A_{13}B_3^2 - 2A_{14}B_2B_3$$

$$\rho_{33}^s(\vec{B}) = \rho_{33}^0 + A_{31}(B_1^2 + B_2^2) + A_{33}B_3^2$$

$$\rho_{23}^s(\vec{B}) = A_{41}B_1^2 - A_{41}B_2^2 + 2A_{44}B_2B_3$$

$$\rho_{13}^s(\vec{B}) = 2A_{44}B_1B_3 + 2A_{41}B_1B_2$$

$$\rho_{12}^s(\vec{B}) = 2A_{14}B_1B_3 + (A_{11} - A_{12})B_1B_2. \quad (6.1b)$$

Equations (6.1b) have been given by Juretschke (1955) but are repeated here with corrected signs for A_{14} and A_{41} in agreement with Okada (1955a). The form of these equations enables one to obtain readily, using

$$E_i = \rho_{ij}(\vec{B})J_j, \quad (6.2)$$

the experimental configurations required for measurement of a particular tensor component.

To measure these twelve low field tensor components, sets of three single crystal, parallelepiped (about 2.0 x 0.2 x 0.2 cm) specimens, oriented along the x, y and z axes, have been used. Crystals were aligned using the symmetry shown on Laue back-reflection photographs (and the sense of the y-axis checked by etch pit orientation) as described in section (6.2.3). Samples were spark-cut from these oriented crystals. The four-probe configuration usual for galvanomagnetic effect measurements was employed. Voltage probes were copper wire (37 gauge) soldered to the sample with a solder consisting of a eutectic mixture of Bi and Cd (melting point -140°C) which does not become superconducting above 0.8K. The sample current was about 0.5 Ampere. For temperature measurements copper-constantan (above 77K) and Au/Fe - Cromel (for low temperatures) thermocouples were attached to each end of the sample. We have noticed that thermocouples not electrically insulated from the sample can give rise to stray voltages; thus the thermocouples were electrically insulated from the sample by using very thin mica plates. Magnetic fields up to

about 8 kG (0.8T) were provided by a water-cooled electromagnet. Measurements of low field tensor components between 77K and room temperature were made by experimental techniques similar to those described by Jeavons and Saunders (1969), Jeavons (1969) and Sumengen (1971). A standard liquid helium cryostat was employed for lower temperature measurements.

Sets of low field magnetoresistivity tensor components measured at selected temperatures between 1.5K and 300K (room temperature (-300K), nitrogen (77K), pumped nitrogen (-50K), helium (4.2K) and pumped helium (-1.5K)) are given in tables (6.4a, 6.4b) together with the magnetoconductivity tensor components obtained from

$$\rho_{ij}(\vec{B}) \sigma_{jk}(\vec{B}) = \delta_{ik}. \quad (6.3)$$

The appropriate relationships are given in the correct sign convention in Appendix I as equations (AI.4). The anisotropies of resistivity and the Hall coefficients are quite marked: $\rho_{11}^0/\rho_{33}^0 = 1.6$, $R_{123}/R_{231} = 5$. In the alloy ρ_{11}^0 is larger than ρ_{33}^0 , behaviour which resembles that of antimony ($\rho_{11}^0/\rho_{33}^0 = 1.3$) rather than that of arsenic ($\rho_{11}^0/\rho_{33}^0 = 0.8$). On the other hand the anisotropy ratio of the Hall coefficients (R_{123}/R_{231}) is more like that of arsenic (-6) than that of antimony (-1.1). Negative signs of R_{123} and R_{231} are found for all three materials. The magnetoresistivity components A_{ij} for the alloy are much smaller than those of the parent elements: this is a consequence of lower carrier mobilities in the alloy. The signs of A_{41} and A_{14} are both positive in agreement with

those in arsenic and antimony for the same choice of sign and axial conventions: this finding implies that the tilt angles of the electron and hole ellipsoids have the same sense as in the parent elements, as the computations confirm.

The temperature dependences of the zero field resistivity components ρ_{11}^0 and ρ_{33}^0 are compared in Figure (6.9) with those of similar compositions measured by Saunders et al. (1965) and by Saito and Maezawa (1970); the resistivity of the present samples is much lower than those in the earlier work. The positive temperature coefficients of ρ_{11}^0 and ρ_{33}^0 over the whole temperature range show that the arsenic (25.5 at.%) - antimony alloy has metallic behaviour between 1.5 and 300K in direct contradiction to the findings of Ohyama (1966).

The low field magnetoconductivity components show very weak temperature dependences at low temperatures. Above about 60K, the σ_{ij} obey approximately $T^{-0.4}$, the $\sigma_{ijk}, T^{-0.9}$ and the $S_{ij}, T^{-1.2}$ (figure 6.10).

The magnetoconductivity tensor components $\sigma_{ij}(\vec{B})$ have themselves been directly related (Aubrey 1971) to the band model parameters and to obtain these parameters measurements have also been made of certain $\rho_{ij}(\vec{B})$. To ensure that sufficient data points are available to enable extraction of a complete set of model parameters, measurements have been made of the angular dependence of certain $\rho_{ij}(\vec{B})$ in a constant magnetic field taken right round the xy and xz planes of 10°

intervals. Results obtained at 4.2K, 77K and 300K for $\rho_{11}(B_1, B_2, 0)$, $\rho_{11}(B_1, 0, B_3)$ and $\rho_{21}(B_1, 0, B_3)$ are shown in Figures (6.11a), (6.11b) and (6.12) respectively. The results were obtained on the same x-cut specimens as those used for the low field components so that a direct comparison between the model parameters could be made under identical physical conditions. The specimens used for galvanomagnetic measurements have been examined by electron microprobe analysis: the composition along each specimen length has been found to be the same within the experimental error ($\leq \pm 0.5\%$ composition change) of the probe.

6.3.2 Computation

In the absence of any theoretical band structure calculations for the arsenic-antimony alloys, interpretation of the galvanomagnetic effects must rest on certain assumptions concerning the nature of the Fermi surface. It is now established (see Dresselhaus 1971 for a review) that the electron Fermi surfaces of arsenic and antimony each consist of three, approximately ellipsoidal pockets centred on the L points in the Brillouin zone. The six hole pockets in antimony are located near the T point, each has mirror symmetry but is rather more warped than the electron pockets. The single hole surface of arsenic may be thought of as six warped pockets near the T point joined by six thin necks (Lin and Falicov 1966). Analysis of the galvanomagnetic

effects in antimony (Öktü and Saunders 1967, Bresler and Red'ko 1972) and arsenic (Jeavons and Saunders 1969) has been based on the assumption that the electron and hole pockets are ellipsoids. As the general form, including sign and anisotropy, of the measured low field components of the magnetoresistivity tensor of the alloy (tables (6.4a) and 6.4b) resembles those of the parent elements, it is reasonable to assume that the carriers in the alloy are also contained in two sets of tilted ellipsoids.

With the assumption that the electron (N) and hole (P) densities are equal ($N = P$), there are nine band model parameters for this model of the Fermi surface. The equations which relate the band model parameters to the low field magnetoconductivity tensor components was first derived in principle from the Boltzmann transport equation by Abeles and Meiboom (1956) and by Drabble and Wolfe (1956). The appropriate forms for the two band, tilted ellipsoidal model are given in S.I. units in Appendix I, equation (AI.1), (AI.2) and (AI.3). A least-mean-squares fit procedure (Jeavons and Saunders 1969, Saunders and Sümengen 1972) has been used to provide the best fit of model parameters to the measured low field magnetoresistivity tensor components by a programme which include equations (AI.1 - AI.4) in Appendix I. A copy of the computer programme is given in Appendix III. The solution obtained for the computed model parameters are given in table (6.5a). The model parameters at different temperatures show a satisfying self-consistency which attests to the

choice of a reasonable model.

A further test is to use the polar data for the $\rho_{1j}(\vec{B})$ shown in Figures (6.11) and (6.12) to obtain the model parameters and then compare them with those found from the low field components. Using the two band tilted ellipsoidal Fermi surface model, Aubrey (1971) has obtained explicit expressions for the magnetoconductivity tensor $\sigma_{ij}(\vec{B})$, valid over the classical range of magnetic fields. These equations have been extended here to analyse the data taken when the magnetic field is in the xy, yz, and xz planes; the resultant equations are given in Appendix II. To transform the measured magnetoresistivity tensor components to the magnetoconductivity tensor components the following relations have been used:

$$\rho_{11}(B_1, B_2, 0) = \frac{\sigma_{22}(B_1, B_2, 0)\sigma_{33}(B_1, B_2, 0) - \sigma_{32}(B_1, B_2, 0)\sigma_{23}(B_1, B_2, 0)}{|\sigma_{1j}(B_1, B_2, 0)|}$$

$$\rho_{11}(B_1, 0, B_3) = \frac{\sigma_{22}(B_1, 0, B_3)\sigma_{33}(B_1, 0, B_3) - \sigma_{32}(B_1, 0, B_3)\sigma_{23}(B_1, 0, B_3)}{|\sigma_{1j}(B_1, 0, B_3)|}$$

$$\rho_{21}(B_1, 0, B_3) = \frac{-\sigma_{21}(B_1, 0, B_3)\sigma_{33}(B_1, 0, B_3) - \sigma_{31}(B_1, 0, B_3)\sigma_{23}(B_1, 0, B_3)}{|\sigma_{1j}(B_1, 0, B_3)|}$$

(6.4)

where $|\sigma_{1j}(B_1, B_2, 0)|$ and $|\sigma_{1j}(B_1, 0, B_3)|$ are the determinants of the magnetoconductivity tensor when $B_3 = 0$ and $B_2 = 0$ respectively. Using these transformations and the expressions for $\sigma_{ij}(\vec{B})$ given in Appendix II, a minimization procedure (sim-

ilar to that adopted for solution of the low field components) has been used to obtain best fit solutions for the model parameters from the data in Figures (6.11) and (6.12) for $\rho_{11}(B_1, B_2, 0)$, $\rho_{11}(B_1, 0, B_3)$ and $\rho_{21}(B_1, 0, B_3)$ taken all together at a given temperature. The solutions obtained at 4.2K, 77K and 300K are given in table (6.5b). There is good agreement between the model parameters obtained by both methods. This confirms that the expressions for $\sigma_{ij}(\vec{B})$ derived by Aubrey (1971) for the general case of group V semimetals apply directly to this arsenic-antimony alloy. The polar plots have been measured—and therefore the complete set of model parameters obtained—on one sample alone, a great advantage especially for alloys.

6.3.3 Discussion of the model parameters

The results in table (6.5) present, for the first time for an arsenic-antimony alloy, details of the carrier densities, mobilities and the tilt angle of the Fermi surface pockets. Physical insight into these data can be gained by a comparison of the model parameters of the alloy with those of the parent elements (table 6.6). As in the elements, the holes occupy pockets of large tilt angle and the electrons those of smaller tilt and the tilt angles have a negative sense. The tilt angles of the electron ellipsoids are much the same in all three materials (table 6.6). In the parent elements the electron ellipsoids are highly elongated, and the components of the electron mobility tensor reflect this. In all three materials μ_2 is at least an order of magnitude smaller than

either μ_1 or μ_3 . The hole pocket tilt of the alloy lies between those of arsenic and antimony, and is closer to that in the latter.

The alloy Fermi surface probably bears a marked similarity to that of antimony. A useful parameter for comparison between the alloy and the elements is the relative proportion of the Brillouin zone filled by carriers. This is equivalent to the ratio of the Fermi surface volume V_{FS} to that V_{BZ} of the Brillouin zone. This ratio is equal to $N/2N_v$ where N is the carrier density per band and N_v is the number of unit cells in unit volume. Values of $N/2N_v$, and thus of V_{FS}/V_{BZ} , calculated at room temperature are 1.27×10^{-3} , 1.78×10^{-3} and 4.65×10^{-3} for antimony, the alloy and arsenic respectively. The size of the Fermi surface in relation to the Brillouin zone volume of the alloy is much closer to that of antimony than arsenic.

The temperature dependence of the electron and hole mobility components is shown in figure (6.13). At low temperatures the mobilities are essentially independent of temperature above about 60K vary at $T^{-0.4}$. The temperature dependence of the mobility is quite different from that in the elements ($T^{-1.7}$ for arsenic, Jeavons and Saunders 1969; $T^{-1.5}$ for antimony, Öktü and Saunders 1967). The mobility in this solid solution seems to be dominated by the disordered atomic array of lattice sites occupied at random by the two different atom types which scatters more efficiently than the lattice vibrations or carrier-carrier interactions.

The carrier density is almost independent of temperature (table 6.5). And although this alloy lies in the middle of the composition range over which the arsenic-antimony alloys were said by Ohyama (1966) to be semiconductors, the carrier density is greater than that of antimony itself (table 6.6). This finding and the positive temperature coefficient of electrical resistivity (figure 6.9) demonstrate that this alloy is semimetallic.

6.4 ELECTRON AND HOLE TILT ANGLES IN THE A7 STRUCTURE SEMIMETALS.

It is now known that the electron pockets of As, Sb and Bi are centred at the "L" points of the Brillouin zone and are tilted with respect to the trigonal plane. The hole pockets of As and Sb are located at the so-called "H" points in the mirror planes and are also tilted with respect to the trigonal plane. Brown et al (1968) have unambiguously described the sign of the electron Fermi surface tilt angle in Bi. Here we follow their description and generalize it so that it includes the Fermi surface tilt angles of As and Sb and the As-Sb alloy. To achieve this end:

- (i) We refer to the crystallographic right-handed orthogonal axial set (see, section 2.2 and figures 2.1 to 2.9);
- (ii) we assume that all the Fermi surface pockets are ellipsoidal;
- (iii) we take $m_1^* // a_1 // b_1 // c_1 // +x$ (+binary) direction and the other two axes of the ellipsoids in the mirror plane.

So far all the reported theoretical and experimental work does agree that the cross sections of the ellipsoids in the mirror planes are highly anisotropic, the long axes of the ellipses (heavy mass direction) are usually denoted by $m_{2,e}^*$ (or $m_{2,h}^*$). We shall use this common observed feature to describe the tilt of the Fermi ellipsoids in As, Sb, Bi and the As-Sb alloy.

We now define the tilt angle as the smaller angle between the $+k_y$ and $m_{2,e}^*$ (or $m_{2,h}^*$) directions. Of course, the hole ellipsoid of Bi is not tilted and so it is excluded from this definition. All the tilt angles will be measured from the $+k_y$ direction. A positive tilt angle is then defined when $m_{2,e}^*$ (or $m_{2,h}^*$) is opened towards ΓL direction and negative when $m_{2,e}^*$ (or $m_{2,h}^*$) is moved towards ΓX direction in the Brillouin zone. According to this definition, the electron tilt angle of Bi is positive, and the electron and hole tilt angles of Sb, As and the alloy are negative.

Armed with a firm description of the tilt angles, we shall now show how to introduce them into the galvanomagnetic equations. The key equation (see, Herring and Vogt 1956) is

$$\vec{\mu} = \frac{e\vec{\tau}}{\vec{m}^*} = e\vec{\tau} \cdot \vec{\alpha} \quad (6.5)$$

where $\vec{\mu}$ is the mobility tensor, $\vec{\tau}$ is the relaxation time tensor, \vec{m}^* is the effective mass tensor and $\vec{\alpha}$ is the inverse effective mass tensor ($\vec{\alpha} = (\vec{m}^*)^{-1}$). All the tensors in equation (6.5) are second rank polar. Equation (6.5) is

defined only when all the tensors refer to the same point in the Brillouin zone. The symmetry of this point restricts the form of these tensors. Since equation (6.5) relates the mobilities to the effective masses via the relaxation time, it may be called the bridge equation, i.e., results obtained from the galvanomagnetic measurements can be related to the fundamental parameters via equation (6.5).

Let us see how the tilt angle enters into the mobility equations expressed in the crystallographic orthogonal set. For this we use the passive convention and employ clockwise and anticlockwise rotations. Rotation of an ellipsoid axes about the binary (+x) direction (which is parallel to the 1 axis of the ellipsoid) is represented by

$$R = \begin{pmatrix} 1 & 0 & 0 \\ 0 & \cos\theta & \pm\sin\theta \\ 0 & \mp\sin\theta & \cos\theta \end{pmatrix} \quad (6.6)$$

where the upper sign is for clockwise rotations and the lower sign for anticlockwise rotations, θ is the tilt angle and its range is $0^\circ < \theta < 90^\circ$. It is convenient to insert the sign of the tilt angle into the transformation matrix R (equation 6.6) so that θ takes positive values only.

Example 1: the principal electron ellipsoid of bismuth. The tilt angle is positive. We need to employ a clockwise rotation, that is the upper sign in equation (6.6) is used. The mobility tensor components transform as

$$\mu_{ij} = R_{ip} R_{jq} \mu_{pq}^* \quad (6.7)$$

where R_{ip} and R_{jq} are obtained from equation (6.6) and

$\mu_{pq}^* = \mu_p \delta_{pq}$. Thus

$$\left. \begin{aligned} \mu_{11} &= \mu_1 \\ \mu_{22} &= \mu_2 \cos^2 \theta + \mu_3 \sin^2 \theta \\ \mu_{33} &= \mu_2 \sin^2 \theta + \mu_3 \cos^2 \theta \\ \mu_{23} &= \frac{1}{2} (\mu_2 - \mu_3) \sin 2\theta \end{aligned} \right\} \quad (6.8)$$

The tilt angle is given by (Hartmann 1969)

$$\tan 2\theta = \frac{2\mu_{23}}{(\mu_{22} - \mu_{33})} \quad (6.9)$$

where $\mu_{23} < 0$ and $(\mu_{22} - \mu_{33}) < 0$.

Example 2: the principal electron ellipsoids of As, Sb and the alloy.

The tilt angles are negative, that is, the lower sign in equation (6.6) is used. The mobility tensor components transform as

$$\left. \begin{aligned} \mu_{11} &= \mu_1 \\ \mu_{22} &= \mu_2 \cos^2 \theta + \mu_3 \sin^2 \theta \\ \mu_{33} &= \mu_2 \sin^2 \theta + \mu_3 \cos^2 \theta \\ \mu_{23} &= \frac{1}{2} (\mu_3 - \mu_2) \sin 2\theta \end{aligned} \right\} \quad (6.10)$$

The tilt angle can be obtained by

$$\tan 2\theta = \frac{2 \mu_{23}}{(\mu_{33} - \mu_{22})} \quad (6.11)$$

where $\mu_{23} > 0$ and $(\mu_{33} - \mu_{22}) > 0$.

Example 3: the principal hole ellipsoids of As₃B and the alloy. The tilt angles are negative. The hole mobility tensor components transform as

$$\left. \begin{aligned} v_{11} &= v_1 \\ v_{22} &= v_2 \cos^2 \theta + v_3 \sin^2 \theta \\ v_{33} &= v_2 \sin^2 \theta + v_3 \cos^2 \theta \\ v_{23} &= \frac{1}{2}(v_3 - v_2) \sin 2\theta \end{aligned} \right\} \quad (6.12)$$

The tilt angle can be obtained by

$$\tan 2\theta = \frac{2 v_{23}}{(v_{33} - v_{22})} \quad (6.13)$$

The difficulty arises when $45^\circ < |\theta| < 90^\circ$, that is, for the hole tilt angle of arsenic; $|\theta| = 50^\circ$. For this case $v_{23} > 0$, but $(v_{33} - v_{22}) < 0$ therefore equation (6.13) yields the complimentary tilt angle with a negative sign. This difficulty may be removed by rewriting equations (6.13) as

$$\tan 2\psi = - \frac{2 v_{23}}{(v_{33} - v_{22})} \quad \text{and} \quad \theta = \frac{\pi}{2} - \psi \quad (6.14)$$

Thus when $45^\circ < |\theta| < 90^\circ$ equation (6.14) is used instead of equation (6.9) or (6.11) or (6.13).

Let us examine the elements of equation (6.5) in more detail.

$\bar{\mu}$ is symmetric (essentially this is due to the Onsager reciprocity relations, in fact we have shown that partial $\bar{\mu}$ or \bar{V} is also symmetric in the A7 structure semimetals) so it can be geometrically represented by an ellipsoid (or rather a quadric) and is diagonal when it is referred to its principal axes.

\bar{m}^* (or its inverse $\bar{\alpha}$) is symmetric by definition. It is obtained from the expansion of the carrier energy $E(\vec{k})$ about \vec{k} in the vicinity of a minimum or maximum as

$$E(\vec{k}) = \frac{\hbar^2}{2m_0} \vec{k} \cdot \bar{\alpha} \cdot \vec{k} + \dots \quad (6.15)$$

or in suffix notation

$$E(\vec{k}) = \frac{\hbar^2}{2m_0} k_i \alpha_{ij} k_j \quad (i, j = 1, 2, 3). \quad (6.16)$$

Thus the principal axes of \bar{m}^* and $\bar{\alpha}$ coincides (see, section 3.3.3).

$\bar{\tau}$ is the relaxation time tensor which can be considered in the following three separate situations

case 1: $\vec{\tau}$ is a scalar. For this case, the principal axes of \vec{m}^* , \vec{a} and $\vec{\mu}$ coincide.

case 2: a) $\vec{\tau}$ is symmetric and diagonal in the same orthogonal set as \vec{m}^* or $\vec{\mu}$. Again the principal axes of \vec{m}^* and $\vec{\mu}$ coincide. This is the case considered by Herring and Vogt (1956), "Oktu" and Saunders (1967), Jeavons and Saunders (1969) and Hartman (1969).

b) $\vec{\tau}$ is symmetric, but not diagonal in the same orthogonal set as \vec{m}^* or $\vec{\mu}$. This can only happen when $a_{22} = a_{33}$, i.e. for an ellipsoid of revolution which is not necessarily correct so we exclude this particular case.

case 3: $\vec{\tau}$ is not symmetric. That is the only restriction to the form of $\vec{\tau}$ is from the symmetry of the point L. Equation (6.5), for this case, becomes

$$\begin{pmatrix} \mu_{11} & 0 & 0 \\ 0 & \mu_{22} & \mu_{23} \\ 0 & \mu_{23} & \mu_{33} \end{pmatrix} = e \begin{pmatrix} \tau_{11} & 0 & 0 \\ 0 & \tau_{22} & \tau_{23} \\ 0 & \tau_{32} & \tau_{33} \end{pmatrix} \cdot \begin{pmatrix} a_{11} & 0 & 0 \\ 0 & a_{22} & 0 \\ 0 & 0 & a_{33} \end{pmatrix} \quad (6.17)$$

where $\mu_{23} = e \tau_{23} a_{33} = e \tau_{32} a_{22}$.

$$\text{Thus } \frac{\tau_{23}}{\tau_{32}} = \frac{a_{22}}{a_{33}} = \frac{m_3^*}{m_2^*} \quad (6.18)$$

A similar condition to that in equation (6.18) appropriate to the band structure of Bi_2Te_3 was first given by Korenblit (1961) and later supported by Hübner (1967), Füscher et al (1970) and Ashworth et al (1971).

Case 3 automatically implies that tilt angles of the mobility and the mass ellipsoids can be different. In other words, the tilt angle calculated from the galvanomagnetic data does not necessarily equal to that obtained from the measured effective mass tensor components. As an example, consider the tilt angle of the hole pockets in Sb. Öktü and Saunders (1967) and Kechin (1968) from the low field galvanomagnetic data obtain -24° , while Windmiller (1966) and Ishizawa (1968) from the dHvA effect measure -37° (a -13° difference). Furthermore, Falicov and Lin (1966), from the pseudopotential approach, calculate -49° . This discrepancy has usually been attributed to the deviations from the ellipsoidal shape and to the nature of the different experimental techniques, but it may not be all that: we propose (by considering case 3) that the tilt angle obtained from the galvanomagnetic effects corresponds to the mobility ellipsoid and that of measured from the dHvA effect corresponds to the mass ellipsoid. We have used the hole effective mass tensor components of Datars and Vanderkooy (1964) together with the hole mobility tensor components (at 77K) of Öktü and Saunders (1967) expressed (by a 13° clockwise rotation) in the principal mass ellipsoid axes and calculated the nonsymmetric relaxation time tensor components. They are listed in the following table. Those given by Öktü and Saunders (1967), by considering case 2(a), are also included.

	τ_{11}	τ_{22}	τ_{33}	τ_{23}	τ_{32}
Öktü and Saunders (1967)	9.1	8.9	6.1		
This work	9.1	14.12	5.8	1.23	22.6

τ_{ij} in units of 10^{-10} sec.

Furthermore we have collected, in table (6.7), the smallest and largest reported electron and hole tilt angles of As, Sb and Bi. The variation of the reported tilt angles over a wide range may be taken as an evidence that $\bar{\tau}$ is nonsymmetric i.e. the principal axes of the mobility (or rather conductivity) and mass ellipsoids do not coincide.

TABLE (6.1): Possible dislocations in the A7 crystal structure in general and in the 25.5 at.% arsenic-antimony alloy in particular.

Burgers vector (b)	No. of equivalent Burgers vectors.	$ \vec{b} ^2$	Angle between (b) and [111]
$\langle 10\bar{1} \rangle$	6	$4a^2 \sin^2 \frac{\alpha}{2} = 0.88a^2$	90°
$\langle 100 \rangle$	6	a^2	33°
$\langle 1\bar{1}1 \rangle$	6	$a^2(1+4\sin^2 \frac{\alpha}{2}) = 1.88a^2$	52°
$\langle 110 \rangle$	6	$4a^2 \cos^2 \frac{\alpha}{2} = 3.11 a^2$	18°
$\langle 111 \rangle$	2	$3a^2(1+4\cos^2 \frac{\alpha}{2}) = 6.34a^2$	0°

TABLE (6.2): Angles between pseudo-axes and +y axis in the A7 structure semimetals.

Material	Pseudo-threefold: angle between $[12\bar{1}]_{prh}$ and the normal to $(010)_{prh}$	Pseudo-fourfold: angle between $[12\bar{1}]_{prh}$ and the normal to $(101)_{prh}$
As	17.167°	31.717°
Sb	18.317°	33.496°
Bi	18.366°	33.578°
As(25.5 at.%)–Sb	17.984°	32.933°

TABLE (6.3) : Details of etching and orientation of the pits obtained.

Material	ETCHING REAGENT		Orientation of Pits
	Composition	Ref	
Arsenic	10% Iodine in methanol	(1)	Type B
	CH ₃ COOH, HF, HNO ₃ , HCl, Br ₂ (24 : 1 : 2 : 1 : 1)	(1)	Type B
	CH ₃ COOH, HF, HNO ₃ (1 : 2 : 1)	(2)	Type A
Antimony	CH ₃ COOH, HF, HNO ₃ , Br ₂ (3 : 3 : 5 : 1)	(3)	Type A
	CH ₃ COOH, HF, HNO ₃ , HCl, Br ₂ (24 : 1 : 2 : 1 : 1)	(4)	Type A
	CH ₃ COOH, HF, HNO ₃ , Br ₂ (28 : 4 : 5 : 3)	(5)	Type A
Bismuth	1% iodine in methanol	(6)	Type B
	33% HNO ₃ in water	(7)	Type A
Arsenic (25.5at%) -Antimony Alloy	CH ₃ COOH, HF, HNO ₃ (3 : 3 : 5) and a few drops of bromine	(8)	Type A
	CH ₃ COOH, HF, HNO ₃ , HCl, Br ₂ (24 : 1 : 2 : 1 : 1)	(4)	Type A
Antimony- (2at%) Germanium Alloy	CH ₃ COOH, HF, HNO ₃ , Br ₂ (3 : 3 : 5 : 1)	(4)	Type A

(1) Shetty and Taylor (1968).

(2) Jeavons and Saunders (1968).

(3) Wernick et al (1958).

(4) Akgöz et al (1972).

(5) Kosevich (1961).

(6) Lovell and Wernick (1959).

(7) Brown et al (1968).

(8) Akgöz and Saunders (1971).

Table (6.4a)

The measured low field magnetoresistivity tensor components of As(25.5 at.%) - Sb alloy crystals.

Temp. (K)	ρ_{ij}^0		R_{ijk}		A_{ij}							
	ρ_{11}^0	ρ_{33}^0	$-R_{123}$	$-R_{231}$	A_{11}	A_{12}	A_{13}	A_{31}	$-A_{44}$	A_{33}	A_{14}	A_{41}
300	10.64	6.80	18.5	3.5	1.4	3.1	1.5	1.9	0.9	0.8	0.2	0.4
77	6.30	3.65	25.0	3.9	2.7	5.6	2.9	3.0	1.6	1.5	0.5	0.9
50	5.95	3.41	25.8	4.0	3.2	6.7	3.3	4.5	2.0	2.2	0.7	1.1
4.2	5.87	3.32	26.4	4.1	3.5	7.7	3.8	4.9	2.1	2.4	0.8	1.2
1.5	5.85	3.30	26.5	4.1	3.5	7.8	3.8	5.0	2.1	2.5	0.8	1.2
approx error (%)	5	6	6	25	10	9	10	15	20	15	20	25

Units: ρ_{ij}^0 , $10^{-7} \Omega m$; R_{ijk} , $10^{-9} \Omega mT^{-1}$; A_{ij} , $10^{-9} \Omega mT^{-2}$.

Table (6.4b)

Low field magnetoconductivity tensor components of the As-Sb alloy crystals.

Temp. (K)	σ_{ij}^0			σ_{ijk}			S_{ij}						
	σ_{11}^0	σ_{33}^0	σ_{123}	σ_{1jk}	σ_{231}	σ_{312}	$-S_{11}$	$-S_{12}$	$-S_{13}$	$-S_{31}$	S_{44}	$-S_{33}$	$-S_{14}$
300	9.4	14.7	16.3	4.8	4.8	12.4	27.5	16.1	41.3	12.8	17.3	1.8	5.5
77	15.8	27.4	62.9	16.9	16.9	68.0	142	98	226.9	66.2	112.5	12.6	39.1
50	16.8	29.3	72.8	19.7	19.7	90.4	190.6	125	389.3	99	189.2	19.7	54.2
4.2	17.0	30.1	76.6	21.0	21.0	101.6	224.9	145	447.1	112.5	217.7	23.2	61.6
1.5	17.1	30.3	77.4	21.2	21.2	102.3	229.4	146	461.7	113.6	229.5	23.4	62.2

Units: $\sigma_{ij}^0, 10^5 \Omega^{-1} m^{-1}$; $\sigma_{ijk}, 10^3 \Omega^{-1} m^{-1} T^{-1}$; $S_{ij}, 10^2 \Omega^{-1} m^{-1} T^{-2}$.

Table (6.5a)

Computed model parameters (from the low field data) for As(25.5at.%) - Sb.

Temp. (K)	Carrier Density (N=P)	Electrons				Holes			
		μ_1	μ_2	μ_3	θ_μ	ν_1	ν_2	ν_3	θ_ν
300	6.4	7.4	1.1	5.7	-7°	5.9	0.5	12.5	-34°
77	6.2	10.1	1.6	9.6	-7°	11.0	0.8	22.0	-34°
50	6.15	14.2	1.9	12.9	-6.5°	13.7	0.8	24.5	-35°
4.2	6.1	15.5	2.1	14.1	-6.8°	15.4	1.0	26.3	-34°
1.5	6.1	15.6	2.1	14.2	-6.8°	15.5	1.1	26.4	-33°

Units: N, 10^{25} m^{-3} ; $\mu_1, \nu_1, 10^{-2} \text{ m}^2 \text{ V}^{-1} \text{ s}^{-1}$; θ_μ, θ_ν , degrees.

Table (6.5b)

Model parameters computed from the angular dependence of $\rho_{11}(B_1, B_2, 0)$,

$\rho_{11}(B_1, 0, B_3)$ and $\rho_{21}(B_1, 0, B_3)$ at $B = |\vec{B}| = 0.7 \text{ Tesla}$.

Temp (K)	Carrier Density (N=P)	Electrons				Holes			
		μ_1	μ_2	μ_3	θ_μ	ν_1	ν_2	ν_3	θ_ν
300	6.50	7.0	1.0	5.6	-7.4°	5.8	0.6	12.6	-34°
77	6.25	11.0	1.4	10.2	-7.5°	10.9	0.8	22.0	-33°
4.2	6.0	15.3	2.0	14.5	-7°	15.0	0.9	26.5	-32°

Units are the same as in table(6.5a).

Table (6.6)

Comparison between the model parameters at 77K of the
As-Sb alloy and those of the parent elements.

	Electrons			Holes			
	Carrier Density		Tilt Angle	Mobility		Tilt Angle	
	$N = P$						
As*	19.2	μ_1 46.0	μ_3 53.0	θ_μ -8°	ν_1 87.0	ν_3 66.0	θ_ν -51°
Sb†	3.8	162.0	126.0	-5°	236.0	214.0	-24°
As(25.5at.%) - Sb	6.2	10.1	9.6	-7°	11.0	22.0	-34°

Units: $N, 10^{25} \text{ m}^{-3}$; $\mu_i, \nu_i, 10^{-2} \text{ m}^2 \text{ V}^{-1} \text{ s}^{-1}$; θ_μ, θ_ν , degrees.

* Jeavons and Saunders (1969)

† Öktü and Saunders (1967)

TABLE (6.7): Range of the reported electron and hole tilt angles in As, Sb, Bi and the As-Sb alloy. The smallest and largest (in magnitude) reported values are listed only.

Material	electron tilt angle	hole tilt angle	
As	theoretical	-8° (a)	-46° (a)
	experimental	-4° (b) to -8° (c)	-50° (c) to -53° (d)
Sb	theoretical	-7° (e)	-49° (e)
	experimental	-2.3° (f) to -8° (g)	-24° (h) to -37° (f)
Bi	theoretical	$+3.5^{\circ}$ (i) to $+10^{\circ}$ (j)	—
	experimental	$+4.3^{\circ}$ (k) to $+8^{\circ}$ (l)	—
As (25.5 at.%)—Sb experimental	-7° (m)	-34° (m)	

- | | |
|-----------------------------------|---|
| (a) Lin and Falicov (1966) | (h) Öktü and Saunders(1967). |
| (b) Datars and Vanderkooy (1966). | (i) Ferreira (1968). |
| (c) Jeavons and Saunders (1969). | (j) Golin (1968). |
| (d) Priestley et al (1967). | (k) Smith et al (1964). |
| (e) Falicov and Lin (1966). | (l) Gregers-Hansen (1971). |
| (f) Windmiller (1966). | (m) This work and Akgöz
and Saunders (1974). |
| (g) Kechin (1968). | |

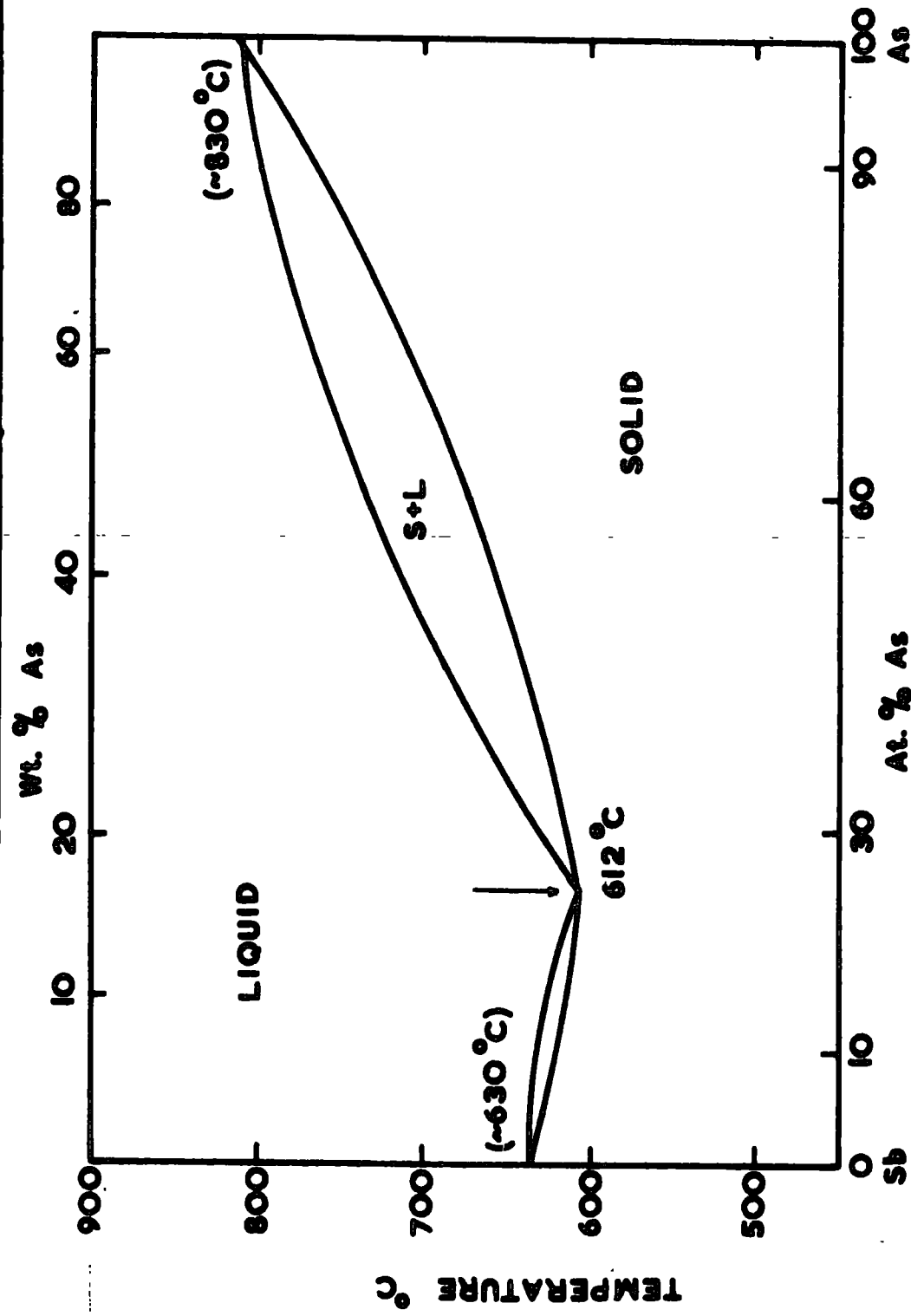
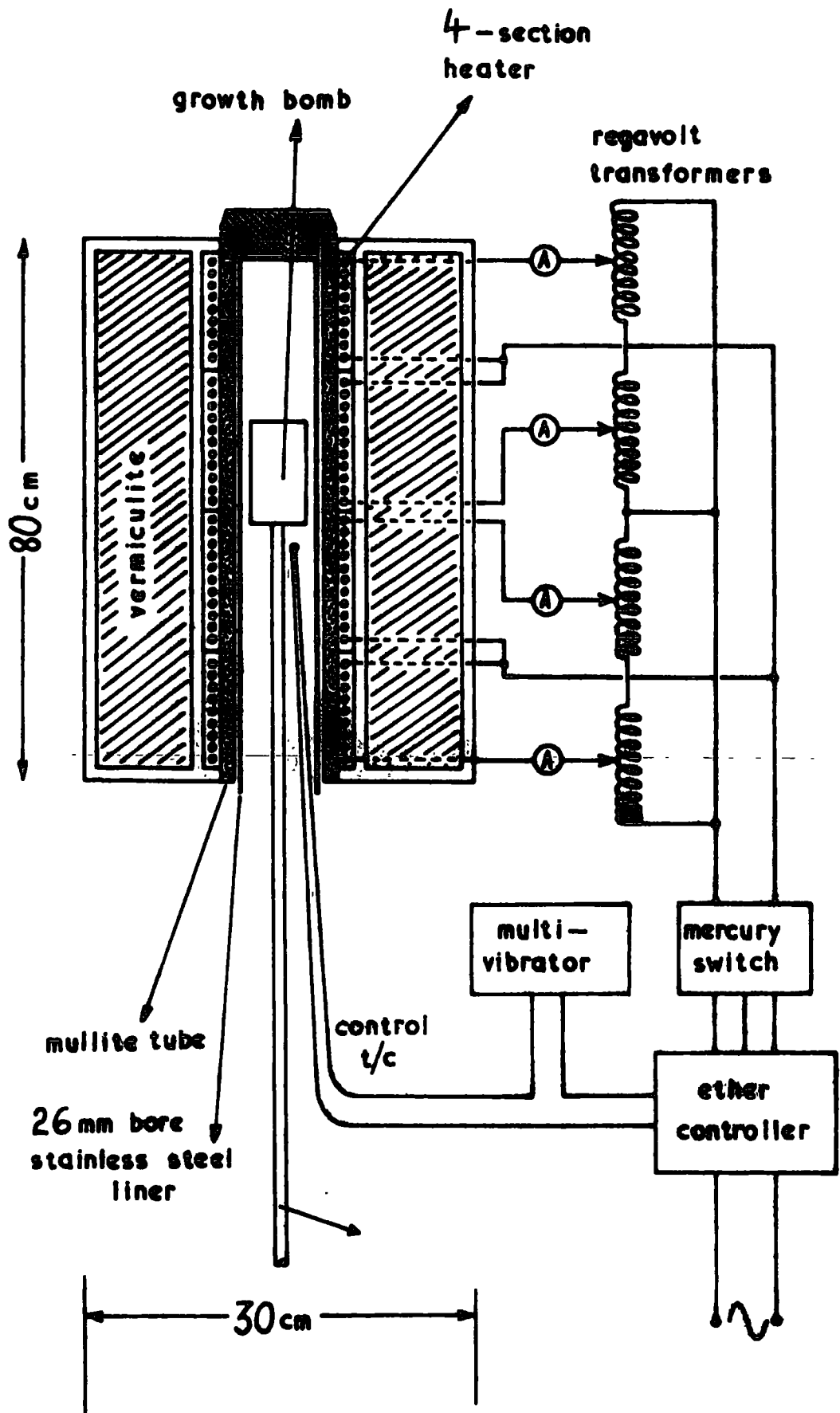


FIGURE (6.1) : THE ARSENIC-ANTIMONY PHASE DIAGRAM.

(After M. HANSEN, 1958 Constitution of binary alloys: McGraw Hill p.178.)



FIGURE(6.2): Crystal growth furnace.

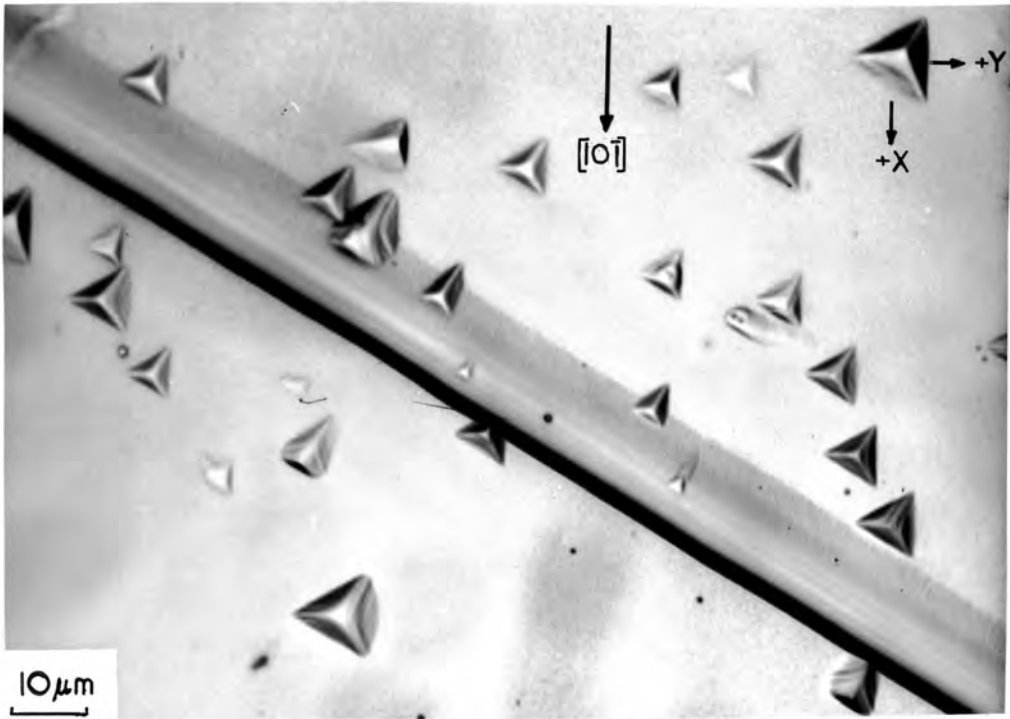


FIGURE (6.3): The pyramidal etch pits and a slip line. The etch pit orientation is shown with respect to an orthogonal (+x,+y,+z) axial set (+z is directed normally out from the plane of the photograph).

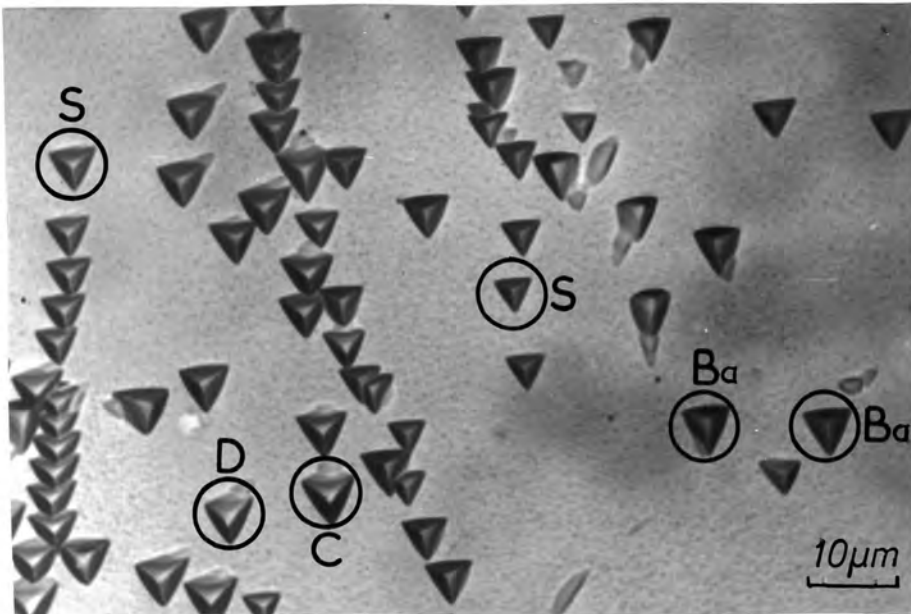


FIGURE (6.4): A variety of etch pits. Symmetrical (S), asymmetrical with projected apex deflected (B_α) towards a base (C) towards a corner and (D) completely asymmetric.

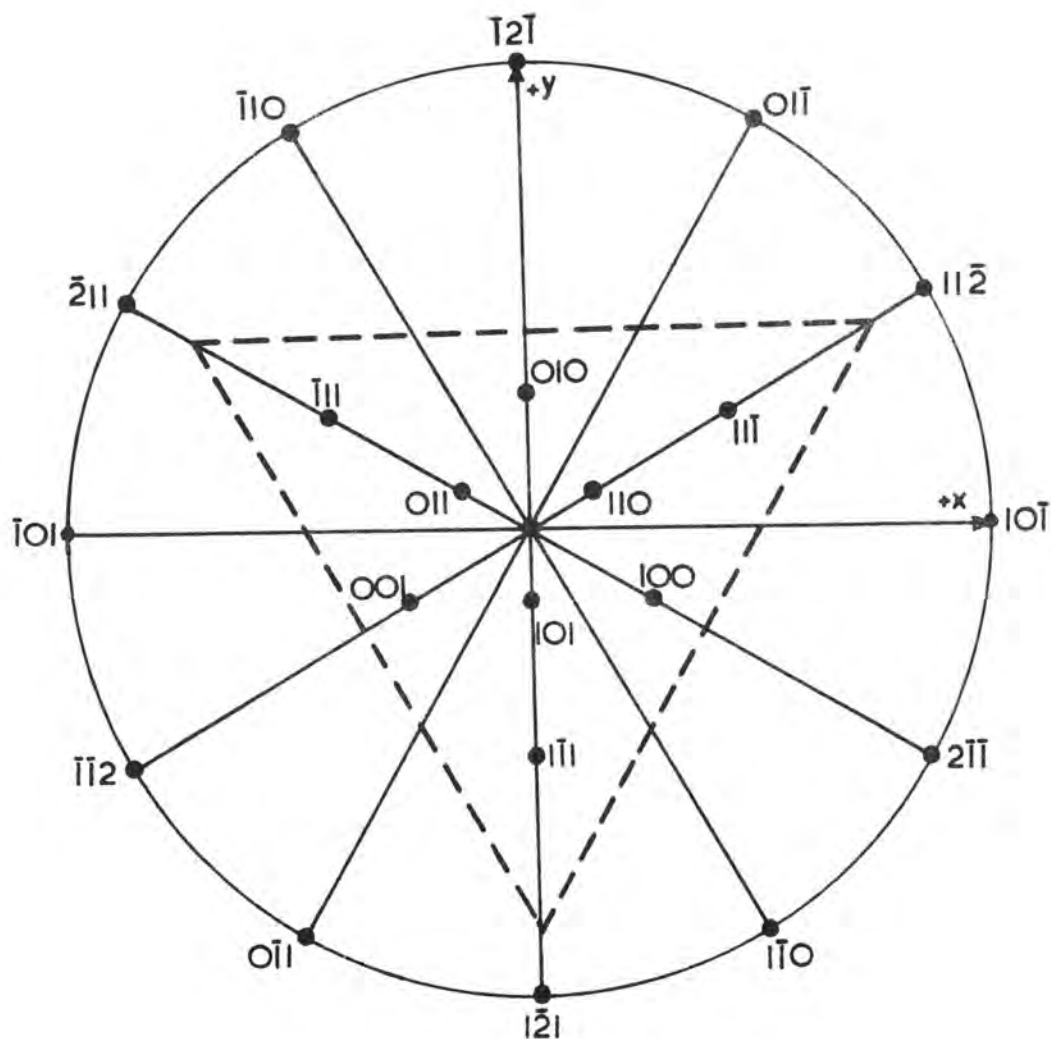


FIGURE (6.5): Standard (111) projection for directions in an arsenic (25.5 at.%) - antimony alloy, showing those directions of particular interest in dislocation studies. The orientation of a "type A" etch pit is also shown.

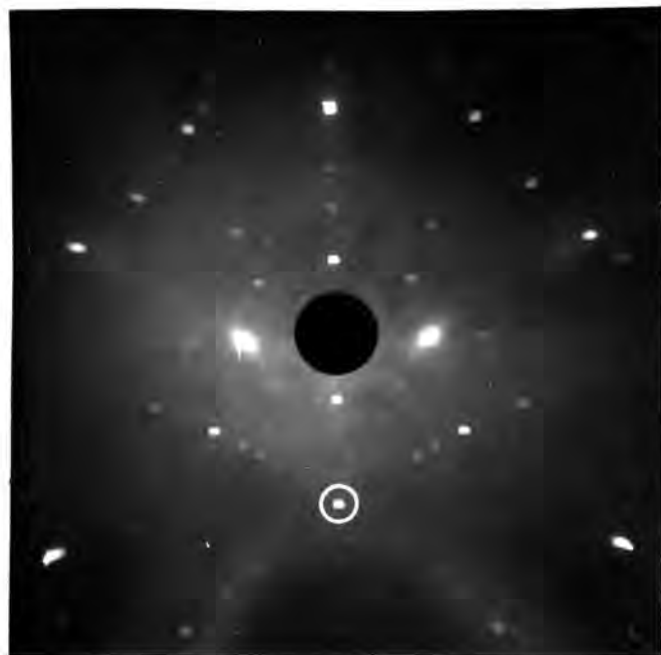


FIGURE (6.6): Back reflection photograph of As(25.5 at.%) - Sb alloy taken with the X-ray beam in a bisectrix direction and the cleavage plane horizontal. The pseudo-threefold spot (ringed) lies in the lower half of the photograph so that for a +z axis chosen vertically upwards the +y axis lies in the direction of the incident X-ray beam.

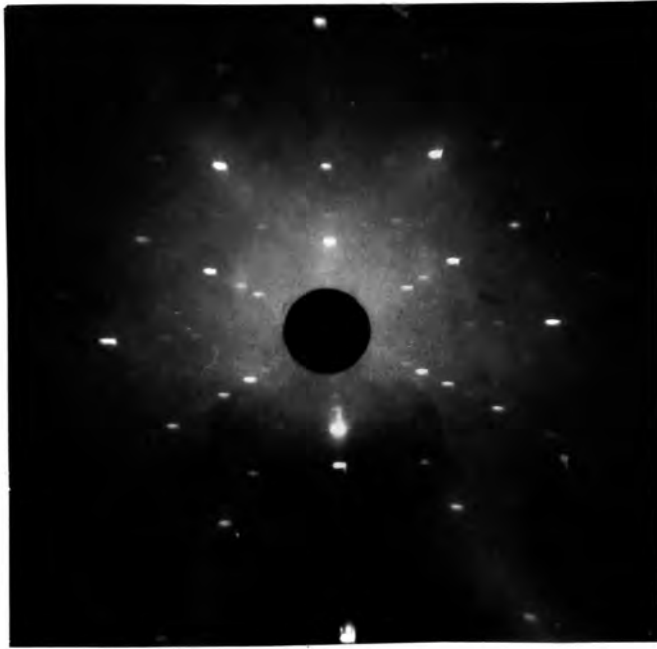
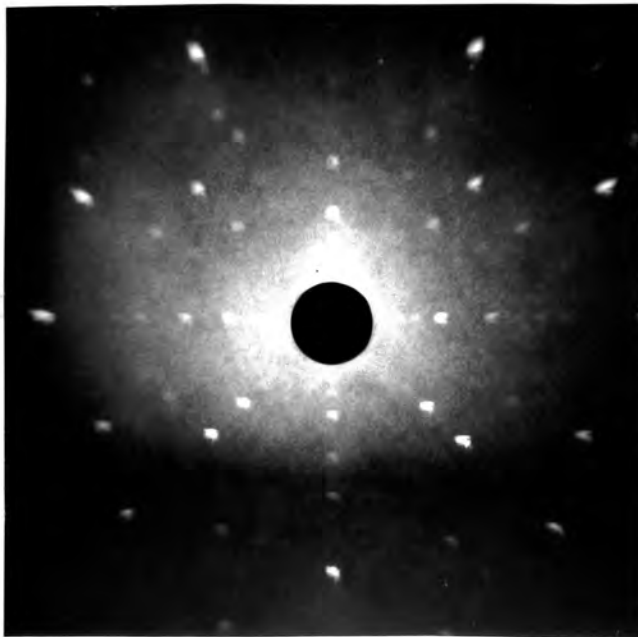


FIGURE (6.7): Back reflection photograph of As(25.5 at.%) - Sb alloy taken with the X-ray beam incident along a pseudo-threefold axis.



FIGURE(6.8): Back reflection photograph of As(25.5 at.%) - Sb alloy taken with the X-ray beam incident along a pseudo-fourfold axis.

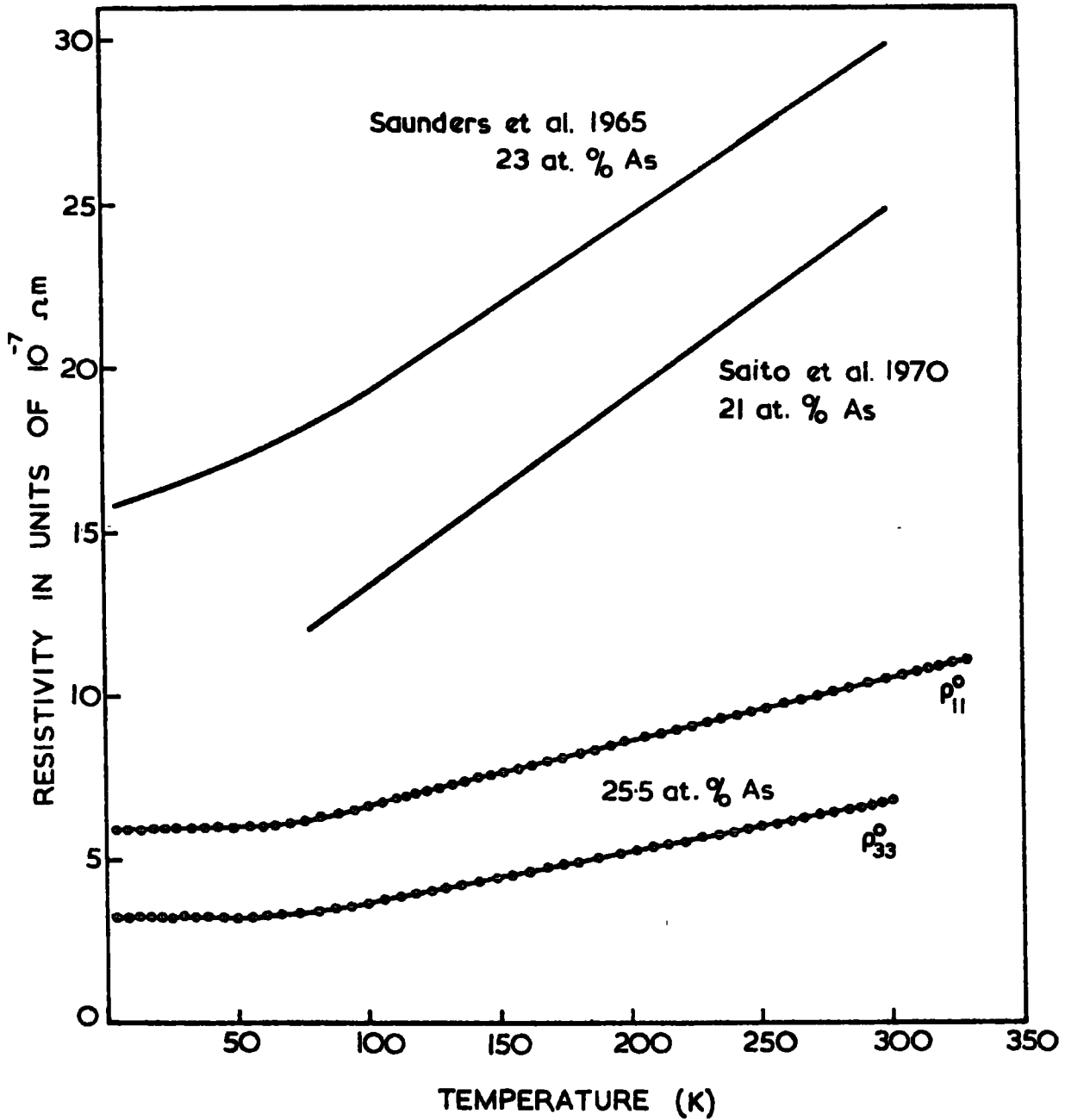


FIGURE (6.9): The temperature dependence of the electrical resistivity of arsenic-antimony alloys.

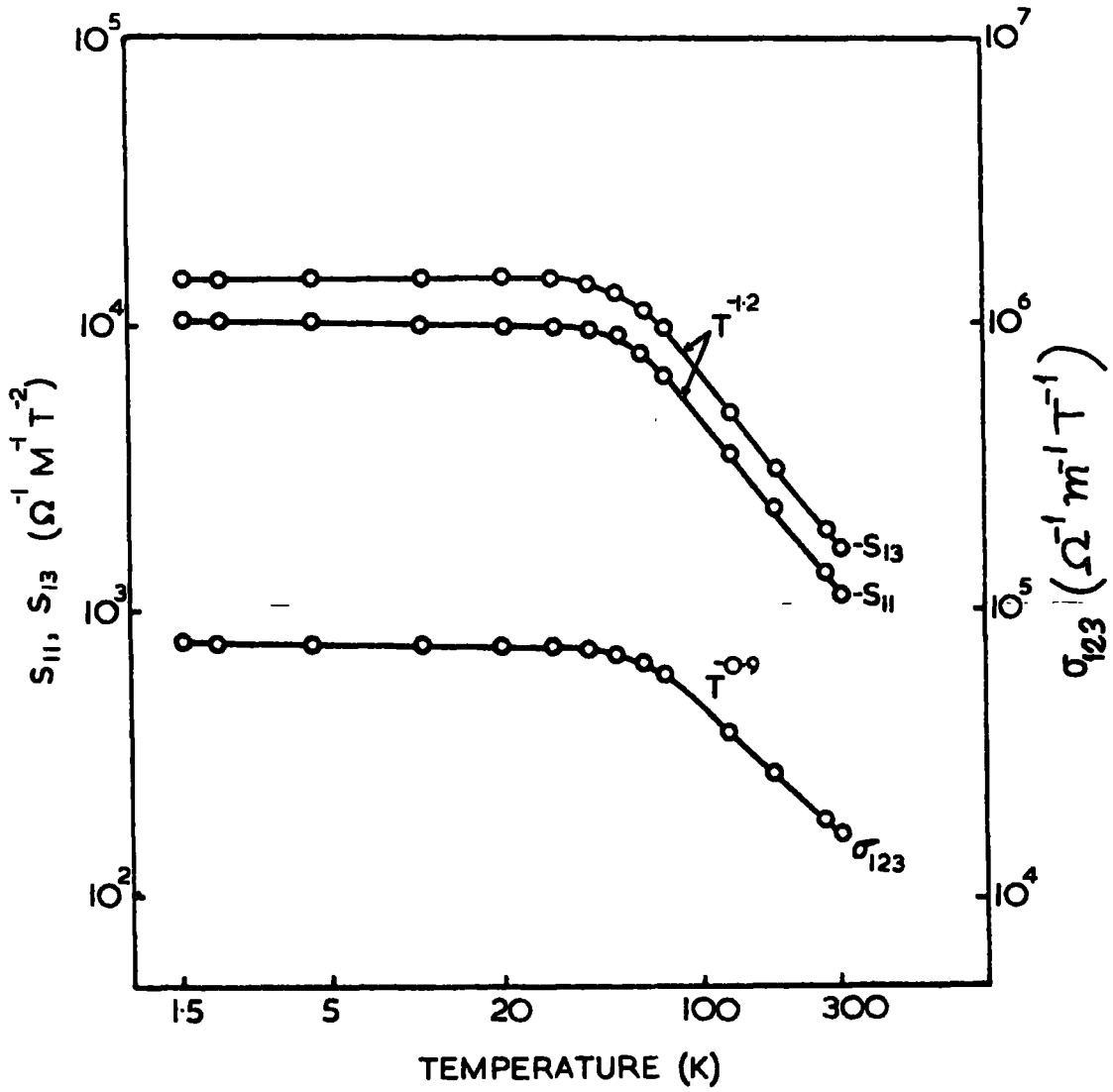


FIGURE (6.10): The temperature dependence of the magnetoconductivity tensor components S_{11} , S_{13} and σ_{123} .

FIGURES (6.11a) and (6.11b):

Magnetoresistance voltage increment ΔV_1 (in microvolts) which is related to (a) $\rho_{11}(B_1, B_2, 0)$ and (b) $\rho_{11}(B_1, 0, B_3)$ by

$$E_1 = \frac{(V_0 + \Delta V_1)}{d_1} = \rho_{11}(B)J_1$$

where V_0 is the voltage without an applied magnetic field and J_1 is the current density and have values of:

$$V_0 = 10190.3 \times 10^{-7} \text{V}, \quad J_1 = 21.7 \times 10^4 \text{ Am}^{-2} \text{ at } 4.2\text{K}$$

$$V_0 = 10785.6 \times 10^{-7} \text{V}, \quad J_1 = 21.4 \times 10^4 \text{ Am}^{-2} \text{ at } 77\text{K}$$

$$V_0 = 17364.5 \times 10^{-7} \text{V}, \quad J_1 = 20.4 \times 10^4 \text{ Am}^{-2} \text{ at } 300\text{K}$$

d_1 ($= 0.8 \times 10^{-2} \text{m}$) is the distance between the potential probes. $|\vec{B}| = 0.7$ Tesla and is taken round

(a) the xy and

(b) the xz planes at 10° intervals.

FIGURE (6.12):

The Hall voltage V_2 (in microvolts) which is related to the tensor component $\rho_{21}(B_1, 0, B_3)$ by

$$E_2 = \frac{V_2}{d_2} = \rho_{21}(B_1, 0, B_3)J_1.$$

The current density J_1 takes the same values as in Fig.(6.11) . . . $|\vec{B}| = 0.7$ Tesla and is taken round the xz plane at 10° intervals. The distance d_2 ($= 20.3 \times 10^{-4} \text{m}$) is that between the Hall potential probes.

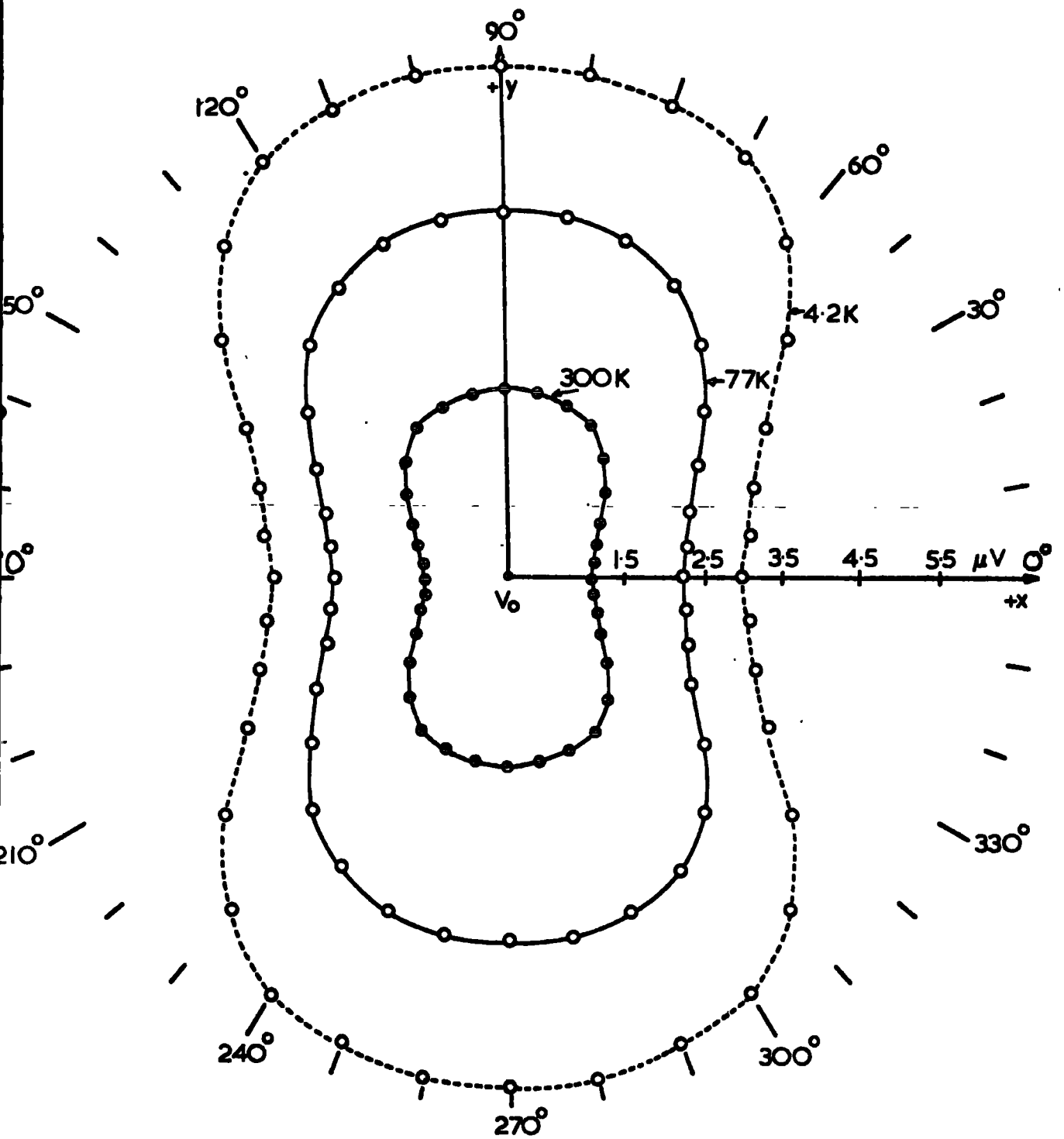


FIGURE (6.11a)

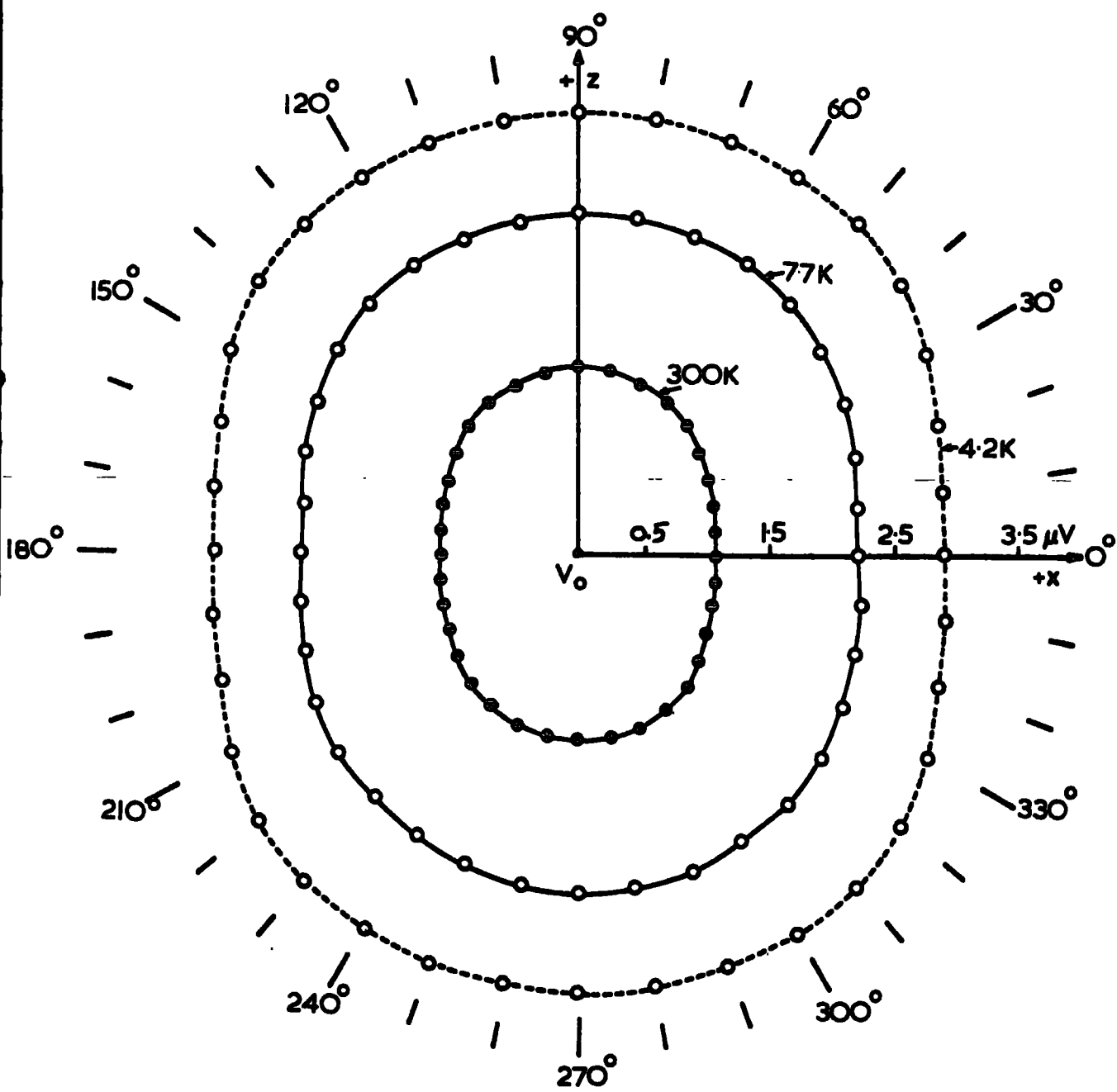


FIGURE (6.11b)

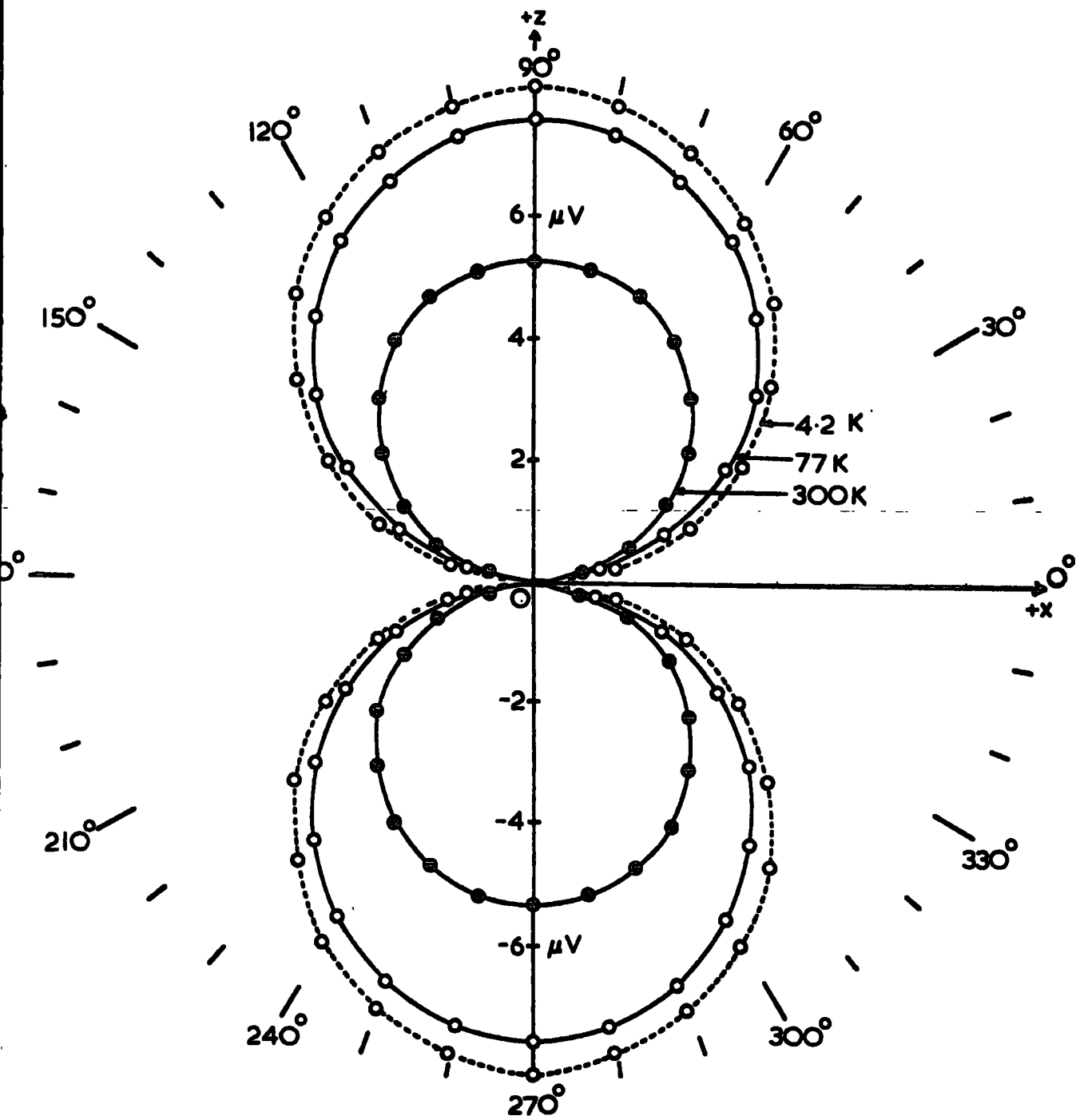


FIGURE (6.12)

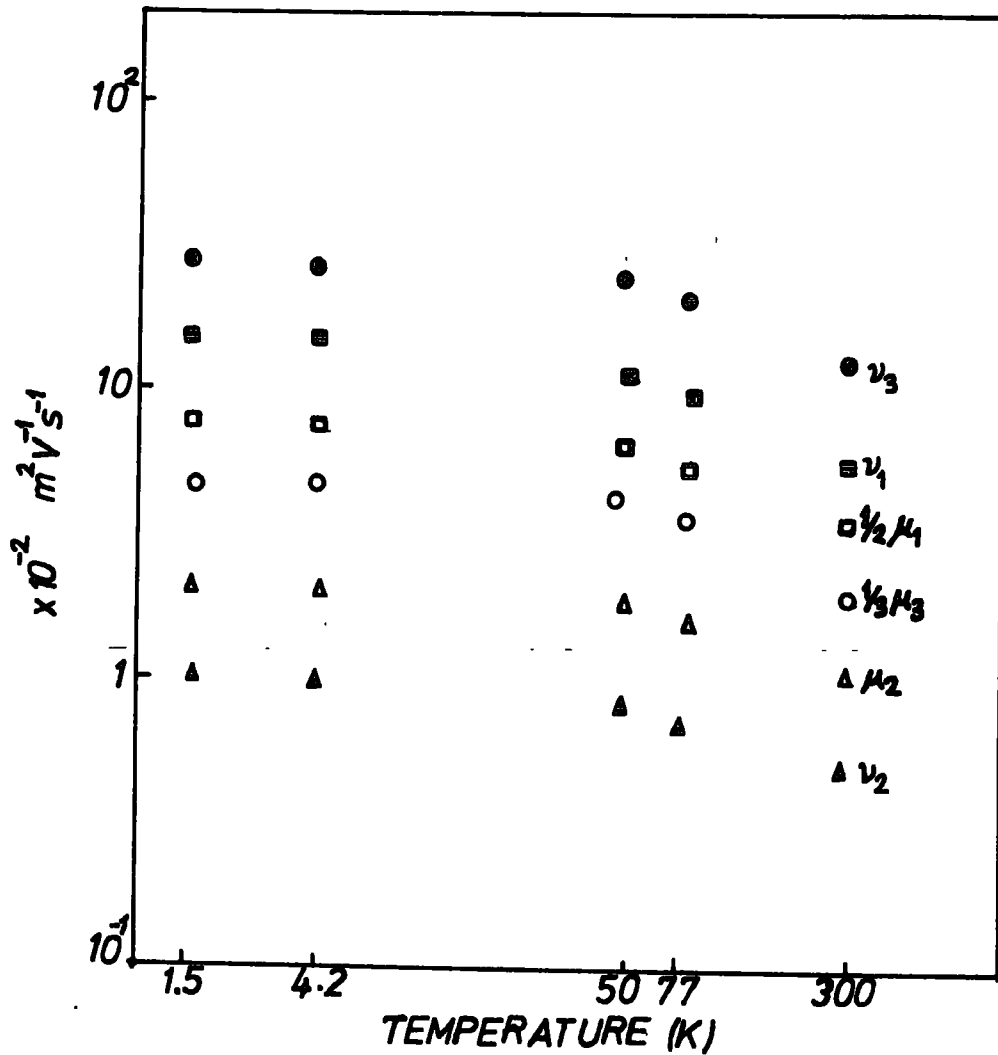


FIGURE (6.13): The temperature dependence of the electron and hole mobility tensor components of As(25.5 at.%)–Sb alloy. For clarity, μ_1 and μ_3 have been divided by 2 and 3 respectively.

REFERENCES

- Abeles B. and Meiboom S. 1956 Phys. Rev. 101 544
- "
Akgöz Y.C. and Saunders G.A. 1971 J. Mater. Sci. 6 395
- "
Akgöz Y.C. and Saunders G.A. 1974 J.Phys.C.: Solid state
phys. 7 1655
- "
Akgöz Y.C., Farley J.M. and Saunders G.A. 1972 J.Mater. Sci.
7 598
- Allgair R.S. 1973 Phys. Rev. B8 4470
- Ashworth H.A., Rayne J.A. and Ure R.W. 1971 Phys. Rev B3 2646
- Aubrey J.E. 1971 J.Phys.F: Metal Phys. 1 493
- Azároff L.V. 1968 "Elements of X-ray Crystallography"
(McGraw-Hill) p.49
- Bacon D.J., Heckscher F. and Crocker A.G. 1964 Acta Cryst. 17
760
- Baranskii P.I., Baidakov V.V., Dahovskii I.V. and Samoilovich
A.G. 1971 Phys. Stat. Sol. 46 785
- Beer A.C. Solid State Phys. 1963 supplement 4.
- Bhagavantam S. 1966 "Crystal Symmetry and Physical Properties"
(Academic Press, London)
- Bhagavantam S. and Suryanarayana D. 1949 Acta Cryst. 2 21
- Birss R.R. 1966 "Symmetry and Magnetism" (North-Holland,
Amsterdam)
- Blatt F.J. 1968 "Physics of Electronic Conduction in Solids"
(McGraw-Hill, New York)
- Bloss F.D. 1971 "Crystallography and Crystal Chemistry"
(Holt, Rinehart and Winston Inc., New York) p.63.
- Bradley C.J. and Cracknell A.P. 1972 "The Mathematical Theory
of Symmetry in Solids" (Clarendon-Oxford)
- Bresler M.S. and Red'ko N.A. 1972 Sov.Phys. - JETP 34 149 -
- Brown R.D., Hartman R.L. and Koenig S.H. 1968 Phys. Rev. 172
598
- Buerger M.J. 1971 "Introduction to Crystal Geometry"
(McGraw-Hill) chapter 6.

- Calvert L.D. and Taylor J.B. 1972 J.Mater. Sci. 7 595
- Callen H.B. 1948 Phys. Rev. 73 1349
- Casimir H.B.G. 1945 Rev. Mod. Phys. 17 343
- Casimir H.B.G. and Gerritsen A.N. 1941 Physica 8 1107
- Chiang Yu.N. and Schevchenko O.G. 1974 Phys. Stat. Sol. (b)
62 K9
- Cohen M.H. 1961 Phys. Rev. 121 387
- Cohen M.H., Falicov L.M. and Golin S. 1964 IBM J.Res.Develop
8 215
- Connell R.A. and Marcus J.A. 1957 Phys. Rev. 107 940
- Cracknell A.P. 1973 J.Phys. C: Solid State Phys. 6 826
- Datars W.R. and Vanderkooy J. 1964 IBM J.Res.Develop. 8 247
- Datars W.R. and Vanderkooy J. 1966 J.Phys. Soc.Jap 21(Suppl.)
657
- Doershel J. 1972 Kristal und Technik 7 197
- Douglas R.J. and Datars W.R. 1973 Can.J.Phys. 51 1770
- Drabble J.R. and Wolfe R. 1956 Proc.Phys.Soc. B69 1101
- Dresselhaus M.S. J.Phys. Chem. Solids 32 Suppl.1 3-33
- Falicov L.M. 1966 "Group Theory and Its Physical Applications"
(Chicago University Press)
- Falicov L.M. and Golin S. 1965 Phys. Rev. 137 A871
- Falicov L.M. and Lin P.J. 1966 Phys.Rev. 141 562
- Ferreira L.G. 1968 J.Phys. Chem. Solids 28 1891 and 29 537
- Fieschi R., De Groot S.R. and Mazur P. 1954 Physica 20 259
- Frawley J.J. and Childs W.J. 1970 J.Appl. Phys. 41 1862
- Fumi G.F. 1952a Acta Cryst. 5 44
- 1952b Nuovo Cim. 9 739
- Fuchser T.D., Mackey H.J. and Sybert J.R. 1970 Phys. Rev. B2
3863
- Garcia-Moliner F. 1959 Proc. Roy. Soc. A249 73.

- Gitsu D.V., Bodiul P.P. and Fedorko A.S. 1969
Phys. Stat. Sol. 33 K143
- Gitsu D.V., Muntyanu F.M. and Federko A.S. 1970
Phys. Stat Sol. 42 173
- Goldberg C. and Davis R.E. 1954 Phys. Rev. 94 1121
- Goldsmid H.J. 1970 Phys. Stat. Sol.(a) 1 7
- Golin S. 1968 Phys. Rev. 166 643
- Grabner L. 1960 Phys. Rev. 117 689
- Grabner L. and Swanson J.A. 1962 J.Math. Phys. 3 1050
- Gregers-Hansen P.F. 1971 J.Phys. Chem. Solids 32 1881
- "Grüneisen E. and Gielessen J. 1936 Ann. Phys 26 449
- Hall L.H. 1969 "Group Theory and Symmetry in Chemistry"
(McGraw-Hill, New York)
- Hansen M. 1958 "Constitution of Binary Alloys" (McGraw-Hill)
- Hansen O.P. and Nielsen H. 1974 To be published.
- Harman T.C. and Honig J.M. 1967 "Thermoelectric and
Thermomagnetic effects and Applications"
(McGraw-Hill, New York).
- Harman T.C., Honig J.M. and Tarmy B.M. 1965 Adv. Ener. Conv.
5 1
- Hartman R. 1969 Phys. Rev. 181 1070
- Hattori T. 1968 J.Phys. Soc. Jap. 24 762
- Hermann C. 1934 Z. Krist. 89 32
- Herring C. and Vogt E. 1956 Phys. Rev. 101 944
- "Hübner U. 1967 Z. Naturforsch 22 2086
- Hurd C.M. 1972 "The Hall Effect in Metals and Alloys"
(Plenum, New York)
- Hurd C.M. 1974 Adv. Phys. 23 315
- Ishizawa Y. 1968 J. Phys. Soc. Jap 25 150
- Jacobson D.M. 1973 Phys. Stat. Sol.(b) 58 243
- Jahn H.A. 1937 Z. Krystallogr. 98 191
- 1949 Acta Cryst. 2 30
- Jain A.L. 1959 Phys. Rev. 114 1518
- Jan J.-P. 1957 Solid State Phys. 5 3

(x)

- Jan J.-P. 1972 Can.J.Phys. 50 925
- Jeavons A.P. and Saunders G.A. 1968 Brit. J. Appl. Phys. (J.Phys.D.) Series 2, 1 869
- Jeavons A.P. and Saunders G.A. 1969 Proc. Roy. Soc. A310 415
- Jones H. 1960 "Theory of Brillouin Zones and Electronic States in Crystals" (North-Holland) p.57.
- Juretschke H.J. 1955 Acta Cryst. 8 716
- Kachinskii V.N. 1961 Sov. Phys. - Doklady 5 1260
- Koa L.P. and Katz E. 1958 J.Phys. Chem.Solids 6 223
- Kechin V.V. 1968 Sov.Phys.-Solid State 9 2828
- Klauder J.R. and Kunzler J.E. 1961 Phys.Rev. Lett. 6 179
- Kleiner W.H. 1966 Phys. Rev. 142 318
- Koch K.M. 1955 Z. Naturforsch 10a 496
- Kohler M. 1934 Ann. Physik 20 891
- Korenblit I. Ya. 1961 Sov.Phys. - Solid State 2 2738
- 1969 ————— Semicond. 2 1192
- Kosevich V.M. 1961 Sov. Phys. Cryst. 5 715
- Landau L.D. and Lifshits E. 1960 "Electrodynamics of Continuous Media" (Pergamon-Press)
- Lifshits I.M., Azbel M.Ya. and Kaganov M.I. 1973 "Electron Theory of Metals" (Consultants Bureau)
- Lin P.J. and Falicov L.M. 1966 Phys.Rev. 142 441
- Logan J.K. and Marcus J.A. 1952 Phys.Rev. 88 1234
- Lovell L.C. and Wernick J.H. 1959 J.Appl.Phys. 30 234
- Lyubarskii G. Ya. 1960 "The Application of Group Theory in Physics" (Pergamon Press - Oxford)
- Mansuri Q.A. 1928 J. Chem. Soc. Part 2 2107
- Mase S. 1958 J.Phys. Soc. Jap. 13 434
- Mason W.P. 1966 "Crystal Physics of Interaction Processes" (Academic Press-New York)
- Mason W.P., Hewitt W.H. and Vick R.P. 1953 J.Appl.Phys. 24 166
- Michenaud J.P., Streydio J.M., Issi J.P. and Luyckx A. 1970 Solid State Commun. 8 455

- Mulliken R.S. 1933 Phys. Rev. 43 279
- Nye J.F. 1960 "Physical Properties of Crystals"
(Clarendon Press - Oxford).
- Ohyama M. 1965 J.Phys. Soc. Jap. 20 1538
 ————— 1966 ————— 21 1126
- Okada T. 1955a Mem. Fac. Sci. Kyushu Univ. B1 157
 ————— 1955b ————— 168
- Öktü Ö and Saunders G.A. 1967 Proc. Phys. Soc. 91 156
- Onsager L. 1931 (a and b) Phys. Rev. 37 405 and 38 2265
- Pace W.G., Saunders G.A. and Sumengen Z. 1970 J.Phys.Chem.
Solids 31 1467
- Pantulu P.V. and Sudarshan E. 1970 Acta Cryst. A26 163
- Parravano N. and de Cesaris P. 1912 Z.für Metall. 2 70
- Pinchuk I.I. 1967 Phys. Stat. Sol. 20 537
- Pippard A.B. 1965 "The Dynamics of Conduction Electrons"
(Gorden and Breach, London) p.92
- Priestley M.G., Windmiller L.R., Ketterson J.B. and
Eckstein Y. 1967 Phys. Rev. 154 671
- Quensel P., Ahlborg K. and Westgren A. 1937 Geol. Foren.
Stockholm Forh. 59 135
- Saito Y. and Maezawa K. 1970 Proc. 12th Int.Conf.Low.Temp.
Phys. 583
- Salkovitz E.I. 1956 AIME Trans. J.Metals 206 176
- Saunders G.A. and Öktü Ö. 1968 J.Phys.Chem. Solids 29 327
- Saunders G.A. and Sumengen Z. 1972 J.Phys.F: Metal Phys. 2
972
- Saunders G.A. and Akgöz Y.C. 1973 Proc. Int. Conf. of the
Physics of Semimetals and Narrow Gap Semiconductors
(Nice - Cardiff, Sept. 1973) In Press
- Saunders G.A., Cooper G., Miziumski C. and Lawson A.W. 1965
J.Phys. Chem. Solids 26 533
- Schiferl D. and Barrett C.S. 1969 J.Appl. Cryst. 2 30
- Shetty M.N. and Taylor J.B. 1968 J.Appl. Phys. 39 3717
- Shih C.H. and Peretti E.A. 1956 Am.Soc.Metal Trans. 48 706
- Shoenberg D. 1935 Proc. Cambridge Phil. Soc. 31 265

- Shtrikman S. and Thomas H. 1965 Solid State Commun. 3 147
- Smith A.C., Janak J.F. and Adler R.B. 1967 "Electronic Conduction in Solids" (McGraw-Hill, New York)
- Smith G.E., Wolfe R. and Haszko S.E. 1964 Proc.Int. Conf. Semicond. Phys. Paris p.399
- Smith G.E., Baraff G.A. and Rowell J.M. 1964 Phys. Rev. 135 A1118
- Steele M.C. and Babiskin J. 1955 Phys. Rev. 98 359
- "
Sumengen Z. 1971 Ph.D. Thesis University of Durham
- "
Sumengen Z. and Saunders G.A. 1972a J.Phys.C: Solid State Phys. 5 425
- "
Sumengen Z. and Saunders G.A. 1972b Solid State Commun. 10 37
- "
Sumengen Z., Turetken N. and Saunders G.A. 1974 J.Phys. C: Solid State Phys. 7 2204
- Tinkham M. 1964 "Group Theory and Quantum Mechanics" (McGraw-Hill, New York)
- Trzebiatowski W. and Bryjak E. 1938 Z.anorg.Chem. 238 255
- Uher C. and Goldsmid H.J. 1974 Phys.Stat.Sol.(b) 63 163
- Vickers W. 1957 AIME Trans. J. Metals 207 827
- Windmiller L.R. 1966 Phys.Rev. 149 472
- Wooster W.A. 1973 "Tensors and Group Theory for the Physical Properties of Crystals" (Clarendon Press - Oxford).

APPENDIX I

The model parameters are related to the low field conductivity tensor components by the following equations:

zero field conductivity components:

$$\begin{aligned}\sigma_{11}^0 &= \frac{1}{2}Ne (\mu_1 + C_e^2 \mu_2 + S_e^2 \mu_3) + \frac{1}{2}Pe (v_1 + C_h^2 v_2 + S_h^2 v_3) \\ \sigma_{33}^0 &= Ne (S_e^2 \mu_2 + C_e^2 \mu_3) + Pe(S_h^2 v_2 + C_h^2 v_3)\end{aligned}\quad (A1.1)$$

low field Hall conductivity components:

$$\begin{aligned}\sigma_{123} &= -Ne \mu_1 (C_e^2 \mu_2 + S_e^2 \mu_3) + Pe v_1 (C_h^2 v_2 + S_h^2 v_3) \\ \sigma_{231} &= \left(\frac{1}{2}Ne\right)\{-\mu_2 \mu_3 - \mu_1 (S_e^2 \mu_2 + C_e^2 \mu_3)\} + \left(\frac{1}{2}Pe\right)\{v_2 v_3 + v_1 (S_h^2 v_2 + C_h^2 v_3)\}\end{aligned}\quad (A1.2)$$

Low field magnetoconductivity tensor components can be written as the sum of electron and hole parts:

$$(S_{ij})_{\text{total}} = (S_{ij})_{\text{electron}} + (S_{ij})_{\text{hole}}$$

The electron contribution terms are:

$$\begin{aligned}S_{11} &= \left(-\frac{1}{8}Ne\right)\{S_e^2 \mu_2 (\mu_1 - \mu_3)^2 + C_e^2 \mu_3 (\mu_1 - \mu_2)^2 + 3C_e^2 S_e^2 \mu_1 (\mu_2 - \mu_3)^2\} \\ S_{12} &= \left(-\frac{1}{8}Ne\right)\{3S_e^2 \mu_2 (\mu_1^2 + \mu_3^2) + 3C_e^2 \mu_3 (\mu_1^2 + \mu_2^2) + C_e^2 S_e^2 \mu_1 (\mu_2 - \mu_3)^2 \\ &\quad + 2\mu_1 \mu_2 \mu_3\} \\ S_{13} &= \left(-\frac{1}{2}Ne\right)(\mu_1 + C_e^2 \mu_2 + S_e^2 \mu_3) (C_e^2 \mu_1 \mu_2 + S_e^2 \mu_1 \mu_3) \\ S_{31} &= \left(-\frac{1}{2}Ne\right) (S_e^2 \mu_2 + C_e^2 \mu_3) \{\mu_2 \mu_3 + \mu_1 (S_e^2 \mu_2 + C_e^2 \mu_3)\}\end{aligned}$$

(xiv)

$$\begin{aligned}
S_{44} &= \left(\frac{1}{2}Ne\right) (S_e^2 \mu_2 + C_e^2 \mu_3) \{\mu_1 (C_e^2 \mu_2 + S_e^2 \mu_3)\} \\
S_{33} &= (-Ne) C_e^2 S_e^2 \mu_1 (\mu_2 - \mu_3)^2 \\
S_{14} &= \frac{1}{4} Ne C_e S_e \mu_1 (\mu_2 - \mu_3) (-\mu_1 + C_e^2 \mu_2 + S_e^2 \mu_3) \\
S_{41} &= \frac{1}{4} Ne C_e S_e (\mu_2 - \mu_3) \{\mu_2 \mu_3 - \mu_1 (S_e^2 \mu_2 + C_e^2 \mu_3)\} \quad (A1.3)
\end{aligned}$$

The hole contribution parts can be obtained by replacing μ_i , N , C_e , S_e by ν_i , P , C_h , S_h respectively. μ_i and ν_i are positive quantities which are expressed in the principal ellipsoidal axis system. $C_e = \cos \theta_\mu$, $C_h = \cos \theta_\nu$, $S_e = \sin \theta_\mu$, $S_h = \sin \theta_\nu$ where θ_μ and θ_ν are the tilt angles of the electron and hole pockets respectively. $N (= P)$ is the total electron (or hole) carrier density and $e = |e|$ is the electronic charge.

The following relations between the measured low field resistivity tensor components and the low field conductivity tensor components are obtained by solving equation(6.3). Apart from notational differences, they are the same as those given by Okada (1955b).

$$\begin{aligned}
\rho_{11}^o &= \frac{1}{\sigma_{11}^o} & A_{13} &= -\frac{S_{13}}{(\sigma_{11}^o)^2} - \frac{\sigma_{123}^2}{(\sigma_{11}^o)^3} \\
\rho_{33}^o &= \frac{1}{\sigma_{33}^o} & A_{31} &= -\frac{S_{31}}{(\sigma_{33}^o)^2} - \frac{\sigma_{231}^2}{\sigma_{11}^o (\sigma_{33}^o)^2} \\
R_{123} &= -\frac{\sigma_{123}}{(\sigma_{11}^o)^2} & A_{44} &= -\frac{S_{44}}{\sigma_{11}^o \sigma_{33}^o} + \frac{1}{2} \frac{\sigma_{123} \sigma_{231}}{(\sigma_{11}^o)^2 \sigma_{33}^o} \\
R_{231} &= -\sigma_{231} / (\sigma_{11}^o \sigma_{33}^o) & A_{33} &= -S_{33} / (\sigma_{33}^o)^2 \\
A_{11} &= -S_{11} / (\sigma_{11}^o)^2 & A_{14} &= -S_{14} / (\sigma_{11}^o)^2 \\
A_{12} &= -\frac{S_{12}}{(\sigma_{11}^o)^2} - \frac{\sigma_{231}^2}{(\sigma_{11}^o)^2 \sigma_{33}^o} & A_{41} &= -\frac{S_{41}}{\sigma_{11}^o \sigma_{33}^o} \quad (A1.4)
\end{aligned}$$

(xv)

APPENDIX II

On the basis of Aubrey's expressions (7) and (8), the following magnetoconductivity tensor components $\sigma_{ij}(B_1, B_2, 0)$ have been derived

$$\vec{B} = (B_1, B_2, 0)$$

$$\begin{aligned} \sigma_{11}(B_1, B_2, 0) &= (\mu_{11} + d_e B_1^2)U_1 + \frac{1}{4} (\mu_{11} + 3\mu_{22} + 4d_e B_1^2)(U_2 + U_3) \\ &+ (v_{11} + d_h B_1^2)W_1 + \frac{1}{4} (v_{11} + 3v_{22} + 4d_h B_1^2)(W_2 + W_3) \end{aligned}$$

$$\begin{aligned} \sigma_{22}(B_1, B_2, 0) &= (\mu_{22} + d_e B_2^2)U_1 + \frac{1}{4} (3\mu_{11} + \mu_{22} + 4d_e B_2^2)(U_2 + U_3) \\ &+ (v_{22} + d_h B_2^2)W_1 + \frac{1}{4} (3v_{11} + v_{22} + 4d_h B_2^2)(W_2 + W_3) \end{aligned}$$

$$\sigma_{33}(B_1, B_2, 0) = \mu_{33}(U_1 + U_2 + U_3) + v_{33}(W_1 + W_2 + W_3)$$

$$\begin{aligned} \sigma_{12}(B_1, B_2, 0) &= (\mu_{11}\mu_{23}B_2 + d_e B_1 B_2)U_1 + \{g_e - \frac{1}{2}\mu_{11}\mu_{23}(-\sqrt{3} B_1 + B_2) + d_e B_1 B_2\}U_2 \\ &+ \{-g_e - \frac{1}{2}\mu_{11}\mu_{23}(\sqrt{3} B_1 + B_2) + d_e B_1 B_2\}U_3 \\ &+ (-v_{11}v_{23}B_2 + d_h B_1 B_2)W_1 + \{g_h - \frac{1}{2}v_{11}v_{23}(\sqrt{3}B_1 - B_2) + d_h B_1 B_2\}W_2 \\ &+ \{-g_h - \frac{1}{2}v_{11}v_{23}(-\sqrt{3}B_1 - B_2) + d_h B_1 B_2\}W_3 \end{aligned}$$

$$\begin{aligned} \sigma_{13}(B_1, B_2, 0) &= \mu_{11}\mu_{33}B_2U_1 + \left\{ \frac{\sqrt{3}}{2} \mu_{23} - k_e B_1 + \frac{1}{4}(\mu_{11}\mu_{33} + \frac{3d_e}{\mu_{11}}) B_2 \right\}U_2 \\ &+ \left\{ -\frac{\sqrt{3}}{2} \mu_{23} + k_e B_1 + \frac{1}{4}(\mu_{11}\mu_{33} + \frac{3d_e}{\mu_{11}}) B_2 \right\}U_3 - v_{11}v_{33}B_2W_1 \\ &- \left\{ -\frac{\sqrt{3}}{2} v_{23} - k_h B_1 - \frac{1}{4}(v_{11}v_{33} + \frac{3d_h}{v_{11}}) B_2 \right\}W_2 \\ &+ \left\{ -\frac{\sqrt{3}}{2} v_{23} - k_h B_1 - \frac{1}{4}(v_{11}v_{33} + \frac{3d_h}{v_{11}}) B_2 \right\}W_3 \end{aligned}$$

(xvi)

$$\begin{aligned}
\sigma_{23}(B_1, B_2, 0) &= (\mu_{23} - \frac{d_e}{\mu_{11}} B_1) U_1 + \{-\frac{1}{2} \mu_{23} - \frac{1}{4}(3\mu_{11}\mu_{33} + \frac{d_e}{\mu_{11}}) B_1 + k_e B_2\} U_2 \\
&+ \{-\frac{1}{2} \mu_{23} - \frac{1}{4}(3\mu_{11}\mu_{33} + \frac{d_e}{\mu_{11}}) B_1 - k_e B_2\} U_3 \\
&+ (v_{23} + \frac{d_h}{v_{11}} B_1) W_1 + \{-\frac{1}{2} v_{23} + \frac{1}{4}(3v_{11}v_{33} + \frac{d_h}{v_{11}}) B_1 - k_h B_2\} W_2 \\
&+ \{-\frac{1}{2} v_{23} + \frac{1}{4}(3v_{11}v_{33} + \frac{d_h}{v_{11}}) B_1 + k_h B_2\} W_3
\end{aligned}
\tag{AII.1}$$

where

$$\begin{aligned}
d_e &= \mu_{11} (\mu_{22}\mu_{33} - \mu_{23}^2) & d_h &= v_{11} (v_{22}v_{33} - v_{23}^2) \\
g_e &= \frac{\sqrt{3}}{4} (\mu_{11} - \mu_{22}) & g_h &= \frac{\sqrt{3}}{4} (v_{11} - v_{22}) \\
k_e &= \frac{\sqrt{3}}{4} (\mu_{11}\mu_{33} - \frac{d_e}{\mu_{11}}) & k_h &= \frac{\sqrt{3}}{4} (v_{11}v_{33} - \frac{d_h}{v_{11}})
\end{aligned}
\tag{AII.2}$$

$B_1 = B \cos \phi, B_2 = B \sin \phi$ where $B = |\vec{B}|$ and ϕ is the rotation angle taken round the xy plane (the sense of rotation is taken from $+x$ direction towards $+y$ direction)

$$\begin{aligned}
U_1 &= ne \left(1 + \frac{d_e}{\mu_{11}} B_1^2 + \mu_{11}\mu_{33} B_2^2\right)^{-1} \\
U_2 &= ne \left\{1 + \frac{1}{4}(3\mu_{11}\mu_{33} + \frac{d_e}{\mu_{11}}) B_1^2 + \frac{1}{4}(\mu_{11}\mu_{33} + \frac{3d_e}{\mu_{11}}) \right. \\
&\quad \left. \times B_2^2 - \frac{\sqrt{3}}{2}(\mu_{11}\mu_{33} - \frac{d_e}{\mu_{11}}) B_1 B_2\right\}^{-1} \\
U_3 &= ne \left\{1 + \frac{1}{4}(3\mu_{11}\mu_{33} + \frac{d_e}{\mu_{11}}) B_1^2 + \frac{1}{4}(\mu_{11}\mu_{33} + \frac{3d_e}{\mu_{11}}) \right. \\
&\quad \left. \times B_2^2 + \frac{\sqrt{3}}{2}(\mu_{11}\mu_{33} - \frac{d_e}{\mu_{11}}) B_1 B_2\right\}^{-1}
\end{aligned}
\tag{AII.3}$$

where n is the number of carriers per ellipsoid.

W_1, W_2, W_3 are obtained from equations (AII.3) by replacing U_i by V_i, μ_{ij} by ν_{ij} and d_e by d_h . The remaining tensor components $\sigma_{21}(B_1, B_2, 0), \sigma_{31}(B_1, B_2, 0),$ and $\sigma_{32}(B_1, B_2, 0)$ can be obtained from the Onsager relation $\sigma_{ij}(\vec{B}) = \sigma_{ji}(-\vec{B})$. The magnetoconductivity tensor components $\sigma_{ij}(B_1, 0, B_3)$ in the xz plane, and $\sigma_{ij}(0, B_2, B_3)$ in the yz plane can be obtained in a similar way.

The transformation equations from the ellipsoidal axis system to the crystallographic system for the mobilities are:

$$\begin{aligned}
 \mu_{11} &= \mu_1 & \nu_{11} &= \nu_1 \\
 \mu_{22} &= \mu_2 \cos^2 \theta_\mu + \mu_3 \sin^2 \theta_\mu & \nu_{22} &= \nu_2 \cos^2 \theta_\nu + \nu_3 \sin^2 \theta_\nu \\
 \mu_{33} &= \mu_2 \sin^2 \theta_\mu + \mu_3 \cos^2 \theta_\mu & \nu_{33} &= \nu_2 \sin^2 \theta_\nu + \nu_3 \cos^2 \theta_\nu \\
 \mu_{23} &= \frac{1}{2}(\mu_2 - \mu_3) \sin 2\theta_\mu & \nu_{23} &= \frac{1}{2}(\nu_2 - \nu_3) \sin 2\theta_\nu
 \end{aligned}
 \tag{AII.4}$$

where μ_i and ν_i are the diagonal components of the mobility tensors in the ellipsoidal axis system, μ_{ij} and ν_{ij} are the electron and hole mobility tensor components expressed in the crystallographic axial system. The tilt angles θ_μ (electron tilt) and θ_ν (hole tilt) are given by

$$\tan 2\theta_\mu = \frac{2\mu_{23}}{(\mu_{22} - \mu_{33})} \quad \tan 2\theta_\nu = \frac{2\nu_{23}}{(\nu_{22} - \nu_{33})}
 \tag{AII.5}$$

Here tilt angles take negative values, i.e. $-90^\circ < \theta_\mu$ (or θ_ν) $< 0^\circ$ (for a general description of the tilt angles in the A7 structure semimetals, see section 6.4).

APPENDIX III

```

***MOBILITY CALCULATIONS FROM LOW FIELD DATA ***
DIMENSION X(9),SMAX(9),SMIN(9),STEP(9),EL(12),HOL(12),
1S(12),CO(12),Z(12),WE(12),W(12),Q(12),SUM(2),H(9),
2P(9),TIL(2),U(1),ET(1),HT(1)
INTEGER I,J,K,L,M,N
REAL Q,SMALL
1  FORMAT (9E8.1)
2  FORMAT(20X,'INITIAL SOLUTIONS FITTED :',//,
120X,'MEASURED COEFFICIENTS',/,2(6(E12.4,1X),/))
4  FORMAT(20X,'RATIOS='/(2(6F12.3/)))
5  FORMAT(20X,'SUM :',2F15.5//)
6  FORMAT(20X,'MEASURED COEFFICIENTS CO(K)='/,2(6(E12.4,1X),/))
9  FORMAT(20X,'ELEC.TILT IN DEG.='F8.2,/,20X,'HOLE TILT IN DEG.='
1,F8.2/)
10 FORMAT(20X,'CALCULATED COEFFICIENTS Z(K)='/,2(6(E12.4,1X),/))
59 FORMAT(20X,'SOLUTIONS',/,3E12.3,4X,F8.3,3E12.3,4X,F8.3,E12.3,/))
80 FORMAT(20X,'STEPS='/,9E12.3,/))
100 FORMAT(/4X,'ELECTR CONTR',5X,'HOLE CONTR',5X,'TOTAL COEFF')
101 FORMAT (12F5.1)
102 FORMAT (8E10.1)
103 FORMAT(/1X,3E15.4)
104 FORMAT(/40X,'CHECK: S(10)='E12.4/)
105 FORMAT(20X,'MOBILITIES IN THE PRINC COORD AXES SYSTEM ARE:'//
15X,'MU1PRIME',5X,'MU2PRIME',5X,'MU3PRIME',5X,
2'MU4PRIME',5X,'NU1PRIME',5X,'NU2PRIME',5X,'NU3PRIME',
35X,'NU4PRIME'/1X,8E13.3/)
106 FORMAT(20X,'SUM :',2F15.5/)
107 FORMAT('1',10X,'MOBILITIES IN THE ELLIPSOIDAL AXES SYSTEM ARE:'
1//8X,'MU1',10X,'MU2',10X,'MU3',5X,'SIN(ET)',5X,'NU1',10X,'NU2',
210X,'NU3',5X,'SIN(HT)',4X,'N=P'/1X,3E13.3,F7.2,3E13.3,F7.2,E13.3/)
108 FORMAT('1',2X,'***** MINIMIZATION STARTS *****'//)
50 READ (5,1,END=99) (X(I),I=1,9)
   READ(5,1)(STEP(I),I=1,9)
   READ (5,101) (W(K),K=1,12)
   READ (5,1) (SMAX(I),I=1,9)
   READ (5,1) (SMIN(I),I=1,9)
   READ (5,102) (CO(K),K=1,12)
   SMALL=0.0001
   HK=0.0
   DO 7 I=1,9
7  H(I)=1
   SUM(1)=0.0
   SUM(2)=0.0
   DO 16 L=1,10
   DO 19 M=1,100
   DO 13 I=1,9
   SUM(2)=0.0
   X(I)=X(I)+HK*STEP(I)
   IF(X(I).GT.SMAX(I)) GO TO 15
   IF(X(I).LT.SMIN(I)) GO TO 15
   CALL ELMA (X,Z,S,EL,HOL,U)
   DO 18 K=1,12
   Q(K)=CO(K)/Z(K)
   SUM(2)=SUM(2)+(W(K)*(Q(K)-1.0)**2
18 CONTINUE
   IF (HK.EQ.1.0) GO TO 77

```

(xix)

```
WRITE (6,108)
WRITE (6,59) (X(K),K=1,9)
WRITE (6,80) (STEP(K),K=1,9)
WRITE (6,10) (Z(K),K=1,12)
WRITE (6,2) (CO(K),K=1,12)
WRITE (6,4) (Q(K),K=1,12)
WRITE (6,5) (SUM(K),K=1,2)
77 CONTINUE
IF (HK.EQ.0.0) SUM(1)=SUM(2)
HK=1.0
IF (SUM(1)-SUM(2)) 15,14,14
15 IF (H(I)-37) 21,21,22
21 X(I)=X(I)-STEP(I)
STEP(I)=-STEP(I)
H(I)=H(I)+1
GO TO 13
22 X(I)=X(I)-STEP(I)
STEP(I)=-0.91*STEP(I)
H(I)=1
GO TO 13
14 IF (SUM(2)-SMALL) 16,16,20
20 SUM(1)=SUM(2)
13 CONTINUE
19 CONTINUE
WRITE (6,59) (X(K),K=1,9)
WRITE (6,80) (STEP(K),K=1,9)
WRITE (6,10) (Z(K),K=1,12)
WRITE (6,6) (CO(K),K=1,12)
WRITE (6,4) (Q(K),K=1,12)
WRITE (6,5) (SUM(I),I=1,2)
16 CONTINUE
ET(1)=(180.0/3.1416)*ATAN(X(4)/(SQRT(1.0-X(4)**2)))
HT(1)=(180.0/3.1416)*ATAN(X(8)/(SQRT(1.0-X(8)**2)))
WRITE (6,107) (X(I),I=1,9)
WRITE (6,9) ET,HT
WRITE (6,10) (Z(K),K=1,12)
WRITE (6,6) (CO(K),K=1,12)
WRITE (6,4) (Q(K),K=1,12)
WRITE (6,106) (SUM(I),I=1,2)
WRITE (6,100)
WRITE(6,103) (EL(I),HGL(I),S(I),I=1,12)
WRITE (6,104) U
P(1)=X(1)
SESQ=X(4)**2
CESQ=1.0-X(4)**2
P(2)=X(2)*CESQ+X(3)*SESQ
P(3)=X(2)*SESQ+X(3)*CESQ
P(4)=X(4)*SQRT(CESQ)*(X(2)-X(3))
TIL(1)=(90.0/3.1416)*ATAN(2.0*P(4)/(P(2)-P(3)))
P(5)=X(5)
SHSQ=X(8)**2
CHSQ=1.0-X(8)**2
P(6)=X(6)*CHSQ+X(7)*SHSQ
P(7)=X(6)*SHSQ+X(7)*CHSQ
P(8)=X(8)*SQRT(CHSQ)*(X(6)-X(7))
TIL(2)=(90.0/3.1416)*ATAN(2.0*P(8)/(P(6)-P(7)))
WRITE (6,105) (P(I),I=1,8)
WRITE (6,9) TIL
GO TO 50
99 STOP
END
```

(xx)

```
SUBROUTINE ELMA (A,Z,S,EL,HOL,U)
DIMENSION A(9),EL(12),HOL(12),Z(12),S(12),U(1)
Q=1.6
SESQ=A(4)**2
CESQ=1.0-SESQ
SHSQ=A(8)**2
CHSQ=1.0-SHSQ
X1=CESQ*A(2)+SESQ*A(3)
Y1=CHSQ*A(6)+SHSQ*A(7)
X2=SESQ*A(2)
X3=CESQ*A(3)
X=X2+X3
Y2=SHSQ*A(6)
Y3=CHSQ*A(7)
Y=Y2+Y3
A23=A(2)*A(3)
A67=A(6)*A(7)
X4=CESQ*SESQ*(A(2)-A(3))**2
Y4=CHSQ*SHSQ*(A(6)-A(7))**2
X5=A(4)*SQRT(CESQ)*(A(2)-A(3))
Y5=A(8)*SQRT(CHSQ)*(A(6)-A(7))
G=A(9)*Q
EL(1)=0.5*G*(A(1)+X1)
HOL(1)=0.5*G*(A(5)+Y1)
S(1)=EL(1)+HOL(1)
EL(2)=G*X
HOL(2)=G*Y
S(2)=EL(2)+HOL(2)
EL(3)=-1.0*G*(A(1)*X1)
HOL(3)=G*(A(5)*Y1)
S(3)=EL(3)+HOL(3)
EL(4)=-0.5*G*(A23+A(1)*X)
HOL(4)=0.5*G*(A67+A(5)*Y)
S(4)=EL(4)+HOL(4)
EL(5)=0.125*G*(X2*(A(1)-A(3))**2+X3*(A(1)-A(2))**2
+3.0*A(1)*X4)
HOL(5)=0.125*G*(Y2*(A(5)-A(7))**2+Y3*(A(5)-A(6))**2
+3.0*A(5)*Y4)
S(5)=EL(5)+HOL(5)
EL(6)=0.125*G*(3.0*X2*(A(1)**2+A(3)**2)+3.0*X3
+1*(A(1)**2+A(2)**2)+A(1)*X4+2.0*A(1)*A23)
HOL(6)=0.125*G*(3.0*Y2*(A(5)**2+A(7)**2)+3.0*Y3
+1*(A(5)**2+A(6)**2)+A(5)*Y4+2.0*A(5)*A67)
S(6)=EL(6)+HOL(6)
EL(7)=0.5*G*((A(1)+X1)*A(1)*X1)
HOL(7)=0.5*G*((A(5)+Y1)*A(5)*Y1)
S(7)=EL(7)+HOL(7)
EL(8)=0.5*G*(X*(A23+A(1)*X))
HOL(8)=0.5*G*(Y*(A67+A(5)*Y))
S(8)=EL(8)+HOL(8)
EL(9)=-0.5*G*(X*A(1)*X1)
HOL(9)=-0.5*G*(Y*A(5)*Y1)
S(9)=EL(9)+HOL(9)
EL(10)=G*(A(1)*X4)
HOL(10)=G*A(5)*Y4
S(10)=EL(10)+HOL(10)
EL(11)=0.25*G*(A(1)*X5*(-A(1)+X1))
HOL(11)=0.25*G*(A(5)*Y5*(-A(5)+Y1))
S(11)=EL(11)+HOL(11)
```

(xxi)

```
FL(12)=0.25*G*(X5*(A23-A(1)*X))
HQL(12)=0.25*G*(Y5*(A67-A(5)*Y))
S(12)=EL(12)+HQL(12)
U(1)=0.5*(-S(6)+3.0*S(5)-2.0*S(9))
Z(1)=1.0/S(1)
Z(2)=1.0/S(2)
Z(3)=S(3)/(S(1)**2)
Z(4)=S(4)/(S(1)*S(2))
Z(5)=S(5)/(S(1)**2)
Z(6)=S(6)/S(1)**2-S(4)**2/(S(1)**2*S(2))
Z(7)=S(7)/S(1)**2-S(3)**2/(S(1)*S(1)*S(1))
Z(8)=S(8)/S(2)**2-S(4)**2/(S(1)*S(2)**2)
Z(9)=S(9)/(S(1)*S(2))-0.5*S(3)*S(4)/(S(1)**2*S(2))
Z(10)=S(10)/S(2)**2
Z(11)=S(11)/S(1)**2
Z(12)=S(12)/(S(1)*S(2))
RETURN
END
```

PUBLICATIONS

1. "DISLOCATION ETCH PITS AND GROWTH OF ARSENIC - ANTIMONY SINGLE CRYSTALS"
Y.C. Akgöz and G.A. Saunders 1971 J.Mater.Sci. 6 395-402
2. "ELASTIC WAVE PROPAGATION in $\text{Bi}_{1.60}\text{Sb}_{0.40}\text{Te}_3$ and Bi_2Te_3 "
Y.C. Akgöz, G.A. Saunders and Z. Sümengen 1972
J.Mater.Sci. 7 279-88.
3. "CONVERSELY ORIENTED ETCH PITS IN A7 STRUCTURE SEMIMETALS"
Y.C. Akgöz, J.M. Farley and G.A. Saunders 1972
J.Mater.Sci. 7 598-600.
4. "ELASTIC BEHAVIOUR OF InBi SINGLE CRYSTALS"
Y.C. Akgöz, J.M. Farley and G.A. Saunders 1973
J.Phys.Chem. Solids 34 141-9.
5. "THE MAGNETORESISTIVITY TENSOR OF As(25.5 at.%) -Sb ALLOY SINGLE CRYSTALS."
Y.C. Akgöz and G.A. Saunders 1973 Paper read at IOP Solid State Physics Conference, Manchester.
6. "GALVANOMAGNETIC EFFECTS OF As(25.5 at.%) -Sb ALLOY CRYSTALS"
Y.C. Akgöz and G.A. Saunders 1974
J.Phys.C: Solid State Phys. 7 1655-70.
7. "DEFECTS AND ALLOYING IN THE GROUP V SEMIMETALS"
G.A. Saunders and Y.C. Akgöz. To be published in the Proc. Int.Conf. on the physics of semimetals and narrow-gap semiconductors (Nice-Cardiff, September 1973).
8. "SPACE-TIME SYMMETRY RESTRICTIONS ON THE FORM OF TRANSPORT TENSORS" I. Galvanomagnetic effects.
Y.C. Akgöz and G.A. Saunders (In Preparation)
9. "SPACE-TIME SYMMETRY RESTRICTIONS ON THE FORM OF TRANSPORT TENSORS" II. Thermomagnetic effects.
Y.C. Akgöz and G.A. Saunders (In Preparation).